Numerical Modelling
of the Human Cervical Spine
in Frontal Impact

by

Matthew Brian Panzer

A thesis

presented to the University of Waterloo

in fulfillment of the

thesis requirement for the degree of

Master of Applied Science

in

Mechanical Engineering

Waterloo, Ontario, Canada, 2006

I hereby declare that I am the sole author of this thesis. This is a true copy of the thesis, including any required final revisions as accepted by my examiners.

I understand that my thesis may be made electronically available to the public.

Matthew B. Panzer

Abstract

Motor vehicle accidents continue to be a leading cause of cervical spine injury despite a conscientious effort to improve occupant safety. Accurately predicting occupant head and neck response in numerical crash simulations is an essential part of the process for developing better safety solutions.

A biofidelic model of the human cervical spine was developed with a focus on accurate representation of the cervical spine at the local tissue level. These tissues were assembled to create a single segment model that was representative of *in vitro* spine in quasi-static loading. Finally, the single segment models were assembled to create a full cervical spine model that was simulated in dynamic loading and compared to human volunteer response.

Models of each segment were constructed from the basic building blocks of the cervical spine: the intervertebral disc, the vertebrae, the ligaments, and the facet joints. Each model was simulated in all modes of loading and at different levels of load. The results of the study indicate that the cervical spine segments performed very well in flexion, compression, and tension. Segment response to lateral bending and axial rotation was also good, while response in extension often proved too compliant compared to the experimental data. Furthermore, the single segment models did not fully agree with the experimental shear response, again being more compliant.

The full cervical spine model was assembled from the single segment models incorporating neck musculature. The model was simulated dynamically using a 15 G frontal impact test. Active muscles were used to simulate the response of the human volunteers used in the study. The response of the model was in reasonable agreement with the experimental data, and compared better than current finite element cervical spine models. Higher frequency oscillation caused most of the disagreement between the model and the experimental data, which was attributed to a lack of appropriate dynamic material properties of the soft tissues of the spine. In addition, a study into the active properties of muscle indicated that muscle response has a significant influence on the response of the head.

A number of recommendations were proposed that would improve the biofidelity of the model. Furthermore, it was recommended that the future goal of this model would be to implement injury-predicting capabilities through the development of advance material models.

Acknowledgements

I would to thank a number of people who were influential in my time as a Master's student at the University of Waterloo. Without their support, this would not have been possible.

I am pleased to thank my advisor, Duane Cronin, for his inspiration and encouragement throughout this entire graduate experience. I would also like to thank him for introducing me to the exciting field of impact biomechanics, even when he tries to instrument my head with accelerometers.

I am grateful for the support of Yih-Charng Deng and our friends at General Motors, who have always realized the importance of collaboration between industry and academia.

I would like to thank General Motors Ltd., Partners for the Advancement of Collaborative Engineering Education (PACE), the Ontario Graduate Scholarship Program, the University of Waterloo, and the Department of Mechanical Engineering for all the financial assistance I received throughout my studies.

I would like to thank my all friends for putting up with my absence during my time writing this thesis. I would like to thank my all officemates for putting up with my presence during my time writing this thesis. I especially would like to thank Alayna Gillespie for her unwavering support through this whole writing process, Jason Hynes for being a good friend by helping ease my stress with dozens of chicken wings, and Christian Kaufmann for being a great officemate and helping me submit my thesis on time.

Finally, I would like to thank my parents, Rob and Brenda, and brother, Derek, who have always encouraged me in all my endeavors. My success in achieving my goals is a direct result of your confidence in me. Thank you.

Table of Contents

List of Tables

List of Figures

Chapter 1
Introduction

1.1 Motivation for Research

Despite the persistent development of occupant protection methods in the automotive industry, the cervical spine continues to be a major region for serious injury caused by motor vehicle accidents. It is estimated that 40 % to 65 % of all spine-related injuries are caused by motor vehicle accidents, with the cervical spine being the primary severe injury site (Yoganandan et al., 1989b). Furthermore, there is a very high incidence rate of minor injuries to the cervical spine in rear impact vehicular accidents (commonly known as whiplash) that can potentially leave a victim with long-term pain and disability (Yoganandan et al., 1989b).

Minor neck injuries such as sprains and strains are the most frequently reported insurance claim in the United States, accounting 66% of all bodily injury claims in 2002 (Insurance Institute for Highway Safety). Claims in which neck pain was the most serious resulted in a cost to society of approximately $8.5 billion dollars.

To ensure that occupants are adequately protected during motor vehicle accidents, automotive manufactures are required to conform and certify compliance with specific safety regulations mandated by government agencies. In the United States, these guidelines and requirements are outlined in the Federal Motor Vehicle Safety Standards (FMVSS) and Regulations, and the Canadian Motor Vehicle Safety Standards (CMVSS) for vehicles in Canada. The specific standard for outlining the tolerances of occupant response in frontal crash tests is FMVSS #208.

Crash testing is a form of destructive testing that is done to ensure design of the vehicle meets the required safety standards. Anthropometric dummies (crash-test dummies) are seated in the vehicle as physical human surrogate models, and are used to measure the occupant response during the crash test. Crash-test dummies were first employed as a human surrogate model in the late 1940's. Since that time, numerous models have been developed for specific types of loading, and upgraded to increase their human-like response (biofidelity). In 1976, General Motors developed the detailed Hybrid III dummy model for occupant response in frontal impact. The Hybrid III has since become

the standard model to use for FMVSS 208 frontal crash tests, as well as in other applied biomechanics research.

Crash testing vehicles is a necessary process that ensures all safety criteria for the vehicle are met. However, this process is very expensive, as it requires the destruction of a new vehicle with each test. Also involved are massive amounts of instrumentation used for high-speed data acquisition of both the vehicle and the dummies during the test. This requires a significant amount of time to setup since rigorous scientific standards are employed to ensure that quality data is obtained from the test.

Due to the high costs associated with crash testing, automotive manufactures have begun using numerical methods to understand crash. This reduces the cost of vehicle testing, as the number of destroyed vehicles is minimized. Numerical modelling allows for surrogate experiments that are characterized by definite repeatability. Whereas physical testing can be limited by measurement and instrumentation feasibility, numerical models have near infinite capabilities to measure response, including internal response such as stress. The downside to numerical modeling is that models require an extensive amount of evaluation and validation with experimental studies.

For the automotive industry to assess the crashworthiness of a vehicle in simulation, numerical occupant models are required to simulate the response of a human. Human numerical models have been used in biomechanics research for many decades, but only in the last 10 years has computer power allowed researchers to create highly detailed models. While much of the human body model development has been stimulated by the automotive industry, research from sports injury and medicine have also been major players in advancing the field. A current trend in the impact biomechanics field is to use numerical simulation of human body models as a tool for analyzing and understanding the response of the human body to impact.

1.2 Research Objectives and Approach

The objective of this research is to develop a numerical model of the human cervical spine for use in frontal impact conditions. A previously developed model by Deng et al (1999) was the basis for the new cervical spine model. Justification for developing new cervical spine model was based on the necessity for simulating the cervical spine at high levels of loading, while providing the framework for enhancing the model into an injury-predictive tool.

The approach taken in developing this model was one that concentrated on accurate representation of the local tissues using the mechanical properties discovered through fundamental research. Persistent

evaluation of the model during each development stage ensured that the tissue was properly characterized based on anatomy, physiology, and mechanics. In no instances was the scientific integrity of the tissue models compromised by model calibration or adjustment to achieve a desired output. This rigorous method allowed for an accurate tissue representation, and provided a solid foundation to build the model on.

The tissue models were then assembled to complete an individual spine segment. The segment models were simulated in all types of loading, and the response of the model was compared to a wide range of experimental studies. The load-displacement response of each segment was analyzed using procedures documented by the comparable experimental studies. The results were scrutinized to identify model strengths and weaknesses. Furthermore, the segment models were simulated at very high loads of compression to identify the injury mechanisms and failure loads of the vertebral body.

The segment models were then combined to create a full cervical spine model. Neck musculature was added to the spine, and a muscle activation scheme was developed that allowed the cervical spine to exhibit physiological response. Some material models were enhanced to include the viscoelastic response seen during relaxation or high-strain rate testing. The full spine model was compared to a human volunteer test series using the 15 G frontal impact case in an attempt to validate the model. A study into the effects of muscle activation on the response of the cervical spine model was accomplished.

All numerical simulation of the cervical spine model will be done as finite element analysis, using the commercial code LS-DYNA. LS-DYNA is a nonlinear, explicit finite element analysis program developed by Livermore Software Technology Corporation (LSTC). It is an evolving code that is used in a wide range of applications, such as crashworthiness simulation, impact biomechanics, and blast simulation.

1.3 Organization of the Thesis by Chapter

This thesis is presented in a format that is comparable to the approach taken in developing the cervical spine model. Chapter 2 focuses on the anatomy and physiology of the various tissues of the cervical spine. This background research is an essential phase of the development process, as accurate anatomy is one of the main pillars required for producing a biofidelic model.

Another pillar required for accurate modelling of biological systems is found in the extensive background research presented in Chapter 3, which delves into the complex mechanical properties of

tissue. This research provides the fundamental detail of the mechanical response of the tissue, and provides insight into the requirements for the material models.

Chapter 4 investigates the causes of injury and the injury mechanisms associated with the cervical spine. As well, the current injury criteria methods used to assess injury potential are discussed. Chapter 4 also highlights the vast amount of experimental studies focused on understanding the biomechanics and injury of the cervical spine. Background research includes tests done with spine segments, isolated cervical spines, post-moterm human subject testing, and finally human volunteer response.

Previous efforts in cervical spine numerical models are described in Chapter 5. Various spine segment models, including those from the lumbar spine region, are reviewed to provide the history of modelling techniques. Full cervical spine models of both multi-body and finite element types are discussed and compared.

Chapter 6 outlines the process used in the development of the new cervical spine model. Modelling techniques used in constructing the numerical model are first discussed. Various measures of cervical spine model geometry are presented as a verification tool, comparing the model anatomy with that described in Chapter 2. Finally, the development of material models based on the tissue mechanics presented in Chapter 3 is illustrated.

A summary and analysis of the results of the single segment models are presented in Chapter 7. The results are compared to various sources of experimental data to validate the model. The model response is critiqued, and conclusions and recommendations are made. The complete results of the single segment model simulations are found in Appendix A, while a more detailed presentation of the flexion and extension results are found in Appendix B.

The results from the frontal impact simulation of the full cervical spine model are found in Chapter 8. The motion of the head during the impact simulation is compared to the response corridors of human volunteers. The dynamic response of the model is critically evaluated, and suggestions are made for improving the results. A study involving the activation scheme of the neck muscles is also presented.

Finally, Chapter 9 and Chapter 10 provide the overall conclusions and recommendations for the model. The model is assessed in its current state, and the results from both the single segment and the full spine model simulations are discussed. Recommendations are made based on improving the response of the model, as well as to provide some direction for future development of the model.

Chapter 2

Functional Anatomy

Anatomy is the study of the structure of the human body. Functional anatomy is the study of anatomy in its relation to function. Finally, physiology is the study of how various body parts function. All three areas of study are important in the field of biomechanics. The human body tends to follow the 'form follows function' such that to understand the function of the body, we must first learn how it is constructed.

Anatomical descriptions are based on three imaginary planes that intersect the human body (Figure 2-1). These planes are the frontal plane, the transverse plane, and the sagittal plane. The frontal plane divides the body into front and back parts, while the transverse plane divides the body into top and bottom. The sagittal plane divides the body into right and left sides, and is called the median plane when passing directly through the centre of the human body.

Various anatomical terms are used to describe relative direction and position within the human body (Figure 2-1). The superior and inferior directions are opposite each other, and are created by the intersection of the sagittal and frontal planes. The anterior and posterior directions are also opposite, and are created by the sagittal and transverse planes. The third direction is treated a little differently since using terms such as left or right can be ambiguous depending on the viewer's perspective. Instead, the term medial is used to describe the direction perpendicular and towards the medial plane, while lateral is used to describe the direction away from the medial plane.

Other anatomic terms used to describe structures relative to the surface of the body are superficial, intermediate, and deep. Superficial is used to describe structures near the surface, while deep refers to structures far away from the surface. Intermediate is a term used for structures between superficial and deep.
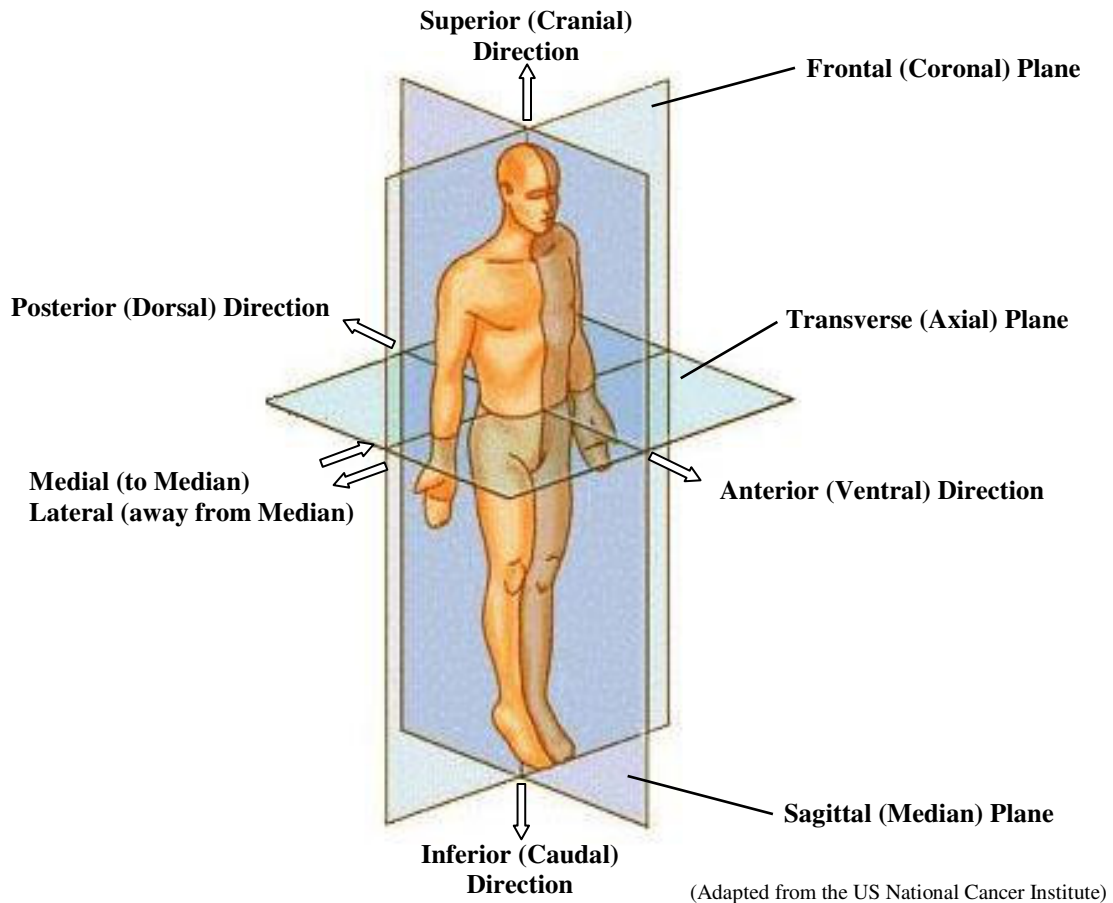
Figure 2-1: Anatomical Planes and Directions

The anatomical terms for the movement of the cervical spine and head are lateral bending, axial rotation, extension, and flexion (Figure 2-2). Lateral bending, or just simply bending, refers to the motion of the head and neck rotating about the anterior-posterior axis in the frontal plane. Axial rotation, or simply rotation, refers to motion of the head and neck rotating about the superior-inferior axis in the transverse plane. Flexion and extension refer to motion of the head and neck rotating about the lateral axis in the sagittal plane. Extension is the term used when this rotation results in the head 'looking up', and flexion is the term used when the rotation results in the head 'looking down'.

| Lateral Bending (Tilted Head) | Axial Rotation (Turned Head) | Extension (Looking Up) | Flexion (Looking Down) |
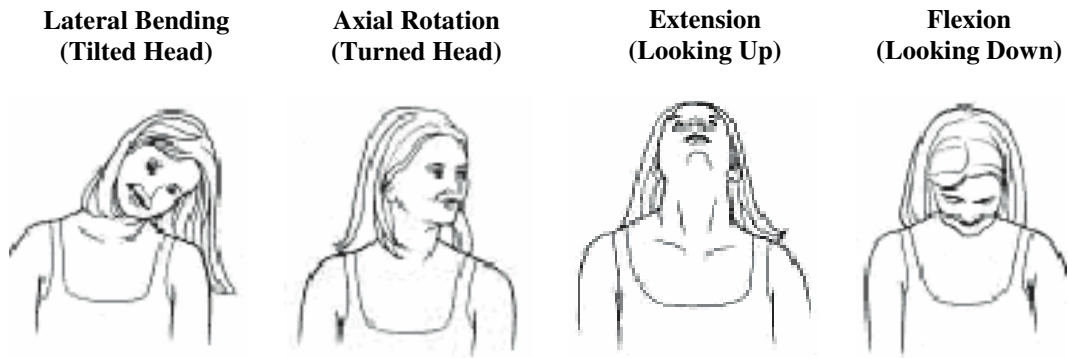
(Adapted from Contemporary Pediatrics)

Figure 2-2: Terms of Movement for the Head and Cervical Spine

2.1 Vertebrae

The vertebrae are the basic bony structures that constitute the spinal column. There are 33 vertebrae in the human body, divided up into three regions (cervical, thoracic, and lumbar), the sacrum, and the coccyx. An intervertebral disc separates each vertebra, except in the upper cervical spine (C1 & C2), and in the sacrum and coccyx, where the vertebrae are fused together. A diagram of the entire human spinal column can be seen in Figure 2-3.
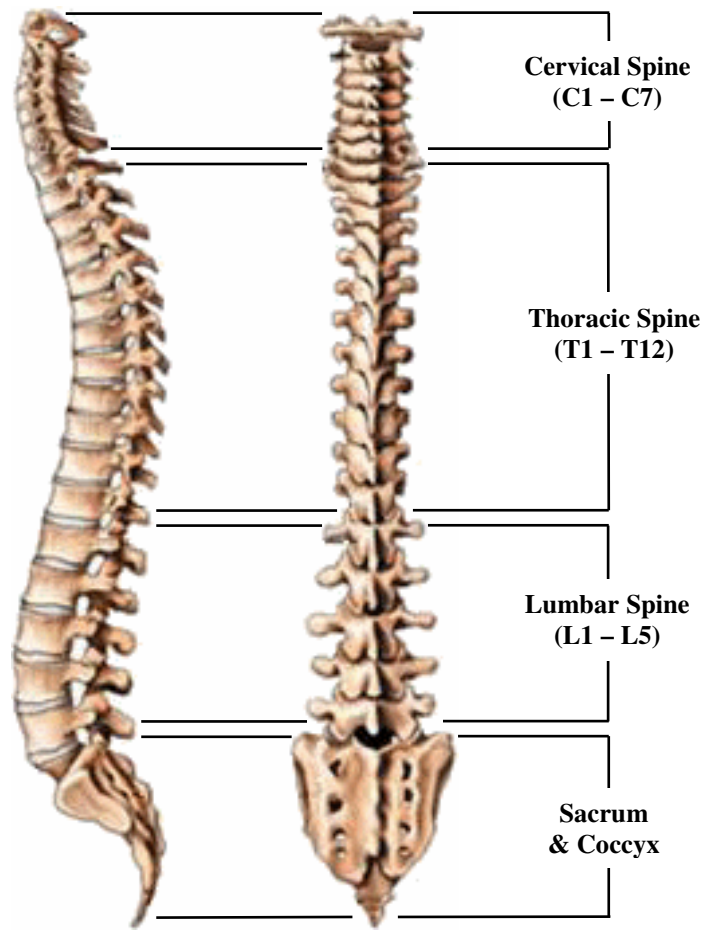
Figure 2-3: Different Regions of the Human Spinal Column

The cervical spine, which constitutes the bony structures in the neck, consists of seven vertebrae. It is common for the cervical spine to be divided in three sections: the upper cervical spine (C1 and C2), the middle cervical spine (C3 – C5), and the lower cervical spine (C6 – T1). The first thoracic vertebra is commonly included in the cervical spine because it forms the lowest cervical intervertebral joint with C7. These regions can be seen in the diagram of the entire cervical spine in Figure 2-4.
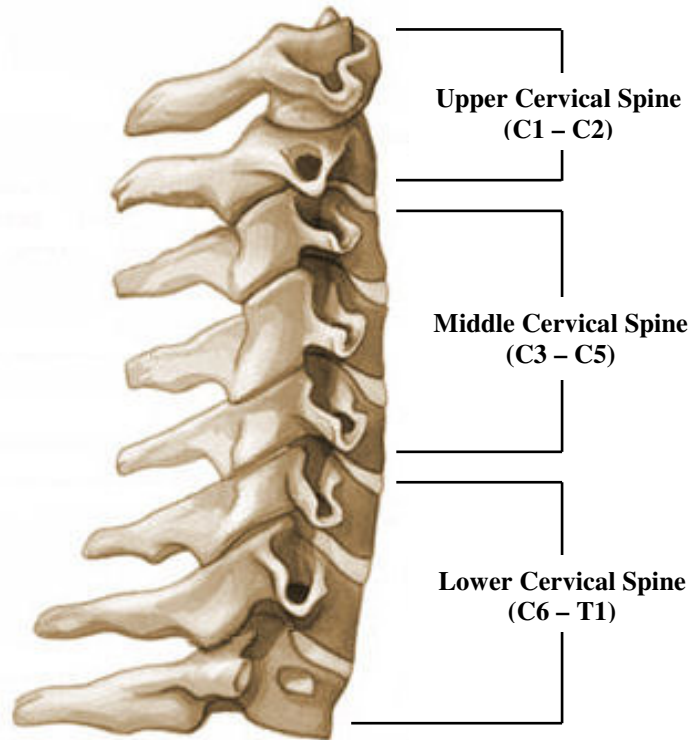
Figure 2-4: Different Regions of the Human Cervical Spine

2.1.1   Vertebral Anatomy

The anatomy of the middle and lower cervical vertebrae (C3 – C7) share the same basic characteristics as other vertebrae in the spinal column (Gray, 1918). The basic structure of the vertebra is divided into two essential parts: the anterior segment (the vertebral body) and the posterior segment (the vertebral arch, made up of the laminae, the pedicles, and seven processes). The processes consist of four articular processes, two transverse processes, and one spinous process. The vertebral arch is constructed in a way such that various foramens (orifices) are formed. These details can be seen in Figure 2-5.
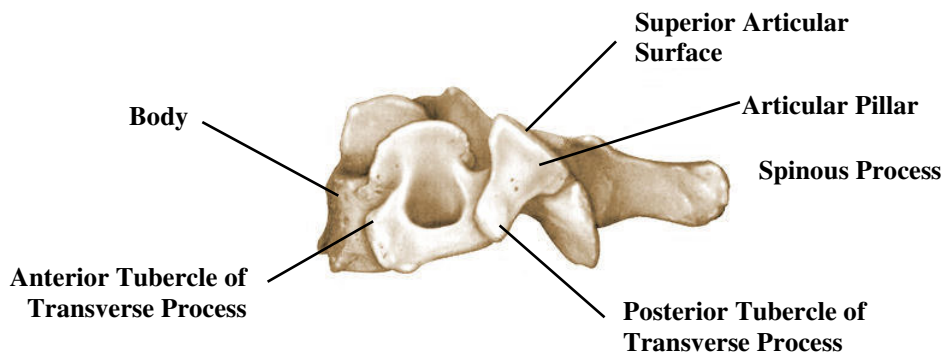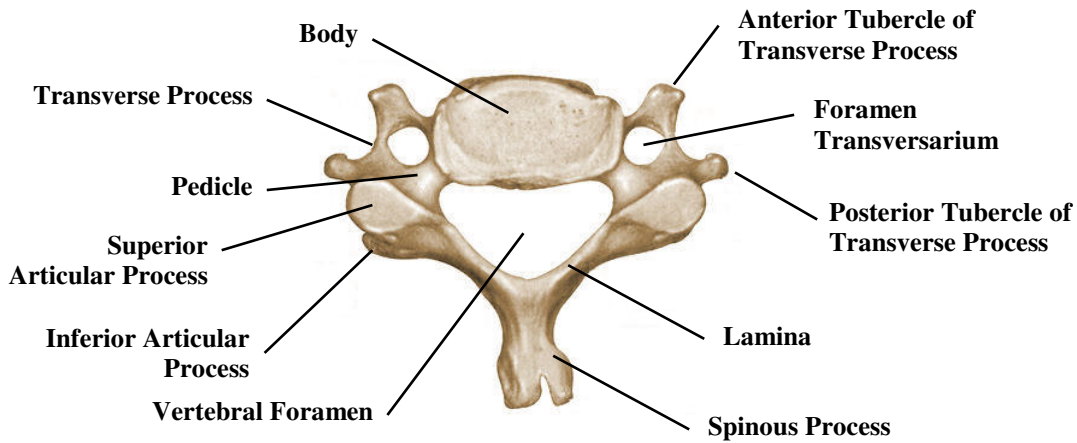
Figure 2-5: Anatomic Details of the Middle and Lower Cervical Vertebrae

The vertebral body is the largest structure in the cervical vertebrae, resembling an elliptical cylinder. The superior and inferior surfaces of the vertebral body (also known as the osseous endplates) are flattened and rough for the attachment of the intervertebral discs. The anterior surface of the body is often convex, whereas the poster surface is slightly concave. The typical size of the cervical body height is between 13 and 15 mm, with an elliptical cross-section of approximately 15 mm depth and 30 mm width (Gilad and Nissan, 1986; Pooni et al., 1986; Panjabi et al., 2001a).

The pedicles are two short, thick structures that attach to the middle portion of the posterolateral vertebral body. The laminae are two broad plates that are connected to the pedicles, and are directed in the posteromedial direction from the pedicles until they are fused together in the sagittal plane. The posterior surface of the body along with the pedicles and the laminae, form the vertebral foramen through which the spinal cord passes.

At the lateral junction of the pedicles and the laminae is the articular pillar. The articular pillar is a structure that fuses together the superior and inferior articular processes. The surfaces of the articular processes (facets joints) are oriented between 70° and 100° from the sagittal plane (increasing from C3 to C7), and between 45° and 65° from the transverse place (also increasing from C3 to C7) (Pal et al., 2001).

The spinous process is a prominent structure stemming from the union of the laminae, and used as an attachment point for muscle and ligaments. The spinous process of the cervical vertebra is much smaller in proportion to the spinous process in the lumbar vertebra, except for in the C7 vertebra, where it is much more pronounced. The tips of each spinous process are between 13 and 20 mm apart when the cervical spine is in a neutral position (Gilad and Nissan, 1986). The two transverse processes exist at the junction of the pedicles and laminae, attached to the articular pillar. It forms the foramen transversarium with the pedicle, which allow passage for vertebral arteries and veins, as well as sympathetic nerves bundles. Attached to the transverse process are tubercles, which serve as attachment points for muscle and ligaments.

The upper cervical spine has two different types of vertebrae that are unlike any other in the human body. These two vertebrae are referred to as the atlas (C1) and the axis (C2) because of their basic shape. The atlas does not have a vertebral body or a spinous process. It resembles a bony ring consisting of anterior and posterior arch, and two lateral masses (Figure 2-6). The anterior arch, which is about 20% of the circumference of the ring, has the anterior tubercle on its anterior surface and the concave articular facet for the odontoid process (dens) on its posterior surface. The posterior arch, which is about 40% of the circumference of the ring, has a posterior tubercle that is rudiment of a spinous process (Gray, 1918).

Connecting the anterior arch to the posterior arch are two lateral masses, which are the solid, compact portion of the atlas used for supporting the weight of the head. On the superior surface of the lateral masses are the superior facets, which are large, concave, elliptical surfaces that form to the occipital condyles of the skull. The inferior facets of the atlas, on the other hand, are large, convex, circular surfaces that contact with the superior articular surfaces of the axis.

Figure 2-6 labels (top view): Anterior Arch, Anterior Tubercle, Transverse Process, Foramen Transversarium, Superior Facet, Vertebral Foramen, Posterior Tubercle, Posterior Arch

Figure 2-6 labels (bottom view): Lateral Mass, Inferior Facet, Articular Facet for Dens, Anterior Arch
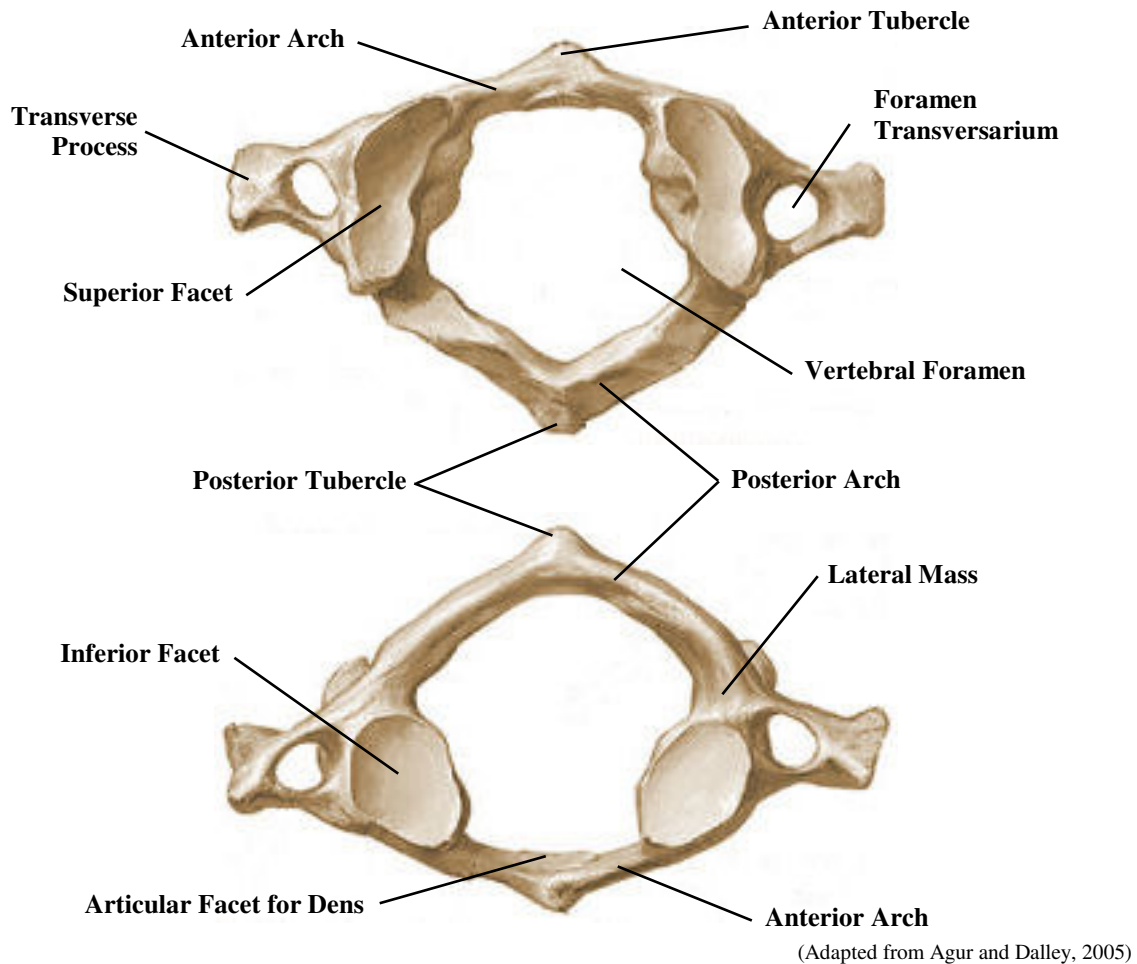
(Adapted from Agur and Dalley, 2005)

Figure 2-6: Anatomic Details of the Superior (Top) and Inferior (Bottom) View of the Atlas

The axis (C2) is a large vertebra similar to the middle and lower cervical vertebra except for the presence of the prominent odontoid process (dens) that rises superiorly from the vertebral body (Figure 2-7). On the anterior surface of the odontoid process is an articular facet for contact with the anterior arch of the atlas. The posterior surface of the odontoid process has a slightly grooved articular surface for contact with the transverse ligament. The odontoid process attaches to the large vertebral body, which is connected to pedicles and laminae similar to other vertebrae. However, both the pedicles and the laminae are much larger and stronger in the axis than in the other cervical spine vertebrae (Gray, 1918).

The superior articular facets of the axis are slightly convex to support contact with the atlas while allowing relatively free translational movement between the two surfaces. The inferior articular

surfaces are similar to the articular surfaces of other cervical vertebrae. The assembly of the atlas and axis can be seen in Figure 2-8. More detail regarding the upper cervical spine joint complex can be seen in Figure 2-21 and Figure 2-22.

Articular Facet for Anterior Arch of Atlas

Odontoid Process

Superior Facet

Inferior Facet

Pedicle

Vertebral Body

Articular Surface for Transverse Ligament

Transverse Process

Foramen Transversarium

Spinous Process

Laminae
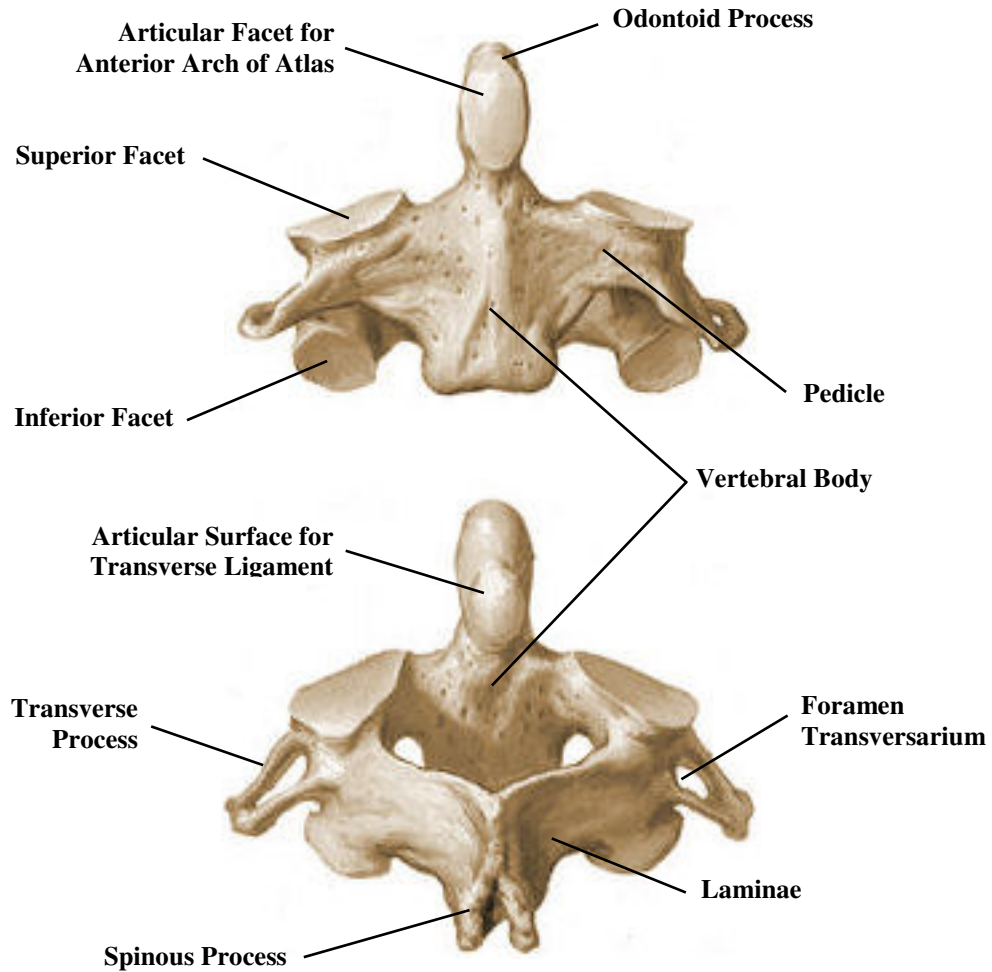
(Adapted from Agur and Dalley, 2005)

Figure 2-7: Anatomic Details of the Anterior (Top) and Posterior (Bottom) View of the Axis

Atlas (C1)

Axis (C2)

C3

C4
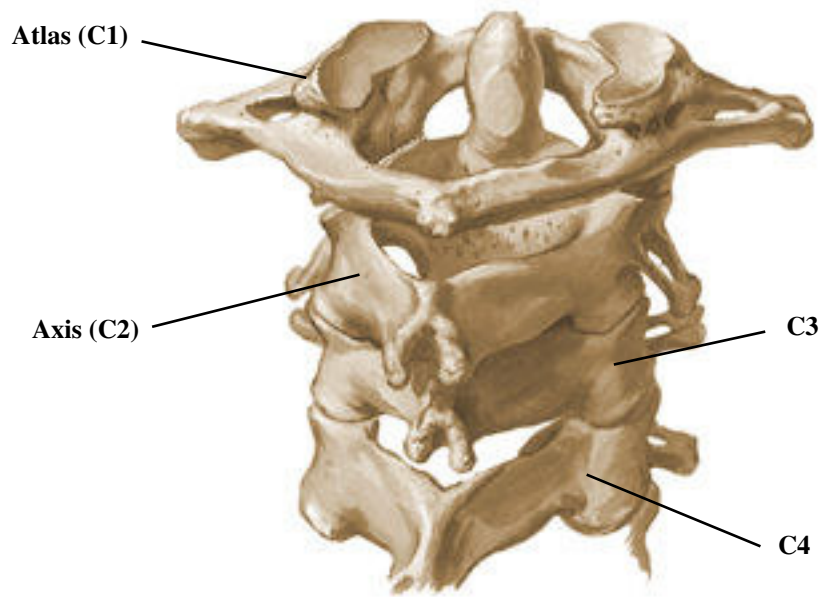
Figure 2-8: Posterior View of the Upper Cervical Spine Joint with C3 and C4

Each vertebra is constructed from a cancellous bone core surrounded by a thin cortical bone shell. The construction of the human vertebra can be seen in Figure 2-9. The size of the cervical vertebrae is relatively small compared to other bones in the human body, with the vertebrae being roughly 2 x 1½ x ¾ inches in size. The dimensions of the vertebral body as measured by Gilad and Nissan (1986) and Panjabi et al (1991e) can be seen in Table 2-1.The vertebral body is shaped similar to an elliptical cylinder, with the dimensions in the lateral direction (width) being slightly larger than the dimensions in the anterior-posterior direction (depth). The distance from the anterior face of the vertebral body to the tip of the spinous process is slightly larger than the distance between the tips of each transverse process.
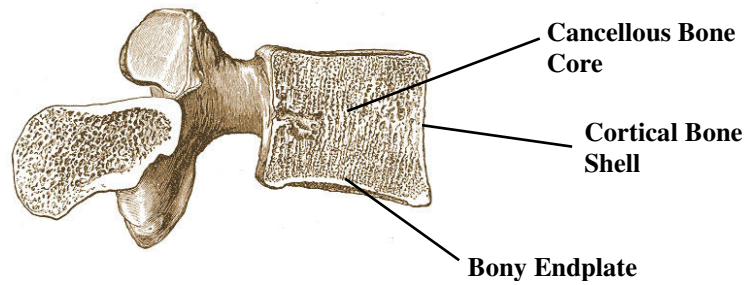
Figure 2-9: Sagittal Plane Cross-Section of a Human Lumbar Vertebra

The cortical shell and bony endplates surrounding the vertebral body is very thin, ranging from 0.40 mm to 0.70 mm thick (Panjabi et al., 2001a). Measured thicknesses of the cortical bone and bony endplates can be found in Table 2-1. Around the posterior elements of the cervical vertebrae, the cortical shell is much thicker (Gray, 1918).

Table 2-1: Vertebral Dimensions and Bone Thickness

Vertebral Dimension	C2	C3	C4	C5	C6	C7
Vertebral Body Depth						
(Superior)	12.6 mm	14.8 mm	15.5 mm	15.5 mm	16.0 mm	16.4 mm
(Inferior)	15.3 mm	15.6 mm	15.8 mm	16.1 mm	16.6 mm	16.3 mm
Vertebral Body Height						
(Anterior)	19.0 mm	14.1 mm	13.4 mm	12.7 mm	13.0 mm	14.6 mm
(Posterior)	16.6 mm	14.5 mm	13.9 mm	13.8 mm	13.9 mm	14.9 mm
Vertebral Body Width						
(Superior)		15.8 mm	17.2 mm	17.5 mm	18.5 mm	16.8 mm
(Inferior)	17.5 mm	17.2 mm	17.0 mm	19.4 mm	22.0 mm	23.4 mm
Spinous Process Length	33.7 mm	29.6 mm	30.3 mm	28.5 mm	34.2 mm	45.7 mm
Transverse Process Width	52.6 mm	50.3 mm	48.5 mm	46.4 mm	49.5 mm	66.6 mm
Cortical Thickness						
(Anterior)		0.51 mm	0.55 mm	0.62 mm	0.66 mm	0.70 mm
(Posterior)		0.41 mm	0.41 mm	0.44 mm	0.49 mm	0.48 mm
Endplate Thickness						
(Superior)		0.63 mm	0.62 mm	0.55 mm	0.63 mm	0.60 mm
(Inferior)		0.58 mm	0.56 mm	0.62 mm	0.65 mm	0.67 mm

The cancellous bone core has an apparent density between 0.1 g/cm^3 and 0.3 g/cm^3 (Kopperdahl and Keaveney, 1998). This is on the lower end of apparent density for cancellous bone from other sites of the human body (Keaveny et al., 2001). Furthermore, vertebral cancellous bone density decreases approximately 50% from age 20 to age 80 for normal individuals (Mosekilde et al., 1987). The architecture of the vertebral cancellous bone is characterized by thick vertical rods and columns sustained by thinner horizontal trabeculae (Mosekilde et al., 1987; Kopperdahl and Keaveny, 1998). This allows for strength in the primary load-direction (axial compression) while maintaining a

minimal bone mass (Cowin, 2001). A fluid phase of blood vessels, blood, marrow, nerve tissue, interstitial fluid, and miscellaneous cells fills the remaining voids of the cancellous bone *in vivo* (Carter and Hayes, 1977).

2.1.2 Vertebral Physiology

The major physiological load on the spine is axial compression (White and Panjabi, 1990). Unlike many other bones in the human body, the cancellous core is a major contributor to the physiological load-carrying capacity (White and Panjabi, 1990). Compressive load is transmitted from the superior endplate to the inferior endplate through either the cancellous core or the cortical shell. Because the cortical shell is so thin, it only contributes a small amount to the strength of the vertebral body (Rockoff et al., 1969; White and Panjabi, 1990). It was found that for younger vertebrae (< 40 years), the cancellous core carried as much as 55% of the applied compressive load (Rockoff et al., 1969). As the density of the cancellous bone decreased with age (> 40 years), a larger portion of the load was carried by the cortical shell, resulting in 35% of the load being carried by the cancellous core (Rockoff et al., 1969).

Under compressive loading, the build-up of hydrostatic pressure in the adjacent intervertebral disc causes the bony endplate to deform into the vertebral body (White and Panjabi, 1990). The resulting endplate deformation has been estimated to be half the size of the bulge of the annulus fibrosus at the same applied load (Brickmann and Horst, 1985). An example of this can be seen in Figure 2-14. The increase in strain in the endplate because of compressive loading can lead to fracture in high load cases (White and Panjabi, 1990).

Since the articular surfaces of the lower and middle cervical spine are approximately 45° to the transverse plane, these surfaces are capable of transmitting compressive load from one vertebra to the next, reducing the share of load seen on the intervertebral disc and vertebral body. Under physiologic loading, the facet joints carry approximately 10% of the total compressive force seen on the vertebra (Goel et al, 1998). This load share increases significantly when the spine is loaded in extension, axial rotation, and lateral bending, where the facets joints carry about 85%, 33%, and 37% of the total load respectively (Goel et al, 1998). In flexion, the facet joints are separated, and thus no compressive load is carried.

In the upper cervical spine, 100% of the axial compressive load is transferred from the head to the cervical spine (C2) via the articular facets. The occipital condyles (sometimes referred to as the C0), are convex articular surfaces on the skull and sit in the concave superior articular surfaces of the atlas.

This allows for relatively free motion between the skull and the atlas in flexion and extension, while limiting relative motion in axial rotation and lateral bending (Bogduk and Mercer, 2000).

The articular facets between the axis and the atlas are both convex, which naturally allow free planar motion between the surfaces. With the odontoid process secured to the anterior arch of the atlas via the transverse ligament, the C1 is permitted to rotation around the odontoid process relatively uninhibited. The rotational range-of-motion between C1 and C2 is almost 180°, and accounts for approximately 55% of the total cervical spine rotation (White and Panjabi, 1990; Chang et al., 1992).

Instantaneous Axis of Rotation
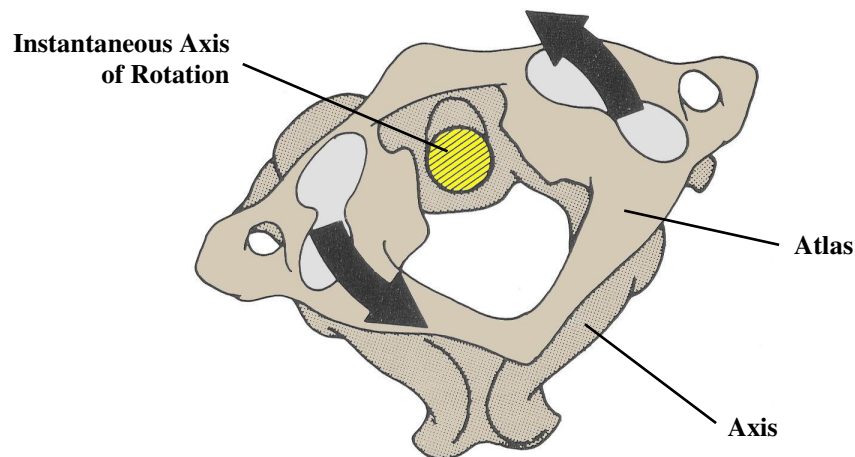
Atlas

Axis

(Adapted from White and Panjabi, 1990)

Figure 2-10: Relative Rotational Motion Between the Atlas and the Axis

2.2 Facet Joints

The facet joints of the cervical spine are important for two main reasons: they are a direct source for neck injury and pain, and they are a principal structure for cervical spine stability (White and Panjabi, 1990). These joints are formed between articular surfaces of adjacent vertebrae, and are a complex structure of fluid, hard, and soft tissue.

2.2.1 Facet Joint Anatomy

The facet joints are synovial joints similar to the joints in the knee and elbow. A synovial joint consists of two matching bony articular surfaces (on the articular pillars) covered with articular cartilage (Figure 2-11). Between the articular cartilages is a gap filled with synovial fluid, a viscous fluid that lubricates the cartilage for ultra-low friction sliding. Containing the synovial fluid within the

synovial joint is the flexible synovial membrane. In the cervical facet joint, the capsular ligament encases the facet joint to provide joint strength in tension.
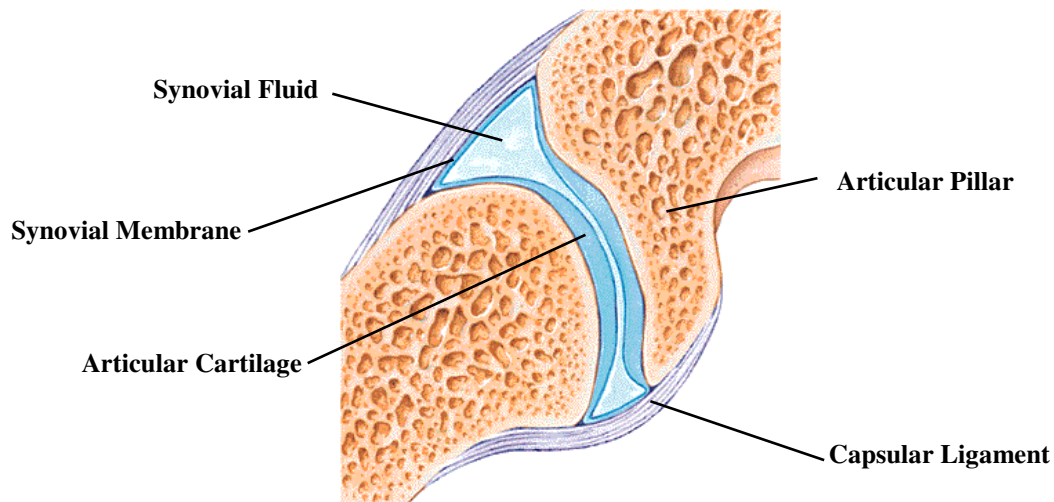
Figure 2-11: Cross-Sectional View of the Synovial Facet Joint of the Cervical Spine

Articular cartilage in the facet joints is of the hyaline type, which is a semi-transparent matrix that is extremely strong, but flexible and elastic. The composition of cartilage includes living cells (chondrocytes), a gelatinous ground substance (75% by weight), and a system of collagen fibres (10% by weight) that are arranged in layers within the tissue (Fung, 1993; Mow et al., 1980). Collagen fibres are organized in tightly packed sheets oriented in the plane of the articular surface in the superficial tangential layer of the cartilage. The middle layer of cartilage tissue consists of shorter collagen fibres arranged in a random manner. At the deepest layer, collagen fibres are infused with the underlaying subchondral bone. These fibres form part of the organic matrix that is swollen by fluid, giving cartilage its viscoelastic properties.

Synovial fluid is made up of hyaluronic acid that gives it higher viscosity than water (Fung, 1993). The role of the synovial fluid is to provide the lubrication between the articular surfaces for reduced friction and to supply the nutrients to the cartilage. The effectiveness of synovial fluid as a lubricant is far superior to many other types of lubricants. The synovial membrane is a very smooth, dense connective tissue that encloses and secretes synovial fluid.

The size and orientation of the cervical facet joints are important factors that determine the functional biomechanics of the joint and of the cervical spine (Pal et al., 2001). However, there are very few studies on the geometry of the cervical facet joint (Yoganandan et al., 2003). The facet joint surfaces

are elliptical in shape, being slightly larger in width (lateral direction) than in height (anterior-posterior direction). The orientation of the facet joints in the cervical spine are commonly posterolateral, with the average plane of their surfaces forming an angle between 30 and 65° with the transverse plane, and 0 to 15° with the sagittal plane. The results from a number of studies on the size and orientation of the cervical facet joints can be found in Table 2-2. For the definition of each dimension and angle, refer to Figure 6-13.

Table 2-2: Summary of the Size and Orientation of the Cervical Facet Joints

Study	Level	Inferior Surface				Superior Surface			
		Width	Height	α_T	α_S	Width	Height	α_T	α_S
Francis, 1955	C1	17.2 mm	18.0 mm			11.6 mm	23.4 mm		
	C2	11.8 mm	11.4 mm			17.7 mm	19.0 mm		
	C3	12.2 mm	11.5 mm			11.8 mm	11.3 mm		
	C4	12.7 mm	11.4 mm			12.2 mm	11.5 mm		
	C5	13.2 mm	11.2 mm			12.6 mm	11.2 mm		
	C6	13.6 mm	11.0 mm			13.1 mm	10.8 mm		
	C7	14.8 mm	12.4 mm			14.0 mm	10.2 mm		
Panjabi et al, 1993	C2	10.9 mm	12.4 mm	33.8°	72.6°	16.4 mm	17.9 mm	37.1°	116.3°
	C3	11.4 mm	12.4 mm	42.6°	77.3°	11.1 mm	11.6 mm	52.0°	74.2°
	C4	11.6 mm	12.3 mm	42.6°	74.7°	11.5 mm	12.2 mm	48.4°	84.6°
	C5	11.7 mm	11.2 mm	51.7°	73.6°	12.1 mm	11.6 mm	45.6°	83.6°
	C6	12.9 mm	12.3 mm	54.9°	82.4°	12.4 mm	11.0 mm	47.6°	79.0°
	C7	13.3 mm	12.7 mm	49.5°	81.3°	12.6 mm	11.4 mm	55.5°	82.9°
	T1	12.6 mm	12.9 mm	64.3°	75.5°	13.7 mm	12.6 mm	60.0°	85.9°
Pal et al, 2001	C3					10.3 mm	10.0 mm	45.8°	69.9°
	C4					10.8 mm	10.7 mm	50.8°	81.7°
	C5					11.3 mm	9.7 mm	52.3°	91.0°
	C6					12.3 mm	9.0 mm	56.0°	95.7°
	C7					13.6 mm	8.6 mm	64.7°	94.1°
	T1					14.3 mm	8.8 mm	68.8°	99.3°
Yoganandan et al, 2003	C0		18.6 mm						
	C1		16.7 mm				18.6 mm		
	C2		11.5 mm				16.7 mm		
	C3		11.9 mm				11.5 mm		
	C4		10.6 mm				11.9 mm		
	C5		10.8 mm				10.6 mm		
	C6		11.1 mm				10.8 mm		
	C7		12.4 mm				11.1 mm		
	T1						12.4 mm		

2.2.2 Facet Joint Physiology

The facet joints of the cervical spine have two main roles: they are responsible for bearing a significant amount of compressive load acting on the spine (Goel and Clausen, 1998), and they help control the primary and secondary motions of the cervical spine (Boduk and Mercer, 2000). Goel and Clausen (1998) observed each facet joint carrying 6% of the entire compressive load (4.6N of 73.6 N each), while this load increased dramatically to 51% of the compressive load with the inclusion of extension. Significant load increases were also seen in one of the joints in axial rotation and lateral.

Because of the geometry of the facet joints (oriented approximately 45° in the transverse plane), axial rotation is inevitably coupled with lateral bending (Bogduk and Mercer, 2000). For example, under going an axial rotation, the superior articular surface of the facet joint must slide up the inferior surface, causing a lateral bending motion between the vertebrae. Conversely, when undergoing a lateral bend, the superior articular surface of the compressed facet joint will slide downwards and posteriorly, causing a rotation between the vertebrae.

2.3 Intervertebral Discs

The intervertebral disc is a fibrocartilaginous structure situated between adjacent vertebral bodies serving as a shock absorber for the spinal column. It is arguably the most widely studied anatomic structure of the entire spine due to its significant role in spinal motion and injury (White and Panjabi, 1990). The structure of the spine involving the vertebrae and the intervertebral disc can be seen in Figure 2-12.
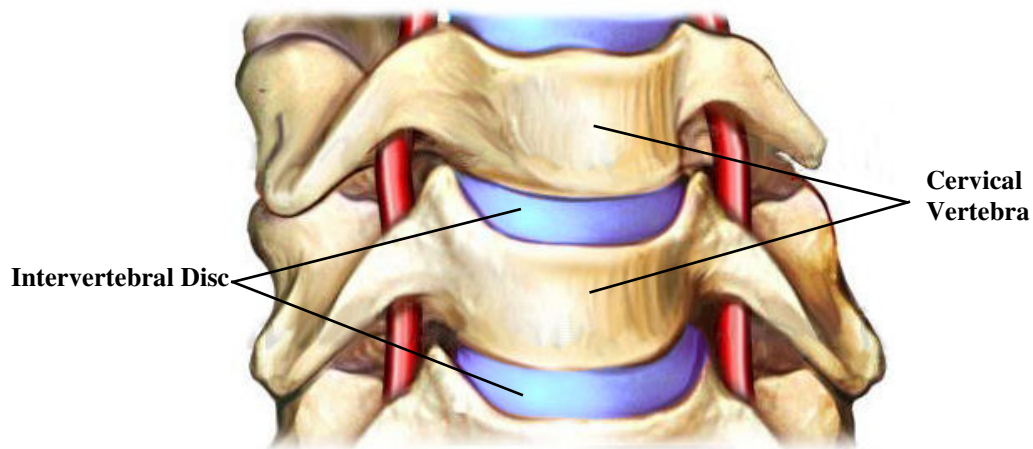
(Adapted from www.doereport.com)

Figure 2-12: Intervertebral Disc Between Two Adjacent Vertebral Bodies

2.3.1   Intervertebral Disc Anatomy

The intervertebral disc constitutes approximately 20 – 33% of the entire height of the vertebral column (Gilad and Nissan, 1986; White and Panjabi, 1990). In the cervical spine, the posterior height of the intervertebral disc is approximately 60% of the anterior height, giving the disc a wedge-like shape, as seen in the sagittal plane (Gilad and Nissan, 1986; Pooni et al., 1986; Przybylski et al., 1998). The average cervical disc height is about 50% the average height of a lumbar disc (Gilad and Nissan, 1986). The intervertebral disc heights measured by Gilad and Nissan (1986) and Przybylski et

al (1998) can be found in Table 2-3. In the transverse plane, the cross-sectional area of the intervertebral disc increases from cranial-to-caudal direction, in accordance with increasing acting body weight (Pooni et al., 1986). Cross-sectional area varies between 200 – 400 mm^2, with the disc having an elliptical shape (Pooni et al., 1986).

Table 2-3: Measured Intervertebral Disc Heights

Study	IVD Height	C23	C34	C45	C56	C67	C7T1
Gilad and Nissan, 1986	Anterior	4.8 mm	5.3 mm	5.5 mm	5.4 mm	5.2 mm	4.7 mm
	Posterior	3.4 mm	3.3 mm	3.0 mm	3.0 mm	3.3 mm	3.5 mm
Przybylski et al, 1998	Anterior	5.2 mm	5.3 mm	5.2 mm	4.6 mm	4.9 mm	
	Posterior	3.4 mm	3.4 mm	3.7 mm	3.9 mm	4.3 mm	

The intervertebral disc is comprised of three distinct components: the annulus fibrosus, the nucleus pulposus, and the cartilaginous endplates. The annulus fibrosus is the tissue of the intervertebral disc that encloses the nucleus pulposus and forms the outer boundary of the disc. A cartilagous endplate is located on the superior and inferior surface of the disc to separate the disc from adjoining vertebrae.

The annulus fibrosus has a composite structure consisting of parallel collagen fibres embedded in a homogenous matrix consisting of an aqueous gel of proteoglycans, water, and other proteins (Klisch and Lotz, 2000; Iatridis et al, 1998; Marchand and Ahmed, 1990). This fibrous tissue is arranged in concentric lamina, where fibres are oriented in the same direction of each layer but in opposite direction from adjacent layers (Figure 2-13a). The direction of the fibres in each lamina typically alternate from +/- 30° in the outer layers (Figure 2-13b), to +/- 45° in the inner layers, as measured in the transverse plane of the disc (Cassidy et al., 1989; Marchand and Ahmed, 1990; Wagner and Lotz, 2004; White and Panjabi, 1990). The ends of these fibres (known as Sharpey's fibres) are firmly attached to the cartilagous endplates, securing the intervertebral disc within the spine.
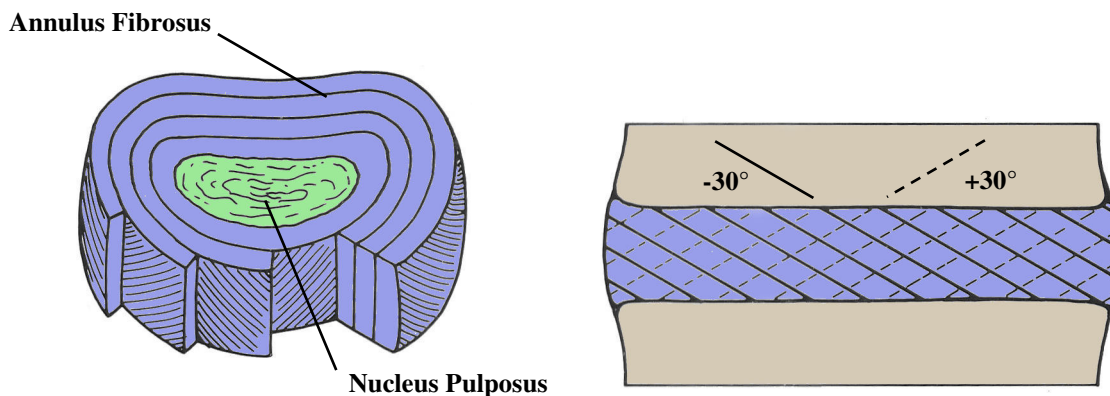
(Adapted from White and Panjabi, 1990)

Figure 2-13: Concentric Layers of the Annulus Fibrosus Oriented +/- 30 in the Outer Layer

Annulus fibrosus tissue is a fibrocartilage consisting predominantly of water, which contributes to 65 – 75% of the total tissue weight (Kraemer et al., 1985). Most of the remaining annulus tissue consists of laminae of collagen fibres, long fibrous structural proteins that are ubiquitous throughout the human body. The outer layers of annulus fibrosus laminae contain mostly Type I collagen fibres, which is the common collagen type found in ligaments and tendons. There is a gradual replacement of Type I collagen with Type II collagen (common building block of cartilage) as the lamina get closer to the inner disc and the nucleus pulposus (Skaggs et al., 1994). This change of tissue structure is one of the main hypotheses for the regional variation of mechanical properties within the annulus fibrosus.

The inner annulus fibrosus encases the nucleus pulposus, which makes up approximately 30 - 60% of the cross-sectional area of the non-degenerate intervertebral disc (Pooni et al., 1986; Iatridis et al., 1996). Consisting of a very loose collection of proteoglycans and collagen (type II, VI, IX, and XI), the nucleus is around 90% water at birth, decreasing to 70% water in the 6th decade (Yang and Kish, 1998; White and Panjabi, 1990; Iatridis et al., 1996). Due to the high water content in the nucleus, it has often been assumed that this tissue behaves as an enclosed fluid.

The nucleus pulposus is bound on its superior and inferior surface by the cartilagous endplates. The endplate is a thin layer of hyaline cartilage consisting primarily of collagen, proteoglycans, and water (Setton et al., 1993b). Calcification of the endplate proceeds with age, causing the annulus fibres to insert directly into the vertebral body (Setton et al., 1993b). While the cartilagous endplate is firmly attached to the disc through the Sharpey's fibres, the interface between the cartilagous endplate and the osseous (bony) endplate of the vertebral body is relatively weak and often a site of avulsion (Maat and Mastwijk, 2000).

2.3.2 Intervertebral Disc Physiology

The physiological behaviour of the intervertebral disc is a result of the interaction of the annulus fibrosus and the nucleus pulposus. When a compressive load is applied to a disc, hydrostatic pressure increases in the nucleus. This pressure causes radial forces to act on the layers annulus fibrosus, resulting in the disc bulging outwards (Figure 2-14). The bulging of the annulus fibrosus puts the annular fibres in tension, which resists further deformation of the annulus and supports the hydrostatic pressure within the nucleus (Holzapfel et al., 2005). Since many lamina of alternating fibre orientation are in tension, the general annulus fibrosus tissue (consisting of multiple layers) is in biaxial tension in both the axial and circumferential directions (Bass et al., 2004). This function of the

intervertebral disc is analogous to pressure vessel theory, with the annulus being the pressure vessel and the nucleus being the enclosed fluid or gas. There is also some bulging of the endplate into the vertebral body under high compressive loading (White and Panjabi, 1990).

In bending, the nucleus acts as a pivot for the vertebrae to rotate around (White and Panjabi, 1990). In flexion, the posterior section of the disc will be subject to tension loading that causes the annulus to contract toward the centre of the disc (White and Panjabi, 1990). The anterior section of the disc will bulge outward from the disc due to compressive loading. This will cause the nucleus to shift slightly to the posterior of the disc (White and Panjabi, 1990). The opposite is true for extension. The nucleus is not under significant hydrostatic pressure in bending.
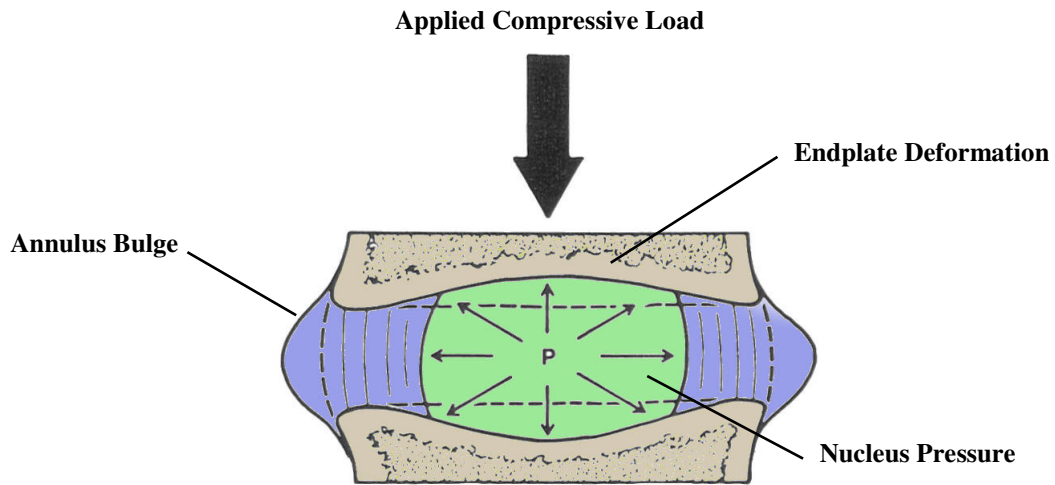
(Adapted from White and Panjabi, 1990)

Figure 2-14: Pressure in the Nucleus Forcing the Annulus to Bulge Outward

Applied Bending Load

Tensile Stress

Compressive Stress
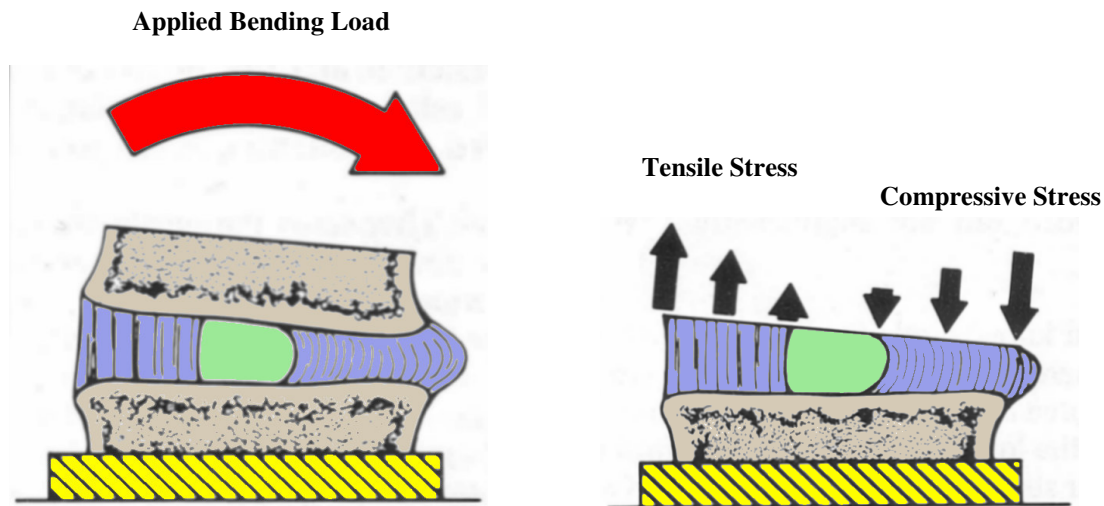
Figure 2-15: Bulging and Stress Distribution of the Annulus from Disc Segment Bending

When the disc is in axial tension, the annular fibres provide all of the tensile stiffness of the disc since the nucleus behaviour is fluid-like. However, since most of the annular fibres are oriented away from the vertical disc axis (as much as 60° from vertical axis), the disc is not as stiff in tension as it is in compression. Likewise, when the disc is loaded in axial torsion, only half of the fibres are able to support the given load, since half the fibres will be loaded in compression. Thus, the strength of the disc in torsion is relatively low.

Much of the physiological behaviour of the intervertebral disc is dependant on the highly oriented and composite structure of the annulus fibrosus tissue. The structure and function of the annulus fibrosus is responsible for guiding the motions of the disc, serving as an intervertebral ligament (Bass et al., 2004). The tensile stresses developed in the annulus are carried by the collagen fibres contained within the laminate structure, since fibre stiffness is magnitudes higher than the matrix it is in (Elliott and Setton, 2000; Iatridis and ap Gwynn, 2004; Pezowicz et al., 2005). Given the various types of loading seen on the intervertebral disc, the annulus is often subject to large and multi-directional loads (White and Panjabi, 1990).

Studies have shown that the presence of non-degenerate nucleus pulposus is important for the function of the intervertebral disc (White and Panjabi, 1990; Meakin et al., 2001). When the nucleus is surgically removed (a treatment option for herniated discs), the inner annulus has been shown to bulge inward due to a lack of internal pressure. This causes in an increase in intralaminar shear stress

in the annulus, leading to an increase risk of delamination and disc injury (Meakin et al., 2001). Furthermore, and degenerated nucleus pulposus (caused by the reduction in water content with age) decreases the mobility of the spine, and leads to an increase in spine injury risk (Ng et al., 2005).

Finally, it is believed that the role of the cartilagous endplate is to facilitate the diffusion transport of nutrients to the intervertebral disc from the vertebral body (Setton et al., 1993b). This is an important role in the health of the disc, since the intervertebral disc is the largest avascular organ in the body (Selard et al., 2003). It is believed that the cartilagous endplate does not play a significant role in the physiological behaviour of the disc, but is an important aspect of disc injury.

2.4 Ligaments

Ligaments are the ribbon-like fibrous tissues that connect the bony structures to form joints. They consist of varying amounts of elastin and type I collagen, arranged in parallel to provide effective tensile resistance to distractions in the direction of the fibres (Myklebust et al., 1988; Yoganandan et al., 2001; Silver et al., 2002).

2.4.1 Ligament Anatomy

The middle and lower cervical spine segments have the same general ligamentous structures as seen throughout the entire human spine. The major ligaments in these spine segments are the longitudinal ligaments (anterior and posterior), the accessory ligaments (the ligamenta flava, the interspinous ligaments, and the nuchal ligament), and the joint capsules. A summary of the geometric measurements of the lower and middle cervical spine ligaments can be found in Table 2-4. It should be noted that discrepancies between the anthropometric studies are a result of the different methodologies used in defining the ligament (Yoganandan et al., 2000a).

The anterior longitudinal ligament (ALL) (Figure 2-16) is a strong, broad band of fibres that extends along the anterior surface of the vertebral bodies. It is attached to the body of the axis (C2 vertebrae), and runs continuously down the spine, supporting the intervertebral discs and the adherent to the prominent margins of the vertebrae. The posterior longitudinal ligament (PLL) (Figure 2-16) is similar to the ALL as it extends from the axis, and is continuous throughout the entire cervical spine. This ligament is situated within the vertebral canal, adhering to the posterior surface of the vertebral body while supporting the intervertebral disc. The PLL is slightly wider than the ALL (approximately 10 mm and 9 mm respectively), and the width of both ligaments increases slightly from middle to lower cervical spine (Przybylski et al., 1998).

Posterior Longitudinal Ligament

Vertebral Body

Anterior Longitudinal Ligament

Intervertebral Disc
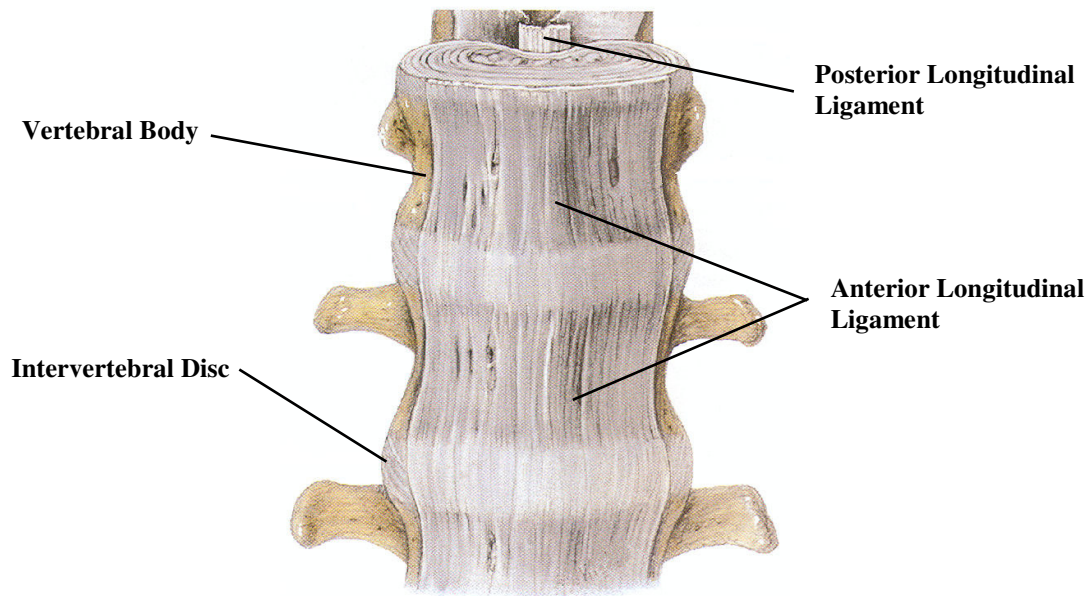
(Adapted from Agur and Dalley, 2005)

Figure 2-16: Anterior View of the Spine Detailing the Location of the ALL and PLL

The ligamenta flava (LF) (Figure 2-17) are a long, thin, but broad band of tissue that connects the lamina of two adjacent vertebrae. They are present from the C2-C3 vertebral joint all the way down the spine, and form the posterior wall of the vertebral canal. Each ligament consists of two portions that begin on either side of the roots of the articular processes, and extend to the point where the lamina meets to form the spinous process.

Lamina of the Vertebral Arch

Ligamenta Flava

Intervertebral Disc
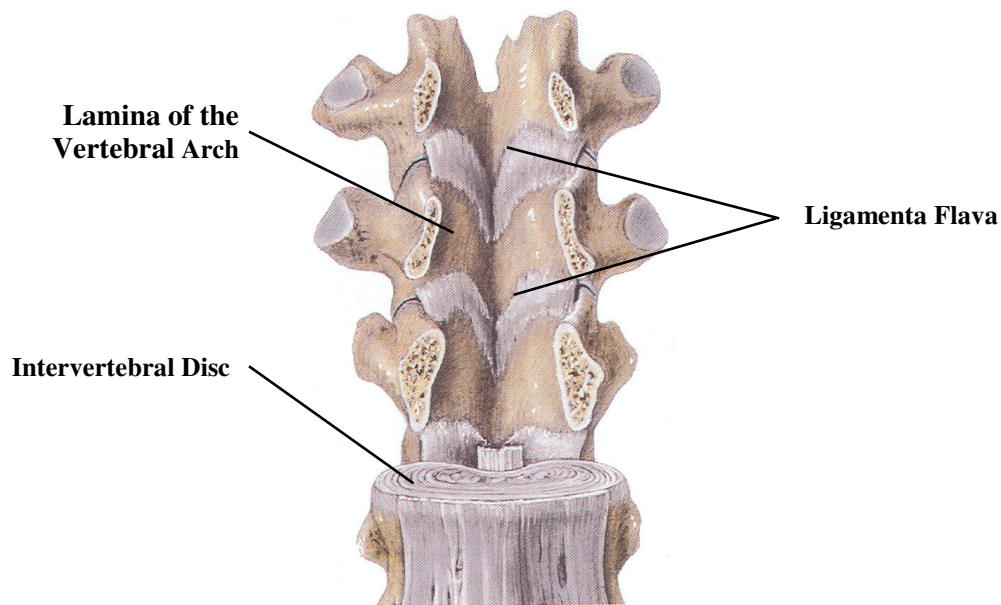
Figure 2-17: Anterior View (Sectioned) Detailing the Location of the Ligamenta Flava

The interspinous ligament (ISL) (Figure 2-18) connects the spinous processes of adjacent vertebrae. These thin, weak ligaments form a membrane that runs from the root to the apex of each spinous process. These membranous ligaments meet with the LF in the anterior, and the supraspinous ligament (nuchal ligament in the cervical spine) in the posterior. The nuchal ligament (NL) (Figure 2-18) (also referred to as the ligamentum nuchae) is a thick, fibroelastic membrane existing solely in the cervical spine, which represents the supraspinal ligament that exists in the thoracic and lumbar spines (Cross, 2003). The NL extends from the external occipital protuberance on the skull to the spinous process of the seventh vertebrae (C7). The anterior border is attached to the spinous processes of each cervical spine, up to the atlas (C1) and towards the foramen magnum. It is connected to the cord-like supraspinous ligament and the ISL.

27

External Occipital Protuberance

Nuchal Ligament

Interspinous Ligament

Spinous Process of C7

Anterior Longitudinal Ligament
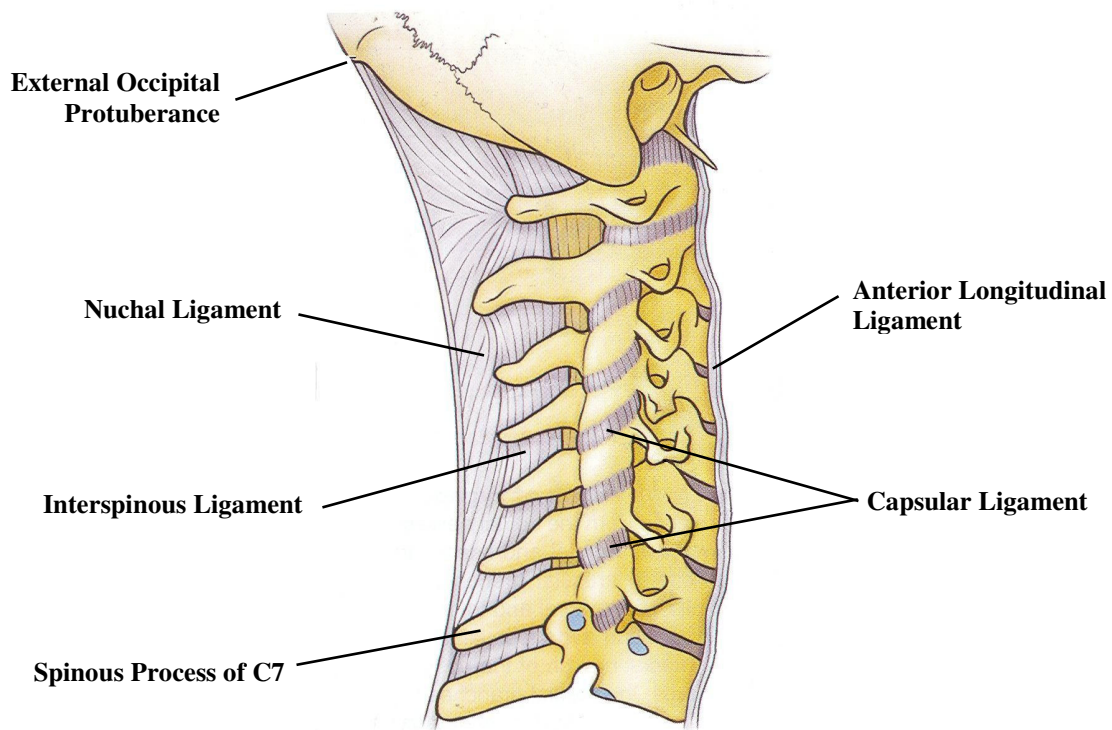
Capsular Ligament

(Adapted from Moore and Dalley, 2006)

Figure 2-18: Right Lateral View of the Spine Detailing Accessory Ligaments

The last significant ligament of the middle and lower cervical spine are the joint capsule ligaments (Figure 2-18). The capsular ligaments (CL) surround the synovial facet (zygapophyseal) joints. These ligaments create a thin, loose articular capsule that is attached to the margins of the articular processes of adjacent vertebrae. The circumference of the CL of the lower cervical spine is approximately 22 mm long, with a thickness just over 0.5 mm (Winkelstein et al., 2001).

While sharing some of the same ligament structures as the lower and middle cervical spine, the upper cervical spine segment has a unique set of ligaments that help in the stability of the skull on the cervical spine. The first group of upper cervical spine ligaments involves the atlanto-occipital ligaments, which connect the atlas to the occipital bone of the skull. The ligaments involved in attaching the atlas to the occipital bone are the anterior and posterior atlanto-occipital membranes, and the articular capsules that are associated with the atlanto-occipital joints.

The anterior atlanto-occipital membrane (AAOM) (Figure 2-19) is a broad, dense ligament that is attached between the anterior arches of the atlas and the anterior margins of the foramen magnum. It is reinforced by a strong, thick cord in the middle that runs from the basilar part of the occipital bone to the anterior tubercle of the anterior arch of the atlas, which is a continuation of the anterior atlanto-axial membrane (Gray, 1918). Likewise, the posterior atlanto-occipital membrane (PAOM) (Figure 2-20) is a broad but thin ligament that attaches the posterior arches of the atlas to the posterior margins of the foramen magnum. This membrane is much weaker than the anterior atlanto-occipital membrane (Gray, 1918). Both the AAOM and the PAOM are continuous with the atlanto-occipital articular capsules. The atlanto-occipital articular capsules (Figure 2-19 and Figure 2-20) of the atlanto-occipital joint are similar to the articular joint capsules of the lower and middle cervical spine. However, the articular capsules between the atlas and the occipital bone surround and connect the superior facets of the atlas to the occipital condyles of the cranium (Gray, 1918).
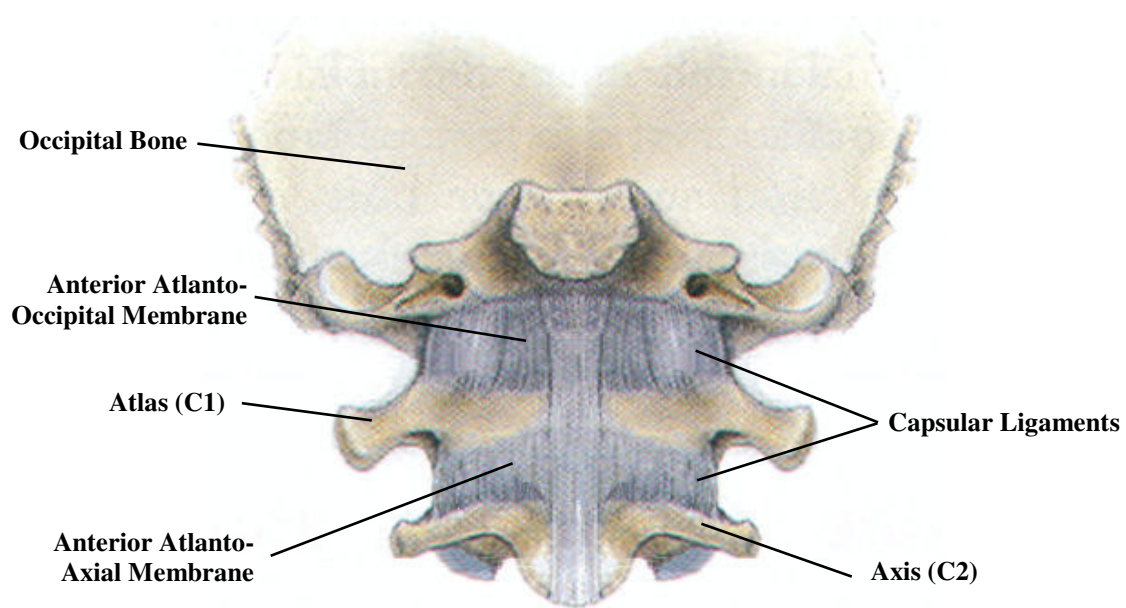
(Adapted from Agur and Dalley, 2005)

Figure 2-19: Anterior View of the Upper Cervical Spine Detailing the Craniovertebral Joint

Occipital Bone

Posterior Atlanto-Occipital Membrane

Atlas (C1)

Posterior Atlanto-Axial Membrane

Capsular Ligaments
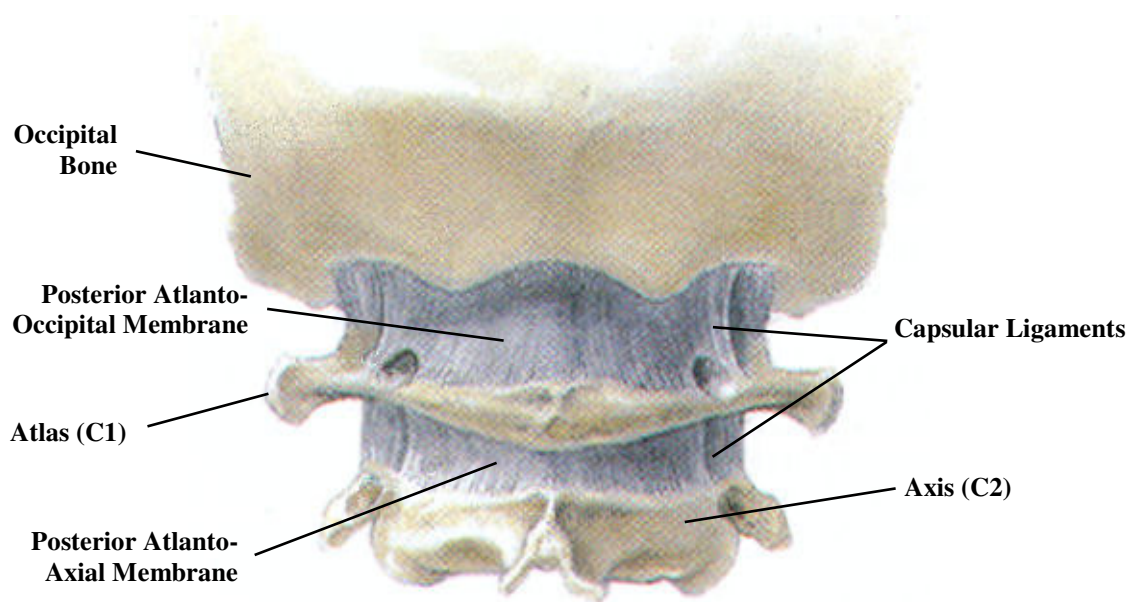
Axis (C2)

(Adapted from Agur and Dalley, 2005)

Figure 2-20: Posterior View of the Upper Cervical Spine

The group providing attachment and support for the complex articulation between the atlas and the axis (C1 and C2) are known as atlanto-axial ligaments. The rotational articulation between the axis and atlas vertebrae is achieved by the unique interaction between the anterior arch of the atlas, the odontoid process (as known as the dens) of the axis, and the transverse ligament. Other atlanto-axial ligaments include the anterior and posterior atlanto-axial membranes, and the articular capsules.

The transverse ligament (TL) (Figure 2-21) is a thick, strong band that keeps the odontoid process of the axis in contact with the anterior arch of the atlas. This ligament is the largest and strongest ligament in the cervical spine (Panjabi et al., 1998). The TL is firmly attached to the lateral masses of the atlas, and extends over the posterior surface of the odontoid process. The middle of the ligament is broader and thicker than at the ends and does not attach to the posterior surface of the odontoid process. The unstretched length of the TL is just over 20 mm long, with a cross-sectional area about 18 mm^2 in the centre (Dvorak et al., 1988).
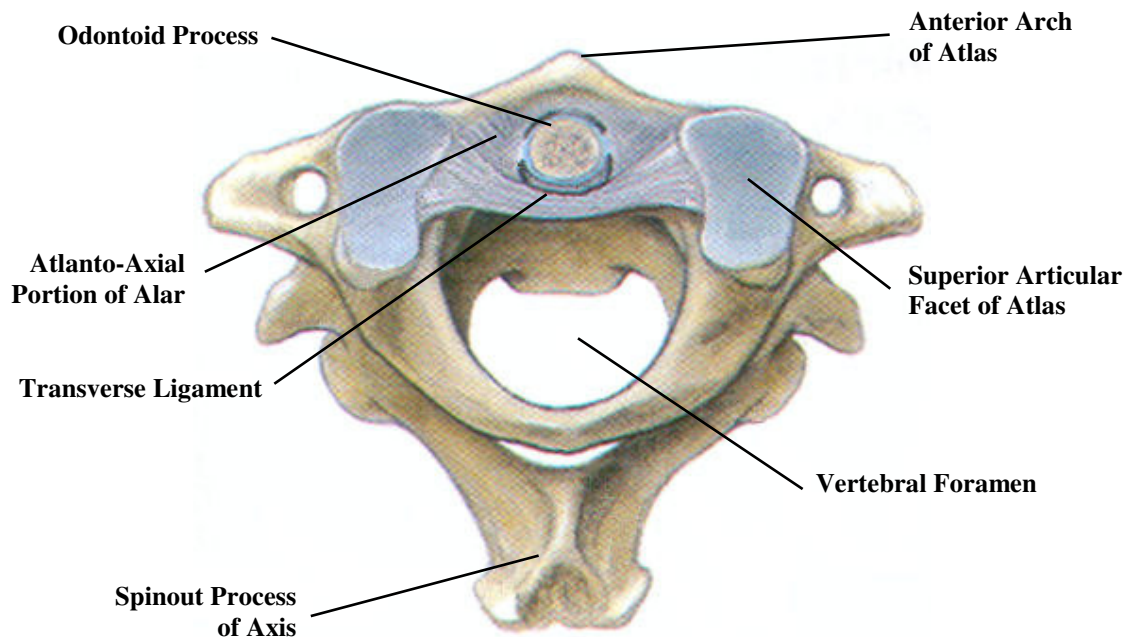
Figure 2-21: Superior View of the Atlanto-axial Joint Complex

In the middle of the TL, where it crosses the odontoid process, a small longitudinal band runs from the posterior fibres of the ligament. The fibres that extend superiorly (superior crus) are attached to the basilar part of the occipital bone, closely situated along the tectorial membrane. Fibres that extend inferiorly (inferior crus) attach to the posterior surface of the axis body. These longitudinal fibres are weak and inconsistently present in the human body (Goel et al., 1988a). The crossing of the longitudinal ligament with the transverse ligament gives the whole ligament the name cruciate ligament of the atlas (Figure 2-22).

The anterior and posterior atlanto-axial membranes (AAAM and PAAM) (Figure 2-19 and Figure 2-20) are similar to their atlanto-occipital counterparts. The AAAM is a strong ligament that is attached to the inferior border of the anterior arch of the atlas, and extends to anterior surface of the axis body. It is strengthened by a thicker cord running between the anterior arch tubercle of atlas to the axis body. The PAAM is thinner than the anterior membrane. It extends from the inferior border of the posterior arch of the atlas to the superior edges of the axis lamina. The PAAM is similar to the LF found on the lower and middle cervical spine, whereas the AAAM is a continuation of the ALL.

31

The atlanto-axial articular capsules (Figure 2-19 and Figure 2-20) are like other articular joint capsule ligaments, which surround the facet joints. The atlanto-axial articular capsules connect the superior articular facets of the axis to the inferior articular facets of the atlas.

The final group of ligaments in the upper cervical spine are the ligaments that attach the axis to the occipital bone. These ligaments consist of the tectorial membrane, alar ligaments, and the apical odontoid ligament. These ligaments further stabilize the occipital-atlanto-axial complex in both extension/flexion and axial rotations. This group of ligaments does not include articular joint capsules, as there is no joint present between the axis and the occipital bone.

The tectorial membrane (TM) (Figure 2-22) is a strong band located in the vertebral canal that covers the odontoid process and its associated ligaments. The TM is fixed inferiorly to the posterior surface of the axis body, and superiorly through the foramen magnum to the basilar groove of the occipital bone. This ligament appears to be a continuation of the PLL found on the middle and lower cervical spine.

(Adapted from Moore and Dalley, 2006)
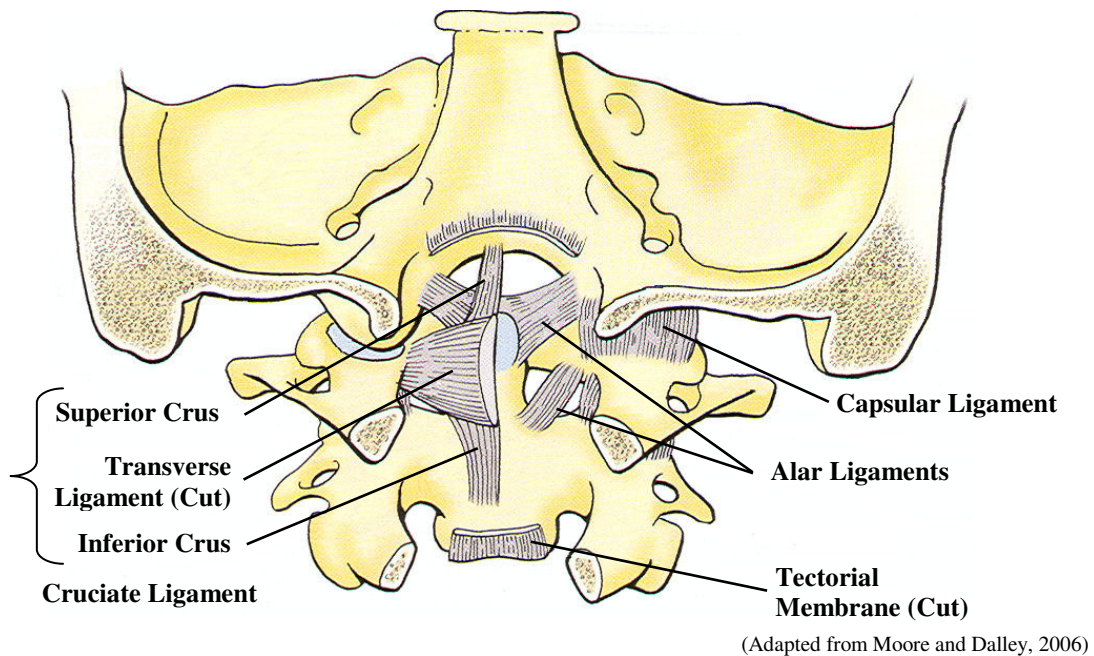
Figure 2-22: Posterior View (Sectioned) of the Upper Cervical Spine

The alar ligaments (Figure 2-22) are strong elliptical cords that stem from either side of the upper part of the odontoid process of the axis to the medial sides of the occipital condyles. They are approximately 10 mm long, with an elliptical cross-section of 3 x 6 mm (Dvorak and Panjabi, 1987). The pair of alar ligaments often forms an angle between 140° and 180° in the transverse plane to each

other (Panjabi et al., 1991d). There is also an often-debated atlanto-axial portion of the alar ligaments. Some anatomic texts state that the alar ligaments are only attached between the axis and the occipital condyles (Gray, 1918). However, documented anatomical studies have shown that a small portion of the inferior alar ligament attaches to the anterior lateral masses of the atlas (Dvorak and Panjabi, 1987; Dvorak et al., 1988; Goel et al., 1988a; Panjabi et al., 1991a).

The apical odontoid ligament is a thin ligament extending from the tip of the odontoid process to the anterior margin of the foramen magnum. This ligament, approximately 24 mm long, blends with the deep portion of the AAOM and the superior crux of the TL (Panjabi et al., 1991a).

Table 2-4: Measured Dimensions of the Lower and Middle Cervical Spine Ligaments

Study	Level	ALL		PLL		LF		CL		ISL	
		Length	Width	Length	Width	Length	Width	Length	Width	Length	Width
Panjabi et al, 1991a	C12	23.1 mm[*]	3.8 mm[*]	30.7 mm[**]	3.7 mm[**]					12.0 mm	
	C23	14.6 mm	5.6 mm	13.4 mm	6.2 mm	5.2 mm	9.4 mm	8.4 mm	6.7 mm	9.8 mm	
	C34	13.5 mm	7.5 mm	10.1 mm	7.1 mm	6.2 mm	10.4 mm	8.8 mm	8.3 mm	9.8 mm	
	C45	12.3 mm	7.8 mm	12.0 mm	8.9 mm	6.2 mm	10.8 mm	9.0 mm	7.4 mm	11.2 mm	
	C56	11.5 mm	7.3 mm	11.7 mm	7.6 mm	6.5 mm	10.9 mm	9.0 mm	5.5 mm	12.3 mm	
	C67	13.7 mm	7.6 mm	13.3 mm	7.4 mm	7.7 mm	10.6 mm	8.6 mm	8.0 mm	16.1 mm	
	C7T1	13.3 mm	7.4 mm	15.0 mm	7.5 mm	8.8 mm	10.3 mm				
Przybylski et al, 1998	C23				8.6 mm						
	C34	5.8 mm	7.3 mm	4.3 mm	9.6 mm						
	C45	5.8 mm	9.3 mm	4.7 mm	10.3 mm						
	C56	5.7 mm	9.9 mm	5.0 mm	11.3 mm						
	C67	5.2 mm	9.8 mm	5.2 mm	10.8 mm						
		5.4 mm	9.8 mm	5.3 mm							
Yoganandan et al, 2000a	C2-C5	18.8 mm		19.0 mm		8.5 mm		6.9 mm		10.6 mm	
	C5-T1	18.3 mm		17.9 mm		10.6 mm		6.7 mm		9.9 mm	

* - Anterior Axial-Atlanto Membrane

** - Cruciate Ligament

2.4.2 Ligament Physiology

The primary role of a ligament is to resist or restrict motion of a joint to provide stability to the biological structure (White and Panjabi, 1990). This means that the ligaments are responsible for providing the boundaries for articulation of a particular joint. In the cervical spine, ligaments connect to the vertebral bodies to limit the mobility of spinal articulation. In particular, these ligaments are effective for resistance of motion in the sagittal plane, as well as provide resistance and stability to external tensile loads. They also absorb some of the energy during trauma (Panjabi et al., 1991a).

The vertebrae pivot on the nucleus pulposus in the intervertebral disc during spinal articulation. This causes the ligaments posterior to the intervertebral disc to be in tension during flexion. These ligaments include the PLL, the LF, the ISL, and the CL of the facet joints. In extension, only the ALL is in tension to provide resistance to bending.

The effectiveness of these ligaments to resist the motion of the spine is based on the stiffness of the ligament, and the location of the ligament from the axis of rotation (i.e. the intervertebral disc). While both the ALL and PLL are much stiffer than the LF and the ISL, the close proximity to the intervertebral disc make the longitudinal ligaments small contributor to the bending stiffness of the spine.

The ligaments in the upper cervical spine primarily provide the articulation constraints for the head. These ligaments, along with the unique anatomy of the C1 and C2 vertebrae, provide the stability of the head to perform actions such as nodding (the "yes" movement), rotating (the "no" movement), and tilting (Gray, 1918). The main ligaments responsible for the stability of the upper cervical spine are the alars and the transverse ligament (Panjabi et al., 1998).

Rotational motion between of the upper cervical spine complex is chiefly constrained by the alar ligaments (Panjabi et al., 1991d). The motion of head rotation to the right is limited by the left alar ligament, and vice versa (Dvorak and Panjabi, 1987; Panjabi et al., 1991d). The TM, the atlanto-axial membranes, and the capsular ligaments also support the alar in restricting rotation movement (Dvorak and Panjabi, 1987).

The TL maintains the stability between the atlas and the axis by securing the odontoid process of the axis to the anterior arch of the atlas. While the TL restrains much of the translational movement

between C1 and C2, it allows effortless rotational motion to occur between these two vertebrae (Panjabi et al., 1998). It is also a key ligament in flexion, with support from the TM and the longitudinal fibres of the cruciate ligament (Dvorak and Panjabi, 1987).

Other ligaments in the upper cervical spine play smaller roles in providing stability. The atlanto-occipital ligaments are mainly responsible for limiting the heads movement in nodding (the 'yes' movement). AAOM provides some resistance when 'looking up' (extension) and the PAOM provide some resistance when 'looking down' (flexion). The atlanto-axial portion of the alars ligaments help provide support for the TL in restricting displacement between the atlas and the axis, and are influential in lateral bending (Dvorak and Panjabi, 1987). A summary of the function of each ligament in the cervical spine can be found in Table 2-5.

Table 2-5: Summary of the Functional Anatomy of Cervical Spine Ligaments

Ligament	Spine Region	Motion of Limiting
Anterior Longitudinal Ligament	C2 – T1	Extension
Posterior Longitudinal Ligament	C2 – T1	Flexion
Ligamenta Flava	C2 – T1	Flexion
Capsular Ligament	C0 – T1	Flexion & Rotatation
Interspinous Ligament	C1 – T1	Flexion
Nuchal Ligament	C0 – C7	Flexion
Anterior Atlanto-Axial Membrane	C1 – C2	Extension & Rotation
Posterior Atlanto-Axial Membrane	C1 – C2	Flexion & Rotation
Anterior Atlanto-Occipital Membrane	C0 – C1	Extension
Posterior Atlanto- Occipital Membrane	C0 – C1	Flexion
Alar Ligaments	C0 – C2	Rotation
Transverse Ligaments	C1 – C2	Flexion & Translation
Tectorial Membrane	C0 – C2	Flexion & Rotation
Apical Ligament	C0 – C2	Flexion
Inferior and Superior Crux	C0 – C2	Flexion

2.5 Muscle

There are three types of muscle in the human body: skeletal, heart, and smooth. Skeletal muscles, which are responsible for the production of force and movement, make up the majority of the muscle of the body (Fung, 1993). In the human neck, the complex group of skeletal muscles is essential to providing stability in a given posture, producing movement during physiological activity, and protecting the spine during trauma (White and Panjabi, 1990).

2.5.1 Muscular Anatomy

Skeletal muscle is soft tissue with a complex microstructure of multiple levels (Figure 2-23). A single muscle is made up of a collection of fascicles surrounded by strong connective sheath called the epimysium. Each fascicle is made up of a collection of muscle fibres (or muscle cells), which are also surrounded by a sheath called the perimysium. The muscle fibre can range from a few millimeters to 30 cm long and is between $10 - 60$ µm in diameter (Fung, 1993). A muscle fibre is considered the basic unit of the muscle tissue.
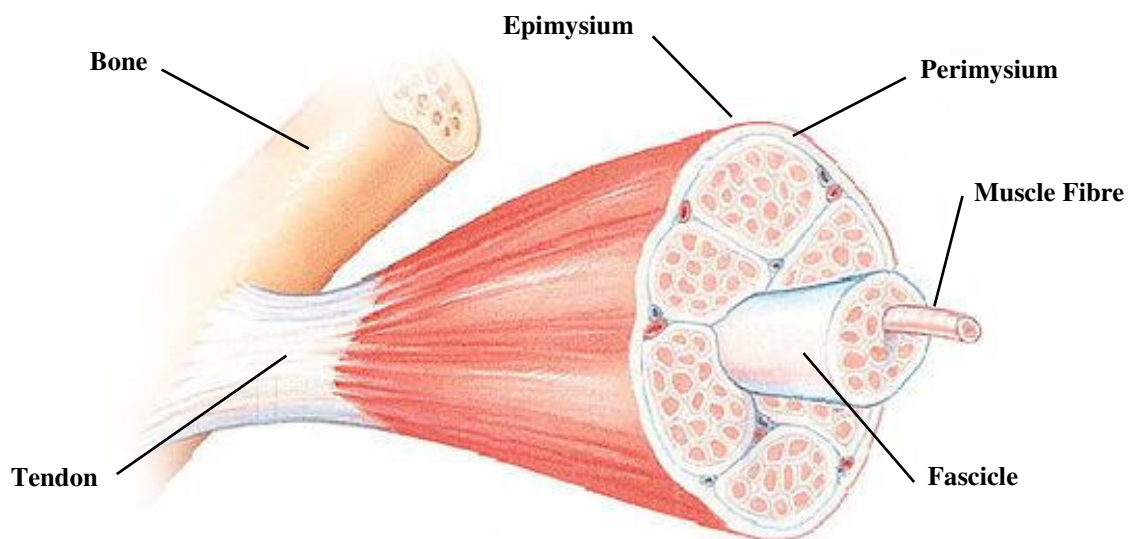
(Adapted from training.seer.cancer.gov)

Figure 2-23: Microstructure of Skeletal Muscle

Each muscle fibre is composed of a collection of myofibrils, which are about 1µm in diameter. Myofibrils are bundles of myofilaments, which are made up of the proteins actin and myosin and sub-divided into units called sarcomeres (around 2.6 µm long) (Knaub et al., 1999). The relative sliding between the actin and myosin proteins, initiated by an electro-chemical process, causes the sarcomere to shorten (Figure 2-24). While the shortening of an individual sarcomere may be very small (around 1µm), the cumulative effect of many sarcomeres (nearly 100,000 sarcomeres in a single muscle fibre), can produce an effective overall contraction for the entire muscle.

(Adapted from www.tmd.ac.jp)
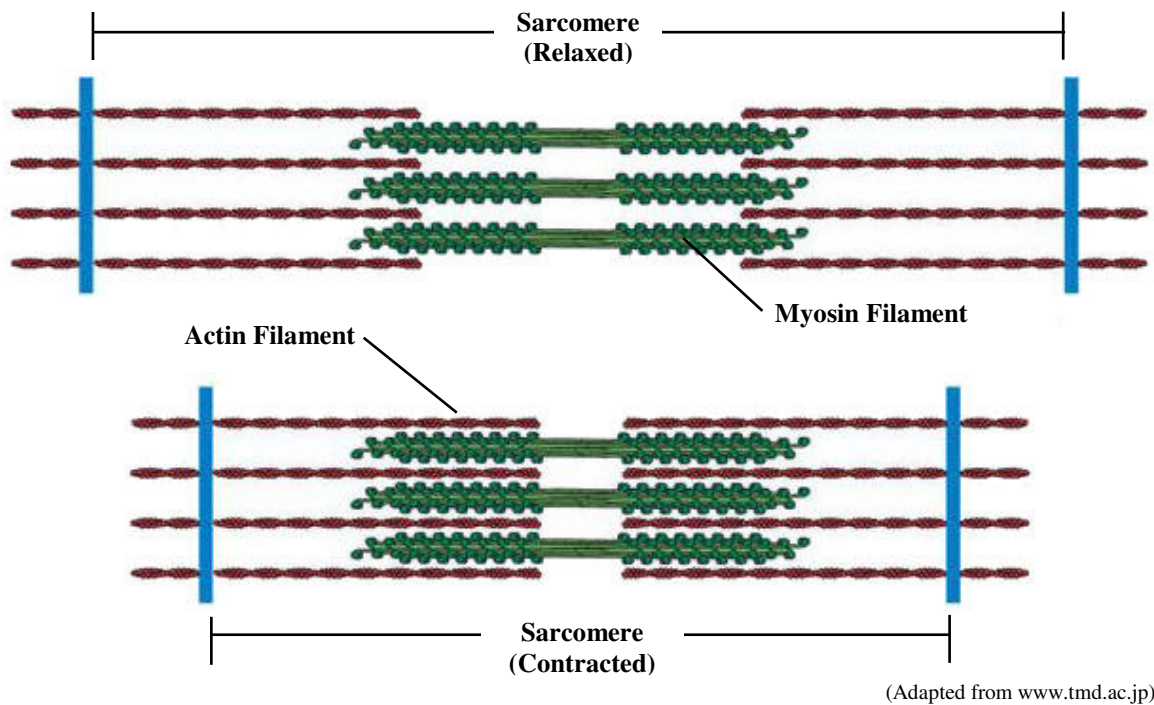
Figure 2-24: Structure of the Sarcomere in a Relaxed and Contracted State

Skeletal muscles are attached to bone through the intervention of the fibrous tendons (Figure 2-23). The attachment points of end of the muscle are referred to as the origin and the insertion. The origin point is the part of the bone where muscle attaches and does not move during contraction, whereas the insertion point is located on a bone that moves during contraction.

There are 31 muscles pairs in the human neck (Knaub and Myers, 1998). Muscle pairs in the neck are symmetric about the medial plane, such that a muscle on the left side of the neck is also present on the right side of the neck. These muscles are divided into six groups: hyoid muscles, anterior muscles, lateral muscles, suboccipital muscles, back muscles, and vertebral column muscles (Gray, 1918).

The hyoid muscle group (Figure 2-25) is a collection of thin muscles attached to the hyoid bone that are associated with swallowing food (Gray, 1918). These muscles are further separated into the suprahyoids and the infrahyoids. The suprahyoids (digastric, geniohyoid, mylohyoid, and stylohyoid muscles) are all muscles that are superior to the hyoid bone and connect with either the mandible or the skull. The infrahyoids (omohyoid, sternohyoid, sternothyroid, and thyrohyoid muscles) are all

37

muscles that are inferior to the hyoid bone and connect with the sternum, scapula, or thyroid cartilage. It is believed that the suprahyoid muscles do not significantly affect the motion of the cervical spine, but a study has shown that the infrahyoid muscles may be a significant contributor to flexion motion (Gray, 1918; Chancey et al, 2003).
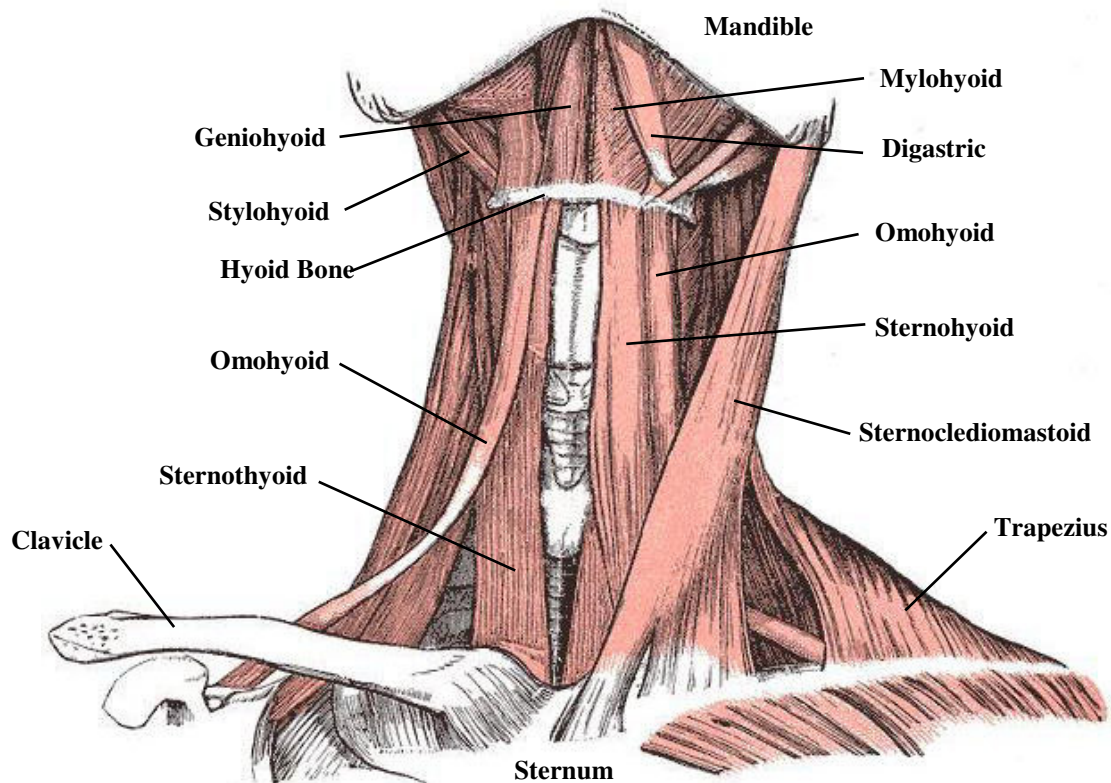
Figure 2-25: Anterior View of Superficial Neck Muscles

The anterior muscle group (Figure 2-26) are a set of deep muscles located adjacent to the anterior side of the vertebral column. The anterior muscle group consists off the anterior and lateralis rectus capitis, the longus capitis, and the longus colli. The rectus capitis muscles are short muscles that connect the atlas to the occipital bone, and are responsible for producing rotation and lateral bending of the head. The longus capitis is a long muscle running from the middle cervical spine to the skull that contributes to the flexion movement of the neck. The longus colli is also a long muscle running from the thoracic spine to the upper cervical spine, and is split into three portions.
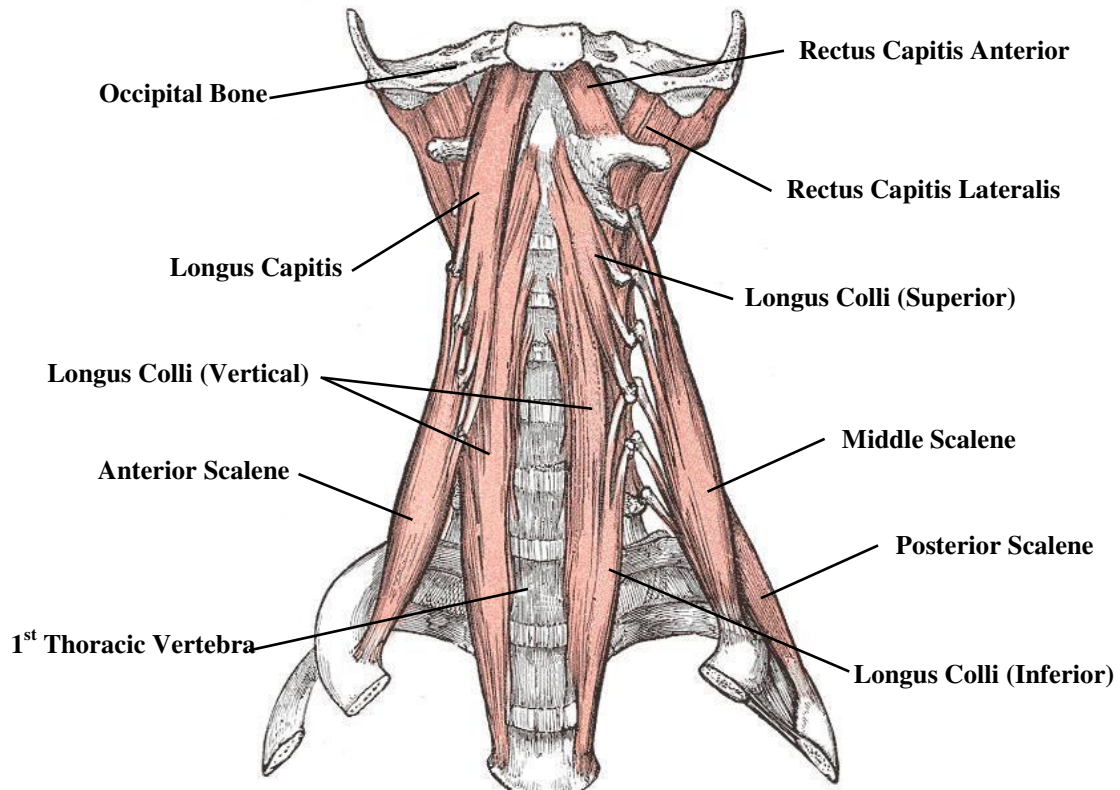
(Adapted from Gray, 1918)

Figure 2-26: Anterior View of Deep Neck Muscles

The lateral muscle group (Figure 2-27) is a group of muscles that run on beside side of the vertebral column, and provide much of the force required for lateral bending. This group of muscles consists of the scalene muscles (anterior, middle, and posterior), and the sternocleidomastoid. The scalene muscles run from the lateral processes of the middle and lower cervical vertebra to the first two ribs. The sternocleidomastoid is a thick muscle attached to both the sternum and clavicle at one end, and the mastoid process of the temporal bone of the skull.

Mylohyoid

Digastric

Stylohyoid

Hyoid Bone

Thyrohyoid

Sternothyoid

Omohyoid

Clavicle

Sternoclediomastoid

Splenius Capitis

Levator Scapula

Middle Scalene

Anterior Scalene

Trapezius
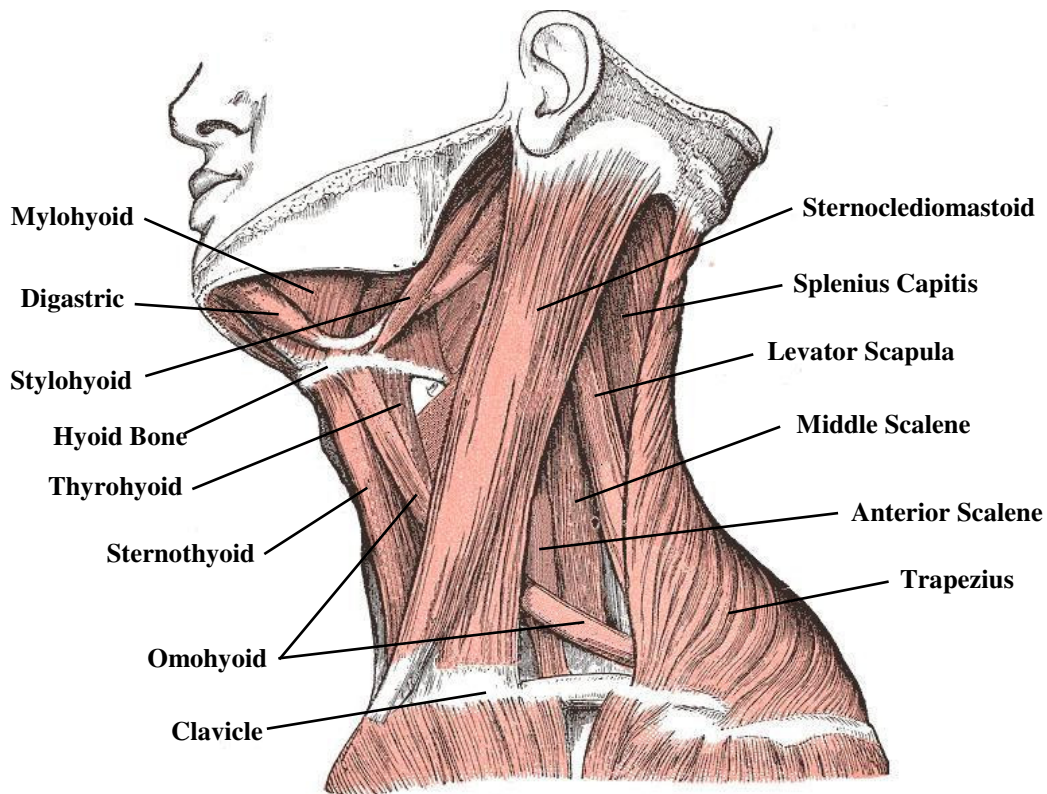
(Adapted from Gray, 1918)

Figure 2-27: Lateral View of Neck Muscles

The suboccipital muscle group (Figure 2-28) is a collection of short muscles within the upper cervical spine. These muscles are primary used for the control of head motion relative to the cervical spine. The suboccipital muscle group includes the superior and inferior oblique capitis muscles, and the major and minor posterior rectus capitis muscles. Both the rectus capitis posterior minor and the oblique capitis superior muscles originate on the atlas and insert on the occipital bone. The rectus capitis posterior major and the oblique capitis inferior muscles originate on the spinous process of the axis, and attach to the occipital bone and the atlas respectively.

Occipital Bone

Rectus Capitis
Posterior Minor

Oblique Capitis
Superior

Rectus Capitis
Posterior Major

Oblique Capitis
Inferior

Multifidus

Semispinalis Cervicis

Longissimus Cervicis

1st Thoracic Vertebrae

Semispinalis Capitis

Longissimus Capitis

Longissimus Cervicis

Iliocostalis
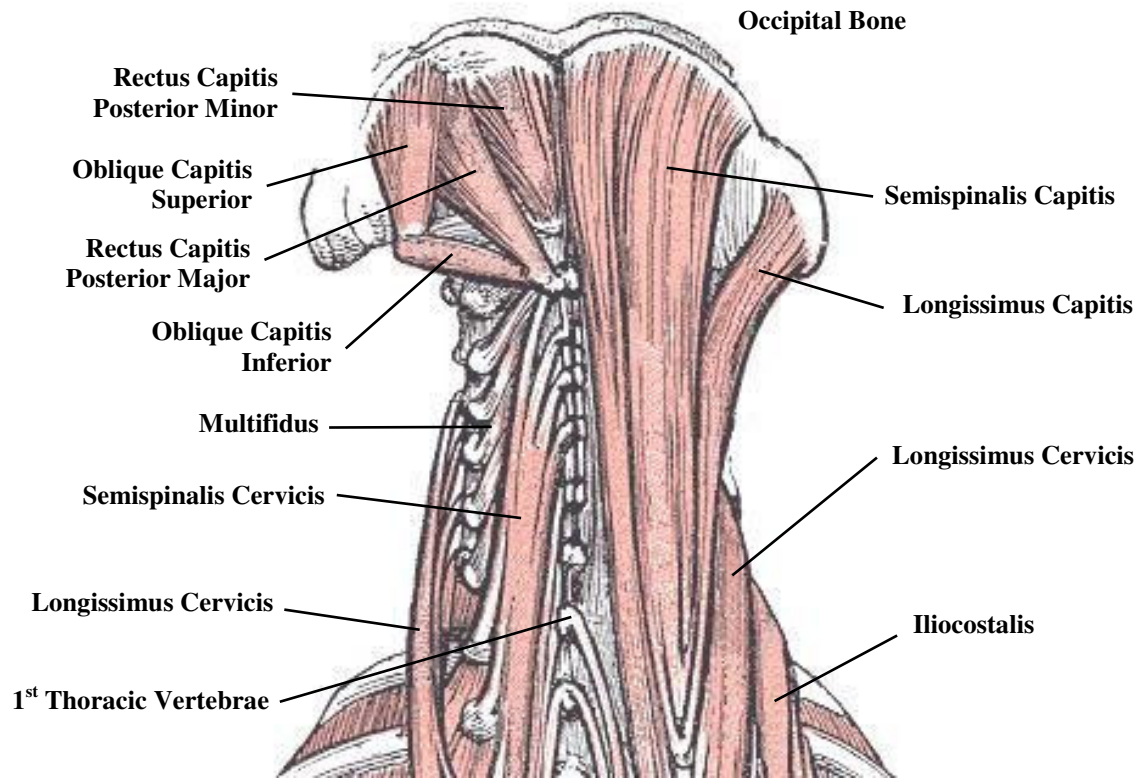
(Adapted from Gray, 1918)

Figure 2-28: Posterior View of Deep Neck and Back Muscles

The back muscle group (Figure 2-29) is a set of long muscles located posterior to the cervical spine, and are primarily used to move the cervical spine in extension. Included in the back muscle group are the longissimus muscles, the semispinalis muscles, the splenius muscles, the iliocostalis, and the multifidus muscle. The longissimus capitis, the semispinalis capitis, and the splenius capitis muscles originate in the upper thoracic spine and insert all the way to the occipital bone. The longissimus cervicis, the semispinalis cervicis, and the splenius cervicis muscles also originate in the upper thoracic spine, but insert into the middle cervical spine. The multifidus muscle, present over the entire human spine, originates on the articular process and inserts on the spinous process of the vertebra three levels up (Gray, 1918).

Occipital Bone

Splenius Capitis &
Splenius Cervicis

Sternocleido -
mastoid

Nuchal Ligament

7th Cervical Vertebrae

Levator Scapula

Minor Rhomboid

Trapezius
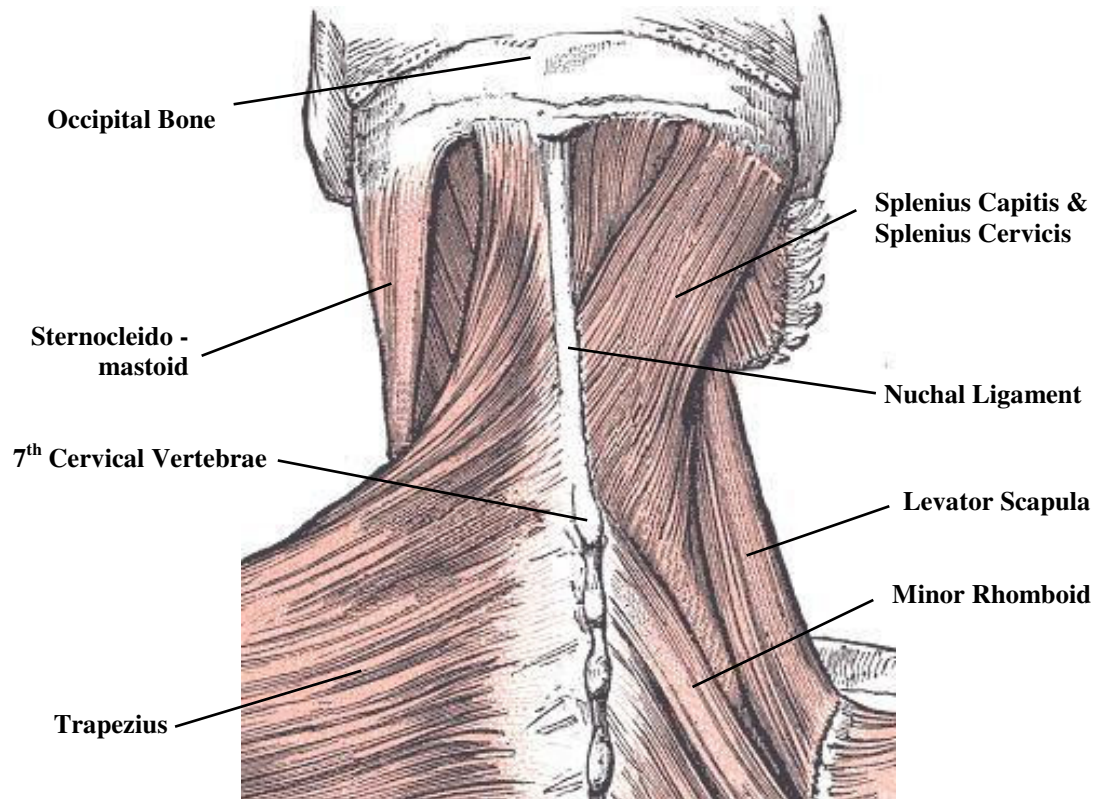
(Adapted from Gray, 1918)

Figure 2-29: Posterior View of Superficial Neck and Back Muscles

Finally, the vertebral column muscle group (Figure 2-29) is a set of muscles that connect the upper extremities to the vertebral column. These muscles include the levator scapula, the minor rhomboid, and the trapezius muscle. These muscles are primarily for moving the scapula towards the spine; however, these muscles can be used to laterally bend the cervical spine.

2.5.2 Muscular Physiology

The only active function of a muscle is to generate a contractile force causing the muscle to shorten in length. Muscles cannot lengthen by themselves, so the activation of other muscles is required to stretch the muscle. Muscles that work together to contract/relax in unison are called antagonistic pairs. Every muscle in the human body has at least one antagonistic muscle.

The maximum force generated during muscle contraction is dependent on the cross-sectional area of the muscle (Winters and Stark, 1988). A muscle with a large cross-sectional area has more muscle fibre to contract than that of a muscle with a small cross-section. The effective cross-sectional area of a muscle, typically measured in the midpoint between the insertion and origin, is known as the physiological cross-sectional area (PCSA). Muscles such as the infrahyoids are very small with PCSA values less than 1 cm^2, while muscles such as the sternocleidomastoid and most of the back muscles are significantly larger (greater than 3 cm^2).

Since the muscles in the cervical spine are reflected in the medial plane, the function of each muscle depends on whether it acts unilaterally (only one side is contracted), or bilaterally (both sides are contracted). Furthermore, the result of unilateral or bilateral contract of a muscle depends on its location within the neck. For instance, a muscle pair that is posterior and lateral of the cervical spine will cause the cervical spine extension when contracted bilaterally (since the lateral forces cancel each other out), and will cause cervical spine rotation when contracted unilaterally.

A summary of the muscles of the cervical spine can be found in Table 2-6. Included in the summary is the origin and insertion points (Gray, 1918; Chancey et al, 2003), the unilateral and bilateral action (Gray, 1918), the PSCA (Knaub and Myers, 1998), and resting sarcomere length (S_{rest}) of each muscle (Knaub and Myers, 1998).

Table 2-6: Summary of the Functional Anatomy of Cervical Spine Muscles

Muscle	Muscle Group	Primary Action (Unilateral / Bilateral)	Origin	Insertion	PCSA (cm²)	S_{rest} (μm)
Oblique Capitis Inferior	Suboccipital	Rotation	C2 (SP)	C1 (TP)	1.95	2.6
Oblique Capitis Superior	Suboccipital	Lat Bend / Extension	C1 (TP)	Occipital Bone	0.88	2.6
Rectus Capitis Posterior Major	Suboccipital	Rotation / Extension	C2 (SP)	Occipital Bone	1.68	3.1
Rectus Capitis Posterior Minor	Suboccipital	Extension	C1 (Post. Arch)	Occipital Bone	0.92	
Longus Capitis	Anterior	Flexion	C3 – C6 (TP)	Occipital Bone	1.37	2.9
Longus Colli (Superior Portion)	Anterior	Rotation / Flexion	C3 – C5 (TP)	C1 (Ant. Arch)	0.69	
Longus Colli (Inferior Portion)	Anterior	Rotation / Flexion	T1 – T2 (Ant. Body)	C5 – C6 (TP)	0.69	
Longus Colli (Vertical Portion)	Anterior	Rotation / Flexion	C5 – T3 (Ant. Body)	C2 – C4 (Ant. Body)	1.37	
Rectus Capitis Anterior	Anterior	Flexion	C1 (Lat. Mass)	Occipital Bone		
Rectus Capitis Lateralis	Anterior	Lat Bend	C1 (TP)	Occipital Bone		
Anterior Scalene	Lateral	Lat Bend / Flexion	C3 – C6 (TP)	1ˢᵗ Rib	1.88	3.1
Middle Scalene	Lateral	Lat Bend / Flexion	C2 – C7 (TP)	1ˢᵗ Rib	1.36	2.8
Posterior Scalene	Lateral	Lat Bend / Flexion	C5 – C7 (TP)	2ⁿᵈ Rib	1.05	2.6
Sternocleidomastoid	Lateral	Lat Bend / Rotation / Flexion	Sternum/Clavicle	Temporal	4.92	2.9
Digastric	Suprahyoid	Swallowing	Temporal Bone	Hyoid Bone		
Geniohyoid	Suprahyoid	Swallowing	Mandible	Hyoid Bone		
Mylohyoid	Suprahyoid	Swallowing	Mandible	Hyoid Bone		
Stylohyoid	Suprahyoid	Swallowing	Temporal Bone	Hyoid Bone		
Omohyoid	Infrahyoid	Swallowing	Scapula	Hyoid Bone	0.75	2.5
Sternohyoid	Infrahyoid	Swallowing	Sternum	Hyoid Bone	0.58	2.6
Sternothyroid	Infrahyoid	Swallowing	Sternum	Thyroid Cartilage	0.65	
Thyrohyoid	Infrahyoid	Swallowing	Thyroid Cartilage	Hyoid Bone		
Iliocostalis	Back	Lat Bend / Extension	3ʳᵈ – 6ᵗʰ Rib	C3 – C6 (TP)	1.04	
Longissimus Capitis	Back	Lat Bend / Extension	C5 – T5 (TP)	Occipital Bone	0.98	2.4
Longissimus Cervicis	Back	Lat Bend / Extension	T1 – T5 (TP)	C2 – C6 (AP)	1.49	2.6
Multifidus	Back	Rotation / Stabilization	C4 – T1 (AP)	C2 – C6 (SP)		
Semispinalis Capitis	Back	Rotation / Extension	C4 – T6 (TP)	Occipital Bone	5.52	2.5
Semispinalis Cervicis	Back	Rotation / Extension	T1 – T6 (TP)	C2 – C5 (TP)	3.06	2.4
Splenius Capitis	Back	Rotation / Extension	C7 – T4 (SP)	Occipital Bone	3.09	2.7
Splenius Cervicis	Back	Rotation / Extension	C7 – T4 (SP)	C1 – C3 (TP)	1.43	2.6
Levator Scapula	Vertebral Column	Lat Bend	C1 – C4 (TP)	Scapula	3.12	2.5
Minor Rhomboid	Vertebral Column	Lat Bend	C7 – T1 (SP)	Scapula	1.02	2.4
Trapezius (Cervical Portion)	Vertebral Column	Extension	C0 – T2 (SP)	Scapula	13.73	2.8

AP – Articular Process, SP – Spinous Process, TP – Transverse Process

Chapter 3
Biological Tissue Mechanics

The cervical spine is composed of two generalized types of biological tissue: hard (bony) tissues, and soft tissues. Soft tissues play an important role in the kinematic and dynamic behaviour of the human cervical spine. These tissues connect to the supporting bony tissues (vertebrae) to allow for the relative movement between these structures. The development of a predictive, biofidelic model of the human cervical spine requires accurate knowledge of the mechanical behaviour each of these tissues. Understanding the fundamental mechanics of biological tissue at the local level is an essential step to understanding the mechanics of biological structures at the global level.

3.1.1 General Mechanics

The mechanical properties of both hard and soft tissues are a function of their microstructure and composition (Fung, 1993). One of the primary microstructural elements in both hard and soft tissue is collagen (Fung, 1993). Type I collagen is the most abundant, occurring in almost every type of human tissue, including both hard and soft, while Type II, IX, X, and X collagens are primarily located in cartilage-like materials. The type of collagen is dependent on its molecular structure, with Types I, II, III, V, and IX collagen having a fibre-forming molecular structure (Fung, 1993). Collagen provides the strength and support to most biological tissues, as steel girders would in a building (Fung, 1993).

The primary function of collagen fibre is to resist tension (Fung, 1993). When pulled in tension, the stress response of collagen fibre is nonlinear and in three distinct regions (Figure 3-1). In the first region (the 'toe' region), the stress increases exponentially with increasing deformation. This region transforms into a second region with linear response, with a modulus around 1.24 GPa (Fung, 1993). The third region is again nonlinear with decreasing stiffness until the fibre ruptures. Because collagen fibre is a nonlinear material, many of the biological tissues with collagen as a predominant component also exhibit nonlinear response.

The arrangement of the collagen fibres is also an important aspect of tissue mechanics, as fibre orientation determines the degree of apparent orthotropy of a tissue. Tissues that have collagen fibres organized in parallel, such as ligament or annulus fibrosus, display significant orthotropic behaviour,

with stiffness in the fibre direction being orders of magnitude greater than stiffness perpendicular to the fibres. Tissues with a random arrangement of collagen fibres, as in the nucleus pulposus, display isotropic material properties.
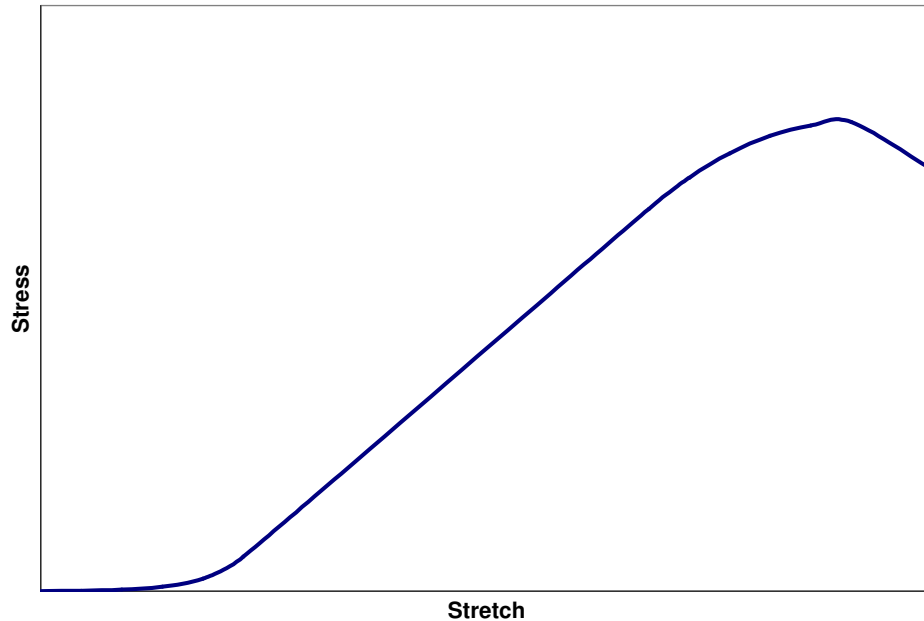
Figure 3-1: Nonlinear Stress-Stretch Response of Collagen Fibre

Hard tissue such as cortical bone can be considered a composite tissue, since collagen fibres are embedded in a matrix of brittle mineral (Cowin, 2001). In soft tissue, collagen fibres are integrated together with an intercellar substance consisting of elastin and a hydrophilic gel called ground substance. Elastin, as the name suggests, is the most elastic material known in the human body, and is primarily concerned with returning soft tissue to its original shape (Fung, 1993). This ground substance is composed of proteoglycans and water, and is the chief reason why soft tissues tend to have viscoelastic characteristics (Fung, 1993).

3.1.2 General Viscoelasticity

Biological tissues, particularly the soft tissues, exhibit a unique mechanical response known as viscoelasticity. Viscoelasticity is the term given to materials that exhibit both viscous and elastic properties. In essence, viscoelastic materials have a time-dependent response (viscous) and a time-independent response (elastic). The viscoelastic effect in most soft tissues comes from two different

mechanisms: flow-dependent viscoelasticity (the result of frictional drag forces caused by interstitial fluid flow), and flow-independent viscoelasticity (intrinsic viscoelastic response of the solid tissue matrix) (Skaggs et al., 1994).

Viscoelastic materials display mechanical phenomena such as stress relaxation, creep, hysteresis, and increasing stiffness with increased strain-rate (Fung, 1993). These phenomena are used to determine the viscoelastic properties of tissue, with stress relaxation and creep testing being the most frequent type of study. Both relaxation and creep are long-term phenomena, and their experiments are often done over extended periods of time (> 1000s)

A stress relaxation experiment involves applying a constant strain to a material, and monitoring the resisting load (stress) over time (Figure 3-2). A pure elastic material will have a stress response that is constant with the applied strain, whereas a pure viscous fluid will reach an instantaneous peak stress that will decay to zero stress over time. However, a viscoelastic material will reach a peak instantaneous stress and will decay to a constant stress over time.
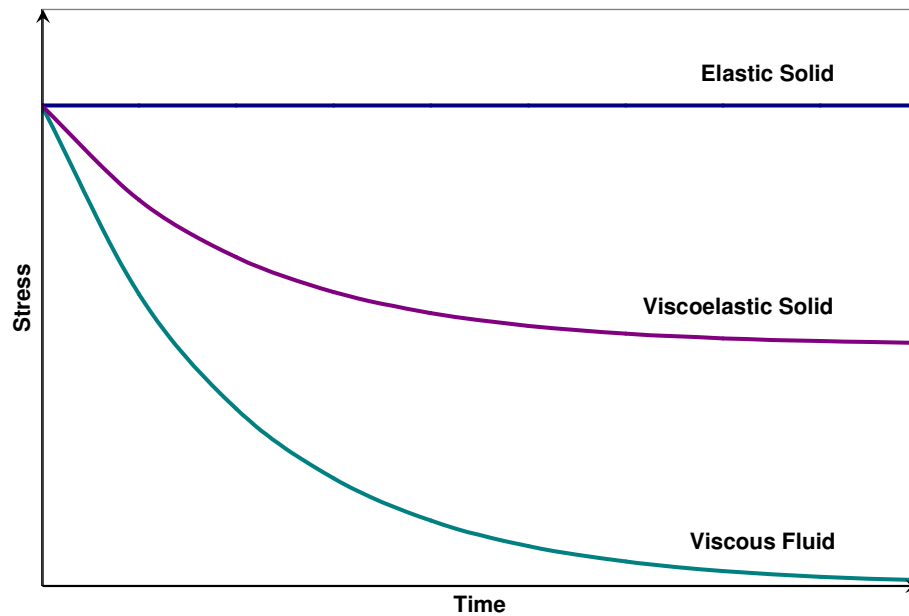
Figure 3-2: Response for Different Types of Materials in Stress Relaxation
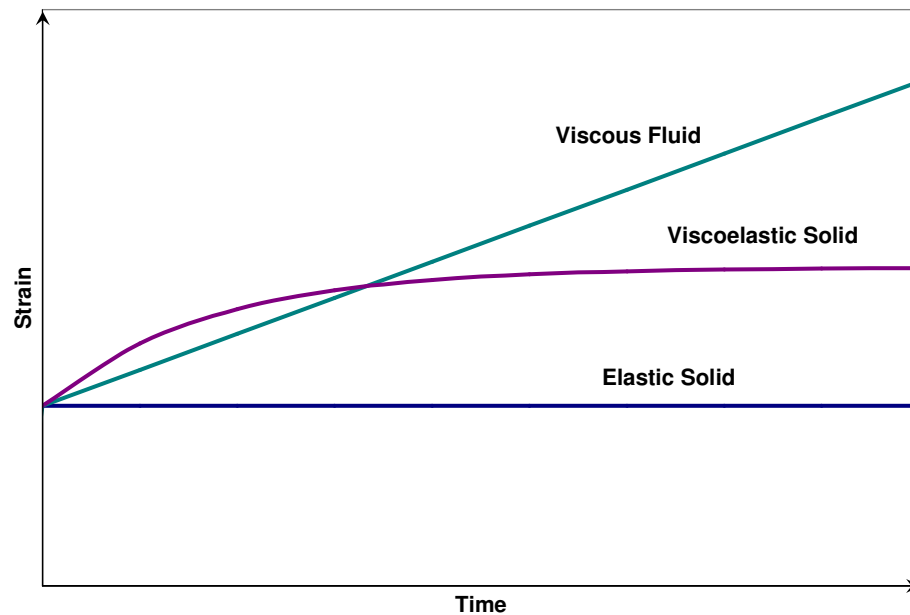
Figure 3-3: Response for Different Types of Materials in Creep

For a creep experiment, a constant applied load (stress) is applied to the material, and the resulting strain is monitored over time (Figure 3-3). As with the relaxation test, a pure elastic material will maintain a constant strain with the applied load, whereas a viscous fluid will theoretically reach an infinite strain over time. However, a viscoelastic material will plateau to a constant strain over time.

While relaxation and creep experiments deal with long-term response, events involving impact are typically very short. The response of a viscoelastic material short-duration strains (or high strain rates) is an increase in stiffness from the time-independent (elastic) response (Figure 3-4). High strain rate testing often deals with a regime of loading that is not considered in creep or relaxation testing, so generalizing the viscoelasticity of a material using only relaxation or creep data may introduce an inaccurate stiffening response of the material at high strain rates seen in impact loading or automotive crash. Additional material testing using other techniques may be required. A list of the various types of material testing techniques and their associated strain-rate regimes can be seen in Figure 3-5.
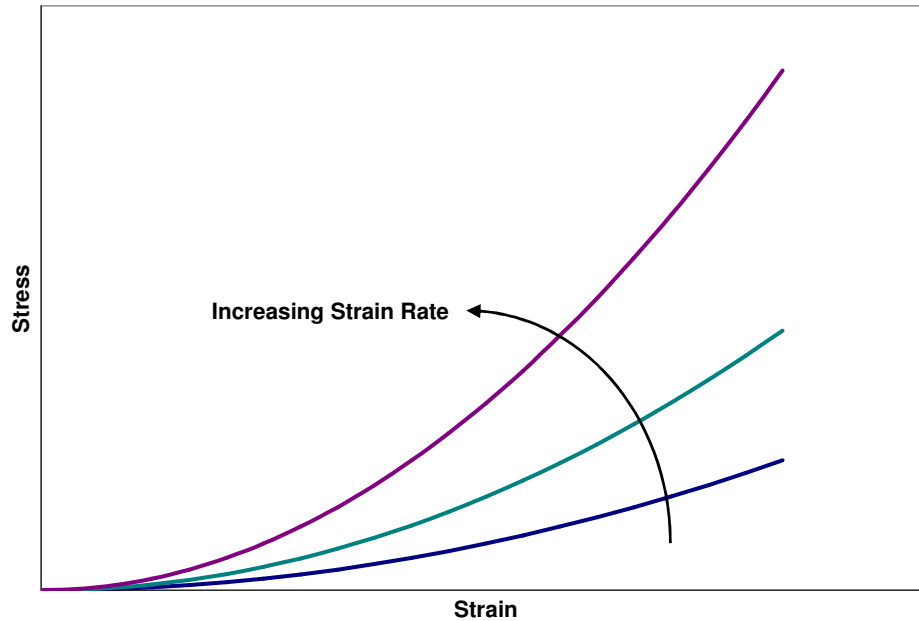
Figure 3-4: Viscoelastic Stress-Strain Response for Increasing Applied Strain-Rate
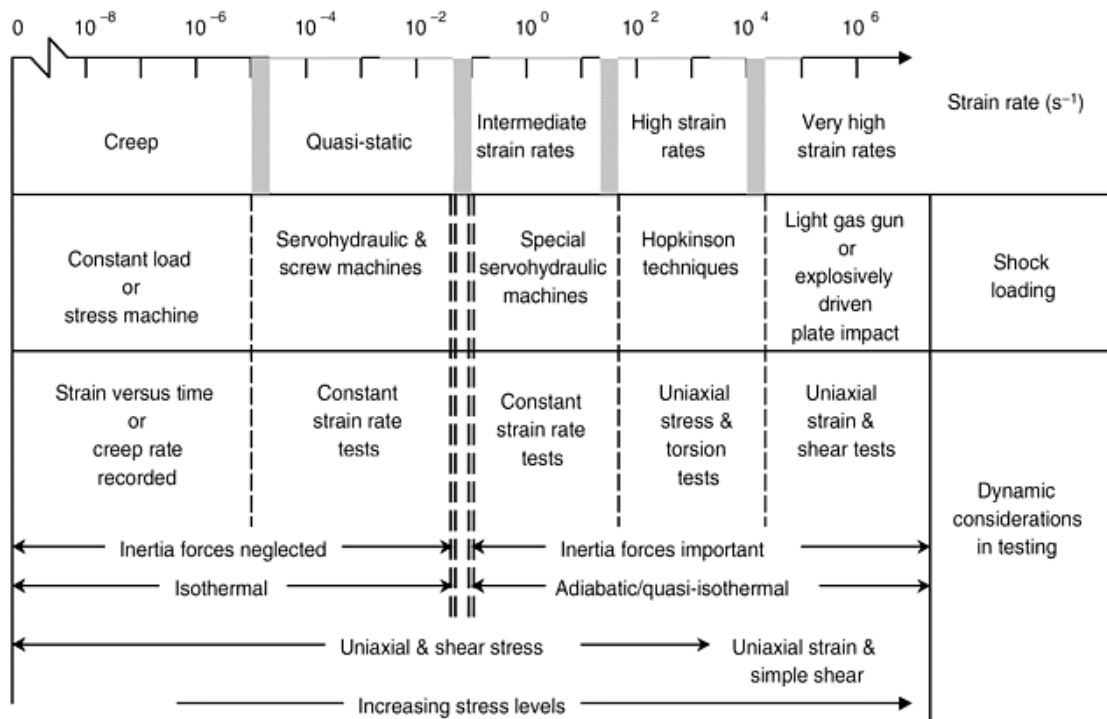
(Adapted from ASM, Vol. 8: Mechanical Testing and Evaluation)

Figure 3-5: Material Testing Techniques for Desired Strain-Rate

3.2 Bone Mechanics

The vertebrae are part of the human skeletal system, being built from osseous (bone) tissue. Bone is a hard biological material, having a composition of 65% mineral (primarily hydroxyapatite) and 35% organic matrix (a mixture of collagen, water, and cells) (Cowin, 2001). There are two basic types of bone in the human body: cortical bone (also referred to as compact bone) and cancellous bone (also referred to as trabecular bone). Cortical bone is a dense, solid material that typically forms the outer surface of a bone. Cancellous bone, on the other hand, is a highly porous material made up of an open latticework of tubular and platen structures called trabeculae. Cancellous bone exists on the inside of bones, surrounded by the cortical bone. Filling the void of the cancellous bone is a fluid mixture of blood and marrow (Carter and Hayes, 1977).

A summary of previous research involving the mechanical properties of both cortical and cancellous bone can be found in Table 3-1 at the end of this section. Human vertebral cancellous bone properties are taken from studies involving the lumbar spine region. Due to the lack of previous studies on the vertebral cortical shell, only select cortical bone properties are reported.

3.2.1 Bone Mechanical Behaviour

Human vertebral cancellous bone is a widely studied tissue because of its significant role in the strength and load-carrying capacity of the vertebra (White and Panjabi, 1990). The mechanical properties of the cancellous bone depend on the mineral density, volume fraction, trabecular architecture, and the trabecular tissue properties (Lindahl 1976; Mosekilde et al., 1987). Mineral density is very important in characteristic of cancellous bone as it is directly related to the apparent stiffness of the bone (Mosekilde et al., 1987). With age, cancellous bone mineral density decreases, reducing the compressive strength of the human vertebrae (Carter and Hayes, 1977; Cody et al., 1991).

Mineral density is also directly related to the volume fraction or apparent density of the cancellous bone (Hansson et al., 1987). An increase in apparent density means that more trabeculae are able to provide structural support for a given load, increasing the stiffness of the bone. Vertebral cancellous bone has an apparent density between 0.1 g/cm^3 and 0.3 g/cm^3 (average approximately 0.2 g/cm^3), whereas tibial and femoral cancellous bone apparent density are much higher, with an averages of 0.4

g/cm^3 and 0.5 g/cm^3 respectively (Rohlmann et al., 1980; Linde al., 1991; Kopperdahl and Keaveney, 1998). An apparent density of 0.2 g/cm^3 corresponds to a volume fraction of 0.1, with trabecular tissue (and cortical bone) having a density of approximately 2.0 g/cm^3 (Keaveney et al., 2001).
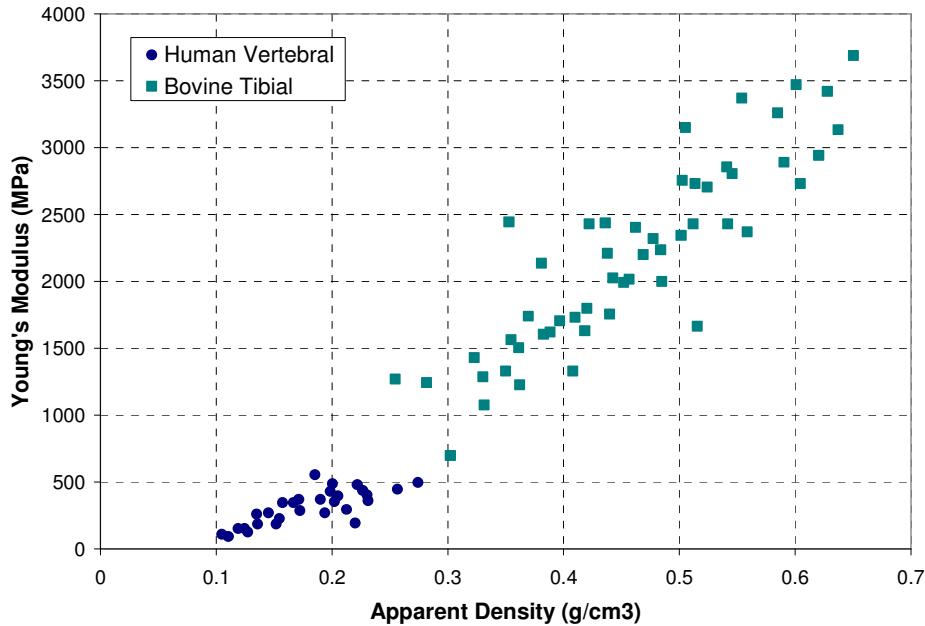
Figure 3-6: Young's Modulus as a Function of Cancellous Bone Apparent Density

The architecture of the trabeculae has influence on the anisotropy of the mechanical properties in cancellous bone (Keaveney et al., 2001). With a volume fraction less than 0.2, vertebral cancellous bone can be considered as an open celled structure (Carter and Hayes, 1977; Linde et al, 1991). This open celled structure follows Wolfe's Law, by being constructed of thick vertical trabecular rods connected by thinner horizontal trabeculae (Mosekilde et al., 1987; Kopperdahl and Keaveny, 1998). This is because the primary loading direction of the cancellous bone is vertical due to the axial compression of the vertebral body. A result of this oriented architecture is that the vertical direction is approximately 3 times stiffer and stronger than in the horizontal direction (Carter and Hayes, 1977; Mosekilde et al., 1987). This anisotropy is accentuated with age, because deterioration of bone density results in a prominent loss of the thin horizontal trabeculae without a significant loss in the thickness of the vertical trabeculae (Mosekilde and Mosekilde, 1986). The ratio of vertical to horizontal stiffness in human cancellous bone has been shown to increase by 63% between the ages of 20 and 80 (Mosekilde and Mosekilde, 1986).
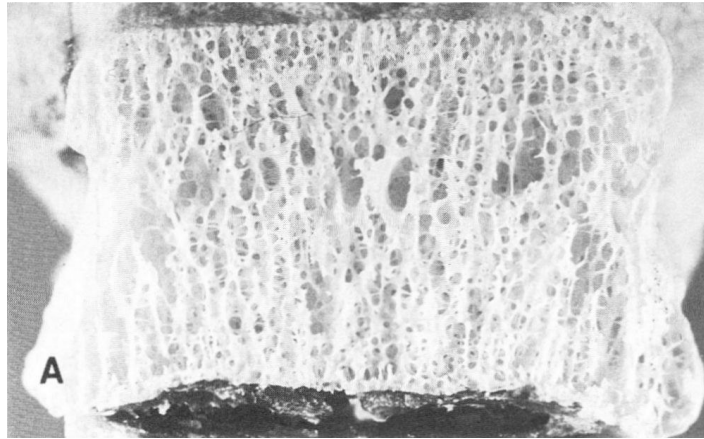
Figure 3-7: Cross-section of the Vertebral Body Showing the Dominate Vertical Trabeculae

The remaining factor involved in the mechanical properties of cancellous bone is the mechanical properties of the trabeculae themselves. It has been found that normal trabecular tissue and cortical bone have similar compositions and tissue densities, and as a result, they have very similar mechanical properties (Carter and Hayes, 1977). Trabecular tissue is relatively stiff and brittle, behaving more like a ceramic material than a metal material (Cowin, 2001).

Because of the similarities between cortical bone and trabecular tissue, cortical bone can be thought of as cancellous bone with a high volume fraction and minimal porosity. The factors that affect the mechanical properties of cortical bone include mineral density, porosity, and the orientation of the collagen fibres present in the organic matrix (Kotha and Guzelsu, 2003). Similar to cancellous bone, a decrease in bone mineral density results in a decrease in elastic modulus, yield strength, and ultimate strength of cortical bone (Kotha and Guzelsu, 2003; Currey, 2004). However, the decrease in bone mineral density with age in cortical bone is not as pronounced as it is in cancellous bone, resulting in an increased role load-bearing capacity for the human vertebrae.

In general, the mechanical behaviour of cortical bone is anisotropic, having different properties in different anatomic sites (Reilly and Burstein, 1975; Cowin, 2001). The orientation of the collagen fibres gives the bone anisotropic behaviour. The presence of these fibres also helps increase the toughness of the cortical bone, reducing the risk of crack propagation (Nalla et al., 2005). The anisotropy in human vertebral cortical shell has not been previously researched, but it hypothesized

that the vertebral shell is not significantly anisotropic due to the relatively low load-carrying capacity. It was found that there is no significant difference in elastic modulus for cortical bone in tensile and compression (Reilly at al., 1974).

3.2.2   Bone Viscoelasticity

The intrinsic viscoelastic properties of both cortical bone and cancellous bone are known to exist, although this effect is often insignificant when compared to the surrounding soft tissue (Cowin, 2001). The mineral portion of bone tissue is considered virtually elastic, having almost no measurable dynamic storage properties (Cowin, 2001). The intrinsic viscoelastic response of bone is a side effect of the organic matrix portion of the tissue. The molecular motion of the cross-linked collagen fibres is believed to provide the mechanism for this viscoelastic effect (Cowin, 2001). Nevertheless, both cortical and cancellous bone exhibit classic viscoelastic behaviour demonstrated by creep, relaxation, and strain-rate stiffening effects (McElhaney, 1966; Carter and Hayes, 1977; Fondrk et al., 1988; Linde et al., 1991; Bowman et al., 1994). Studies have shown that the three phases of creep behaviour (initial rapid response, a steady state creep at constant rate, and a rapid increase in strain just prior to fracture) seen in metals and ceramics, are also seen in both cortical and cancellous bone (Caler and Carter, 1989; Bowman et al., 1994).

With the pores of cancellous bone being filled with a fluid phase (marrow), flow-dependant viscoelastic behaviour is also produced. It was found that the presence of marrow did not influence the viscoelastic behaviour at low to moderate strain rates (Pugh et al., 1973; Carter and Hayes, 1977). It was not until specimens higher strain rates (greater than 10/s) experienced an increase in stiffness, leading to the conclusion that the under moderate, physiological loading, cancellous bone is not hydraulically strengthened by the presence of marrow (Carter and Hayes, 1977).

Creep or fatigue testing of bone are often use to identify bone damage mechanisms as constant and repetitive loading has been known to cause bone failure particularly in mineral-reduced bones (Cowin, 2001). Bone damage is a result of overloading the bone past its physiological threshold. In cortical bone, osteon pullout, microcracking, and void compaction occur as damage mechanisms at the microscopic level (Saha and Hayes, 1976). Cancellous bone damage is apparent in the trabeculae, which undergoes microdamage including longitudinal and transverse microcracks, leading to whole trabecular fracture (Yeh and Keaveny, 2001). Also prevalent in low-density cancellous bone in

compression are trabecular buckling failure mechanisms due to the slenderness ratio of the supporting trabecular struts (Carter and Hayes, 1977; Kopperdahl and Keaveny, 1998).

3.2.3   Bone Injury and Failure

Damage accumulation within bone results in an apparent softening behavior and a corresponding permanent deformation. Onset of material softening is often identified as the yield point, relating bone mechanics to metallic elastic-plastic models. This point is also commonly referred to as the point of bone failure, which not to be mistaken for bone fracture or rupture. Yielding is a simplified description of bone damage, however unlike metals, yield behaviour in bone is not a result of material plasticity, but of microscopic damage described above.

Also different than metal behaviour, bone does not unload along its elastic modulus after plastic deformation has occurred. Instead, bone unloads along a reduced modulus that is not significantly different from the perfect damage modulus idealized in classic brittle materials (Kopperdahl et al., 2000; Yeh and Keaveny, 2001; Kosmopoulos and Keller, 2003). Even subtle damage to the individual trabeculae in cancellous bone can cause a significant reduction in apparent modulus, without entirely fracturing trabeculae (Keaveny et al., 2001). An example of a typical stress-strain curve of an overload specimen of cancellous bone can be in Figure 3-8. Figure 3-9 is a description of the accumulated damaged (measured as a reduction in modulus) of human vertebral cancellous bone.
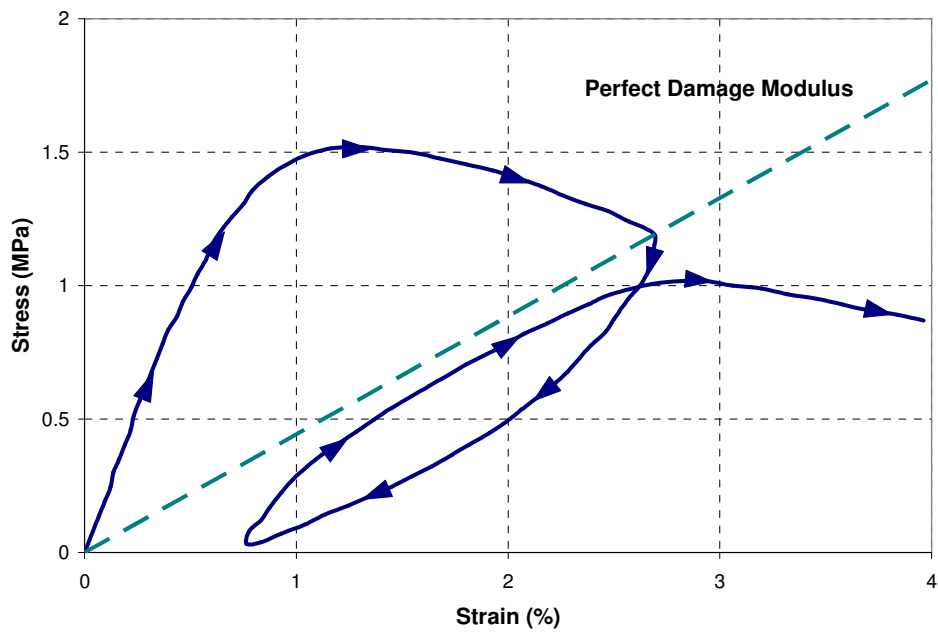
Figure 3-8: Load-Unload-Load Behaviour of Human Vertebral Cancellous Bone
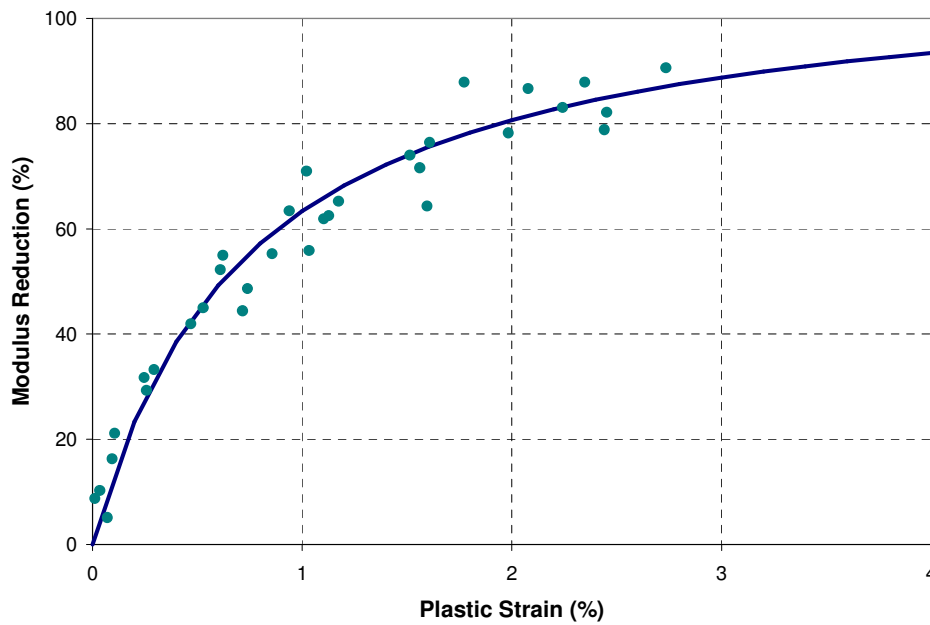
Figure 3-9: Reduction of Elastic Modulus due to Apparent Yield Strain of Cancellous Bone

A strain-based description of bone damage is mathematically simple and statistically powerful since yield strain does not depend on the mineral content, porosity, anisotropy, or histology of the bone (Hansson et al., 1987; Linde et al., 1991; Kopperdahl and Keaveny, 1998; Keaveny et al., 2001; Morgan and Keaveny., 2001; Currey, 2004). However, the post-yield behaviour of cortical bone is highly dependant on the proportion of organic matrix. A high composition of organic matrix in the bone increases the toughness of the bone (Currey, 2004; Nalla et al., 2005). It was also found that wet bone shows more plasticity than that dry bone (Evans and Lebow, 1957). Nevertheless, the plastic deformation of bone in tension is relatively low (approximately 1-2%) before fracture will occur (Reilly et al., 1974). This behaviour is synonymous to brittle materials, which are generally weak in tension (Saha and Hayes, 1976).

It is for the above reasons that damage continuum models for brittle materials (such as ceramics) are ideal for representing the mechanical behaviour of bone. However, these models are complex, and often difficult to apply without appropriate material data. On the other hand, simple elastic-plastic models with yield-strain criteria are easy to implement and adequately accurate for monotonic loading of bone.

A summary of the mechanical properties of bone can be found in Table 3-1.

Table 3-1: Summary of Mechanical Properties Studies of Bone

Study	Bone Source	Type	Test	Results
McElhaney, 1966	Human Femur	Cortical	Compression	$\dot{e}$ = 0.001/s: E = 15.2 GPa, e_{ult} = 1.65%, σ_{ult} = 150.3 MPa $\dot{e}$ = 0.01/s: E = 17.2 GPa, e_{ult} = 1.75%, σ_{ult} = 179.3 MPa $\dot{e}$ = 0.1/s: E = 17.9 GPa, e_{ult} = 1.80%, σ_{ult} = 199.9 MPa $\dot{e}$ = 1/s: E = 22.1 GPa, e_{ult} = 1.78%, σ_{ult} = 220.6 MPa $\dot{e}$ = 300/s: E = 29.6 GPa, e_{ult} = 1.10%, σ_{ult} = 279.2 MPa $\dot{e}$ = 1500/s: E = 40.7 GPa, e_{ult} = 0.95%, σ_{ult} = 317.2 MPa
Reilly et al, 1974	Human Femur	Cortical	Compression and Tension	E = 17.4 GPa, e_{ult} = 2.71%, σ_{ult} = 192.5 MPa (Compression) E = 16.8 GPa, e_{ult} = 2.09%, σ_{ult} = 128.5 MPa (Tension)
Reilly and Burstein, 1975	Human Femur	Cortical	Compression and Tension	E_1 = 17.0 GPa, $E_{2,3}$ = 11.5 GPa, G_{12} = 3.28 GPa σ_{ult1} = 193 MPa, $\sigma_{ult2,3}$ = 133 MPa (Compression) σ_{ult1} = 133 MPa, $\sigma_{ult2,3}$ = 51 MPa (Tension)
Lindahl, 1976	Human Vertebrae	Cancellous	Compression	E = 55.6 MPa, e_y = 6.7%, σ_y = 4.0 MPa, e_{ult} = 9.5%, σ_{ult} = 4.6 MPa
Saha and Hayes, 1976	Human Femur	Cortical	Tension	E = 14.5 GPa, σ_y = 76.7 MPa, e_{ult} = 1.15%, σ_{ult} = 126.3 MPa
Carter and Hayes, 1977	Mulitple	Cancellous	Compression	E = 3790$\dot{e}^{0.06}\rho^3$, σ_y = 68$\dot{e}^{0.06}\rho^2$
Hanson et al, 1987	Human Vertebrae	Cancellous	Compression	E = 22.3 MPa, e_y = 6.0%, σ_y = 1.37 MPa, e_{ult} = 7.4%, σ_{ult} = 1.55 MPa
Mosekilde et al, 1987	Human Vertebrae	Cancellous	Compression	E_1 = 67 MPa, e_{ult1} = 7.4%, σ_{ult1} = 2.45 MPa (Vertical) $E_{2,3}$ = 20 MPa, e_{ult1} = 8.5%, σ_{ult1} = 0.88 MPa (Horizontal)
Linde et al, 1991	Human Tibia	Cancellous	Compression	E = 2232$\dot{e}^{0.047}\rho^{1.56}$, e_{ult} = 0.0256$\dot{e}^{0.03}$, σ_y = 40.2$\dot{e}^{0.073}\rho^{1.65}$
Kopperdahl and Keaveny, 1998	Human Vertebrae	Cancellous	Compression and Tension	E = 291 MPa, e_y = 0.8%, σ_y = 1.9 MPa, e_{ult} = 1.5%, σ_{ult} = 2.2 MPa (C) E = 301 MPa, e_y = 0.8%, σ_y = 1.8 MPa, e_{ult} = 1.6%, σ_{ult} = 2.2 MPa (T)
Morgan and Keaveny, 2001	Human Vertebrae	Cancellous	Compression and Tension	E = 344 MPa, e_y = 0.77%, σ_y = 2.02 MPa (Compression) E = 349 MPa, e_y = 0.70%, σ_y = 1.72 MPa (Tension)
Currey, 2004	Human Femur	Cortical	Tension	E = 16.7 GPa, e_y = 0.72%, σ_y = 112.3 MPa, e_{ult} = 2.93%, σ_{ult} = 165.7 MPa

3.3 Cartilage Mechanics

Numerous studies have been carried out to identify the mechanical properties of articular cartilage, since it is involved in common degenerative diseases such as osteoarthritis (Hori and Mockros, 1976). Many of these studies are listed in Table 3-2 at the end of this section. Early investigations into the mechanical properties of cartilage, using indentation techniques, revealed significant viscoelastic behaviour (Hayes and Mockros, 1971). It has been proposed that the main mechanism for cartilage viscoelasticity is the frictional interactions resulting from interstitial fluid flow, since cartilage is a porous medium (Fung, 1993; Mow and Guo, 2002; Li et al., 2003). When cartilage is loaded in compression, a loss of tissue volume occurs from fluid seepage from the tissue, which also gives rise to significant viscoelastic response (Mow and Guo, 2002). A typical relaxation response of articular cartilage in unconfined compression can be seen in Figure 3-10.
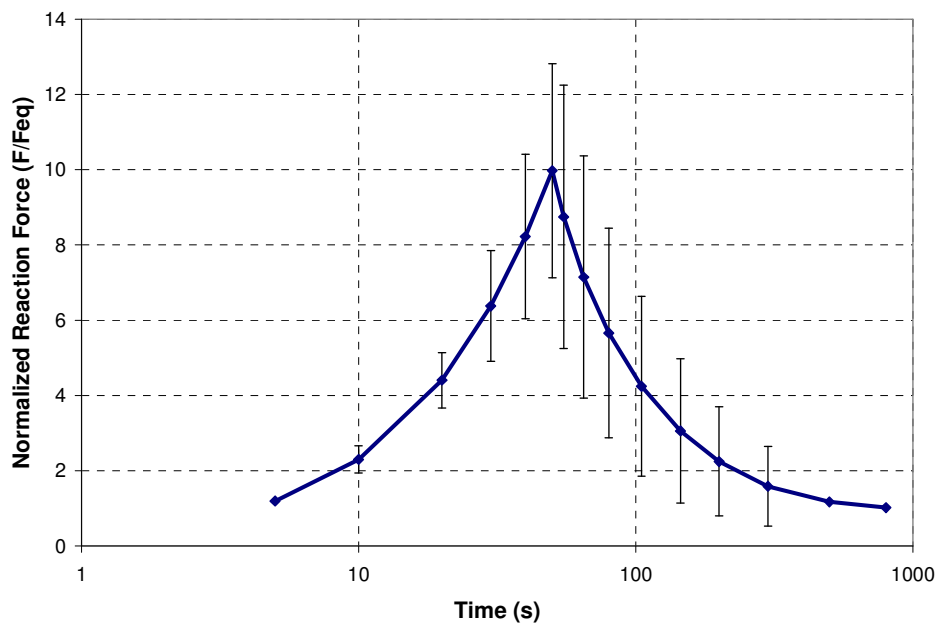
Figure 3-10: Reaction Force of Unconfined Cartilage in Relaxation

The majority of mechanical testing on articular cartilage has been done using viscoelastic methods such as relaxation, creep, or indentation testing (Hori and Mockros, 1976; Woo et al., 1980). The response of the tissue in these tests was found to be largely dependant on the porosity of the tissue (Hayes and Mockros, 1971). This finding led to the development of a biphasic model for cartilage, which consisted of a mixture of permeable solid matrix and incompressible viscous fluid (Mow et al.,

1980). This model was later expanded to include nonlinear permeability, anisotropy, and nonlinear elastic solid behaviour to better fit the results of experiments (DiSilvestro and Suh, 2001).

The results of various studies on the compression of articular cartilage show that, for being a load-bearing tissue, the quasi-static elastic stiffness is relatively low (less than 1 MPa) indicating that hydrostatic pressure in the interstitial fluid is the main source of support (Mow et al., 1980; Ateshian et al., 1997; DiSilvestro and Suh, 2001; Huang et al., 2005). The presence of Type II collagen fibres that make up the solid matrix provide an equilibrium elastic stiffness in tension that is approximately 5 – 25 MPa, many times greater than in compression (Mow and Guo, 2002; Huang et al., 2005). Furthermore, nonlinear mechanical properties can be observed in tension due to the collagen network (refer to Figure 3-1), whereas the elastic properties of cartilage in compression are primarily linear (Mow and Guo, 2002; Huang et al., 2005).

Table 3-2: Summary of Studies on the Mechanical Properties of Articular Cartilage

Study	Type of Experiment
Hayes and Mockros, 1971	Creep and Relaxation in Confined Compression, Torsional Shear
Kempson et al., 1971	Creep Indentation
Hori and Mockros, 1976	Short-time Response in Confined Compression, Torsional Shear
Hayes and Bodine, 1978	Sinusoidal Shear
Mow et al., 1980	Creep and Relaxation in Confined Compression
Woo et al., 1980	Sinusoidal and Relaxation in Tension
Simon et al., 1984	Creep and Relaxation in Tension
Setton et al., 1993a	Creep in Confined Compression
Ateshian et al., 1997	Creep and Relaxation in Confined Compression
Bursac et al., 1999	Relaxation in Unconfined Compression, Confined Compression
DiSilvestro and Suh, 2001	Relaxation in Unconfined Compression, Confined Compression, Indentation

3.4   Annulus Fibrosus Mechanics

The response of the healthy intervertebral disc under various types of loading is predominately due to the load-carrying capabilities of the annulus fibrosus fibres. Numerous experimental studies have been conducted on the annulus in an effort to characterize the mechanical behaviour of the tissue, and identify its role in spinal motion and injury. The mechanical behaviour of the annulus originates from three basic constituents: i) the annular fibres, ii) the homogenous matrix, and iii) the interaction between the fibres and the matrix, and the fibres with each other (Wagner and Lotz, 2004). It is the focus of most annulus studies to address these elements and their effect on the entire annulus tissue. Furthermore, the annulus fibrosus is considered heterogeneous in compression and tension because of its composite structure, thus requiring a significant amount of test data to fully characterize the tissue (Ebara et al., 1996). A summary of the studies of the mechanical properties of the annulus fibrosus can be found in Table 3-3 at the end of this section.

3.4.1   Annulus Fibrosus Mechanical Behaviour

The single annular lamina is considered the basic tensile structural element of the annulus fibrosus tissue (Skaggs et al., 1994). When pulled in tension, a single lamina displays marked non-linear behaviour (Figure 3-11) (Skaggs et al., 1994; Holzapfel et al., 2005). The initial toe region of the stress-strain response is dominated by the straightening of crimped annular fibres with the matrix material (Figure 3-12) (Elliot and Setton, 2001; Pezowicz et al., 2005). As the fibres progressively straighten, the response becomes linear and the fibres begin to carry the tensile load. This nonlinear behaviour also translates to multilayer specimens in both circumferential and axial tension (Galante, 1967; Wu and Yao, 1976; Adams and Green, 1993; Acaroglu et al., 1995; Ebara et al., 1996; Elliott and Setton, 2001; Wagner and Lotz; 2004).
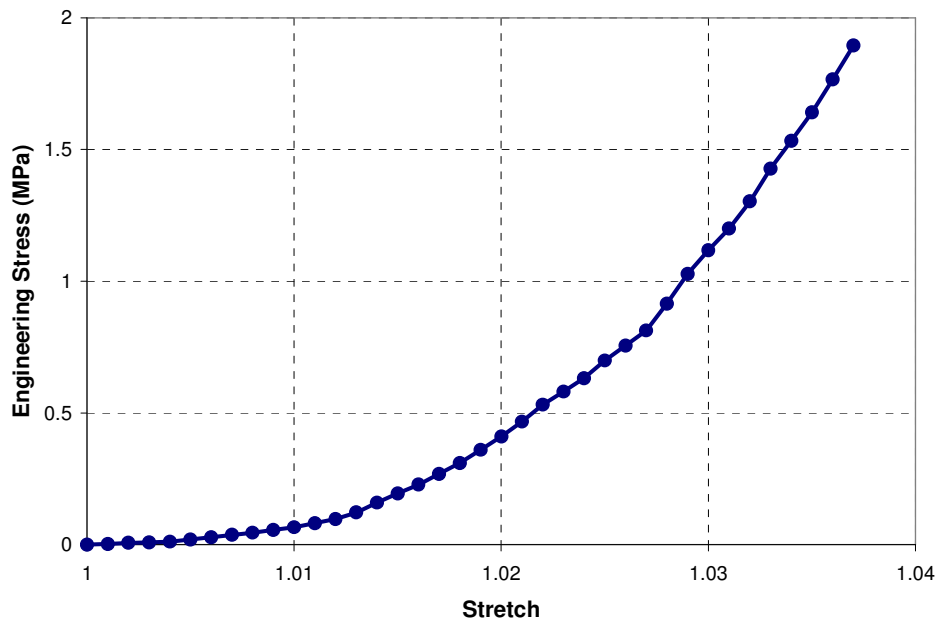
(Reproduced from Holzapfel et al., 2005)

Figure 3-11: Response for a Single Lamina in Tension along the Length of the Fibres

Unloaded **Loaded**
(Adapted from Pezowicz et al., 2005)
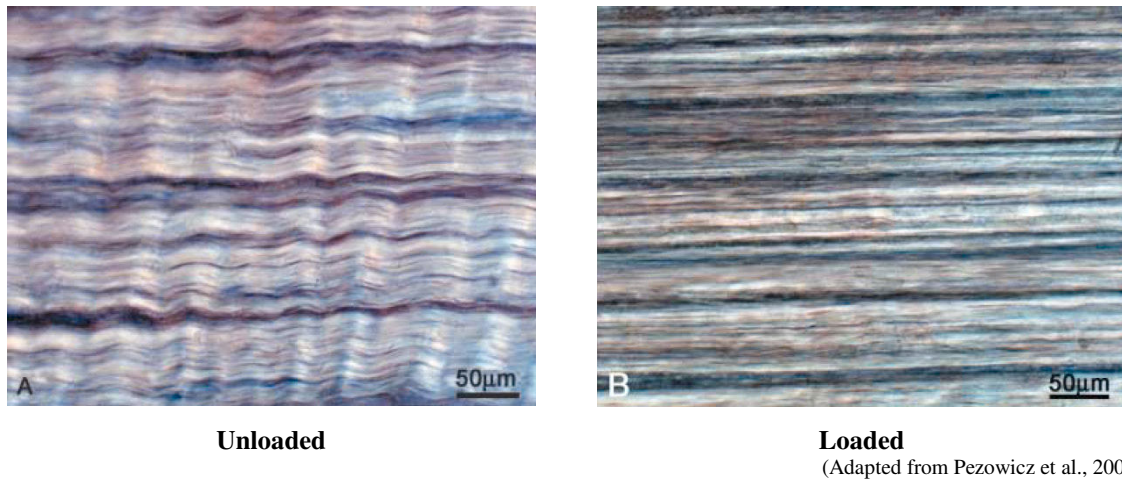
Figure 3-12: Annular Fibres from an Unloaded Crimped State to a Stretched State

The mechanical properties of the single lamina also vary depending on where on the intervertebral disc the specimen was sampled. It has been found that the annulus fibrosus is stiffer in the outer lamina compared to the inner lamina, thus it is possible to create an ideal state of near uniform circumferential stress within the annulus (Skaggs et al., 1994; Holzapfel et al., 2005). This regional variation is also present when testing multilayer specimens in either the circumferential or the axial direction (Acaroglu et al., 1995; Ebara et al., 1996; Elliott and Setton, 2001).

When considering the in-plane tensile properties of the annulus fibrosus in the lamina, it is important to distinguish between single and multilayered samples. Preparing a multilayer specimen from an intervertebral disc requires cutting of the annular fibres. It has been shown that cutting fibres introduces a stress-free edge to the specimen *in vitro* that would have otherwise been supported *in vivo* (Iatridis et al., 2005). This dramatically reduces the strength of the sample (Green et al., 1993). Furthermore, a multilayer specimen often has an unknown number of laminae, which can have a variation of fibre orientation within each lamina. This uncertainty plays a significant role in assessing the quality of data from a multilayer specimen in tension (Holzapfel et al., 2005). Because of the limited nature of in-plane multilayer tensile testing, single layer tensile data is a superior method for determining the mechanical behaviour of the annulus (Holzapfel et al., 2005).

Axial tensile testing of multilayer specimens at various loading rates (ranging from 0.001 1/s to 3 1/s) resulted in a slight increase in tensile stiffness with an increase in strain-rate, while ultimate stress and ultimate strain showed no dependency on strain-rate (Kasra et al., 2004). It was then hypothesized that rate dependence in mechanical properties of the annulus could be primarily due to the annular fibres and not the annulus matrix. However, this hypothesis was disproved when tensile testing of

single layer specimens at a range of low strain-rates (0.1 mm/min to 10 mm/min) resulted in the annular fibres displaying no significant viscoelasticity (Holzapfel et al., 2005). However, the results of these two studies may not be significant for modelling the annulus fibrosus in cervical spine impact, since preliminary full spine model simulations indicate that strain-rates can reach as high as 200 1/s.

The radial properties of the annulus fibrosus (the direction is perpendicular to the annular fibres) are considered the mechanical properties of the homogenous ground substance in which the annular fibres are embedded, since the fibre influence in this direction is negligible (Fujita et al., 1997; Elliott and Setton, 2001). Tests on the tensile behaviour of the ground substance show a distinct non-linear response that is capable of sustaining large deformation (Figure 3-13). However, unlike the tensile properties of the annulus lamina, the tensile properties of the ground substance were found to be independent of annulus region (Fujita et al., 1997).
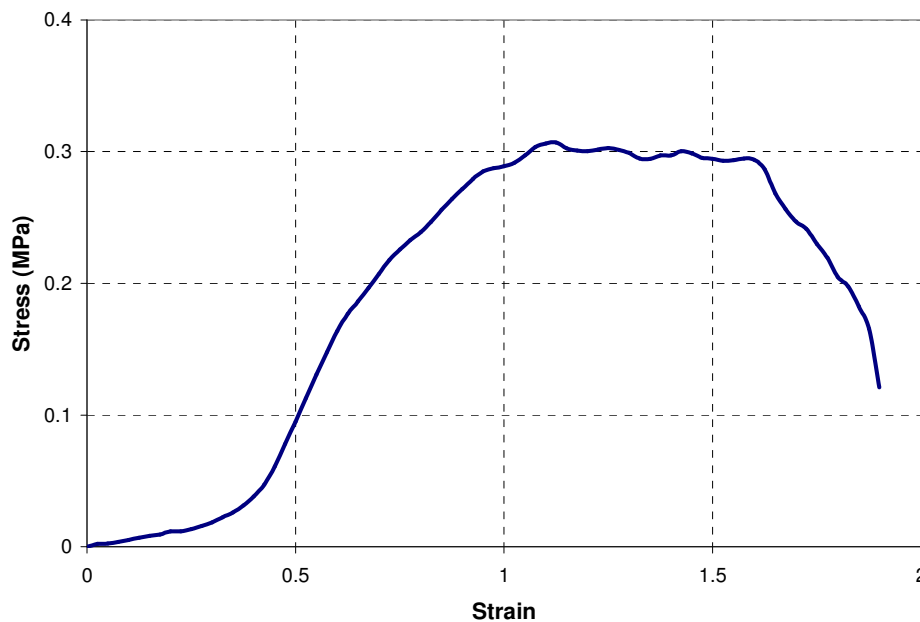
(Reproduced from Fujita et al., 1997)

Figure 3-13: Engineering Stress-Stretch Curve for a Multilayer Specimen in Radial Tension

When comparing compressive response of the annulus ground substance in the axial and radial directions, no significant differences in mechanical response were found suggesting that the ground substance is an isotropic material (Iatridis et al., 1998; Klisch and Lotz., 2000). Compression results also indicate that the compression response of the ground substance is nonlinear, with no site dependence (Figure 3-14) (Iatridis et al., 1998; Klisch and Lotz, 2000).

Finally, studies on the behaviour of the annulus tissue in shear are few, despite the notion that interlaminar shear stresses play a dominant role in annulus fibrosus injury (Goel et al., 1995). Cubes of annular tissue were tested showing that the shear behaviour to be linear and anisotropic, with a small regional dependence (Fujita et al., 2000). However, the difference in shear moduli out-of-plane from the laminae was found to be insignificant, indicating that the description of anisotropy stems from the influence of fibre. Furthermore, shear testing was done for strains up to 10%, so non-linear effects may not have been realized at these relatively small strains (Fujita et al., 2000).
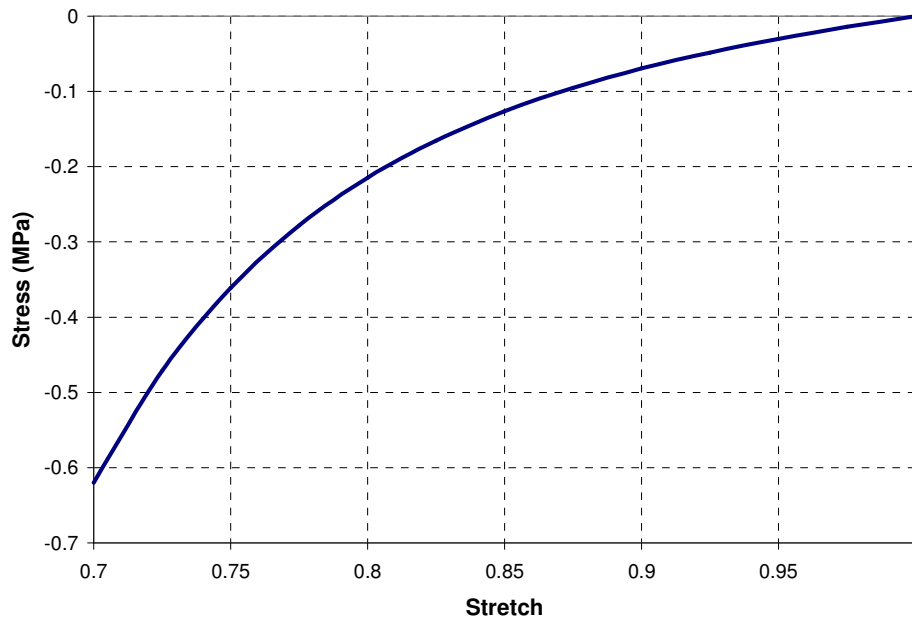
(Reproduced from Iatridis et al., 1998)

Figure 3-14: Engineering Stress-Stretch Curve for the Annulus Fibrosus in Compression

3.4.2   Annulus Fibrosus Viscoelasticity

Relaxation testing of the annulus ground substance tissue in confined compression resulted in a viscoelastic response (Iatridis et al., 1998; Klisch and Lotz, 2000). It is often reported that this viscoelastic effect is a result of the fluid-transport mechanisms described by biphasic mixture theory, since there was a noticeable amount of fluid loss in the tissue (Best et al., 1994; Iatridis et al., 1998; Klisch and Lotz, 2000).

Small-strain dynamic testing in shear, however, can isolate the flow-independent viscoelastic effects from the flow-dependent effects (Iatridis et al., 1999). It was reported that the intrinsic viscoelastic effects of the annulus tissue in shear caused an increase of 1.5 – 2 times the equilibrium stress, whereas in the confined compression cases, the combined viscoelastic effect caused an increase

around six times the equilibrium stress. (Iatridis et al., 1998; Iatridis et al., 1999). This identifies that flow-dependent effects are the dominant viscoelastic mechanisms within the annulus tissue for low strain-rates (Iatridis et al., 1999). Studies of annulus fibrosus viscoelasticity at strain-rates applicable to impact conditions (up to 200 1/s as seen in preliminary impact models), where the fluid does not have sufficient amount to dissipate, are currently unavailable.

3.4.3   Annulus Fibrosus Injury and Failure

Like any biological tissue, overloading the annulus fibrosus will damage the structure of the tissue and affect the physiology of the spinal motion segment. Spinal injury and pain has often been associated with trauma to the intervertebral disc, and many theories pinpoint the failure of annulus as the main injury mechanism source (Iatridis et al., 2005). Failure of the annulus or collagenous network will often result in intervertebral disc injuries such as disc herniation or nucleus prolapse (Iatridis et al., 2005). For example, the posterolateral region of the intervertebral disc is the most frequent area of disc failure, which is caused by a failure in the annulus attributed to the reduced tensile failure stress found in that region (Skaggs et al., 1994; Ebara et al., 1996; Iatridis et al., 2005).

There are three main types of tensile-failure related annulus fibrosus tears: i) radial tears that propagate through multiple laminae, ii) circumferential tears that rupture a lamina on the circumference of the disc, and iii) rim lesions, which is a tearing of the periphery of the annulus at the cartilaginous endplates (Iatridis and ap Gwynn, 2004). These mechanisms are often difficult to accurately reproduce during *in vitro* testing (Natarajan et al., 1994). When testing a bone-annulus-bone specimen in axial tension to failure, the common mechanism of injury was failure of the cartilagous endplate-vertebral body interface rather than the disc itself (Green et al., 1993; Kasra et al., 2004). At higher tensile strain-rates (3 1/s), the injury mechanism switched to failure of the annulus fibrosus, which suggested that strain-rate sensitivity in the annulus is less than in the endplate-vertebral interface (Kasra et al., 2004). However, this study only considered a small range of strain-rates that are below rates seen in impacts (0.001 1/s to 3 1/s).

Tensile failure of the annulus fibrosus is not a catastrophic event, but rather a gradual progression of damage (Figure 3-15) (Pezowicz et al, 2005). Damage initiates in the annulus as localized fibre-endplate anchorage begins to fail (Point A), This event does not propagate a tear across the entire array of fibres, but rather transferring the load to other regions of the tissue. Eventually, these fibres also begin to pullout, leading to isolated fibre bundles sliding with an otherwise intact array

(Pezowicz et al, 2005). The rapid decline in stress (Point A to B) is a result of the cumulative increase in sliding and separation throughout the tissue, until full separation occurs (Point C).

Another theory for annulus fibrosus failure stems from the use of finite element modelling (Goel et al., 1995). It was suggested that interlaminar shear stress was a more relevant injury mechanism in the annulus than the tensile failure of the annular fibres (Goel et al., 1995; Fujita et al., 1997). These shear stresses result in the delamination of the annular layers, which initiate the proliferation of further disc damage (Iatridis and ap Gwynn, 2004; Iatridis et al., 2005). While most of the research into this type of failure mechanism is limited by the lack of clinical research, interlaminar shear stress is an important failure mechanism in traditional composite materials (Goel et al., 1995).
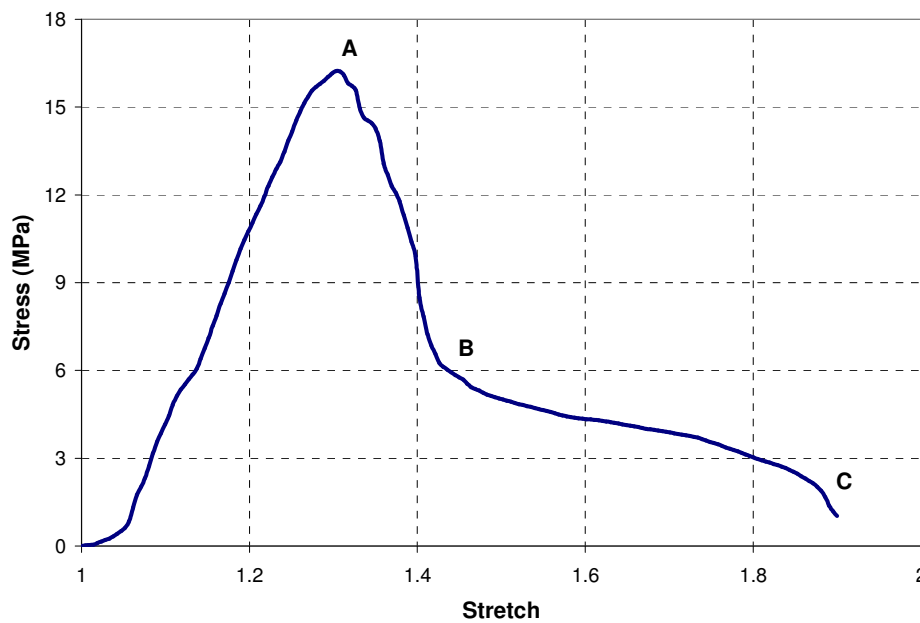
Figure 3-15: Tensile Stress-Strain Response of a Single Lamina along the Fibre Direction

Table 3-3: Summary of Studies on the Mechanical Properties of the Annulus Fibrosus

Study	Specimen Type	Direction of Loading	Type of Experimental Test
Galante, 1969	Multi	Circumferential	Quasi-static Tension
Wu & Yao, 1976	Multi	Circumferential	Quasi-static Tension
Adams & Green, 1993	Multi	Axial	Quasi-static Tension
Green et al., 1993	Multi	Axial	Quasi-static Tension to Failure
Best et al., 1994	Multi	Radial	Creep Confined Compression
Skaggs et al., 1994	Single	Parallel to Fibre	Quasi-static Tension
Acaroglu et al., 1995	Multi	Axial	Quasi-static Tension
Lotz et al., 1995	Multi	Multi-Planar	Relaxation Shear
Ebara et al., 1996	Multi	Circumferential	Quasi-static Tension
Fujita et al., 1997	Multi	Radial	Quasi-static Tension, Dynamic Tension
Iatridis et al., 1998	Multi	Axial, Radial	Relaxation Confined Compression
Iatridis et al., 1999	Multi	Axial Plane	Dynamic Shear
Fujita et al., 2000	Multi, Single	Multi-Planar	Relaxation Shear
Klisch & Lotz, 2000	Multi	Axial, Radial	Relaxation Confined Compression
Elliott & Setton, 2001	Multi	Axial, Radial, Circumferential	Quasi-static Tension
Bass et al., 2004	Multi	In-Plane	Quasi-static Biaxial Tension
Kasra et al., 2004	Multi	Axial	Dynamic Tension to Failure
Wagner & Lotz, 2004	Multi	Circumferential	Quasi-static Tension, Unconfined Compression
Holzapfel et al., 2005	Single	Parallel to Fibre	Quasi-static Tension, Dynamic Tension
Iatridis et al., 2005	Multi	Circumferential	Quasi-static Tension to Failure

3.5   Nucleus Pulposus Mechanics

The nucleus pulposus has not been as extensively studied as the annulus fibrosus, primarily because there has always been the notion that the nucleus was simply an inviscid fluid (Iatridis et al., 1996). More recent testing has shown these assumptions to be false. A dynamic shear study was done to identify the viscoelastic properties of the nucleus pulposus. Under dynamic conditions, the nucleus was found to exhibit viscoelastic-solid like characteristics, with low energy dissipation (Figure 3-16) (Iatridis et al., 1996). However, in a relaxation-type loading condition, the equilibrium stress of the nucleus approached zero, acting as a viscoelastic-fluid (Iatridis et al., 1996). Preliminary analysis of the full cervical spine in impact has revelaed that the nucleus pulposus undergoes a significant amount of shear (up to 65%) due to the relative motion between adjacent vertebrae.

It was also shown that healthy nucleus pulposus has a bulk modulus slightly less than that for water (Yang and Kish, 1988).
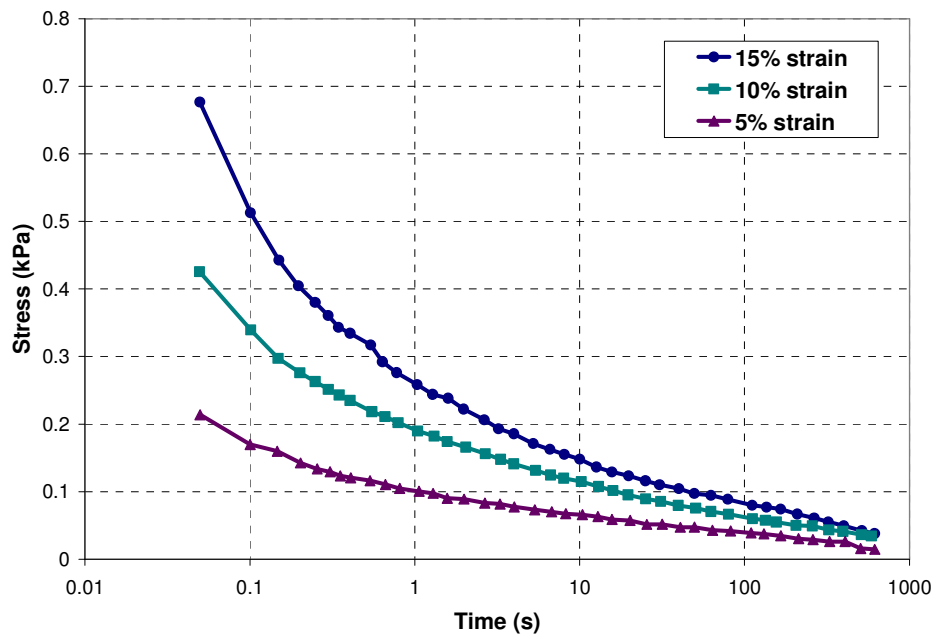
(Reproduced from Iatridis et al., 1997)

Figure 3-16: Shear Relaxation Response for Nucleus Pulposus

3.6 Ligament Mechanics

Quantification of cervical spine ligament behaviour is essential for predicting the functionality of the head and neck during impact loading. As ligaments help maintain the head and neck in a safe range of

motion, accurate definition of the load-deflection characteristics is essential for producing physical behaviour of the cervical spine within the safe range of motion, as well as on the verge of traumatic response. A summary of the available literature for cervical spine failure force and failure deflection can be found in Table 3-5 and Table 3-6.

3.6.1 Ligament Mechanical Behaviour

As with most soft-tissue biological material, testing and quantifying ligaments is often difficult, as most tests are destructive to the ligaments, and require gross-dissection of post-mortem subjects. Ligaments do not support compressive loads and are only effective in uniaxial tensile loading (Yoganandan et al., 2001). This simplifies both the experimental methods and numerical modelling approach to ligament mechanics.

Ligaments are composed of a mixture of elastin and collagen fibres organized in a uniform direction. The share of each of these proteins and the orientation of the collagen fibre are responsible for the mechanical behaviour of the tissue (Panjabi et al., 1998). Ligaments that are high in elastin content, such as the ligamenta flava, tend to be more resilient and are capable of undergoing large deformation without damage (Shim et al., 2006). Ligaments high in collagen content, such the alars and the transverse ligament are much stiffer and do not significant stretch prior to ligament failure (Dvorak and Panjabi, 1987). The interaction between the elastin and collagen fibre also characterizes the mechanics of the ligament.

The load-displacement response of a ligament loaded in uniaxial tension is similar to a sigmoidal curve (Chazal et al., 1985; Yoganadan et al., 1989a; Shim et al., 2006). This type of mechanical behaviour is very similar to the uniaxial tension response of a lamina of annulus fibrosus, also a collagen fibre-dominated tissue. The shape of the response can be broken down into three distinct regions (Figure 3-17).

An initial low-stiffness phase called the 'toe' region occurs as the collagen fibres are engaged and straightened. Stiffness gradually increases as more collagen fibres reach a straightened state, until the overall ligament exhibits a phase of linear stiffness (Chazal et al., 1985; Panjabi et al. 1998). The linear region of the load-displacement response of the ligament continues until the ligament begins to damage (likely the result of individual collagen fibres breaking). This region is known as the sub-traumatic region and is defined by the stiffness of the ligament softening until a point where the maximum load is reached, and the ligament begins to rupture (Chazal et al., 1985). It has been shown that loading into the sub-traumatic region results in permanent deformation, seen as an increase in the

length of the 'toe' region upon reloading (Provensano et al., 2001). A study by Chazal et al. (1985) looked specifically at the shape of this curve, and identified where each of the three regions existed in spinal ligaments. The results of this study are found in Table 3-4.
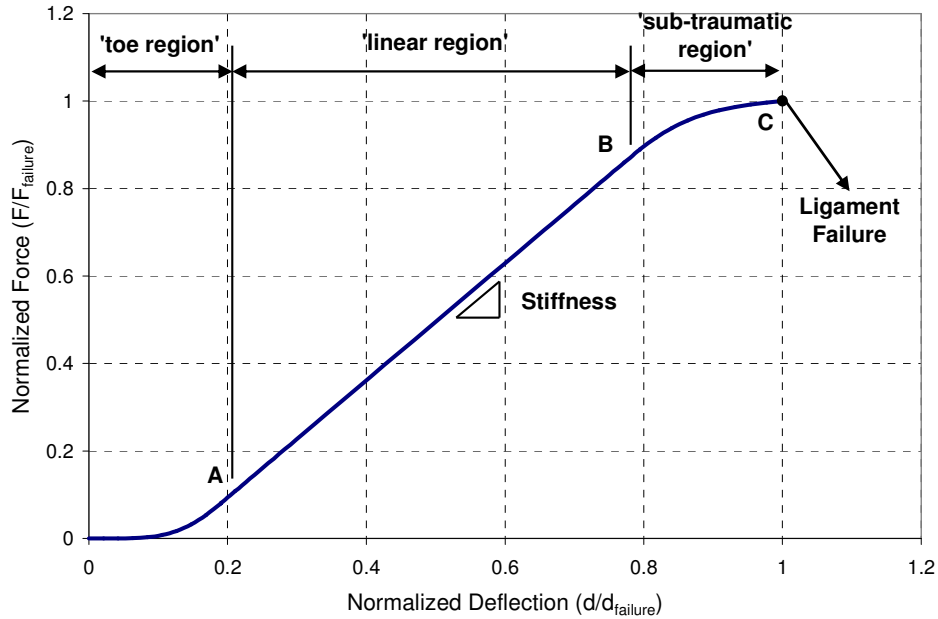
Figure 3-17: Normalized Load-Displacement Response of a Ligament

The 'toe' region of the load-displacement curve occupies the first 20 % – 25 % of displacement when considering the entire deformation to failure for the ALL and PLL (Chazal et al., 1985). This region is slightly longer for elastin-rich ligaments such as the LF and the ISL, having a 'toe' region roughly 30% of total deformation. The force at the end of this region around 10% of failure force for the ALL and PLL, and approximately 20% of failure force for the LF and ISL (Chazal et al., 1985).

Table 3-4: Normalized Force-Deflection Values for Defining Ligament Curve

Ligament	Point A (End of Toe Region)		Point B (End of Linear Region)	
	Deflection	Force	Defection	Force
ALL	21.1 %	10.8 %	77.2 %	85.9 %
PLL	25.0 %	9.8 %	77.3 %	77.9 %
LF	28.6 %	20.9 %	76.2 %	89.3 %
ISL	30.8 %	20.1 %	74.4 %	90.9 %
Average	26.4 %	15.4 %	76.3 %	86.0 %

The onset of the sub-traumatic region is consistent between the ligaments of the lower and middle cervical spine. Sub-traumatic behaviour begins at approximately 75% of the failure deformation, and has a force that is just under 90% of the failure force (Chazal et al., 1985). Using this information, along with experimentally measured failure force and failure deformation data, load-displacement

characteristics for ligaments can be generated. This load-displacement shape information must be assumed for the upper cervical spine ligaments since shape data does not exist for these ligaments.

Few experimental studies have been done on transverse and shear loading of ligaments (Quapp and Weiss, 1998). While results of these studies have shown that both transverse (perpendicular to fibres) and shear loading have a nonlinear response due to the underlying matrix, these are dramatically lower than the response in the uniaxial direction, justifying the 1-D approach to quantifying ligament properties (Quapp and Weiss, 1998; Weiss et al., 2001).

3.6.2 Ligament Viscoelasticity

The ligaments display a significant stiffening response when loaded at high rates of deformation (Yoganandan et al., 1989a; Panjabi et al., 1998; Shim et al., 2006). The shape of the load-displacement response at high rates is similar to the response at quasi-static rates, exhibiting the same three regions as seen in Figure 3-17 (Shim et al., 2006). However, at high rates, the length of the 'toe' region shortens and the stiffness of the linear region increases (Panjabi et al., 1998; Shim et al., 2006). The decrease in 'toe' region is caused by the viscoelastic behaviour of the biological matrix not allowing the collagen fibres to straighten completely (Panjabi et al., 1998). The results from the study by Yoganandan et al (1989a) show an increase in stiffness over a range of loading rates (Figure 3-18).
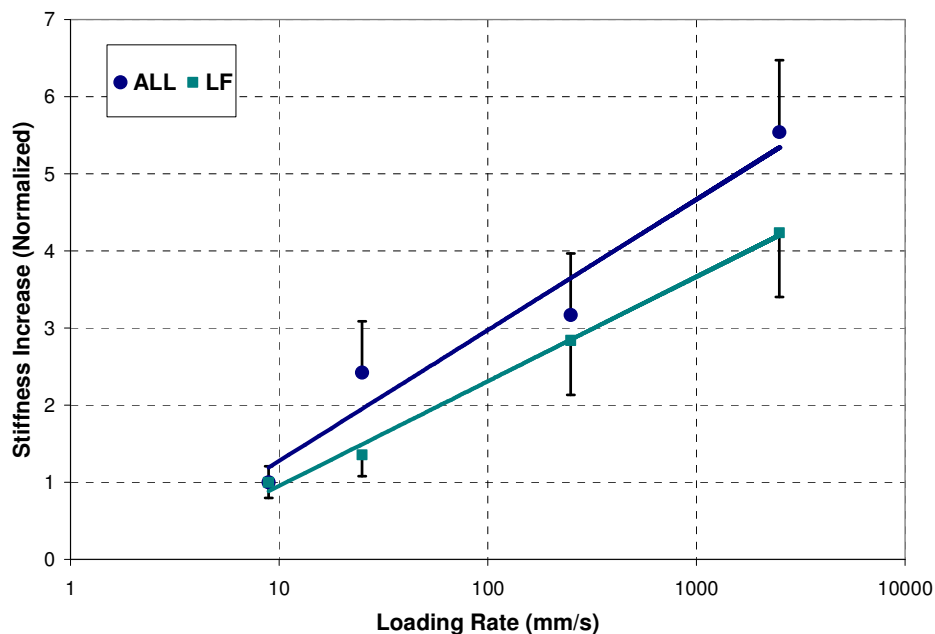
(Reproduced from Yoganandan et al., 1989a)

Figure 3-18: Stiffness Increase for Various Rates of Loading for ALL and LF

3.6.3   Ligament Injury and Failure

In whiplash injuries, ligament trauma is more common than bone-related injury (Maak et al., 2006). Despite this, many specific injury mechanisms associated with ligaments in the cervical spine remain unknown (Maak et al., 2006). Injury is often difficult to identify in the cervical spine ligaments, since sub-traumatic failure often occurs prior to gross ligament failure, and often shows little or no evidence to any type of injury (Winkelstein et al., 2000b). Sub-traumatic damage has been shown to reduce the mechanical properties of the ligament and lengthen the 'toe' region of the force-displacement curve, which results in an increase in joint laxity because of torn or plastically deformed fibres (Panjabi et al., 1996; Provenzano et al., 2002). This will often occur at loads around 40 – 50% of the total rupture force (Siegmund et al., 2001; Lee et al., 2006).

The rate of ligament loading also has an effect on the failure characteristics; however, the effect is often debated (Yoganandan et al., 1989a). High-rate tests by Yoganandan et al (1989a) and Winkelstein et al (2000a) found that increasing the rate of deformation increased the force at ligament failure, but did not significantly effect the deformation at ligament failure. Conversely, the studies by Panjabi et al (1998) and Shim et al (2006) revealed that the high-rate failure strain was greatly reduced from the quasi-static failure strain.

Table 3-5: Summary of Failure Properties of Ligaments of the Middle and Lower Cervical Spine

Study	Spine Level	Rate (mm/s)	ALL		PLL		LF		CL		ISL	
			F_f (N)	d_f (mm)	F_f (N)	d_f (mm)	F_f (N)	d_f (mm)	F_f (N)	d_f (mm)	F_f (N)	d_f (mm)
Yoganandan et al., 1989a	C2-T1	9	121	7.5			131	7.6				
		25	122	5.5			118	5.7				
		250	166	6.4			182	6.3				
		2500	349	6.3			335	8.0				
Myklebust et al., 1988	C0-C1	9	232	18.9			83	18.1	315	11.4		
	C1-C2		263	12.3			111	8.7	315	11.4		
	C2-C3		207	8.7	84	9.6	87	5.8	211	8.9	37	7.0
	C3-C4		47	4.2	82	7.4	75	3.7	240	8.8	33	6.6
	C4-C5		47	4.8	47	3.4	56	12.8	170	9.1	26	6.9
	C5-C6		89	5.0	85	4.8	89	8.0	144	8.7	33	5.5
	C6-C7		176	13.7	102	5.0	160	7.7	277	10.0	31	9.2
	C7-T1		97	7.6	95	6.4	221	9.9	264	6.8	45	8.7
Winkelstein et al., 2000b	C3-C4, C5-C6	0.0083							84.2	5.8		
		100							118.1	5.8		
Yoganandan et al., 2001	C0-C1	9	232	18.9			83	18.1	320	9.9		
	C1-C2		263	11.8			111	9.6	314	9.3		
	C2-C5		93	5.8	71	3.5	121	6.5	120	10.2	39	6.3
	C6-T1		145	6.5	188	6.1	129	9.4	181	7.8	39	6.7

* AAOM, AAAM, PAOM, PAAM are listed in their ALL and LF counterparts

Table 3-6: Summary of Failure Properties of Ligaments of the Upper Cervical Spine

Study	Spine Level	Rate (mm/s)	TM		TL		Apical		Alar		CLV	
			F_f (N)	d_f (mm)	F_f (N)	d_f (mm)	F_f (N)	d_f (mm)	F_f (N)	d_f (mm)	F_f (N)	d_f (mm)
Dvorak et al., 1988	C012				354				214			
Myklebust et al., 1988	C012	9	76	11.9			214	11.5	357	14.1	436	25.2
Panjabi et al., 1998	C012	920			436	0.4			367	0.4		
Yoganandan et al., 2001	C012	9	76	11.9			214	8.0	357	14.1	436	12.5

3.7   Muscle Mechanics

Muscle mechanics is a complicated subject because muscle tissue is unlike any other tissue in the human body. Muscle tissue properties change depending on the state of activity (contraction). Thus, muscle response can be divided into two components: an active (contracted) component, and a passive (relaxed) component. The act of contracting a muscle can be both a conscious effort and a subconscious one (due to autonomic or reflex processes).

The focus on this section will be on macroscopic muscle mechanics rather than microscopic mechanics. The microstructural mechanics of muscle contraction involving microfibres and sarcomeres will not be discussed in this section. Complex electro-chemical process of axons and ions causing muscle contraction will not be discussed.

3.7.1   Passive Muscle Behaviour

Unlike many other tissues in the human body, the mechanical properties of muscle tissue vary significantly depending on testing time from post-mortem (Van Ee et al., 2000a; Van Slightenhorst et al., 2006). This change in post-mortem mechanical properties is particularly noticeable in a phase called rigor mortis, where the stiffness of the muscle increases drastically between five hours post-mortem and 30 hours post-mortem (Van Ee et al., 2000a; Van Slightenhorst et al., 2006). This change in the mechanical behaviour of muscle is due to microstructural alterations from the variation of ionic concentration and enzymatic activity in post-mortem tissue (Myers et al., 1995).

The mechanical properties of muscle exhibit nonlinear, viscoelastic behaviour that is capable of large physiological deformation, while having a variable cross-section. The tissue properties are further complicated by the fact that mechanical properties are sensitive to hydration, temperature, muscle fitness, and the post-mortem period (Myers et al., 1995). This may be a reason why engineering stress-strain behaviour for skeletal muscle has not been extensively reported (Myers et al., 1995). Furthermore, the focus of most muscle research has been testing full *in vivo* animal muscle in tension rather than samples of muscle tissue.

Myers et al (1995) tested rabbit tibialis anterior muscle in tension at different rates (1, 10, and 25 1/s) and the results were that the muscle had a nonlinear response (passive) that was found to have a slight

dependency on strain rate. The results from the passive muscle testing in this study can be seen in Figure 3-19. Other studies have produced results showing the nonlinear response of passive muscle in tension (Yamada, 1970; Hawkins and Bey, 1997; Van Ee et al., 2000; Davis et al., 2003).

Unlike tension, studies into the response of passive muscle in compression are limited (Van Slightenhorst et al., 2006). McElhaney et al (1966) and Van Slightenhorst et al (2006) tested bovine muscle tissue at very high rates (between 1000 1/s and 2300 1/s) and found that the response was significantly rate-dependant. A typical response of bovine muscle tissue at high rate compression using a split Hopkinson bar apparatus can be seen in Figure 3-20.
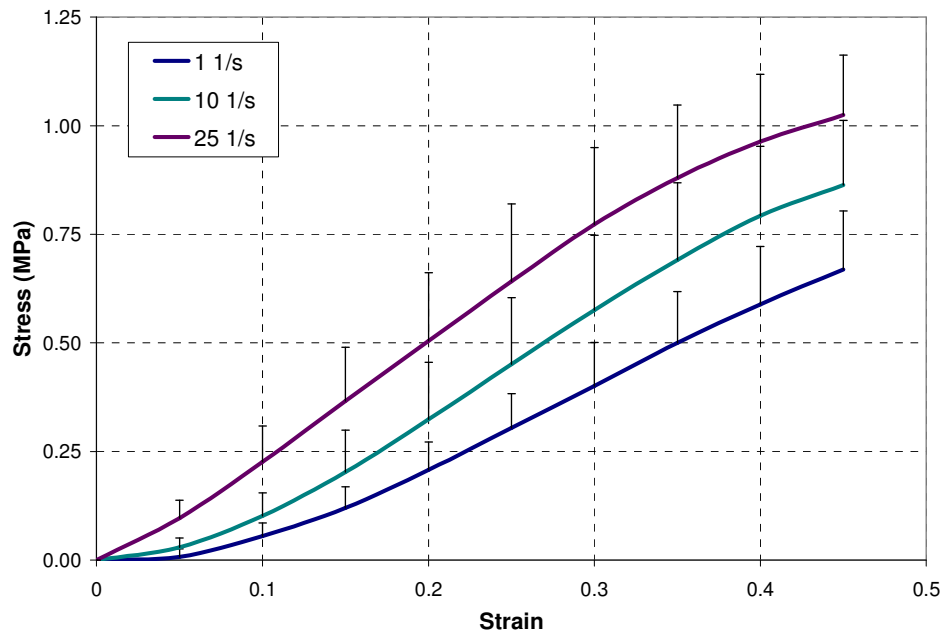
(Reproduced from Myers et al., 1995)

Figure 3-19: Engineering Stress-Strain of Passive Muscle at Various Elongation Rates
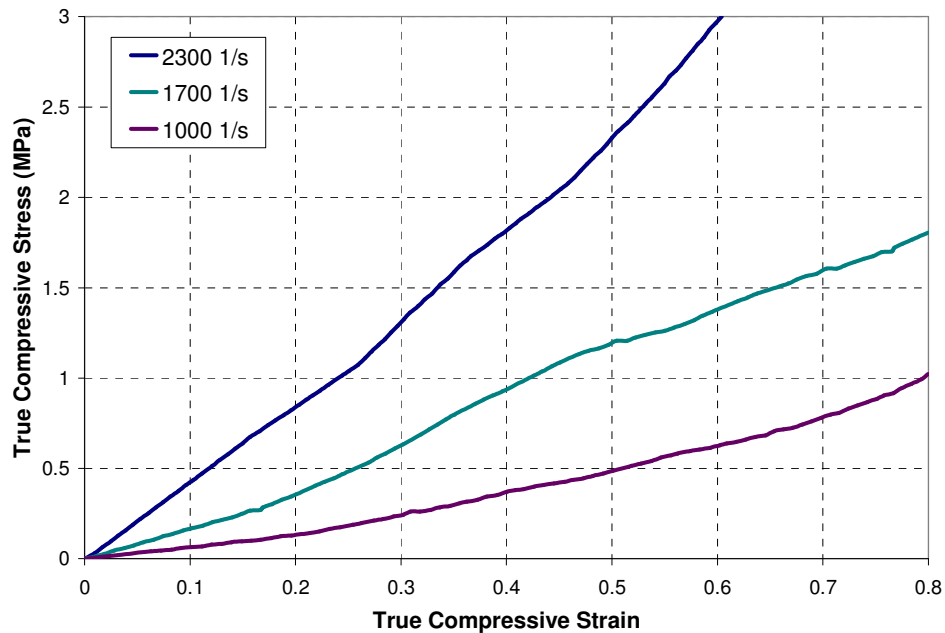
Figure 3-20: True Stress-Strain of Passive Muscle at High Compression Rates

3.7.2 Active Muscle Behaviour

Active muscle contraction is a complex biochemical process involving interaction between the central nervous system and the muscles, and the flow of ions and ATD/ATP molecules. A technique called electromyography (EMG) is often used to measure muscle activation response to nervous stimulation. An EMG test detects the electrical potential generated by muscles cells during contraction. However, most simulation studies use an idealized input for muscle activity using excitation dynamics (Winters and Woo, 1990). The idealized activation level ranges from 0 (completely passive) to 1 (completely activated), and is often used to scale the force generated in the muscle based on the force-tension and force-velocity relationships.

The force-tension relationship associates the amount force generated in the active muscle based on the relative length of the muscle (normalized to a reference or rest length). Muscle can achieve a maximum isometric force (F_{max}) at an optimum normalized length of approximately 1.05 (Winters and Woo, 1990). A current muscle that is shorter or longer than the optimum length will reduce the

muscles capability to generate force. When the muscle is approximately 40% or 150% the optimum length, the available force is nearly zero (Winters and Woo, 1990).

The shape of the force-length relationship resembles a Gaussian curve (solid lines), and can be seen in Figure 3-21 for various levels of muscle activation. The additive response of the passive muscle in tension (discussed in the previous subsection) can also be seen in Figure 3-21 as the dotted lines. Note that passive muscle response is not affected by muscle activation.
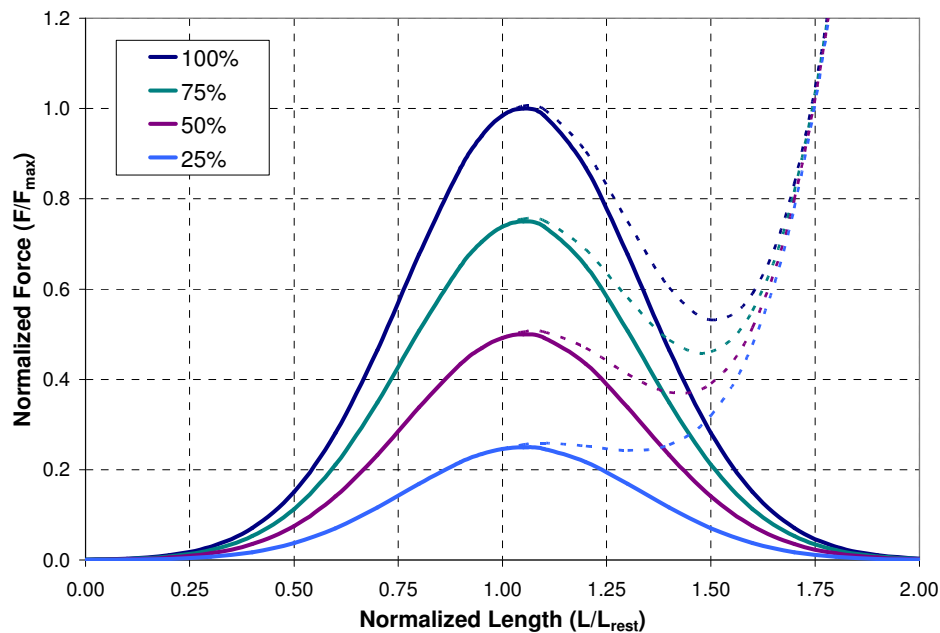
Figure 3-21: Isometric Muscle Force-Length Relationship for Various Levels of Activation

The force-velocity relationship associated the amount of force generated in the active muscle based on the relative velocity of the muscle (normalized to a reference velocity V_{max}). Negative muscle velocity is commonly referred to as 'muscle shortening', while positive muscle velocity is 'muscle lengthening'. When the muscle is shortening, the capacity for muscle force generation decreases nonlinearly until reaching zero at $-V_{max}$ (Winters and Woo, 1990). At zero velocity, the muscle is in its isometric state, and the muscle is able to generate maximum isometric force (F_{max}). A muscle that is lengthening will actually be able to generate more force than F_{max}, however the increase in force is asymptotic around 130% of the isometric force (Winters and Woo, 1990). The shape of the force-velocity relationship for various levels of activation can be seen in Figure 3-22.
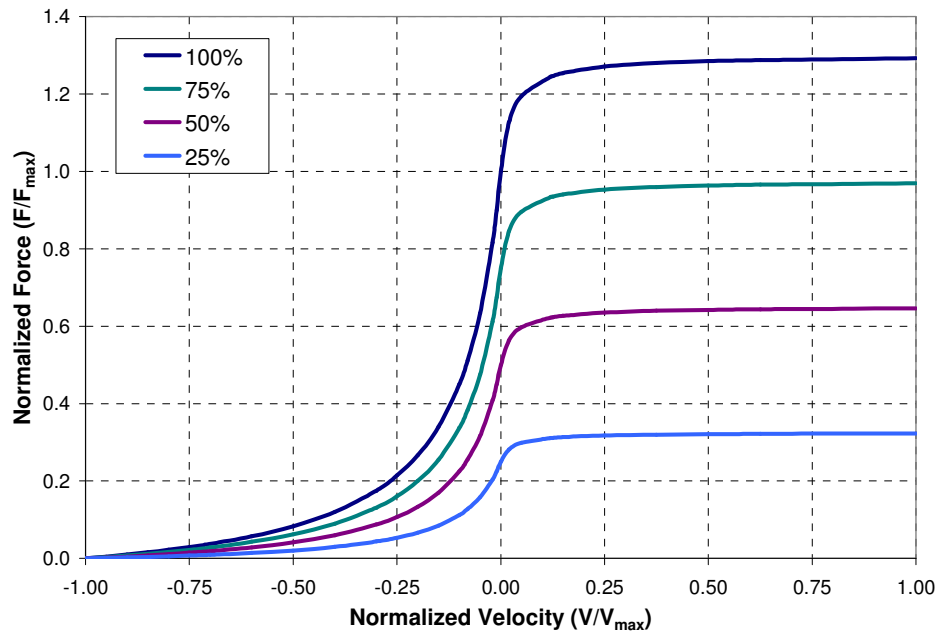
Figure 3-22: Muscle Force-Velocity Relationship for Various Levels of Activation

The relationship between the normalized force-length and force-velocity on the overall mechanics of activated muscle is productive (Winters and Woo, 1990). Mathematically, this means that both the force-length and the force-velocity phenomena of the muscle are independent of each other, and can be multiplied together to represent the capacity of the muscle to generate force. This can be seen in Figure 3-23, where the current state of the muscle (length and velocity) determines the maximum amount of force generated in the muscle.
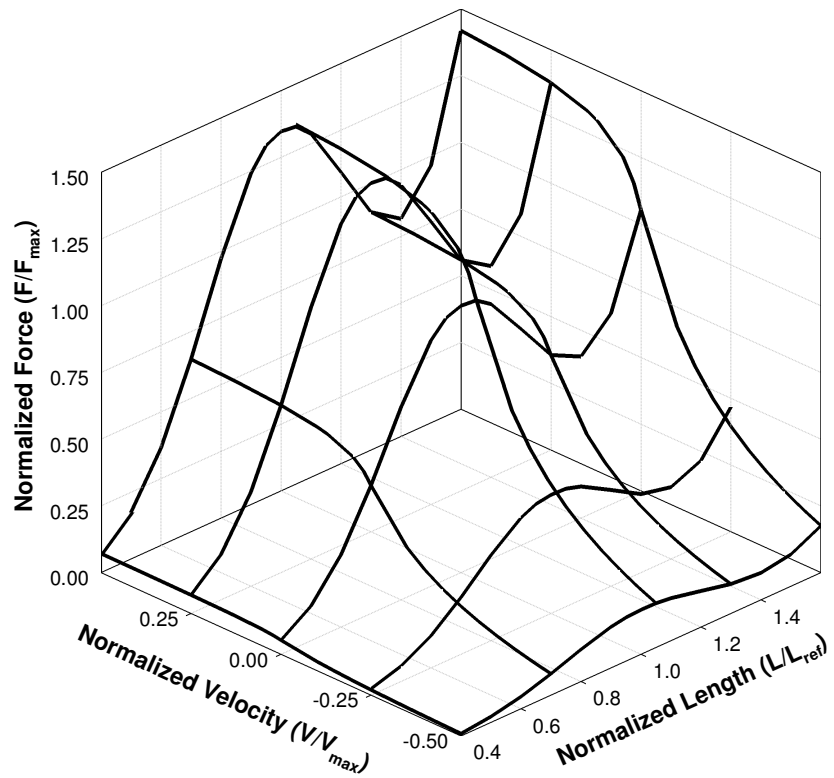
Figure 3-23: 3D Representation of Muscle Behaviour at 100% Activation

Chapter 4

Injury and Biomechanics of the Cervical Spine

Motion studies of the human cervical spine have been carried out for many years (Panjabi and Myers, 1990). There are four types of study commonly used to investigate the mechanical response of the human cervical spine. These are (in order of increasing complexity): spinal segment studies, isolated ligamentous spine studies, post-mortem human subject (cadaveric) studies, and human volunteer studies.

Spinal segment studies investigate the load-displacement characteristics of a section of the spine, often consisting of an *in vitro* vertebra-disc-vertebra motion segment. The typical procedure for a spinal segment study is to fix the inferior vertebra while applying a controlled load or displacement to the superior vertebra. While this method can provide simple and understandable load-displacement response of a single section of the cervical spine, the *in vitro* load and motion of the vertebra may not be realistic of the *in vivo* loads and motion of a living human. However, understanding the mechanics of the cervical spine at a localized (vertebral) level is essential for formulating many of the theories used for the global cervical spine.

A complex, but more realistic type of *in vitro* cervical spine study is done on isolated ligamentous spine. An isolated ligamentous spine is a full cervical spine (usually from C0 to C7 to T1) complete with all soft tissues, but devoid of any musculature. The advantage of using isolated ligamentous spines to study the spine biomechanics is that researchers are able to track the motion of spine during impact using techniques such as high-speed film. Furthermore, resultant injuries can be identified by observation or simple dissection. However, without the presence of neck muscle, isolated ligamentous spine research is mainly limited to axial compressive loading where the role of musculature is minimal.

To overcome the deficit of isolated ligamentous spines, post-mortem human subjects (PMHS) can be used to study the *in situ* mechanics and injury mechanisms of the cervical spine. The advantage of using PMHS to study the cervical spine is that the behaviour of the specimen is very similar to a live

human subject, without any active musculature response. In many impact cases, the loads applied to the person occur well before active muscle contraction can have an influence, making the response of a PMHS similar to live human subject. Furthermore, high levels of impact loads can be applied to the PMHS unlike in human volunteer testing, so PMHS are typically used to define some sort of injury tolerance rather than physiological loading. The downside to PMHS testing is apparent in longer-duration impacts where human reflexes play a significant role in the impact response. It is also difficult to instrument a PMHS to measure local response, and identifying resulting injury requires CT scan, X-Ray, or gross dissection.

Finally, human volunteer testing is the most effective type of study if understanding living phenomena is required. Phenomena such as active muscle response can have a significant influence on the impact biomechanics, as seen in simulated automotive impacts (Wismans et al., 1987). One of the disadvantages of using human volunteers is obviously the fact that the study is limited to physiologic levels of loading.

4.1 Cervical Spine Injury

The purpose of injury biomechanics research is to understand how injuries occur in order to better develop ways to prevent or minimize injury in the impact environment (Viano et al., 1989). Injury to the human body is caused by deformation of biological tissue beyond its physiological limits. This is often characterized in biological tissues by a change in biomechanical properties or physiological function. The rate at which deformation occurs is also an important factor in injury biomechanics, since the risk of injury is related to the impact energy delivered to the body (Viano et al., 1989).

Impact involving the head and neck is a complicated process that can ultimately lead to damage to the cervical spine and intrusion into the spinal cord. The types of injury that can occur to the human spine range from mild to fatal, and are often classified by a certain injury mechanism or loading process (King, 2000).

4.1.1 Epidemiology of Cervical Spine Injuries

Motor vehicle accidents (MVA) are one of the leading causes of cervical spine injury, causing 40 – 65% of all spine traumas (Yoganandan et al., 1989b). The cervical spine was the most commonly injured spine site in car accidents (50.7% of all spine injuries), but the least common spine injury in

motorcycle accidents (17.4%) (Robertson et al., 2002). For serious spine injuries of AIS 3 or greater, the cervical spine was the primary injury site (Figure 4-2) (Yoganandan et al., 1989b).

The reason behind neck injuries in automotive accidents is the magnification of acceleration between the vehicle and the head (White and Panjabi, 1990). This effect can be seen in Figure 4-1 where the occupant's head and shoulder lag the vehicle in a frontal crash scenario. Because the shoulder lags the vehicle, the magnitude of acceleration required to stop the shoulder increases. Furthermore, the head lags the shoulder, causing an even higher magnitude of acceleration. Thus the head, supported by the neck, undergoes amplified loading, even for relatively minor accidents. Finally, the relative load between the head and shoulders is carried by the cervical spine, causing the injury seen in automotive crash.
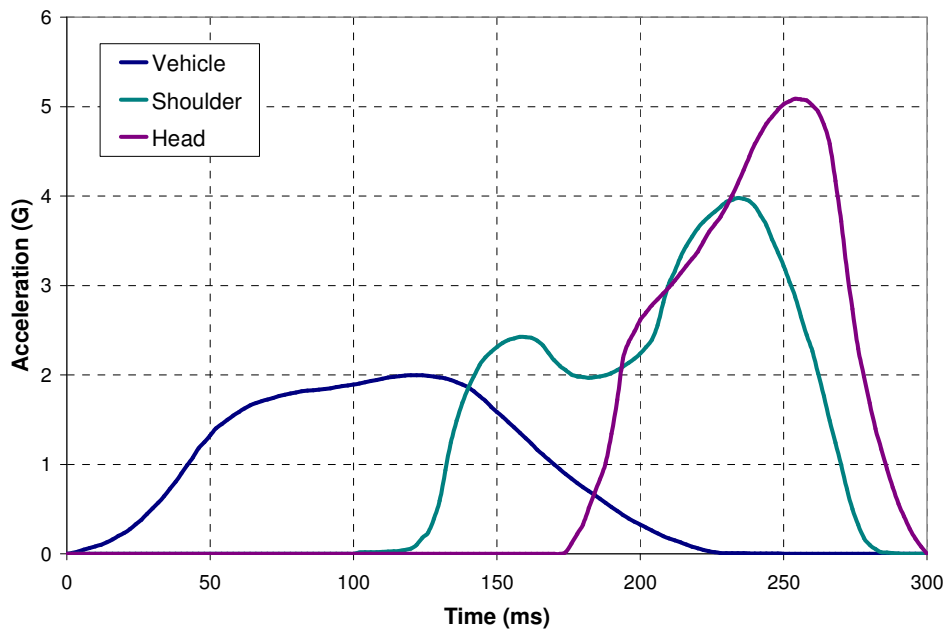
Figure 4-1: Example of Acceleration Magnification of the Shoulder and Head in Frontal Crash

Minor injuries, such as those to the soft tissues, occur in 16% of all MVA (Morris and Thomas, 1996). While the majority of soft tissue injuries occur in the frontal impacts (over 50%), rear impacts have a much higher incidence rate of soft tissue injuries than any other type of MVA (Yoganandan et al., 1989b; Morris and Thomas, 1996). Minor soft tissue injury occurring in rear impacts is commonly referred to as 'whiplash'. However, serious injuries to the cervical spine are more likely to occur in rollover-type MVA (see Figure 4-3 and Figure 4-4).
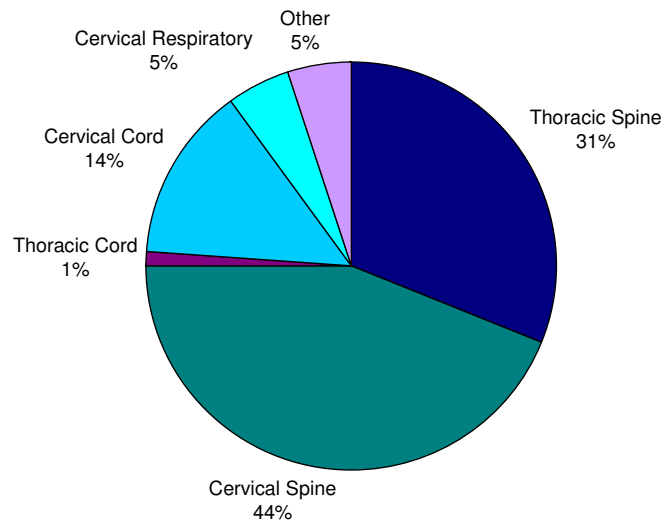
Figure 4-2: Distribution of AIS 3+ Injuries of the Spine in MVA
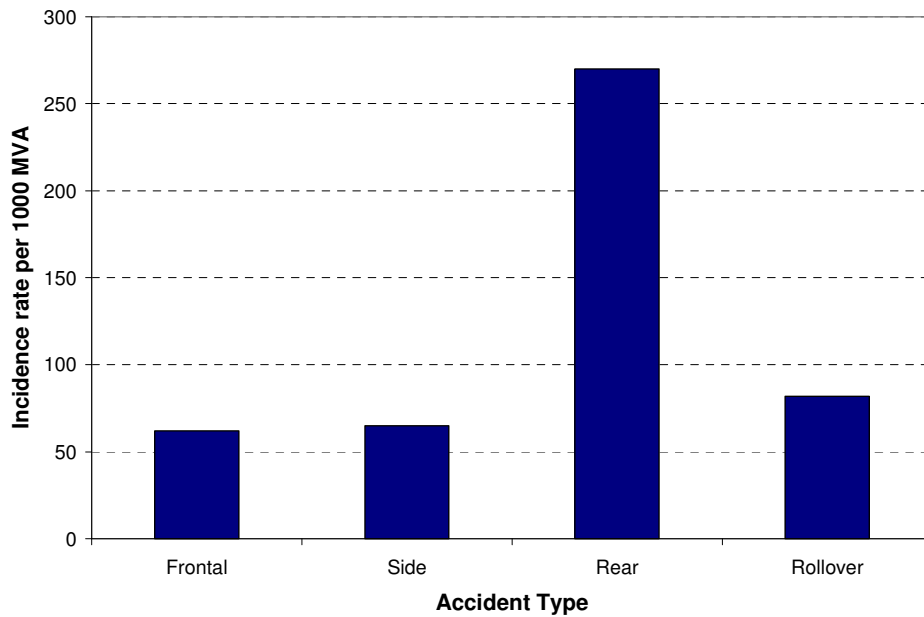
Figure 4-3: Incidence Rates (per 1000 accidents) by Crash Type for AIS 1 (Minor) Injuries
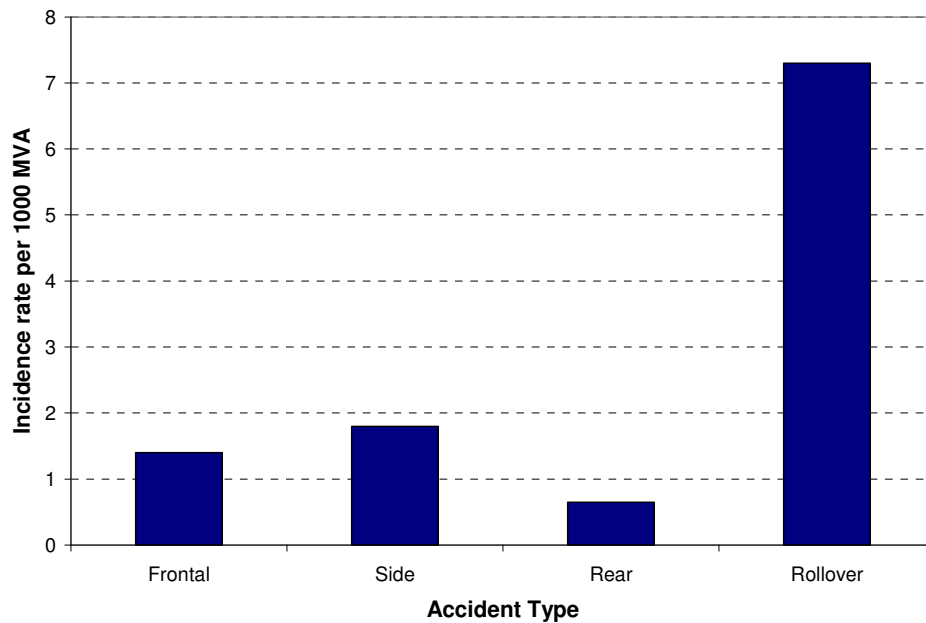
Figure 4-4: Incidence Rates (per 1000 accidents) by Crash Type for AIS 3+ (Serious) Injuries

Cervical spine injuries tend to occur in a few areas of the cervical spine. A study by Daffner et al (2006) found that the upper cervical spine (C0-C2) was the most frequent site of vertebral fracture caused by any type of trauma. The high frequency of upper cervical spine fractures is likely due to its relatively low resistance to motion, aided by the fact that the joint directly connects the heavy head to the rest of the cervical spine. The prominent odontoid process is also susceptible to fracture from translational loading (White and Panjabi, 1990).

The most common type of cervical fracture was to the vertebral body (26% of all fractures) and articular pillars (23% of all fractures) (Daffner et al., 2006). These findings agreed with Robertson et al (2002), who only looked at spine injuries in MVA. The distribution of cervical spine fractures can be seen in Figure 4-5.
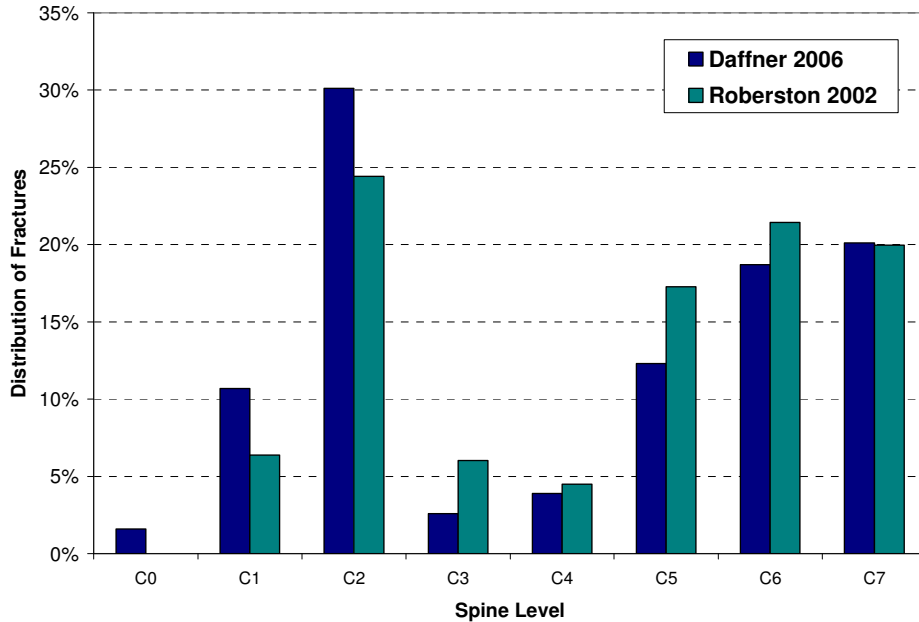
Figure 4-5: Distribution of Cervical Spine Fractures in MVA

4.1.2   Classification of Injury

Classification of the injury mechanisms of the cervical spine is an important communication tool within and between epidemiological, clinical, and biomechanical fields (Carter, 2002). Numerous classification schemes for cervical spine injury have been described in the literature, with no specific scheme universally accepted (Carter, 2002). The scheme for the lower cervical spine injuries described by Argenson et al (2002) is a simple scheme based on injuries produced by a dominate force vector. This classification scheme is described in this section.

Cervical spine injuries are classified as either Type A (compression), Type B (flexion-extension-distraction), and Type C (rotation) injuries (Argenson et al., 2002). Each type of injury was subdivided into three severity levels (I, II, and III). In a study conducted from trauma patients admitted between 1980 and 1994 in France, the three injury classifications (A, B, and C) occurred with equal frequency (Argenson et al., 2002). The breakdown of the frequency of each type of injury, including severity level, can be seen in Figure 4-6.
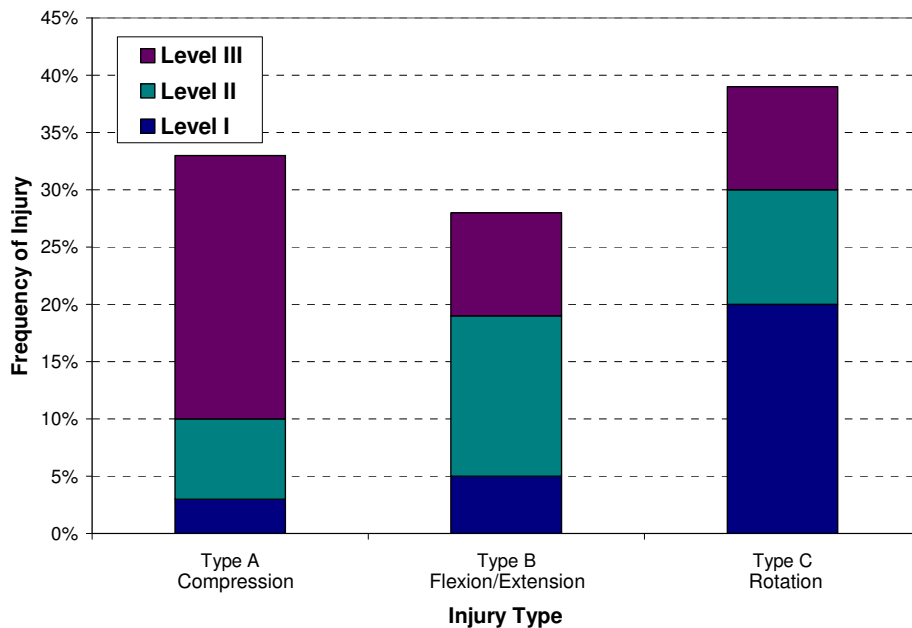
Figure 4-6: Frequency of Cervical Spine Injuries based on Classification Scheme

Compression injuries (Type A) were marked by mainly bone trauma (Figure 4-7). Level I severity is defined by anterior vertebral body compression (wedge fractures). Level II compression injuries are comminuted fractures (burst fractures). Teardrop fractures represent Level III compression injuries, and are influenced by a slight flexion mechanism.
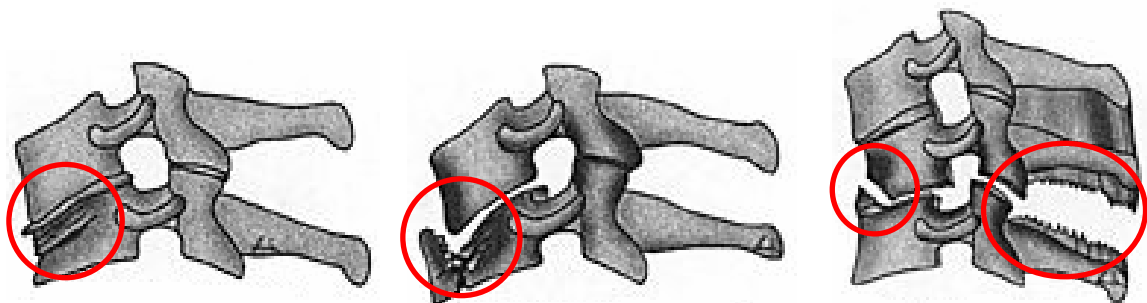
I – Anterior Wedge Fractures   **II – Comminuted Fractures**   **III – Teardrop Fractures**

Figure 4-7: Type A – Compression Injuries of the Lower Cervical Spine

Flexion-extension-distraction injuries (Type B) involve sagittal plane rotations, and the associated distraction (tension) seen on the tissues (Figure 4-8). Moderate sprains (Level I) are common injuries that include 'whiplash' injury. However, only BI injuries that were accompanied by slight

neurological deficits were counted in the study, resulting in an occurrence of 5% of all trauma cases. Level II severity injuries (severe sprains) are marked by posterior longitudinal ligament damage, and result in soft tissue injuries to the intervertebral disc and posterior ligaments, and spinous process fracture. Level III injuries include bilateral fractures and/or dislocation.

| **I – Moderately Sprains** | **II – Severe Sprains** | **III – Bilateral Fracture-Dislocation** |

(Adapted from Argenson et al., 2002)
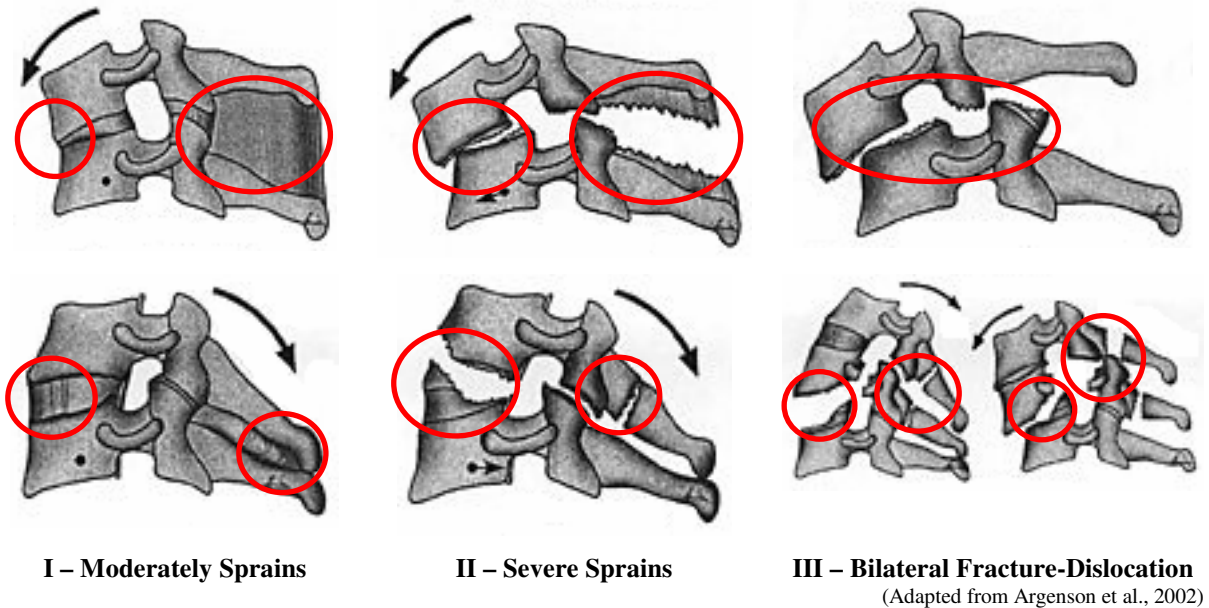
Figure 4-8: Type B – Flexion-Extension-Distraction Injuries of the Lower Cervical Spine

Rotation injuries (Type C) involve axial rotations, which are usually associated with lateral bending due to the mechanical behaviour of the cervical spine (Figure 4-9) (White and Panjabi, 1990). Level I rotation injuries are single facet fractures, whereas level II rotation injuries are fractures of the articulate pillars resulting in separation from the vertebra. Unilateral dislocation injuries are the level III rotational injuries.

| **I – Unifacet Fracture** | **II – Fracture Separation** | **III – Unilateral Dislocation** |

(Adapted from Argenson et al., 2002)
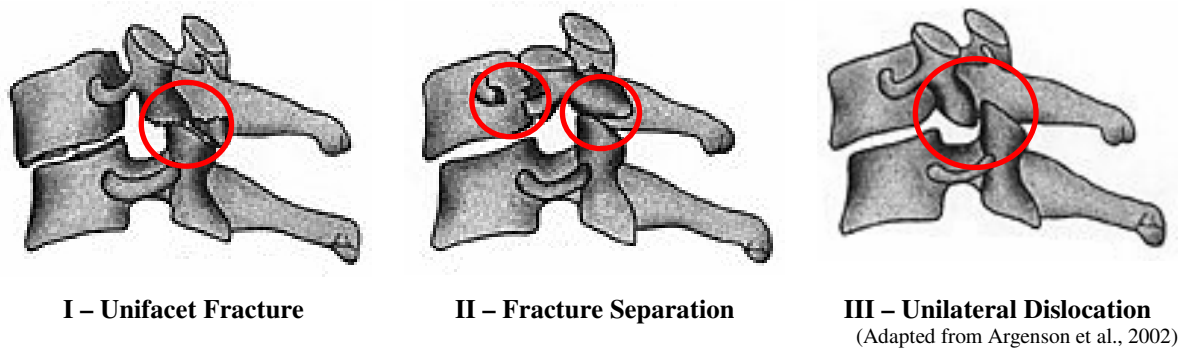
Figure 4-9: Type C – Rotation Injuries of the Lower Cervical Spine

Injury severity is often rated based on the Abbreviated Injury Scale (AIS) or some variation of this scale. First introduced in 1971 by the Association for the Advancement of Automotive Medicine (AAAM), the AIS system is universally accepted as the foundation of injury severity scaling systems. The AIS is used by trauma clinicians, trauma data managers, injury researchers, and public health and policy professionals. The AIS for the cervical spine is found in Table 4-1.

Table 4-1: Abbreviated Injury Scale Description for the Cervical Spine

AIS Score	Description	Possible Injuries
1	Minor	Minor strain with no fracture or dislocation (Whiplash)
2	Moderate	Compression fracture C1-C7 < 20% loss in height of vertebral body
		Fracture and/or dislocation/subluxation of the spinous process, transverse process, or atlanto-occipital joint
		No spinal cord injury
3	Serious (non life-threatening)	Compression fracture/subluxation
		Spinal cord contusion/compression with or without transient neurological signs (weakness, paralysis, loss of sensation)
		Disc rupture/herniation with nerve root damage
		Fracture and/or dislocation/subluxation of the lamina, body, facet, pedicle, or odontoid process
4	Sever (life-threatening)	Lesion (incomplete cord syndrome with preservation of some sensation or motor function)
5	Critical	Vertebral crush (C4 or below)
		Cord laceration (C4 or below)
		Complete cord syndrome (quadriplegia or paraplegia with no sensation) (C4 or below)
		Total transaction (C4 or below)
6	Fatal	Vertebral crush (C3 or above)
		Cord laceration (C3 or above)
		Complete cord syndrome (quadriplegia or paraplegia with no sensation) (C3 or above)
		Total transection (C3 or above)

4.1.3 Injury Criteria

Various post-moterm human subject studies have investigated the human tolerance limits of the neck, and a number of criteria have been developed to predict neck injury. These criteria are applied to the response of the head and neck of the Hybrid III crash test dummy to assess the potential for injury. It is possible to apply these criteria to human volunteer and post-moterm human subject tests by converting the rigid-body motion of the head into axial force and bending moments at the occipital condyles (Mertz and Patrick, 1971).

The most commonly used neck injury criteria is the N_{ij} criteria, which is currently supported by Federal Motor Vehicle Safety Standards and Regulations 208 as the occupant neck load limit in frontal crash (National Highway Traffic Safety Administration, 2002). It should be noted that this

criterion is only valid for neck motion in the extension/flexion direction, and assumes that no lateral force or bending moment is present (Eppinger et al., 1999).

The N_{ij} criterion takes into account the combination of extension/flexion moment and the tension/compression load on the neck (Eppinger et al., 1999). The resulting neck loading can be plotted on a graph, where neck loads within the critical intercepts are considered safe. The critical intercepts for the 50th percentile male are 6160 N in compression, 6806 in tension, 310 Nm in flexion, and 135 Nm in extension. The graphical for the N_{ij} criterion for a 50th percentile male can be seen Figure 4-10 where the shaded area is considered safe. An N_{ij} value of 1 corresponds to probably of 22% for an AIS 3 injury to occur.
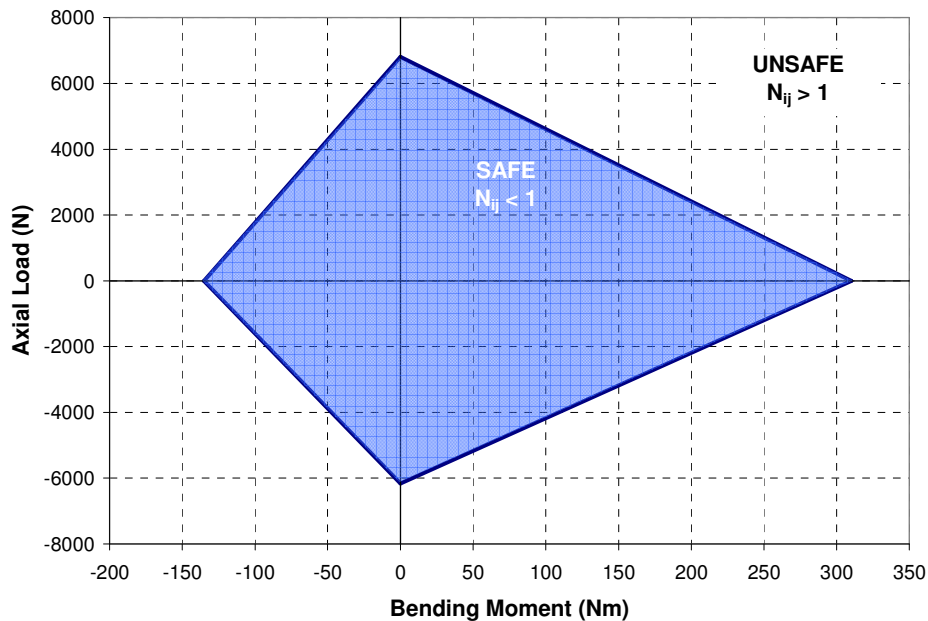
Figure 4-10: Nij Criterion for 50th Percentile Male

The N_{ij} criterion can be evaluated mathematically by normalizing the moment and axial loads with the corresponding critical intercept values, which were determined by experiment. This would allow for a basic formulation that can be used for various sized humans with different critical intercept values (Eppinger, 1999). The N_{ij} is calculated based on the following expression:

$$N_{ij} = \frac{F_z}{F_{zc}} + \frac{M_{ocy}}{M_{yc}} < 1.0$$

Equation 4-1

where F_z is the tension/compression force measured at the C1 vertebrae (equivalent location to the upper load cell of the Hybrid III crash test dummy) and M_{ocy} is the occipital bending moment. These values are measured and calculated concurrent in time (Eppinger et al., 1999).

An additional neck injury criterion was developed by Bostrom et al (1996) specifically for dealing with crash test dummies in rear-impact collisions, called the Neck Injury Criterion (NIC). The NIC evaluates the injury based on the relative acceleration between the upper and lower neck, as well as the corresponding relative velocity (Bostrom et al., 1996). The NIC is calculated based on the following set of equations:

$$NIC = 0.2 \cdot a_{rel} + v_{rel}^2 \qquad \textbf{Equation 4-2}$$

where a_{rel} is the difference between the acceleration of the T1 vertebra and the head, and v_{rel} is the integral of a_{rel}. The suggested human tolerance of NIC is 15 m^2/s^2, but this criterion is still considered in development and not supported in FMVSS 208 (Yoganandan et al., 2000b).

However, an additional load limit is specified by FMVSS 208 in addition to the N_{ij} criterion. The peak tensile force in the upper loading cell of the Hybrid III dummy (equivalent to C1 vertebrae) allowable under FMVSS 208 is 4170 N, while the peak compressive force is 4000 N. These forces are lower than the intercepts used in N_{ij} for axial force.

4.2 Cervical Spine Segment Studies

A spine segment consists of a section of the cervical spine complete with the ligaments but void of any musculature. Typically, spinal segments are made up of a vertebra-disc-vertebra unit (also known as a functional spinal unit). The entire cervical spine is made up of six typical spinal segments (for the six intervertebral discs), with each segment described by the two associated vertebra. For this thesis, the upper cervical spine joint (C0-C1-C2) will also be considered a spine segment, although it does not have an intervertebral disc.

A study by Goel et al (1988a) examined the upper cervical spine under small bending moments (0.3 Nm). It was reported that relatively small applied loads produced large rotations, supporting the idea that the occipital-atlanto-axial ligaments are lax and that the head is chiefly stabilized by muscle

activity. Furthermore, 85 – 90% of axial rotation in the upper cervical spine occurred between the C1 and C2.

For the response of the cervical spine to translational loading, Panjabi et al (1986) looked at the three-dimensional response of the cervical spine segment in compression, tension, and shear. Compression was found to have a coupled extension motion, whereas tension had a coupled flexion motion. Anterior and posterior shear also had coupled flexion and extension motions respectively. The cervical spine segment was found to be least flexible in compression and most flexible in anterior shear, with tension, posterior and lateral shear being roughly equal in stiffness.

A study by Moroney et al (1988) looked at the load-displacement relationship of 35 adult cervical spines in compression, shear, flexion, extension, lateral bending, and axial rotation. A preload of 49 N was applied at the disc centre to each segment prior to testing. The results of these tests were significantly stiffer than previous spine tests. These results were thought to be influenced by differences in experimental techniques and reporting methods, as well as the preload. Furthermore, the results of the cervical spine segments were pooled together, so load-displacement properties for each level were unidentifiable.

Like Moroney et al (1988), Shea et al (1991) examined the load-displacement relationship of cervical spines, however using two-segment specimens rather than single segments. Linear stiffness values were reported for the 18 cervical spines in compression, tension, anterior-posterior shear, and flexion-extension. These results were compared to previous single segment studies by doubling the reported stiffness values of two segments, based on the assumption that each segment had equal stiffness. This study also looked at the effect of pre-torsion on the spine segments, finding that 'toe' region of response was reduced and the stiffness increased.

Another study by Panjabi et al (2001b) looked at the three-dimensional load-displacement response of all cervical spine motion segments (except C7-T1) in flexion, extension, lateral bending, and axial rotation. The neutral zone (0 Nm) and range of motion (1 Nm) was reported for each segment level. Key findings in this study were that a flexion-anterior shear and extension-posterior shear coupled motions were present at all cervical spine levels, and that coupled axial rotation was in the same direction as the lateral bending at all cervical spine levels.

A collection of studies by Nightingale et al (2002, 2006) examined the flexion/extension response of cervical spine segments over a range of applied moments up to 3.5 Nm. The nonlinear stiffening results of each study were conveniently presented using a fitted logarithmic function for the relationship between the applied moment and the resulting rotation for each segment level. No significant differences in the flexion/extension response between the female (Nightingale et al., 2002) and male (Nightingale et al., 2006) cervical spines were found.

The following tables present the results of many experimental studies examining the physiological motion of the cervical spine segment. The results presented in these studies (as well as the following tables) are reported as a 'range-of-motion' value for a specific mode of loading. However, different authors use different definitions of range-of-motion, so the applied load deemed to be the limit for the range-of-motion is also reported. Results for translational loads are typically reported as linear stiffnesses. Depending on the author of the study, these values are also reported at different levels of load. A summary of the results from various cervical spine segment studies can be found in Table 4-2 to Table 4-5 at the end of this section.

Table 4-2: Range-of-Motion of the Cervical Spine Segment in Flexion/Extension

Study	Load	C0-C1	C1-C2	C2-C3	C3-C4	C4-C5	C5-C6	C6-C7	C7-T1
Goel et al, 1984	0.3 Nm					7.1°	10.1°		
Goel et al, 1988a	0.3 Nm	23.0°	10.1°						
Goel et al, 1988b	0.3 Nm				6.4°	6.2°	5.2°	5.7°	2.3°
Moroney et al, 1988	1.8 Nm			9.1°	9.1°	9.1°	9.1°	9.1°	9.1°
Panjabi et al, 1988	1.5 Nm	24.5°	22.4°						
Schulte et al, 1989	0.45Nm					6.5°	4.5°	4.5°	5.2°
Panjabi et al, 1991c	1.5 Nm	28.8°	23.2°						
Wen et al, 1993			23.8°	11.1°	12.0°	13.3°	11.9°	11.6°	
Camacho et al, 1997	1.5 Nm*	28.3°		11.8°	10.4°	10.6°	10.8°	8.3°	5.9°
Richter et al, 2000	2.5 Nm						13.4°		
Winkelstein and Myers, 2000	1.5 Nm*				8.6°		7.6°		
Panjabi et al, 2001b	1.0 Nm	29.2°	24.4°	6.2°	7.7°	10.1°	9.9°	7.1°	
Nightingale et al, 2002	1.5 Nm*	45.8°			14.4°		16.6°		9.1°
Puttlitz et al, 2004	1.0 Nm					9.4°			
Wheeldon et al, 2006	1.5 Nm*			12.5°	11.6°	11.2°	12.9°	12.7°	6.6°
Nightingale et al, 2006	1.5 Nm*	39.6°				12.2°		9.2°	

Table 4-3: Range-of-Motion of the Cervical Spine Segment in Axial Rotation

Study	Load	C0-C1	C1-C2	C2-C3	C3-C4	C4-C5	C5-C6	C6-C7	C7-T1
Goel et al, 1984	0.3 Nm					3.6°	2.8°		
Goel et al, 1988a	0.3 Nm	4.8°	55.6°						
Goel et al, 1988b	0.3 Nm				4.6°	4.6°	4.6°	3.4°	2.8°
Moroney et al, 1988	1.8 Nm			3.7°	3.7°	3.7°	3.7°	3.7°	3.7°
Panjabi et al, 1988	1.5 Nm	14.4°	77.8°						
Schulte et al, 1989	0.45Nm					5.0°	2.6°	2.2°	4.2°
Panjabi et al, 1991d	1.5 Nm	9.3°	71.4°						
Chang et al., 1992	2.0 Nm	59.8°							
Wen et al, 1993			75.9°	11.1°	12.2°	15.5°	11.0°	9.8°	
Richter et al, 2000	2.5 Nm						8.6°		
Winkelstein and Myers, 2000	1.5 Nm*				6.9°		5.6°		
Panjabi et al, 2001b	1.0 Nm	9.9°	56. 7°	3.3°	5.1°	6.8°	5.0°	2.9°	
Puttlitz et al, 2004	1.0 Nm					9.9°			

Table 4-4: Range-of-Motion of the Cervical Spine Segment in Lateral Bending

Study	Load	C0-C1	C1-C2	C2-C3	C3-C4	C4-C5	C5-C6	C6-C7	C7-T1
Goel et al, 1984	0.3 Nm					5.4°	4.6°		
Goel et al, 1988a	0.3 Nm	6.8°	8.4°						
Goel et al, 1988b	0.3 Nm				6.4°	7.2°	4.8°	3.6°	3.0°
Moroney et al, 1988	1.8 Nm			9.4°	9.4°	9.4°	9.4°	9.4°	9.4°
Panjabi et al, 1988	1.5 Nm	11.0°	13.4°						
Schulte et al, 1989	0.45Nm					6.0°	2.4°	2.8°	3.6°
Panjabi et al, 1991c	1.5 Nm	10.7°	20.9°						
Wen et al, 1993			8.3°	11.6°	10.8°	10.5°	10.0°	9.8°	
Richter et al, 2000	2.5 Nm						9.9°		
Winkelstein and Myers, 2000	1.5 Nm[*]				5.5°		5.7°		
Panjabi et al, 2001b	1.0 Nm	9.1°	6.5°	9.6°	9.0°	9.3°	6.5°	5.4°	
Puttlitz et al, 2004	1.0 Nm					13.0°			

Table 4-5: Linear Stiffness of the Cervical Spine Segment in Translational Displacement

Study	Load	Compression	Tension	Lateral Shear	Anterior Shear	Posterior Shear
Liu et al, 1982		3905 N/mm	381 N/mm		20 N/mm	30 N/mm
Panjabi et al, 1986	25 N	140.8 N/mm	52.6 N/mm	52.6 N/mm	33.8 N/mm	52.6 N/mm
Moroney et al, 1988	19.6 N[*]	1318 N/mm		119 N/mm	131 N/mm	49 N/mm
Shea et al, 1991	100 N[**]	1914 N/mm	386 N/mm		246 N/mm	228 N/mm
Van Ee et al, 2000b	300 N		253 N/mm			
Nightingale et al, 2004	200 N		356 N/mm			

* 73.6 N for compression
** 500 N for compression

4.3   Isolated Ligamentous Cervical Spine Studies

The isolated ligamentous cervical spine consists of the cervical spine without the associated musculature. Occasionally, these spine specimens also include the entire head for studies involving impact (required for accurate inertial loading). A summary of previous ligamentous spine studies can be found in Table 4-6.

McElhaney et al (1983) performed relaxation tests on isolated C0-T1 cervical spines in compression. These spines were pre-flexed to vertically align the spine to prevent any bending during compression loading. Relaxation, cyclic, and variable loading rate tests were conducted up to a maximum compression of 7 mm. The spine displayed significant viscoelastic characteristics such as stiffness decay in relaxation, and increasing in stiffness with loading rate. These spines were then loaded to failure at a rate of 640 mm/s in compression. The results were a wide range of failure forces (0.96 kN – 6.84 kN) with injury occurring in the vertebrae of both the upper and lower cervical spine. It was

also noticed that slight eccentricities in the load axis would significantly influence the buckling mode of the spine (in extension or flexion).

In a follow-up study, McElhaney et al (1988) tested vertically aligned ligamentous cervical spines in combined loading under different types of end-conditions. The combined loading was achieved by eccentric axial load, resulting in tension or compression coupled with flexion, extension, or lateral bending. Furthermore, the ends of the cervical spine were either pin jointed or fixed. It was found that the fixed joint specimens were significantly stiffer than pin jointed specimens. Posterior ligament failure (ISL, CL, and LF) was the dominate injury mechanism in compression-flexion loading, with failure moments ranging from 3.0 to 14.6 Nm. The spine was found to be stiffer in tension-based combined loads than in compression-based combined loads. The effects of the end-condition of the spine were also studied in Myers et al (1991).

Goel et al (1988b) investigated the load-deformation behaviour of fresh C2-T2 cervical spines to small (0.3 Nm) bending moments in flexion, extension, axial rotation, and lateral bending. The response of each vertebra was measured for each increment of bending moment, and relative motions between various motion segments were recorded. A coupled motion between axial rotation and lateral bending was observed, while flexion and extension motion were relatively independent. A laminectomy and facet wiring procedure was performed on each spine, and load was re-applied to identify the change in mechanical behaviour in the cervical spine due to an injury and stabilization treatment.

Pintar et al (1990) studied vertically aligned ligamentous cervical spines in axial compression by fixing the inferior vertebra and impacting the still-attached head. Loading rates varied from 2950 to 7140 mm/s, with failure forces ranged from 1177 to 6193 N. The wide variability of this test data is likely the result of the inconsistent loading rates and the viscoelastic effects associated with the high loading rates. Similar studies involving dynamic impacts were done by Yoganandan et al (1991) and Pintar et al (1995) with similar results.

Another series of dynamic axial impact studies was done by Nightingale et al (1996, 1997) where impact velocities were kept much more consistent than the previous studies. Furthermore, they varied the impact surface from rigid to foam to see if these conditions have an effect on injury risk. They found that spine injuries occurred between 2 and 8 ms after head impact for rigid surfaces, and 14 –

30 ms for foam surfaces. The injury force of the foam impacts were slightly less than the rigid impacts (1905 N compared to 2038 N). A consistent buckling mode was identified that resulted in the C2-C5 motion segments being in extension, and the C6-T1 motion segments being in flexion. This loading pattern resulted in corresponding injury-types in each region. A second higher order buckling mode was also observed since in a few specimens were the upper and lower cervical spine would be in flexion, with the middle cervical spine being in extension.

Studies by Camacho et al (1997) and Wheeldon et al (2006) examined the flexion-extension response of cervical spine over a range of applied moments. Camacho et al (1997) used male heads and cervical spines in an apparatus that was capable of applying pure bending moments to the entire spine. Flexion and extension moments up to 1.5 Nm were applied and the resulting vertebral rotations were recorded for each level. These spines were later used in the impact study by Nightingale et al (1997). In a similar study, Wheeldon et al (2006) used cervical spines (C2 to T1) from 'young' donors to record the response under applied moments up to 2 Nm extension or flexion. Both studies reported the response of the cervical spine using a logarithmic function similar to Nightingale et al (2002).

Van Ee et al (2000b) and Nightingale et al (2004) both studied the ligamentous cervical spine in tension. The cervical spine was shown to be highly nonlinear in tension, with relatively low stiffness at small distractions, but gradually reaching a high linear stiffness. As with the compressive response of the spine, the end-condition had a significant effect on the response of the spine. A spine with a fully constrained end resulted in a much stiffer response than the same spine with an unconstrained end. Furthermore, it was shown that the spine was stiffest when loaded directly over the occipital condyles (which is at the top of the spinal column), and least stiff when loaded anterior to the head centre of gravity (which is anterior to the condyles). The spines were not loaded to failure in tension.

A recent series of ligamentous spine studies using an apparatus that simulates frontal and rear impact was done by Panjabi et al (2004a, 2004b) and Ito et al (2004, 2005). This newly developed equipment attempts to replicate inertial loading on the cervical spine using a mini-sled that moves the T1 vertebra in a prescribed acceleration profile. Muscle force on the cervical spine is achieved using tensioned cables. A series of simulations involving a increasing acceleration level is done to identify a tolerance level, using a 2g case as the baseline for physiological loading. A significant increase in rotation from the baseline case was used to indicate a soft tissue injury.

Using these methods, Ito et al (2004) found that soft tissue injuries to the ligaments and disc begin to occur at a 5g rear-impact load case at the C5-C6 level in extension. At slightly higher loads, the C4-C5 and C7-T1 segments were also injured in extension. In the same study, Panjabi et al (2004a) reported potential disc injury occurring in the C4-C5 level at 3.5g. This was based on the IVD fibres exceeding predetermined physiological strain limit. At 5g, discs at the C3-C4 and C5-C6 level were potentially injured. In frontal impact, Panjabi et al (2004b) found that the ISL and LF were at high risk of injury at all levels at 4g. The capsular ligaments were not at risk until the 10g impact case, where potential injuries at the C3-C4 and C5-C6 levels exist. In the same frontal impact study, Ito et al (2005) reported on the corresponding intervertebral disc strains, and suggested that injuries occur at 4g in the C2-C3 disc. At 10g, all discs except at the C3-C4 and C4-C5 levels exceeded the author's defined physiological limit (the strain experienced from a 1.5 Nm static load).

Table 4-6: Summary of Isolated Ligamentous Cervical Spine Studies

Study	Load Case(s)	Common Injuries	Study Details
McElhaney et al, 1983	Compression	Jefferson's fracture C5 fracture	Cervical spine is viscoelastic in compression Failure force ranged from 960 – 6840 N (average ~ 3940 N) Buckling mode sensitive to eccentricity of compressive load-axis
McElhaney et al, 1988	Combined	Rupture of ISL, CL, and LF of lower spine	End-conditions play a significant role in the mechanical response Failure moments ranged from 3.0 – 14.6 Nm (Flexion) Tension-based loads are stiffer than compression-based loads
Goel et al, 1988b	Rotation, Lateral Bending, Flexion, Extension	Not loaded to failure	Pure quasi-static bending moments (up to 0.3 Nm) Coupled motion between lateral bending and axial rotation Tested injured and stabilized spines to compare to normal spines
Pintar et al, 1989	Compression	Upper spine injuries for CE, lower spine in CF	Upper spine injuries were present in compression-extension modes while lower spine injuries were present compression-flexion modes Failure force ranged from 1355 – 3613 N (average ~ 2296 N)
Yoganandan et al, 1989	Compression	Not loaded to failure	Human cervical spine is not as stiff as Hybrid III neck Compressive stiffness 2198 – 2586 N/cm
Pintar et al, 1990	Dynamic Compression	Lower spine burst , wedge fractures	Loading rates between 2950 and 7140 mm/s Failure force ranged from 1177 – 6193 N (average ~ 3508 N)
Myers et al, 1991	Compression-Flexion	Compression and wedge fractures, bilateral facet dislocations	Unconstrained spine did not injure at large displacements Fully constrained spine had failure force average of 4810 N Rotationally constrained spine had failure force average of 1720 N
Yoganandan et al, 1991	Dynamic Compression	Lower spine burst and wedge fractures	Loading rates between 5300 and 8500 mm/s Failure force ranged from 3.3 – 5.6 kN (average ~ 4.5 kN)
Pintar et al, 1995	Dynamic Compression	Lower spine burst and wedge fractures, soft tissue in extension or flexion	Loading rates between 2500 and 8000 mm/s Failure force ranged from 744 – 6431 kN (average ~ 3326 N) Stiffness ranged from 125 – 1375 N/mm (average ~ 555 N/mm)
Nightingale et al, 1996 Nightingale et al, 1997	Dynamic Compression	Upper spine fractures, middle spine ALL tear,	Loading rates between 2430 and 3510 mm/s Injury force ranged was 2038 for rigid impact, 1905 N for foam impact Injuries occurred 2 – 8 ms after rigid impact, 14 – 30 ms for foam impact

(continued…)

Table 4-6: Summary of Isolated Ligamentous Cervical Spine Studies continued…

Study	Load Case(s)	Common Injuries	Study Details
Camacho et al, 1997	Flexion and Extension	Not loaded to failure	Pure quasi-static flexion and extension moments (up to 1.5 Nm) Moment-rotation response at each cervical level was reported using logarithmic curves Same spines used in Nightingale et al (1996, 1997)
Van Ee et al, 2000b	Tension	Not loaded to failure	End-conditions play a significant role in the mechanical response Response is stiffest when loaded over the condyles, least stiff anterior to CG
Ito et al, 2004 Panjabi et al, 2004a	Rear Impact	Soft tissue injury (Extension) IVD injuries	Extension injury occurs at the C5-C6 motion segment at 5g Injury occurs at the C4-C5 and C7-T1 motion segment at 6.5g Injury is likely to occur at the C4-C5 IVD at 3.5g, C3-C4 and C5-C6 at 5g
Nightingale et al, 2004	Tension	Not loaded to failure	Load-displacement is nonlinear, $F(x) = 96.2[\exp(0.32x)-1]$
Panjabi et al, 2004b Ito et al, 2005	Frontal Impact	Posterior ligaments (ISL, LF) IVD injuries	Injury is likely to occur to the ISL and LF at a frontal impact of 4g at all levels Injury is may occur to the CL at a frontal impact of 10g in C3-C4 and C5-C6 Injury is likely to occur at the C2-C3 IVD at 4g, all other discs at 10g
Wheeldon et al, 2006	Flexion and Extension	Not loaded to failure	Pure quasi-static flexion and extension moments (up to 2.0 Nm) Moment-rotation response at each cervical level was reported using logarithmic curves

4.4   Post-Mortem Human Subject Cervical Spine Studies

Post-mortem human subjects are an effective means to studying the mechanical tolerance of the human cervical spine. Studies have often involved impacting PMHS with a load similar to the conditions known to inflict injury (commonly from the reconstruction of an automobile impact or football-injury impact). Many of the studies described in the following section have significant contributions to the current understanding of human neck tolerance. A summary of previous PMHS studies can be found in Table 4-7.

Clemens and Burows (1972) simulated frontal and rear automotive impacts using 53 post-mortem human subjects. Each specimen was belted to a sled with initial speeds around 8 m/s, and varying deceleration times. They found that in frontal impact, the most frequent type of injury was damage to the intervertebral disc, (80% of the test cases), followed by vertebral fractures (75%), ruptures to the capsular ligaments (50%), ruptures of the ligamenta flava (40%) and damage to the longitudinal ligaments (35%). Injuries were most frequent in the lower cervical spine, particularly in the C5-C6 region. In rear impact, damage to the intervertebral disc occurred in 90% of the test cases, followed by ruptures of the anterior longitudinal ligament (80%) and of the capsular ligaments (40%), fracture of the vertebrae (30%) and rupture of the posterior longitudinal ligament and ligamenta flava (10% each). Again, injuries were concentrated in the C5-C6 and C6-C7 region of the cervical spine.

Schmidt et al (1974) tested 30 PMHS in frontal impact using an acceleration sled with a three-point harness. Each simulated impact had an initial speed of 50 km/h with an average deceleration of 25 g's. Of all the test subjects, roughly 25% resulted in fractures to the vertebral body, transverse process, or spinous process. Ligament and disc injuries were reported as rare, but the authors noted that investigation into the soft tissue injuries was not yet finished.

Hodgson and Thomas (1980) performed a series of quasi-static and dynamic impact tests on 16 helmeted PMHS in axial compression. They were able to instrument some of the specimens with strain gages on the vertebral bodies to correlate vertebral movement and loading to strain distribution. It was found that constraining the head in a fixture during impact caused greater exaggeration of flexion or extension in the lower cervical spine that resulted in increased injury. It was also shown that head load did not correlated to vertebral body strain. Studies by Nusholtz et al (1981, 1983) on

neck tolerance to dynamic axial loading produced similar injuries, and concluded that the spinal configuration and impact conditions have a significant influence on both mechanical response and damage.

Injuries to the cervical spine caused by a distributed frontal load on the chest were studied by Cheng et al (1982) to identify injury mechanisms possibly associated with airbag-deployment. A sled was used to apply peak decelerations ranging from 32 to 39 g to six unbelted PMHS, which impacted a pre-inflated airbag. It was found that in three of the cases, severe neck injuries were present that were not normally observed in belted frontal impacts. These injuries included severed spinal cord, fracture of the odontoid process, and atlanto-occipital avulsion. Furthermore, they proposed a resultant load of 6.2 kN as a tolerance for neck fracture, which is in agreement with N_{ij} tolerances.

Another axial impact study by Alem et al (1984) used 19 PMHS to define both sub-injurious response as well as traumatic impacts. Using a 10 kg impactor that impacted the head at speeds between 7 and 10 m/s, they found that both impact force and head injury criterion (HIC) were poor predictors of neck injury, while impulse (the integration of force and time) proved to be the most suitable indicator of injury. Common injuries produced from the axial compressive impact were tearing of the ALL at the C3-C4 and C4-C5 level, fracture of the C2, rupture of the discs at the C3-C4 and C4-C5 levels, and fracture and ligament damage to the lower cervical spine and upper thoracic spine.

A study by Wismans et al (1987) compared the results of PHMS head-neck response in frontal impact, to those produced by the human volunteers in the 15 g Naval Biodynamics Laboratory (NBDL) tests by Ewing and Thomas (1973). Using comparable impact loading, they concluded that the relative head displacements and accelerations of the PMHS were similar to those produced by the volunteers. However, head rotation in the PMHS tests was much larger than in the human volunteer tests, indicating some active muscle activity is present. No injuries were found in the PMHS from the 15 g frontal impact cases, agreeing with the human volunteer study. Only minor injuries (AIS 2 and less) to the intervertebral discs were observed in 23 g impact cases.

A large impact study performed by Kallieris et al (1991) was used to develop an injury criterion of the neck. Forty-three belted PMHS in cars were subjected to frontal and lateral impacts of speeds between 30 and 60 km/h, and in various seats in the automobile. Injuries to subjects in lateral impacts were mostly in the middle cervical spine, with the intervertebral disc frequently damaged. In frontal

impacts, injuries that were most common were the posterior ligaments in the lower cervical spine and upper thoracic spine, and the intervertebral discs of the middle cervical spine. Using the AIS injury severity scale, most lateral impact injuries were only minor (AIS I, 76%), while most frontal impact injuries were either minor (AIS I, 54%) or moderate (AIS II, 39%). Injury severity did not correlate well to the various measures used to predict injury (including neck angular velocity, head velocity, neck angular acceleration, and head acceleration).

Low-speed rear impacts were simulated by Deng et al (2000) to identify the kinematics of the human head and cervical facet joints, without inducing injury. Six PMHS were impacted multiple times under different initial seat conditions, with sled speeds ranging from 5 to 12 km/h, and decelerations ranging from 5 to 8 g. It was found that during low-speed rear impacts, the capsular ligaments experience strains up to 60%, which may exceed tolerance limits and result in pain. It was also found that a seatback at 20° produced more relative rotation between the motion segments than a seatback of 0°, resulting in a greater risk of injury.

In another rear impact study, Yoganandan et al (2000b) attempted to document the soft-tissue injuries in the neck of five PMHS to correlate injury to various dynamic measures taken during the experiment. At 4.3 and 6.8 m/s impacts, four of the subjects had injuries that included tearing of the anterior longitudinal ligament, rupture of the ligamentum flavum, hematoma of the upper facet joint, anterior disc disruption in the lower cervical spine, and capsular ligament tear. By evaluating the PMHS global response, they found that the NIC limit of 15 m^2/s^2 was exceeded for all specimens, while the N_{ij} criteria predicted zero risk of AIS 3+ for all but one specimen. It was suggested by the authors that a minor injury criterion for soft tissues should be developed since injury criteria is typically geared towards moderate to severe (AIS 2+) injuries.

Table 4-7: Summary of Post-Mortem Human Subject Cervical Spine Studies

Study	Load Case(s)	Common Injuries	Study Details
Clemens and Burow, 1972	Frontal, Rear Impact	All injuries concentrated in lower spine region	53 PMHS with impact speeds 8 m.s (25 g) IVD injuries and fractures common in frontal impact IVD injuries and ALL ruptures common in rear impact
Schmidt et al, 1974	Frontal Impact	Fracture to the body, transverse process, and spinous process	30 PMHS with impact speeds 50 km/h (25 g) 25% of subjects had fractures, soft tissues were rare (unexamined)
Hu et al, 1977	Rear Impact	Disc injuries, subluxations, compression fractures of C5-C7	6 PMHS with impact speeds 16 mph (14.5 – 19.1 g) 5 of 6 subjects were injured, with an AIS of 3
Hodgson and Thomas, 1980	Compression	Fracture of C4-C7	16 helmeted PMHS in quasi-static and dynamic impact Significance on head end-condition on response and damage
Nusholtz et al, 1981	Dynamic Compression	Spinous process, transverse process, lamina and body fractures, disc ruptures	12 PMHS impacted with 56 kg between 4.6 and 5.6 m/s Head forces from 1800 – 11100 N Significance on head end-condition on response and damage
Cheng et al, 1982	Frontal Impact	Severed cord, odontoid process fracture, atlanto-occipital avulsion	6 PMHS with distributed chest load under 32 to 39 g Proposed neck tolerance of 6.2 kN
Nusholtz et al, 1983	Dynamic Compression	Middle spine disc rupture, upper spine fractures, ALL tear	8 PMHS dropped head-first from 0.8 – 1.8 m Head forces from 3200 – 10800 N Constraining head resulted in more injury, higher loads
Alem et al, 1984	Dynamic Compression	ALL tearing, disc rupture (C3-C5), C2 fracture, lower spine fracture	19 PMHS impacted with 10 kg between 7 and 10 m/s Impact force, HIC did not predict injury, impulse was best
Yoganandan et al, 1986	Dynamic Compression	Compression fractures, PLL disruptions, spinous process fracture, disc rupture	15 PMHS dropped head-first from 0.9 – 1.5 m Restrained head forces from 9800 – 14600 N Unrestrained head forces from 3000 – 7000 N
Wismans et al, 1987	Frontal Impact	Intervertebral disc injury	2 PMHS in impact similar to 15 g NBDL volunteer tests, 5 PMHS in impact at 23 g PMHS response was similar to volunteer response No injuries found in the 15 g cases
Kallieris et al, 1991	Frontal, Lateral Impact	IVD injuries in lateral impact, posterior ligament injuries and IVD injuries in frontal impact	43 PMHS with impact speeds from 30 to 60 km/h Lateral injuries were minor (AIS I) Frontal injuries were moderate (AIS II)

(continued…)

Table 4-7: Summary of Post-Mortem Human Subject Cervical Spine Studies continued…

Study	Load Case(s)	Common Injuries	Study Details
Deng et al, 2000	Rear Impact	No Injuries	6 PMHS with impact speeds from 5 to 12 km/h (5 – 8 g) Peak capsular ligament strains of 60% Injury more likely in seatbacks of 20° than of 0°
Yoganandan et al, 2000b	Rear Impact	ALL and CL tear, LF rupture, anterior IVD disruption	5 PMHS with impact speeds from 4.3 to 6.8 m/s Soft tissue injury was present in all by 1 subject Current injury criterion did not predict minor injuries

4.5 Human Volunteer Cervical Spine Studies

The most effective means to understand the physiological response of a person in impact is to use human volunteers as test subjects. This is particularly the case when it comes to cervical spine response in crash (Wismans et al., 1987). As seen in Figure 4-1, a significant amount of delay exists between the onset of a crash and the loads seen on the head, that muscle reflex and active muscle behaviour play a role in the response. However, one of the main disadvantages of human volunteer studies is that only sub-injurious levels of load can be investigated.

Of the available cervical spine literature involving human volunteers, three prolific groups have provided most of the current knowledge. These experiments examined the static and dynamic response of the living cervical spine in a few modes of loading. A summary of some of the previous human volunteer studies can be found in Table 4-8.

Mertz and Patrick (1967, 1971) conducted some of the first human volunteer tests that investigated the strength of the cervical spine in flexion and extension. Human volunteers, secured and seated in a sled, used a self-applied load to force the cervical spine to either flex or extend while also attempting to maintain the neck in its original position. Loads were recorded in the apparatus, and using kinematic analysis, determined the static flexion and extension strength of the neck.

In Mertz and Patrick (1971), Patrick subjected himself to a frontal impact sled test of increasing severity. The tests were concluded when Patrick begin to experience pain because of the impact. The results of the frontal impact, also using the same kinematic analysis to calculate occipital condyle torque, established the first dynamic human tolerances for the cervical spine.

A large experimental series conducted by the National Biodynamics Laboratory (NBDL) focused on the kinematic response of the head and neck in various types of impacts. These experiments (separate groups), which looked at human volunteer response in frontal and lateral impacts, were initially reported by Ewing and Thomas (1968, 1969, 1973) and Ewing et al (1975, 1976, 1977a, 1977b). Using military personnel restrained to a sled, volunteers were instrumented with accelerometers to record the response of the T1 vertebra and the head during each impact. Analysis was simplified to comparing the sagittal plane motion of the head, with the horizontal acceleration of the T1.

One of the conclusions to come out of this series of experiments was that the size of the volunteer did not have a significant impact on the response of the head (Ewing and Thomas, 1973). Another finding was that the initial condition of head and neck played a significant role in reducing the loads seen during impact (Ewing et al., 1975). The rate and duration of the sled acceleration pulse was also studied to identify its effect on the head response (Ewing et al., 1976). One of the most significant results of these experiments was the publishing of a consistent set of dynamic response corridors that have been used consistently in validating full cervical spine models.

Another set of NBDL human volunteer sled tests were reported by Wismans and Spenny (1983, 1984) and Wismans et al (1986). These experiments were conducted in an experimental setup similar to the Ewing studies. However, the results of these studies looked at a larger group of frontal, lateral, and oblique sled tests, each tested at different levels of severity. Furthermore, the responses of the sled tests were used to develop a simple two-bar linkage model of the head and cervical spine. Some of the tests reported in Wismans et al (1986) were later reevaluated by Thunnissen et al (1995) to include the rotation of the T1 vertebra as a second input variable (the first being the horizontal acceleration as mentioned above).

Table 4-8: Summary of Human Volunteer Cervical Spine Studies

Study	Load Case(s)	Study Details
Mertz and Patrick, 1967 Mertz and Patrick, 1971	Static Loads Frontal, Rear Impact (Sled)	10 Volunteers for a total of 90 static neck strength tests, 1 Volunteer with sled decelerations from 2g to 9.6g (14 runs) Static loads applied to the head to determine neck strength to resist extension, flexion Tensing of the neck muscles prior to impact reduces the risk of injury Head torque rather than shear or axial force is the major factor in producing neck injury Proposed tolerances of 88.1 Nm in flexion, 47.5 Nm in extension, 1134 N in tension, 1112 N in compression
Ewing and Thomas, 1968 Ewing and Thomas, 1969 Ewing and Thomas, 1973	Frontal Impact (Sled)	12 Volunteers with sled decelerations from 3g to 10g (236 runs analyzed) Obtain neck and heads response data rather than tolerance data Fully restrained torso and pelvis No relationship between head accelerations and sitting height - response similar between differently sized subjects No injuries occurred to the human volunteers
Ewing et al., 1975	Frontal Impact (Sled)	13 Volunteers with sled decelerations of 6g and 10g (26 runs) Looked at initial neck and head positions on frontal impact response Increase in initial head and neck flexion reduced risk of injury (but not significantly)
Ewing et al., 1976	Frontal Impact (Sled)	10 Volunteers with sled decelerations of 6g, 10g, and 15g (81 runs) Looked at the influence of duration, rate of onset, and peak sled acceleration on the dynamic response of the head and neck Increase in sled acceleration, rate of onset, and duration increased the peak head accelerations and risk of injury
Ewing et al., 1977a	Lateral Impact (Sled)	5 Volunteers with sled decelerations from 2g to 11g (84 runs) Reported time-histories for head and neck motion
Ewing et al., 1977b	Frontal Impact (Sled)	1 Volunteer with sled decelerations of 2g to 7g (4 runs) Measurement of pelvic response in addition to T1 and head acceleration
Wismans and Spenny., 1983 Wismans and Spenny., 1984	Lateral Impact (Sled) Frontal Impact (Sled)	Experimental data based on human volunteer tests from NBDL between 1976 and 1980 (Lateral) Experimental data based on human volunteer tests from Ewing and Thomas (1973) and NBDL 1980 databases (Frontal) 6 Volunteers with sled decelerations between 5g and 10g (16 runs) (Lateral) 12 Volunteers with sled decelerations between 8g and 15g (21 runs) (Frontal) Developed a 2-bar linkage model for the neck in dynamic impact
Wismans et al., 1986 Thunnissen et al., 1995	Lateral, Frontal, and Oblique Impacts	15 Volunteers (109 runs) Frontal tests greater than 8g, lateral tests greater than 5g, and oblique tests greater than 7g Reported time-histories for head and neck motion for dummy neck development Developed a 2-bar linkage model for the neck in dynamic impact Reanalyzed frontal impacts to account for T1 rotation (Thunnissen et al., 1995)

Chapter 5

Cervical Spine Models

Numerical models are a versatile tool that can be used to predict the mechanics of the spine for phenomena that cannot be adequately investigated using physical models. In particular, determining internal loads, stresses, and strains in the tissues of the spine is important advantage that numerical models have over physical models (Panjabi, 1998). The simulation results of a numerical spine model can be used to gain insight into inner workings of the cervical spine, including the load carrying mechanisms, the onset of injury, and the effects of injury or age on the behaviour of the spine (Yoganandan et al., 1996a). Numerical models of the spine can also be used in practical applications, providing a tool to evaluate safety systems such as airbags and seatbelts. However, new model require proper validation against physical test data, which typically occurs at the global level.

The ability of a numerical model to accurately reproduce the behaviour of a human body is known as biofidelity. A model with a high degree of biofidelity is one that effectively simulates the behaviour of a human being, while low biofidelic models do not accurately represent a human. Thus, biofidelity is the most important characteristic for a model of the human body.

The important factors that are required for the development of a biofidelic human model are accurate geometry and material properties of the biological material, representative loading conditions, and proper validation using experimental studies (Yoganandan et al., 1996a). Model geometry of the human body is often obtained from CT scans or cryomicrotomy with a high degree of accuracy. It is also essential to properly discretize the model geometry to capture the nuances of soft tissue deformation. Biological material properties are more difficult to characterize because biological tissues are typically heterogeneous materials resulting in anisotropic, nonlinear, viscoelastic behaviour (Yoganandan et al., 1996a). It is also important to characterize material properties for the regime of loading seen during the numerical analysis. Achieving proper loading conditions is the result of accurately representing the external forces and environment acting on the numerical model. Loading conditions range from simplified, quasi-static cases (such as controlled laboratory experiments) to complex, dynamic cases (such as in an automotive accident).

Model validation is a crucial step in numerical model development, as it demonstrates the biofidelity of the model against a set of experimental studies with different loading conditions (Panjabi, 1998). Validation is a term often used erroneously to describe models that were calibrated to a single set of experimental results. Calibration is the process of adjusting numerical or physical modelling parameters (often the material properties) to improve the agreement between the model and experimental data. A calibrated model, while giving good results for a specific loading case, may have no scientific merit when evaluated in other types of loading. Model validation is the process of determining the degree of model accuracy to representing the physical counterpart by comparing the model results to a set of experimental data. A numerical model should only be considered validated in the particular loading condition of the experimental data that the model was compared (Panjabi, 1998). Thus, validating a numerical model in a number of different loading conditions is the only means to obtain a fully validated model (Yoganandan et al., 1996a).

Numerical models of the human cervical spine are historically divided into two groups: numerical models that represent a segment (or a set of segments) of the cervical spine, and numerical models that represent the entire cervical spine, from the T1 vertebrae to the skull.

5.1   Spine Segment Models

Spinal segment models are typically a model of a vertebra-disc-vertebra, but any model that consists of a section of the spine can be considered a segment model. These models are typically compared against experimental data involving simple quasi-static loading to focus on the load-carrying behaviour of the local tissue. Previous spine segment models have provided insight into the internal behaviour of the spine and appropriately used the finite element method to achieve these goals.

When reviewing previously developed cervical spine segment models, it is advantageous to also consider human lumbar spine segment models. Both groups of models follow the same development principles, and have many material properties in common. Furthermore, investigation into spine injury modelling and analysis has been more prevalent in lumbar spine models since the lumbar spine is a frequent injury site for worker-related injury. Only few significant spinal segment models are detailed in this section. A full summary of previous spine models can be found in Table 5-1.

The first numerical model of the human spine was developed over 20 years ago by Belytschko et al (1974). This was a simplified axisymmetric model of a human lumbar spine segment, which was

developed to study stress distribution and intradiscal pressures of the disc in compression loading. All material models were linear isotropic elastic except for the annulus fibrosus that was linear orthotropic. The orthotropy of the AF model accounted for both the ground substance and the annular fibres in one solid continuum. This model was later redeveloped by Kulak et al (1976) to include a nonlinear orthotropic representation of the annulus fibrosus for a more accurate response.

A groundbreaking model developed by Shirazi-Adl et al (1984) incorporated many of the same features used in more recently developed models. This model was the first significant model to utilize actual vertebrae geometry in a three-dimensional model, as well as the first model to develop a linear composite material model for the annulus fibrosus, incorporating truss elements representing collagen fibres embedded in a linear matrix of ground substance. To further advance the capabilities in complex loading (flexion and extension) nonlinear tension-only truss elements were introduced to represent the ligaments (Shirazi-Adl et al., 1986). This model, or slight variations of this model, have been utilized for countless studies involving the biomechanics of the lumbar spine.

A study by Rao and Dumas (1991) examined the influence of material properties of their lumbar spine model on the mechanical behaviour in compression. This was the first comprehensive material study for intervertebral disc properties, identifying that the material properties of the annulus, including its compressibility, have a significant impact on the load response of the disc. Furthermore, it was shown that changes in the nucleus pulposus, cortical and cancellous bone, and cartilaginous endplates have very little effect for the physiological loading applied in the study.

A number of finite element studies into the spinal segment injury were presented in the mid 1990's that attempted to predict injury in areas that could not be addressed experimentally. Bozic et al (1994) studied burst fracture mechanism in the C4 vertebra by developing a model that used apparent bone density determined by CT scan pixels to assign a stiffness and strength. Based on maximum shear failure theory, the model predicted failure in the central cancellous region of the vertebral body. Nataragan et al (1994) looked at damage accumulation in the endplate during compression loading, as well as the onset of annular tears. It was shown that annulus fibrosus injuries are not likely to occur in pure compressive loading, rather in a bending loading such as flexion or compression. Failure in compression always initiated in the endplates. Goel et al (1995) studied annular delamination caused by intralaminar shear stresses as a source for intervertebral disc injury. It was shown that the posterolateral region of the disc was most susceptible to annulus delamination. Despite the fact that

all three injury models are limited by their use of linear material properties, their results have contributed significantly to the study of injury mechanisms in the human spine.

The first use of viscoelastic material models in a spinal segment model is in a study by Lu et al (1996). In this model, both the ligaments and the annulus fibrosus fibres (as truss elements) were modeled using a quasi-linear viscoelastic theory (Maxwell) with a reduced relaxation function. Parameters for the Prony series of the relaxation function were taken from studies involving the time-dependant properties of human lumbar ligament (Yahia et al., 1991). Other spinal segments models to include time-dependant effects are Martinez et al (1997) and Whyne et al (2003), which both used linear poroelastic material models rather than linear viscoelastic theory.

The first significant cervical spine segment model was developed by Yoganandan et al (1996). This model was built from CT scan geometry of a C4-C5-C6 section of the cervical spine. While this model was very detailed geometrically, the material properties used in the model appear to be chosen based on a calibration of the model to experimental data. The material models for both the annulus fibrosus and the nucleus pulposus were isotropic linear elastic. However, recent research has demonstrated that the importance of nonlinear material properties. Despite this, the model response compared well to experimental data. This model was later redeveloped by Kumaresan et al (1999) to include a better model of the annulus fibrosus (a linear composite model) a detailed model of the synovial facet joint.

Finally, the most significant development since Shirazi-Adl et al (1984) to modelling of the annulus fibrosus was presented by Eberlein et al (2001). This model included the development of an anisotropic constitutive model that was based on a neo-Hookean hyperelastic ground substance coupled with a nonlinear tension-only fibre model. A disc using this new anisotropic annulus fibrosus model showed a significant improvement to experimental data than a disc constructed with a linear composite (truss) annulus fibrosus.

Table 5-1: Summary of Previous Spinal Segment Models

Model	Spine	Application for Study	Geometry	Vertebra Material	IVD Details	Ligament Detail	Validation
Belytschko et al., 1974	Lumbar	IVD Stress Distribution	Simple 2D	Iso Linear Cortical Iso Linear Cancellous	Ortho Linear AF Fluid NP		Compression
Kulak et al., 1976	Lumbar	IVD Stress Distribution	Simple 2D	Iso Linear Cortical Iso Linear Cancellous	Ortho Nonlinear AF Fluid NP		Compression
Lin et al., 1978	Lumbar	Material Property Identification	Simple 3D	Ortho Linear	Ortho Linear AF Fluid NP		Compression
Hakim and King, 1979	Lumbar	Dynamic Vertebra Response	Simple 3D	Iso Linear Cortical Iso Linear Cancellous	Linear Spring Elements		Compression
Spilker, 1980 Spilker et al., 1984	Lumbar	IVD Bulge and Deflection Complex Loading Response	Simple 2D	Ortho Linear	Ortho Linear AF Fluid NP		Compression
Shirazi-Adl et al., 1984 Shirazi-Adl et al., 1986	L2-3	IVD Stress Distribution Sagittal Plane Motion Analysis	Actual 3D	Iso Linear Cortical Iso Linear Cancellous	Linear Comp AF (Truss) Fluid NP	Nonlinear Cable	Compression, Flexion/Extension
Ueno and Liu., 1987	L4-5	Torsion Load Response	Actual 3D	Ortho Linear Cortical Ortho Linear Cancellous	Linear Comp AF (Truss) Fluid NP	Linear Cable	Compression, Flexion/Extension
Goel and Kim, 1989 Goel et al., 1995	L3-4	Effects of Injury Study Annulus Fibrosus Delamination	CT Scan 3D	Iso Linear Cortical Iso Linear Cancellous	Linear Comp AF Fluid NP	Bilinear Cable	Compression
Shirazi-Adl, 1989	Lumbar	Annulus Modelling Techniques	Simple 2D	Iso Linear Cortical Iso Linear Cancellous	Linear Comp AF (Shell) Fluid NP		Compression
Rao and Dumas, 1991	L5-S1	Material Sensitivity Study	Simple 3D	Ortho Linear Cortical Ortho Linear Cancellous	Linear Comp AF (Truss) Fluid NP		Compression
Bozic et al., 1994	C4	Burst Fracture Mechanism	CT Scan 3D	Iso Linear (Density Based)	Linear Spring Elements		
Natarajan et al., 1994	L3-4	Initiation Disc of Injury	Simple 3D	Iso Linear Cortical Iso Linear Cancellous	Ortho Linear AF Fluid NP		Compression
Lu et al., 1996	L2-L3	Complex Loading Response	CT Scan 3D	Ortho Linear Cortical Ortho Linear Cancellous	Linear Comp AF (Truss) Fluid NP, Viscoelasticity	Bilinear Cable	Flexion/Extension, Bending, Rotation
Yoganandan et al., 1996b Kumaresan et al., 1997 Kumaresan et al., 1999a	C4-C6	Initial Development Laminectomy and Facetectomy Material Sensitivity Study	CT Scan 3D	Iso Linear Cortical Iso Linear Cancellous	Iso Linear AF Iso Linear NP	Linear Cable	Compression, Flexion/Extension, Bending, Rotation
Clausen et al., 1997 Goel and Clausen, 1998	C5-C6	Uncinate Process Influence Load Sharing Study	CT Scan 3D	Iso Linear Cortical Iso Linear Cancellous	Linear Comp AF (Truss) Fluid NP	Bilinear Cable	Flexion/Extension, Bending, Rotation

Table 5-1: Summary of Previous Spinal Segment Models continued…

Model	Spine	Application for Study	Geometry	Vertebra Material	IVD Details	Ligament Detail	Validation
Martinez et al., 1997	Lumbar	Creep Compression Study	Simple 2D	Iso Linear	Iso Linear Poroelastic AF Iso Linear Poroelastic NP		Creep Compression
Kumaresan et al., 1999b	C4-C6	Eccentric Loading Study	CT Scan 3D	Iso Linear Cortical Iso Linear Cancellous	Iso Linear AF Fluid NP	Nonlinear Cable	Compression
Natarajan and Anderson, 1999	L3-L4	Geometric Sensitivity Study	CT Scan 3D	Iso Linear Cortical Iso Linear Cancellous	Nonlinear Comp AF (Truss) Fluid NP	Nonlinear Cable	Compression, Flexion/Extension, Bending, Rotation
Natarajan et al., 2000	C5-C6	Anterior Cervical Fusion	CT Scan 3D	Iso Linear Cortical Iso Linear Cancellous	Nonlinear Comp AF (Truss) Fluid NP	Nonlinear Cable	Flexion/Extension, Bending, Rotation
Eberlein et al., 2001 　Eberlein et al., 2004	L1-L2 L2-S1	Initial Disc Development Multi-segment Development	CT Scan 3D	Ortho Linear Cortical Ortho Linear Cancellous	Anisotropic Nonlinear AF Fluid NP	Nonlinear Cable	Flexion/Extension, Bending, Rotation
Ng and Teo, 2001 　Teo and Ng, 2001 　Ng et al., 2003 　Ng et al., 2004	C4-C6	IVD Disc Bulge Study Load Sharing Study Spinal Stability Material Sensitivity Study	Actual 3D	Iso Linear Cortical Iso Linear Cancellous	Iso Linear AF Fluid NP	Nonlinear Cable	Compression, Flexion/Extension
Whyne et al., 2001	L1	Tumor Influence Study	Simple 3D	Iso Linear Cortical Ortho Linear Cancellous	Iso Linear AF Fluid NP		
Pitzen et al., 2002	C5-C6	Anterior Cervical Fusion	CT Scan 3D	Iso Linear Cortical Iso Linear Cancellous	Iso Linear AF Iso Linear NP	Linear Cable	Flexion/Extension, Bending, Rotation
Whyne et al., 2003	L1	Burst Fracture	Simple 3D	Iso Poroelastic Cortical Ortho Poroelastic Canc	Iso Nonlinear Poroelastic AF Iso Linear Poroelastic NP	Linear Shell	Compression
Wilcox et al., 2004	Bovine	Burst Fracture	CT Scan 3D	Iso Elastic-Plastic Cortical Iso Elastic-Plastic Canc	Ortho Linear AF Fluid NP	Nonlinear Cable	Dynamic Compression
Noailly et al., 2005	L3-L5	Artificial Disc Study	Simple 3D	Ortho Linear Cortical Ortho Linear Cancellous	Nonlinear Comp AF (Truss) Hyperelastic NP	Nonlinear Cable	Compression
Denoziere and Ku, 2006	Lumbar	Artificial IVD Study	Simple 3D	Iso Linear Cortical Iso Linear Cancellous	Linear Comp AF (Truss) Fluid NP	Nonlinear Cable	Flexion/Extension, Bending, Rotation
Yao et al, 2006	L2-3	IVD Implant Study	Simple 3D	Ortho Linear Cortical Ortho Linear Cancellous	Linear Comp AF Fluid NP		Compression

5.2 Full Cervical Spine Models

Unlike spinal segment models, full cervical spine models are typically compared against experimental data involving dynamic or impact loading, focusing more on the resultant global motion of the head rather than the local tissues. For this reason, multi-body (MB) models have been widely used as the numerical method for the full cervical spine. Multi-body models take a simplified approach to modelling the cervical spine by representing the soft tissues (particularly the intervertebral disc) as spring-damper elements instead of solid continuum elements as in finite element methods. Using this approach, MB models are easily calibrated to the physical response to achieve reasonably accurate kinematic results, while being unable to identify local tissue response.

Finite element (FE) models, on the other hand, use continuum elements to represent the tissues of the cervical spine. This makes an FE model much more complex and computationally demanding than an MB model. For this reason, only a few FE models of the full cervical spine have been developed. But FE models are becoming more practical with the advent of increasing computational power, with the intension to simulate local tissue response in dynamic loading. Despite the advancement of computer power, FE models with fully deformable vertebrae have not been exploited since simulation times would be measured in weeks rather than hours. All previous developed FE models of the cervical spine use rigid body vertebra for computational efficiency. This assumption is reasonable, unless the goal is to simulate failure of the vertebra, since the stiffness of the vertebra are much higher than the stiffness of the intervertebral discs. Only few cervical spine models are detailed in the section. A full summary of previous spine models can be found in Table 5-2.

Williams and Belytschko (1983) developed one of the first cervical spine models for use in impact loading conditions. This model was a simple 3D multi-body model with six degree-of-freedom (DOF) springs to represent the biomechanics of the soft tissues between each rigid vertebra. Also significant about this model was the implementation of active muscles to simulate the behaviour of the live human. The results of this model showed that active muscles are much more accurate that passive muscles when modelling the response of the head during frontal and lateral impact of volunteer test subjects.

The first FE model of the human cervical spine was developed by Kleinberger (1993). This model

represented the intervertebral disc and spinal ligaments using solid elements to connect the simplified vertebra. However, the intervertebral disc was modeled using a single material, and all soft tissue properties were assumed or calibrated. Furthermore, this model lacked any representation of musculature, which was an important feature since this model was being compared to human volunteer impact data.

One of the more prolific multi-body models is one originally developed by de Jager et al (1994, 1996). While this model was certainly not ground breaking at the time, it was the basis for more complex and complete multi-body models such as Yamazaki et al (2000) and van der Horst (2002). The frequent use of this model in cervical spine impact is likely because it is a component of the MADYMO body model developed by TNO, widely used in vehicle crash simulation.

The finite element model developed by Deng et al (1999) was one of the most advanced cervical spine models at the time of development. Specifically, this FE model was the first to use tissue models based on fundamental tissue research rather than calibrated or assumed properties. This incorporating nonlinear, viscoelastic FE elements to represent tissue in dynamic conditions. Another significant achievement with the Deng model was to include active muscles using the Hill muscle model. These muscles were represented using two spring elements (3 points) to allow for realistic muscle-force direction when the neck was flexed.

Finally, the developed by Halldin et al (2000) and Brolin and Halldin (2004) is significant because it is the first FE cervical spine model that details development of the upper cervical spine complex. Previous cervical spine models do not discuss the development of the upper cervical spine, although it is a crucial component since cervical spine models are typically compared to head acceleration data. This model is also significant for incorporating some modelling techniques used in spine segment modelling such as using a composite annulus fibrosus. Active muscle response was added to this model in Brolin et al (2005).

Table 5-2: Summary of Previous Full Cervical Spine Models

Model	Type	Geometry	IVD Details	Ligament Detail	Muscle Detail	Simulated Impact Cases
Williams and Belytschko, 1983	MB	Simple 3D	6 DOF Spring		22 Pairs, Active (Stretch-Reflex)	Frontal, Lateral
Merrill et al., 1984	MB	Traced 2D	6 DOF Spring/Damper		7 Pairs, Passive	Lateral, Rear
Deng and Goldsmith, 1987	MB	Traced 2D	6 DOF Spring/Damper		13 Pairs (3 Pt), Passive	Lateral, Rear
Kleinberger, 1993	FE	Simple 3D	Iso Linear IVD (AF & NP same)	Iso Linear Solid Elements		Frontal, Axial
Dauvilliers et al., 1994	FE	Simple 3D	Linear Composite Disc (Truss)	Linear Spring/Dampers		Frontal, Lateral
De Jager et al, 1994 De Jager et al, 1996	MB	Simple 3D	6 DOF Spring/Damper		15 Pairs, Passive	Frontal, Lateral
Camacho et al, 1997 Camacho et al, 1999	MB	CT Scan 3D	3 DOF (Sagittal) Spring/Damper			Axial
Yang et al, 1998	FE	MRI Scan 3D	Iso Linear AF, Viscoelastic NP	Linear Cables & Membranes		Axial, Lateral
Deng et al, 1999 Deng and Fu, 2002	FE	Actual 3D	Iso Nonlinear AF, Viscoelastic NP	Linear Viscoelastic Membranes	15 Pairs (3 Pt), Active (Hill)	Frontal
Halldin et al, 2000 Brolin and Halldin, 2004 Brolin et al, 2005	FE	CT Scan 3D	Linear Comp AF (Shell) Iso Linear NP	Bilinear Cables (TL is Shell)	14 Pairs, Active (Hill)	Frontal, Lateral, Axial
Yamazaki et al, 2000	MB	Simple 3D	6 DOF Spring/Damper		15 Pairs, Active (Hill)	Frontal, Lateral
Van der Horst, 2002	MB	Simple 3D	6 DOF Spring/Damper	Nonlinear Cables	68 Pairs (Multi Pt), Active (Hill)	Frontal, Lateral, Rear
Lee et al, 2004	MB	Actual 3D	6 DOF Spring	Nonlinear Cables	22 Pairs (Multi Pt), Active (Hill)	Frontal
Meyer et al., 2004	FE	CT Scan 3D	Iso Linear IVD (AF & NP same)	Nonlinear Cables	Solid Elements, Passive	Frontal, Lateral, Rear
Zhang et al, 2006	FE	Traced 3D	Iso Linear AF, Iso Linear NP	Nonlinear Cabl`es		

Chapter 6

Model Development

As discussed in the previous chapter, cervical spine models are commonly grouped into two categories: segment models, and full spine models. Both types of models are used for their own particular applications. Spine segment models were developed for the purposes of understanding the load-carrying capabilities of the spine by examining the stress distribution within the tissue during quasi-static, physiological loading. Full cervical spine models were developed to investigate the response of the head and cervical spine due to impact loading to correlate the motion of the spine with some sort of global injury measure.

Despite the wide number of cervical spine models of each type, none of the current models can be considered a part of both groups. In essence, current full cervical spine models lack the detail needed for an accurate response of local tissue that exists in spinal segment models.

The objective of this chapter is to detail the development of a finite element model of the cervical spine that is capable of predictive human response to impact based on accurate geometry and tissue material properties. This model is loosely based on the model developed by Deng et al (1999). However, in order to achieve accurate representation of the model, from local (tissue) level to global response, the entire model was redeveloped, preserving only the geometry of the vertebrae.

The principle behind the development of this model is to focus on the representation of the fundamental tissues of the cervical spine to ensure accurate response at the local tissue level. Theoretically, if each subcomponent of the spine model is modeled accurately, then the assembly of these subcomponents should also result in accurate representation. Development of the cervical spine model then follows a developmental hierarchy from the fundamental tissues all the way to the full cervical spine. A flowchart outlining the hierarchy used to develop the cervical spine model can be seen in Figure 6-1.

116
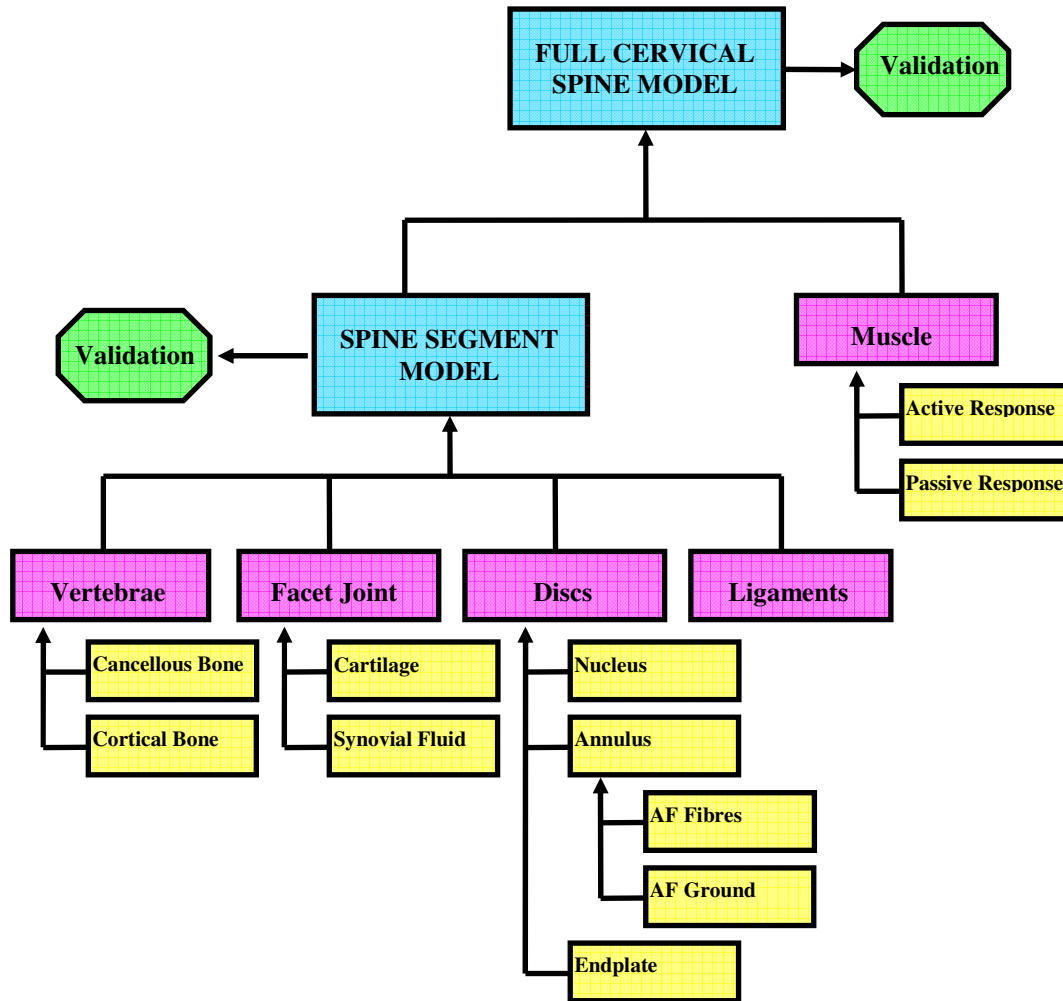
Figure 6-1: Hierarchy of Development for the Cervical Spine Model

Fundamental tissues or properties (yellow), which make up the vertebrae, ligaments, facet joints, and the intervertebral discs, are assembled to create a spinal segment model (blue). Each segment model (seven in total) of the entire cervical spine then come together to complete the model of the full cervical spine (blue). Each level of spine model is rigorously tested to ensure that the model is validated (green) against applicable experimental data.

It should be noted that there are some differences between the material properties of the spinal segment models and that of full cervical spine model. As mentioned in Chapter 3, biological tissues are viscoelastic in nature, and this phenomenon must be accounted for in the full cervical spine model for impact simulation. Furthermore, some compromises in modelling techniques were made in the full cervical spine model, required for computational efficiency. These changes will be discussed throughout the chapter.

6.1 Model Construction

Model construction was the first step in the development of the full cervical spine model. This process involved the generation of the finite element mesh, the classification of each type of element (element formulation), and the definition of the interaction between one part to another. To construct the mesh of cervical spine model, a number of important factors were considered for each part: geometry, mechanical properties, loading conditions, and computational cost. Each of these aspects will be discussed in the following sections for each component of the full cervical spine.

All pre-processing and model construction was done using Hypermesh 7.0 (Altair Engineering Inc., Troy, MI) and LS-Pre/Post2 (LSTC, Livermore, CA). An element-breakdown summary of various parts in the cervical spine model can be seen in Table 6-1 at the end of this section

6.1.1 Vertebrae Construction

In the single spinal segment models, the C1 to C7 vertebrae were modeled as deformable parts, consisting of separate elements for cortical bone, cancellous bone, and the bony endplates. Cancellous bone, forming the bulk of the vertebra, was modeled using 3D solid hexagonal elements. Cortical bone and the bony endplates were both modeled using 2D quadrilateral shell elements, which were overlaid onto the outer surfaces of the solid cancellous bone elements. The choice of using a shell element rather than a solid element for both the cortical bone and the bony endplate is due to the relatively thin (less than 1 mm) nature of these tissues. Shell elements are also computationally cheaper (quicker to process) than solid elements, as through-thickness effects are not considered important for the current model.

The construction of a typical deformable vertebra can be seen in Figure 6-2, while all meshed cervical spine vertebrae (including T1) can be seen in Figure 6-10 at the end of this section. A contact algorithm is enabled for all vertebra in the instances that vertebra-vertebra contact does occur. It should be noted that both the skull (C0) and the T1 vertebrae were modeled as rigid bodies for both the full spine model and the single segment models. For this reason, the skull and T1 were modeled using shell elements only.
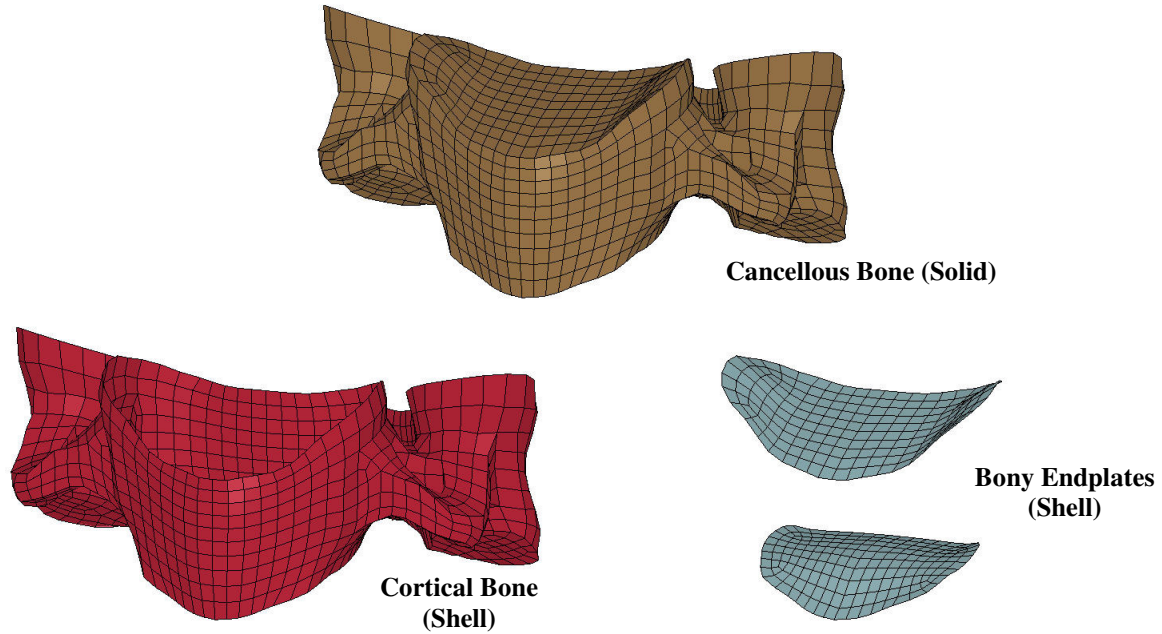
Figure 6-2: Components of Each Deformable Vertebra

6.1.2 Facet Joint Construction

The facet joints between the C2 to T1 vertebrae are represented in the cervical spine model with solid elements for articular cartilage and a simple pressure-volume airbag model for the synovial fluid. The typical facet joint (without capsular ligaments) can be seen in Figure 6-3. All articular cartilages are one solid element thick, except for in the C2-C3 facet joint, where they are two elements thick due to the excessively large gap between artilcular surfaces. Using one-element through the thickness of a part often leads to hourglassing issues, however the cartilage material is constrained one of its surfaces wthich reduced any potential hourglassing.

Capsular ligaments, represented by beam elements surrounding the perimeter of the articular cartilage, connect the complementary pair of articular surfaces (see Section 6.2.4 for more detail). All cartilage elements were attached to the vertebra using a tied contact to allow for attachment of dissimilar meshes (as the cartilage required finer mesh density). Frictionless contact was defined between all articular cartilage surfaces in the model.
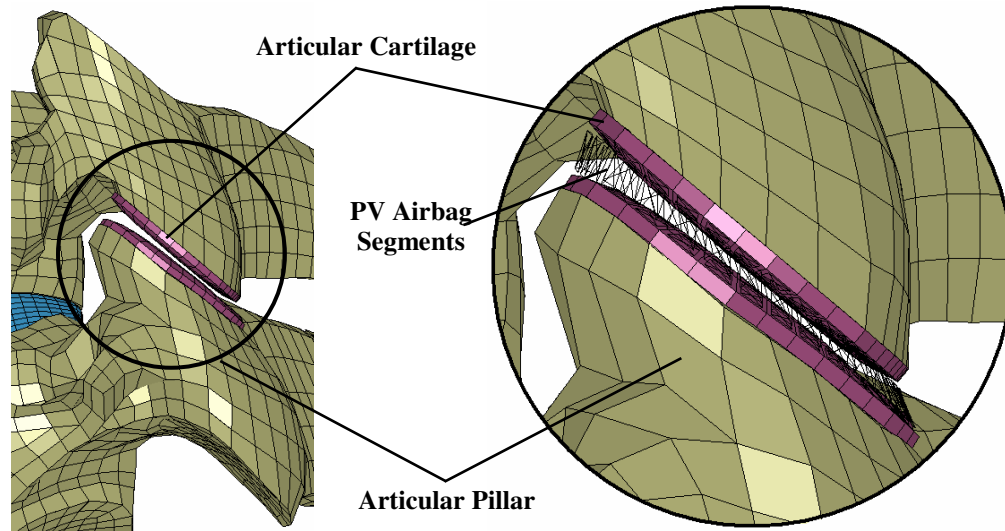
Figure 6-3: Construction of a Typical Facet Joint with Pressure-Volume Airbag

Because of the relative sliding motion between upper and lower articular surfaces of a facet joint during physiological loading, using fluid elements for the synovial fluid between the cartilage can result in highly distorted elements. This can lead to sharply decreasing timestep size and numerical instability. However, omitting the synovial fluid from the model creates unrealistic contact behaviour between the facet cartilages due to the present of an 'empty gap' (Kumaresan et al., 1998). Instead, the synovial fluid was modeled using a simple technique that applies a hydrostatic pressure to the surfaces of a defined volume (Figure 6-3), based on a user-inputted squeeze-film action relationship (detailed in Section 6.3.3). This simple method for modelling the synovial fluid in the facet joint allowed for realistic loading behaviour without a significant computational cost.

Cartilage in the upper cervical spine was also modeled to ensure proper interaction between the C0, C1, and C2 vertebrae. The upper cervical spine cartilage can be seen in Figure 6-4. The difference between the facet joints of the lower and middle cervical spine and that of the upper cervical spine is that no synovial fluid was modeled in the upper cervical spine. The complexity of the shape of the upper cervical spine, and the large relative motion between the C0, C1, and C2 made it difficult to implement the airbag method for the synovial fluid. This is not likely to have major implications in the model, but should be investigated in the future.
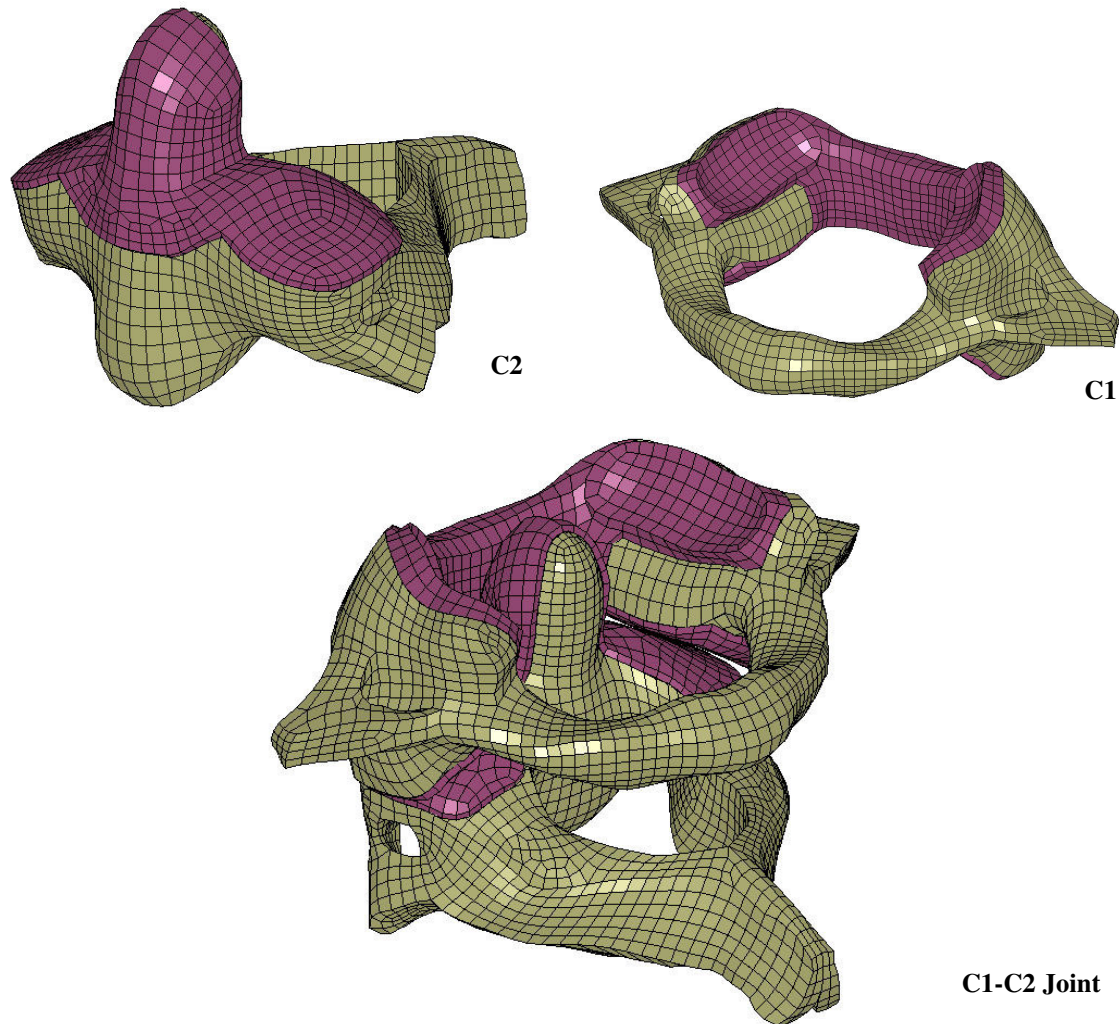
Figure 6-4: Construction of the Cartilage of the Upper Cervical Spine Joint

6.1.3 Intervertebral Disc Construction

The intervertebral disc is based on a structural (composite) annulus fibrosus model with shell layers for annulus fibrosus laminae and solid layers for annulus fibrosus ground substance. Structural AF models are composed of elements representing the fibres in the laminae, and the ground substance. Annular fibres have often been represented by non-linear truss elements imbedded in the ground substance elements (Yin and Elliot, 2005). However, more recently shell-based models of the annular fibres have be proved more representative of the AF tissue, and have improved the results of finite element models (Duncan et al., 1995a; Elliott and Setton, 2001). This type of intervertebral disc model has been utilized in other annulus fibrosus models (Duncan et al., 1995a; Halldin et al., 2000).

Each disc in the cervical spine model is constructed with a 'ring' of solid hexagonal elements of the annulus fibrosus ground substance that was four elements thick and eight elements high. Interlacing the solid ground substance elements were five pairs of concentric shell layers (10 layers total) representing the annulus fibrosus fibre lamina. Encompassed by the annulus fibrosus elements were solid hexagonal elements that represented the nucleus pulposus. An example of the construction of each disc can be seen in Figure 6-5.

Nucleus Pulposus

AF Ground Substance

AF Fibres

Complete Intervertebral Disc
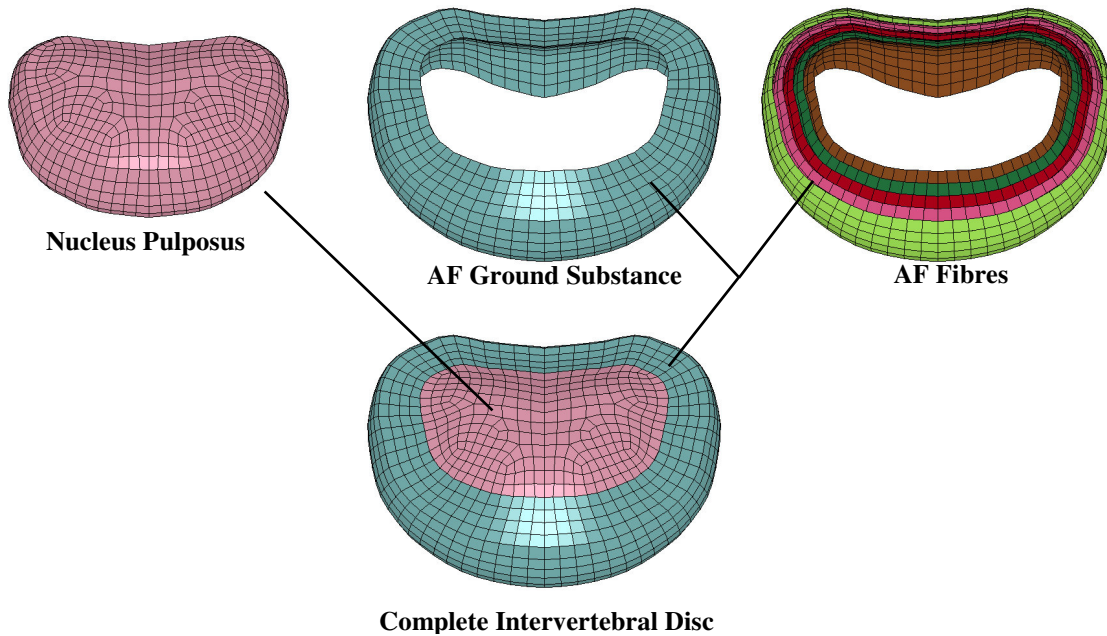
Figure 6-5: Components of Each Intervertebral Disc

A layer of shell elements representing the cartilagous endplate was incorporated on the superior and inferior surfaces of the intervertebral disc model (not shown in Figure 6-5). The cartilagous endplates were attached to the bony endplates of the vertebra by a tiebreak-type contact to allow for attachment of the finer intervertebral disc mesh to the courser vertebral mesh. A tiebreak contact also allowed for failure of the attachment in the case where the interface stresses exceed a defined limit. This type of contact is important for modelling endplate avulsion.

6.1.4   Ligament Construction

The mechanical properties for ligaments are quite complex to model, being non-linear, orthotropic, viscoelastic, and unable to carry compressive load. Additionally, experimental data on ligaments in the cervical spine are often reported as force-deflection rather than stress-strain, since measuring the length and the effective cross-sectional area of the ligament is often difficult (Przybylski et al., 1998).

For this reason, the ligaments in the cervical spine model were modeled using 1D discrete elements rather than 2D shell membrane elements. Discrete elements only provide axial force in tension or compression based on the change in element length, and does not provide bending or torsion strength. The use of discrete elements allows for material characterization from force-deflection data rather than stress-strain data that would be required for a continuum element. Discrete elements have been used to represent cervical spine ligaments in many previous models (Yoganandan et al., 1996b; Clausen et al., 1997; Halldin et al., 2000; Ng and Teo, 2001; Meyer et al., 2004).

Each ligament in the cervical spine was composed of a set of discrete elements spaced closely together and attached their respective vertebra by sharing common nodes. There is only one element between the origin and insertion point. The arrangement of these individual elements to form the whole ligament can be seen in Figure 6-6 for the lower and middle cervical spine.
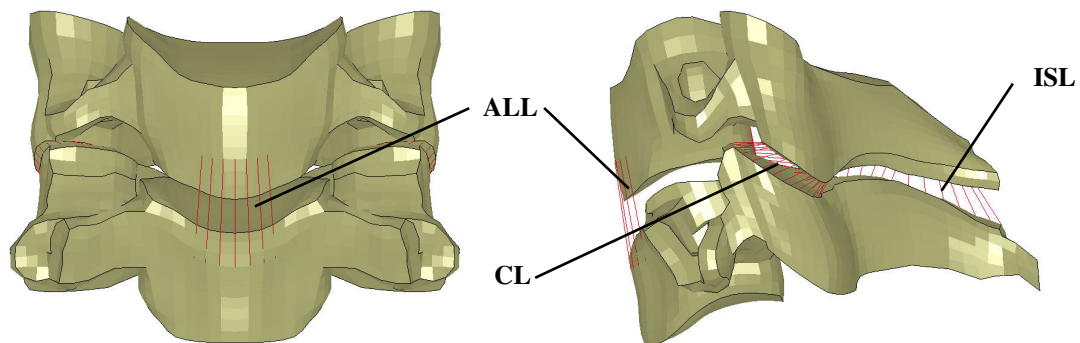
Figure 6-6: Arrangement of Some Ligaments in the Lower and Middle Cervical Spine

6.1.5 Muscle Construction

The cervical spine muscles were modelled using the Hill-type muscle model (as described in Section 6.3.7). This model accounts for the force generated between the origin and insertion points of the muscle from active and passive properties. The modelling of bulk muscle properties was not required since the neck does not often experience direct impact.

Each muscle element was represented using 1D discrete elements, which were broken up into separate segments that accounted for the various origin and insertions points of the muscle (see Table 2-6). This resulted in 90 separate muscle pairs (180 segments in total) representing the 27 different muscles of the cervical spine. Origin and insertions of each muscle segment are listed in Table 6-8 in Section 6.2.5.
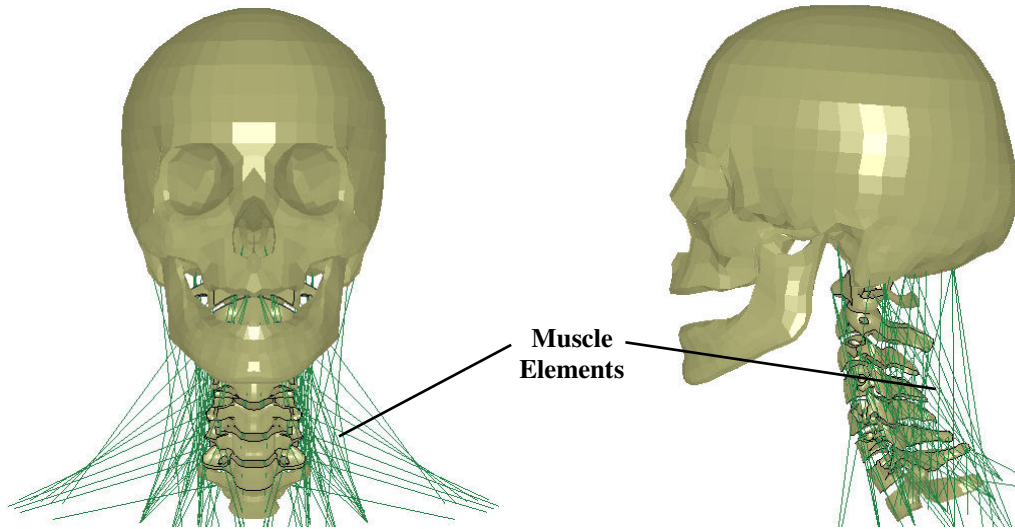
Figure 6-7: Muscle Elements of the Full Cervical Spine Model

To account for the changing load direction from muscle curvature during neck flexion or extension, each muscle segment was divided into equal length elements in series from origin to insertion point. Along with the origin node and the insertion node, intermediate nodes were constrained to a vertebra that the muscle segment spanned. For instance, a muscle segment with an origin on C2 and an insertion on C5 would be made up of three muscle elements with two intermediate nodes constrained to C3 and C4. Nodes that are constrained to the C4 vertebra can be seen in Figure 6-8, along with the effect of this method on the curvature of neck muscles in flexion.
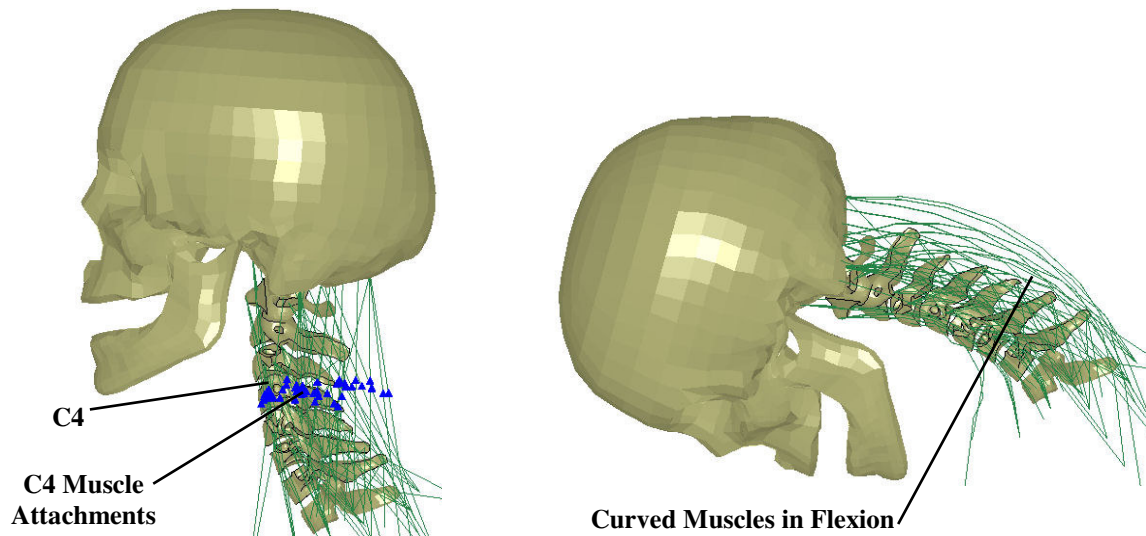
Figure 6-8: Attachment of Muscles to Vertebrae for Curved Muscle Response

The disadvantage to using this method of constrained intermediate nodes is that the force generated within each element a muscle segment may not be equal, and largely depend on the relative rotation

between adjacent vertebrae. Ideally, the nodes constrained to the intermediate vertebrae would serve as a guide for the muscle elements to slipover rather than to constrain. Attempts have been made achieve this effect using a newly implemented contact algorithm in LS-DYNA (*CONTACT_GUIDED_CABLE), but employing the guided cable method was not successful due to numerical stability issues. Preliminary impact studies suggest this force difference is present, but not in amounts that would significantly change the behaviour of the model.

Because discrete elements were used to model the muscles in the cervical spine, mass elements were added to account for the weight of the muscles. The mass of each element (located on a muscle segment node), was based on the volume of the muscle segment and a muscle density of 1.06 g/cm^3 was used (Ward and Lieber, 2005). The distribution of muscle mass in the cervical spine can be seen in Figure 6-9.
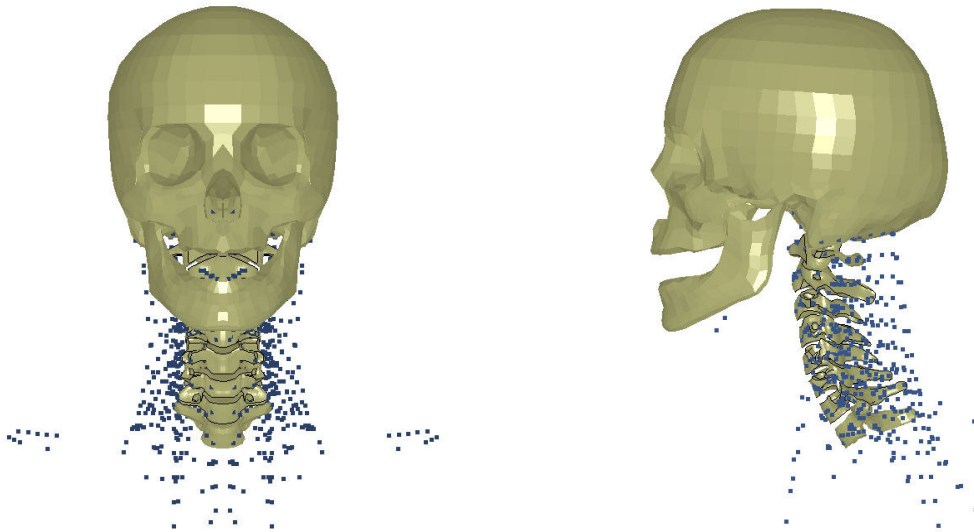
Figure 6-9: Distribution of Muscle Mass Elements

For future extension of the cervical spine model to a full body model, muscles that attach to parts of the human body not included in the cervical spine (scapula, sternum, clavicle, thoracic spine, etc.) were included as if these body parts were present in the model. Attachment of the nodes of these muscles that extended below the first thoracic vertebra were constrained to the first thoracic vertebra since all full cervical spine simulations are based on a prescribed motion to the T1.

Table 6-1: Summary of Elements for Each Part

Part	Level	Solid Elements	Shell Elements	Discrete Elements	Total Elements
Vertebrae					
	Skull	0	2894	0	2894
	C1	4208	2436	0	6644
	C2	7454	3380	0	10834
	C3	5747	3188	0	8935
	C4	3468	2334	0	5802
	C5	4152	2382	0	6534
	C6	3954	2362	0	6316
	C7	7042	3492	0	10534
	T1	0	742	0	742
Cartilage					
	Skull	320	0	0	320
	C1	824	0	0	824
	C2	896	0	0	896
	C3	518	0	0	518
	C4	350	0	0	350
	C5	368	0	0	368
	C6	376	0	0	376
	C7	590	0	0	590
	T1	276	0	0	276
IVD					
	C23	3712	5568	0	9280
	C34	4432	6388	0	10820
	C45	4096	5824	0	9920
	C56	4992	7008	0	12000
	C67	4256	6024	0	10280
	C7T1	4368	6212	0	10580
Ligaments					
	C012	0	18	281	299
	C23	0	0	97	97
	C34	0	0	98	98
	C45	0	0	84	84
	C56	0	0	98	98
	C67	0	0	101	101
	C7T1	0	0	115	115
Muscles					
	C0-T1	0	0	820	820
Total		66399	60252	1694	128345
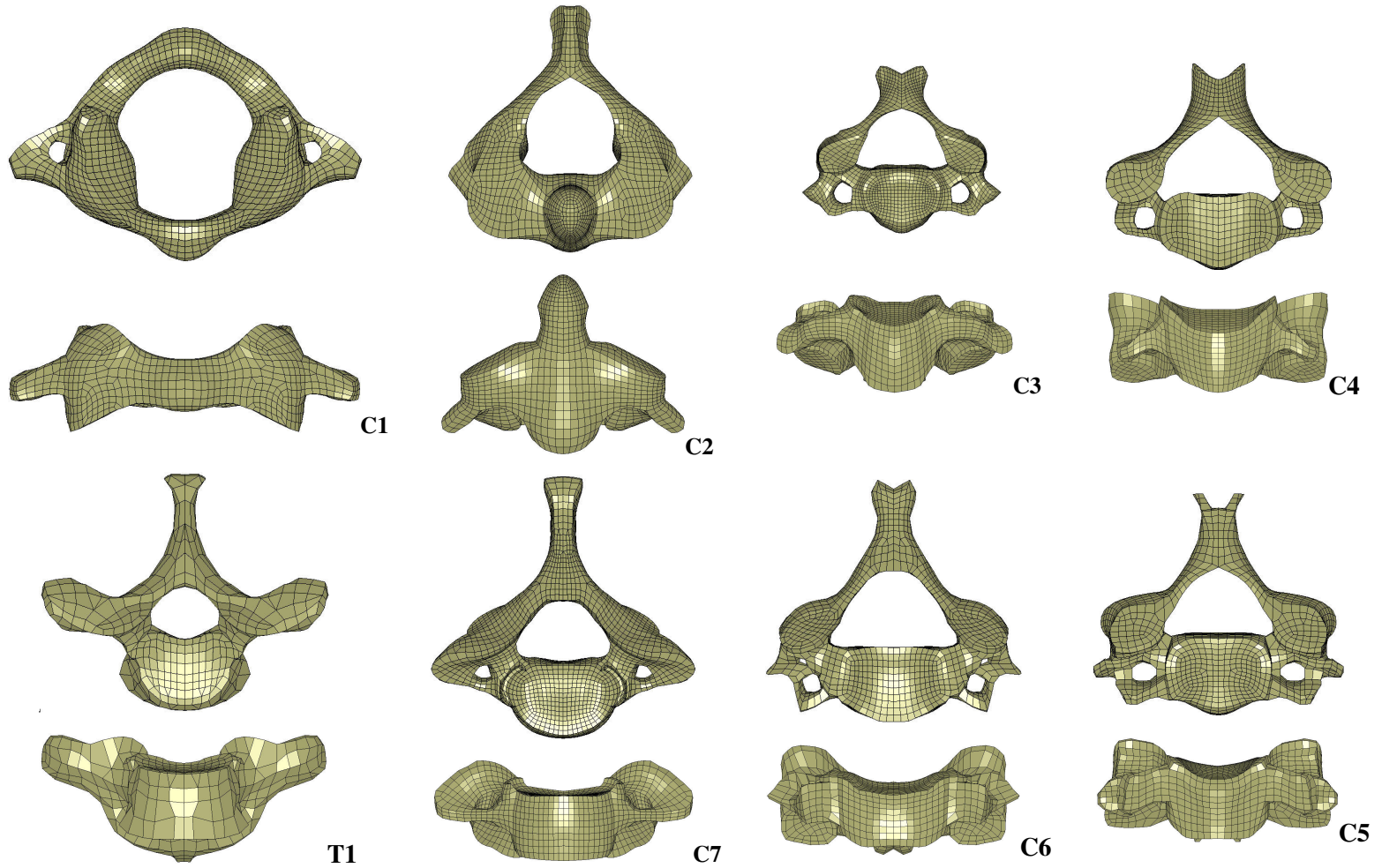
Figure 6-10: Geometry and Mesh of Each Vertebra in the Cervical Spine (To Scale)

6.2   Model Geometry

Model geometry is an important step in ensuring an accurate response during a numerical analysis. The adult human body comes in many shapes and sizes, with common sizes in the automotive industry ranging from the small 5th percentile female, the standard 50th percentile male, and to the very large 95th percentile male. The size and shape of the human body has a significant influence on the response of the cervical spine, particularly during an impact-loading scenario. Thus, it is important to design and verify that a numerical model meets the desired anthropometric size.

The cervical spine model detailed in this thesis was designed to meet the anthropometric specification for a mid-sized male (known as the 50th percentile male). The geometry of each vertebra was based on the model by Deng et al (1999), which was originally constructed from a commercial dataset of 3D surfaces (Viewpoint DataLab, Orem, UT). The entire original cervical spine geometry was scaled such that the dimensions of the skull agreed with the anthropometric data reported in Robbins (1983) for the 50th percentile male.

Soft tissues such as the intervertebral discs, ligaments, and musculature were added to the vertebra based on the qualitative observations from various studies, using the landmarks of the vertebrae as a reference. Detailed anatomic descriptions of the intervertebral discs and geometry can be found in Markolf and Morris (1974), Gilad and Nissan (1986), Pooni et al (1986), and Cassidy et al (1989). Literature on the location and geometry of cervical spine ligaments can be found in Dvorak and Panjabi (1987), Dvorak et al (1988), Panjabi et al (1991a, 1991b), Przybylski et al (1998), Yoganandan et al (2000a), Winkelstein et al (2001), and Mercer and Bogduk (2003). Muscle origin and insertion point can be found in textbooks such as Gray (1918), Agur and Dalley (2005), and Moore and Dalley (2006), as well as Chancey et al (2003).

6.2.1   Vertebral Geometry

Because the geometry of each vertebra was scanned from an individual person, some deviation from the 'ideal' 50th percentile male vertebral dimensions was expected. However, the dimensions of the vertebral bodies in the cervical spine model are all within one standard deviation of the dimensions measured by Gilad and Nissan (1986, see Table 2-1) for the 50th percentile males. The dimensions of each vertebral body are defined in Figure 6-11, and can be seen in Table 6-2.
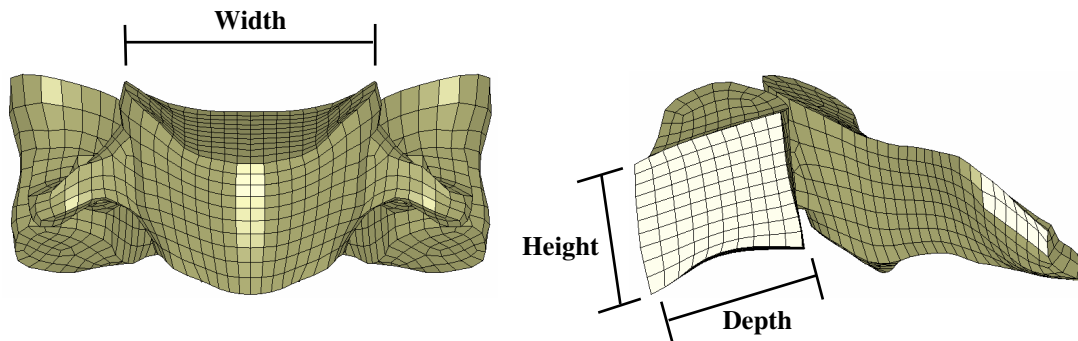
Figure 6-11: Dimensions of the Vertebral Body of the Cervical Spine Model

For the single segment models that use a deformable vertebra, thickness values for the cortical bone and bony endplate were assigned based on Panjabi et al (2001a). Endplate thickness was based on the average measured superior and inferior endplate thickness, while cortical bone thickness was based on the average measured anterior and posterior vertebral shell thickness. Cortical bone and bony endplate thickness in the model can be seen in Table 6-2.

Table 6-2: Vertebra Body Geometry and Bone Thickness of the Cervical Spine Model

Vertebral Body	C2	C3	C4	C5	C6	C7	T1
Depth							
(Superior)	15.4 mm	14.7 mm	17.0 mm	16.3 mm	17.3 mm	16.2 mm	18.5 mm
(Inferior)	15.4 mm	18.1 mm	17.4 mm	18.5 mm	16.0 mm	17.0 mm	18.5 mm
Height							
(Anterior)	24.3 mm	15.8 mm	14.4 mm	14.0 mm	12.0 mm	15.7 mm	15.2 mm
(Posterior)	18.5 mm	15.7 mm	15.1 mm	14.4 mm	13.3 mm	12.7 mm	17.1 mm
Width							
(Superior)	12.6 mm	19.9 mm	27.6 mm	24.2 mm	25.6 mm	24.6 mm	24.5 mm
(Inferior)	16.5 mm	21.0 mm	20.9 mm	22.9 mm	23.9 mm	23.2 mm	30.7 mm
Cortical Thickness	0.46 mm	0.46 mm	0.48 mm	0.53 mm	0.58 mm	0.59 mm	
Endplate Thickness	0.61 mm	0.61 mm	0.59 mm	0.58 mm	0.64 mm	0.64 mm	

Since the skull was constructed from rigid shell elements, mass and inertia properties were defined based on Walker et al (1973). The mass and the moment of inertia in the sagittal plane interia were both measured values, while the out-of-plane inertias were based on the interia ratios reported by Robbins (1983). These values can be found in Table 6-3.

Table 6-3: Mass and Moment of Interia of the Skull

| | Mass | Moment of Interia | | |
		Ixx	Iyy	Izz
Skull	4.376 kg	21060 kg mm^2	23300 kg mm^2	15200 kg mm^2

The centre of mass for the skull was also measured by Walker et al (1973) using X-Rays. The centre of mass of the head was calculated using polar coordinates, with the Frankfort plane as a baseline and the auditory meatus as the origin. It was found that the average position of the centre of mass was located 24.2 mm and 285° from the auditory meatus. The head was also reported to have a 7° tilt, measured between the transverse plane and the Frankfort plane.
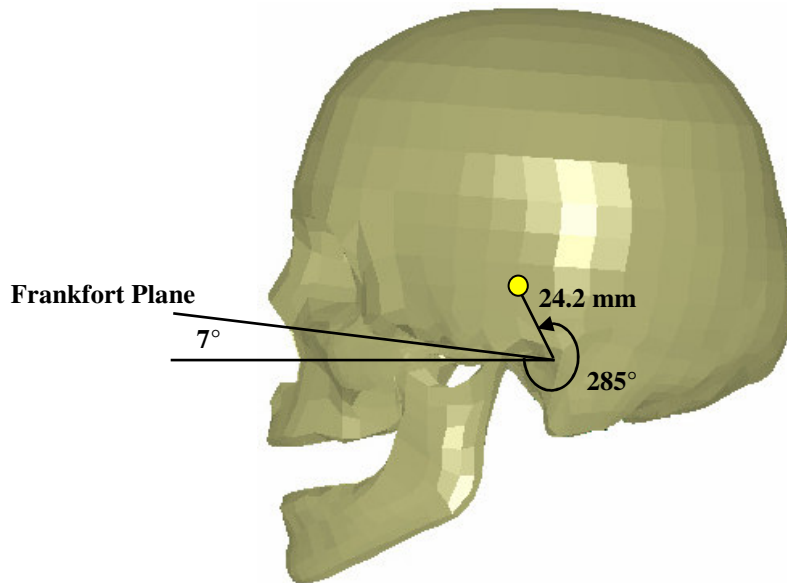
Figure 6-12: Centre of Mass of the Skull

6.2.2 Facet Joint Geometry

The size and shape of the modeled facet joints was dependant on the vertebral geometry described above. The size of the modeled facet joints were in good agreement with some of the facet joint studies listed in Table 2-2 (Francis, 1955; Panjabi et al., 1993; Pal et al., 2001; Yoganandan et al., 2003). The dimensions of the facet joints, and how they were defined, can be found in Figure 6-13 and Table 6-4.
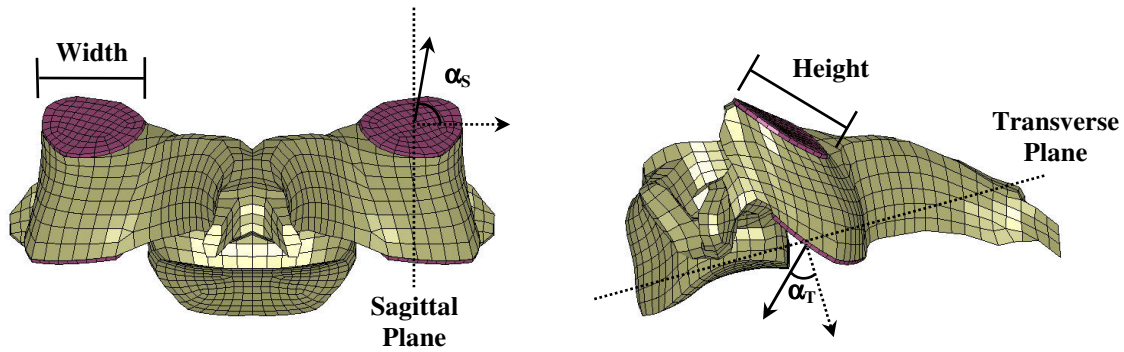
Figure 6-13: Dimensions of the Facet Joints of the Cervical Spine Model

The orientation of the modeled facet joints was also measured and compared to anatomical studies. Using the same method as Panjabi et al (1993), the orientation of the facet joints is measured by the angles made between the plane of the facet joint and the sagittal and transverse planes of the vertebra. The sagittal angle and transverse angle, α_S and α_T respectively, are essentially the angle between the facet plane normal vector, and the normal vectors from the sagittal and transverse planes (refer to Figure 6-13). The orientation of the facet joints in the model can be found in Table 6-4, and were in reasonable agreement with Panjabi et al (1993) and Pal et al (2001) (see Table 2-2).

Table 6-4: Facet Dimensions and Orientation of the Cervical Spine Model

| Facet	C1	C2	C3	C4	C5	C6	C7	T1
Height								
(Upper)	21.2 mm	18.7 mm	11.2 mm	11.0 mm	13.2 mm	12.9 mm	8.9 mm	12.5 mm
(Lower)	18.6 mm	9.2 mm	12.6 mm	9.8 mm	12.3 mm	12.5 mm	12.3 mm	
Width								
(Upper)	9.8 mm	16.4 mm	11.0 mm	13.0 mm	12.3 mm	13.6 mm	13.8 mm	12.4 mm
(Lower)	14.5 mm	12.2 mm	11.5 mm	10.9 mm	13.2 mm	13.2 mm	13.3 mm	
α_T								
(Upper)			55.5°	42.7°	51.1°	58.1°	67.0°	58.0°
(Lower)		52.2°	43.3°	50.7°	54.8°	61.1°	50.6°	
α_S								
(Upper)			91.6°	81.6°	88.7°	77.2°	80.1°	83.7°
(Lower)		95.6°	105.4°	89.2°	77.0°	82.2°	80.7°	

6.2.3   Intervertebral Disc Geometry

The intervertebral discs in the model were situated between adjacent vertebral bodies, so dimensions such as depth and width were based on the vertebral geometry. The anterior and posterior height of each disc was based on the distance between each adjacent vertebra. The vertebrae were arranged to provide disc heights in agreement with Gilad and Nissan (1986, see Table 2-3) for the 50th percentile male while maintaining a neutral spine curvature (discussed later). The height of each disc can be

seen in Table 6-5, while the depth and width of each disc correspond to the dimensions of the attached vertebral body, seen in Table 6-2.

Table 6-5: Intervertebral Disc Heights and Area of the Cervical Spine Model

IVD	C23	C34	C45	C56	C67	C7T1
Height						
(Anterior)	4.00 mm	4.95 mm	4.68 mm	5.42 mm	4.98 mm	5.02 mm
(Posterior)	3.61 mm	3.65 mm	3.94 mm	3.57 mm	3.79 mm	4.23 mm
Transverse Area	216.0 mm^2	340.2 mm^2	308.3 mm^2	354.0 mm^2	299.4 mm^2	358.6 mm^2
NP Area	44.9%	48.9 %	43.2 %	48.0 %	56.5 %	50.9 %

The transverse cross-sectional areas of each disc are within the 200 – 400 mm^2 range reported by Pooni et al (1986). However, Pooni et al (1986) reported increasing cross-sectional area from C2 to T1, but this is not the case in the model. The ratio of the nucleus pulposus area to the total invertebral disc area is approximately 1:2, which is the estimated size of the nucleus in healthy disc (Pooni et al., 1986; Iatridis et al., 1996).

When the vertebrae and intervertebral discs were assembled to create the full spine model, the overall dimensions of the cervical spine agreed with Robbins (1983). The distance between the C7/T1 joint (based on the C7 surface landmark) and the head/neck joint (based on the occipital condyles) is 121.4 mm in the model, compared to 118.8 mm as reported by Robbins (1983) for a mid-sized male. The method of determining the length of the cervical spine (as defined by Robbins) can be seen in Figure 6-14.
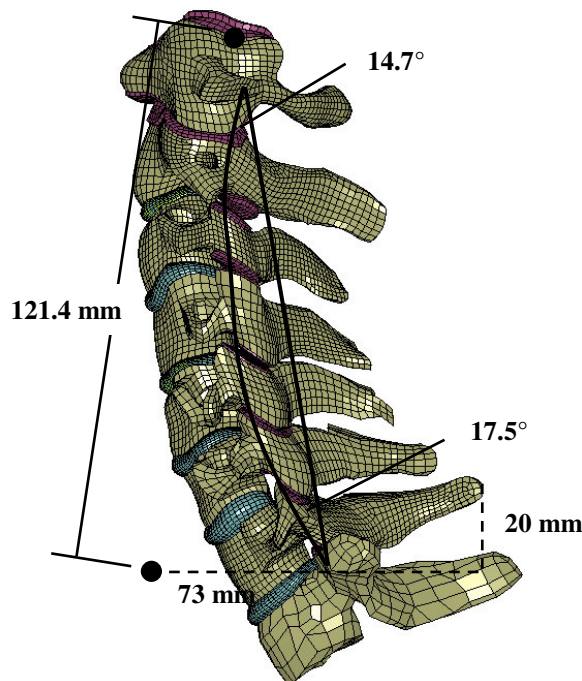

Figure 6-14: Length and Curvature of Cervical Spine Model

A natural cervical spine curvature exists for a seated occupant that is dependant on age, sex, and stature, and has been shown to influence the likelihood of an injury during impact (Klinich et al., 2004). By defining the inferior and superior angles of a cubic Bezier curve that runs from the posterior margins of C2 through C7 vertebral bodies (the method used by Klinich et al), the full spine model had an inferior angle of 17.5° and a superior angle of 14.7° (Figure 6-14). These angles agree well with anthropometric data from Klinich et al (2004) that the full cervical spine model has a curvature that is natural to a seated 50th percentile male.

6.2.4   Ligament Geometry

The ligaments in the model were positioned based on the origin and insertion locations described in various studies and anatomy textbooks mentioned previously. Since the material model used to represent the ligaments used force-deflection type data rather than stress-strain type data, it was not required that ligament geometry (length and cross-section) be modeled exactly as measured in the various anatomical studies (Panjabi et al., 1991a and 1991b; Przybylski et al., 1998; Yoganandan et al., 2000a). It is also evident from Table 2-4 that different laboratories used different techniques and definitions to measure the geometry of cervical spine ligaments, resulting in an inconsistent pool of research data. Nevertheless, the dimensions of all ligaments modeled in the cervical spine model agree with anatomical studies, with the exception of the capsular ligaments. For ease of modelling, the capsular ligaments were modeled extending along the circumferential edge of the vertebral-side of the facet cartilage, which results in a much shorter ligament length. Since the model will used force-deflection based material properties (Section 6.3.6), this is not an issue in the model.

Table 6-6: Dimensions of the Lower and Middle Ligaments of the Cervical Spine Model

Ligament		C23	C34	C45	C56	C67	C7T1
ALL							
	(Length)	11.8 mm	14.1 mm	13.7 mm	11.7 mm	12.5 mm	13.0 mm
	(Width)	10.4 mm	9.1 mm	9.4 mm	9.6 mm	9.8 mm	9.6 mm
PLL							
	(Length)	13.1 mm	11.3 mm	12.5 mm	9.9 mm	10.5 mm	11.5 mm
	(Width)	9.8 mm	8.8 mm	10.3 mm	10.9 mm	10.5 mm	10.7 mm
LF							
	(Length)	9.3 mm	9.8 mm	7.9 mm	9.6 mm	7.7 mm	10.5 mm
	(Width)	17.5 mm	13.2 mm	19.4 mm	20.0 mm	17.3 mm	18.9 mm
ISL							
	(Length)	10.0 mm	9.4 mm	7.3 mm	5.5 mm	5.0 mm	11.2 mm
	(Width)	13.2 mm	8.8 mm	10.7 mm	13.1 mm	16.4 mm	23.3 mm
CL							
	(Length)	4.9 mm	3.4 mm	2.8 mm	2.2 mm	2.6 mm	4.6 mm
	(Circumference)	35.8 mm	39.2 mm	37.2 mm	42.0 mm	40.0 mm	40.6 mm

Table 6-7: Dimensions of the Upper Ligaments of the Cervical Spine Model

Ligament			Ligament			Ligament		
AAOM			CL (C01)			Nuchal		
	(Length)	27.7 mm		(Length)	3.9 mm		(Length)	47.3 mm
	(Width)	16.6 mm		(Circumference)	61.7 mm		(Width)	5.5 mm
AAAM			CL (C12)			Transverse		
	(Length)	17.3 mm		(Length)	4.4 mm		(Length)	30.0 mm
	(Width)	10.1 mm		(Circumference)	61.8 mm		(Width)	6.5 mm
Tectorial Mem			Apical			Sup. Crux		
	(Length)	29.1 mm		(Length)	22..4 mm		(Length)	31.7 mm
	(Width)	4.3 mm		(Width)	4.0 mm		(Width)	4.9 mm
PAOM			Alars (C02)			Inf. Crux		
	(Length)	14.1 mm		(Length)	6.4 mm		(Length)	7.8 mm
	(Width)	42.3 mm		(Width)	5.1 mm		(Width)	3.7 mm
PAAM			Alars (C12)			ISL (C12)		
	(Length)	10.6 mm		(Length)	4.7 mm		(Length)	12.3 mm
	(Width)	29.4 mm		(Width)	3.1 mm		(Width)	4.8 mm

6.2.5   Muscle Geometry

The muscles were added based on the descriptions provided in clinical anatomy textbooks, using landmarks on the vertebrae and skull as a reference. All muscles with origin or insertion points not on the cervical spine were modelled as they would be in a full body model, but constrained to the T1 vertebra for cervical spine simulation. All geometric details of the cervical spine muscle segments can be seen in Table 6-8. The length of each muscle is the straight distance from origin to insertion point, while PCSA and volume information was taken from the literature (Knaub and Myers, 1998). For muscles with multiple segments, PCSA was divided evenly amongst each segment, whereas segment volume was determined based on the relative length of the segment in the muscle.

Table 6-8: Muscle Geometry in Cervical Spine Model

Muscle Segment	Origin	Insertion	Length (mm)	PCSA (cm^2)	Volume (g/cm^3)
Oblique Capitus Inferior	C2	C1	57.13	1.950	8.13
Oblique Capitus Superior	C1	C0	21.88	0.880	3.03
Rectus Capitus Major	C2	C0	49.22	1.680	5.37
Rectus Capitus Minor	C1	C0	14.48	0.920	1.82
Longus Capitis A	C3	C0	62.04	0.343	1.84
Longus Capitis B	C4	C0	86.30	0.343	2.56
Longus Capitis C	C5	C0	103.68	0.343	3.08
Longus Capitis D	C6	C0	121.18	0.343	3.60
Total Longus Capitis				1.370	11.09
Longus Colli Sup A	C3	C1	40.85	0.230	0.76
Longus Colli Sup B	C4	C1	64.55	0.230	1.19
Longus Colli Sup C	C5	C1	81.10	0.230	1.50
Longus Colli Inf A	T1	C5	63.74	0.345	1.76
Longus Colli Inf B	T2	C6	61.05	0.345	1.69
Longus Colli Vert A	C5	C2	76.37	0.457	2.32
Longus Colli Vert B	C6	C3	73.24	0.457	2.23
Longus Colli Vert C	C7	C4	76.93	0.457	2.34

(continued…)

Table 6-8: Muscle Geometry in Cervical Spine Model continued…

Muscle Segment	Origin	Insertion	Length (mm)	PCSA (cm^2)	Volume (g/cm^3)
Total Longus Colli				2.750	13.79
Rectus Capitis Ant	C1	C0	22.74	1.300	1.36
Rectus Capitis Lat	C1	C0	11.88	1.300	1.74
Anterior Scalene A	C3	T1	128.88	0.470	3.13
Anterior Scalene B	C4	T1	104.73	0.470	2.54
Anterior Scalene C	C5	T1	88.20	0.470	2.14
Anterior Scalene D	C6	T1	72.04	0.470	1.75
Total Anterior Scalene				1.880	9.56
Middle Scalene A	C2	T1	122.85	0.227	2.36
Middle Scalene B	C3	T1	116.03	0.227	2.23
Middle Scalene C	C4	T1	97.07	0.227	1.86
Middle Scalene D	C5	T1	80.89	0.227	1.55
Middle Scalene E	C6	T1	69.29	0.227	1.33
Middle Scalene F	C7	T1	54.14	0.227	1.04
Total Middle Scalene				1.360	10.38
Posterior Scalene A	C5	T1	84.75	0.350	2.51
Posterior Scalene B	C6	T1	73.11	0.350	2.17
Posterior Scalene C	C7	T1	57.23	0.350	1.70
Total Posterior Scalene				1.050	6.38
Sternocleido Mastoid A	T1	C0	169.10	2.460	25.54
Sternocleido Mastoid B	T1	C0	202.33	2.460	30.55
Total Sternocleido Mastoid				4.920	56.09
Iliocostalis Cervicis A	T1	C3	120.07	0.260	2.20
Iliocostalis Cervicis B	T1	C4	102.71	0.260	1.88
Iliocostalis Cervicis C	T1	C5	91.46	0.260	1.67
Iliocostalis Cervicis D	T1	C6	79.83	0.260	1.46
Total Iliocostalis Cervicis				1.040	7.21
Longissimus Capitis A	C4	C0	67.15	0.196	1.71
Longissimus Capitis B	C5	C0	84.17	0.196	2.14
Longissimus Capitis C	C6	C0	97.63	0.196	2.49
Longissimus Capitis D	C7	C0	116.60	0.196	2.97
Longissimus Capitis E	T1	C0	118.28	0.196	3.01
Total Longissimus Capitis				0.980	12.33
Longissimus Cervicis A	T1	C2	85.84	0.298	1.68
Longissimus Cervicis B	T1	C3	99.04	0.298	1.94
Longissimus Cervicis C	T1	C4	98.13	0.298	1.92
Longissimus Cervicis D	T1	C5	103.29	0.298	2.02
Longissimus Cervicis E	T1	C6	109.00	0.298	2.14
Total Longissimus Cervicis				1.490	9.71
Multifidus A	C4	C2	42.10	0.200	4.34
Multifidus B	C5	C3	33.99	0.350	3.51
Multifidus C	C6	C4	33.95	0.450	3.50
Multifidus D	C7	C5	44.45	0.450	4.59
Multifidus E	T1	C6	38.75	0.450	4.00
Multifidus F	T1	C7	45.56	0.450	4.70
Total Multifidus				2.350	24.64

(continued…)

Table 6-8: Muscle Geometry in Cervical Spine Model continued…

Muscle Segment	Origin	Insertion	Length (mm)	PCSA (cm2)	Volume (g/cm3)
Semisplenius Capitus A	C4	C0	65.94	0.613	2.53
Semisplenius Capitus B	C5	C0	82.40	0.613	3.16
Semisplenius Capitus C	C6	C0	97.01	0.613	3.72
Semisplenius Capitus D	C7	C0	114.36	0.613	4.39
Semisplenius Capitus E	T1	C0	118.09	0.613	4.53
Semisplenius Capitus F	T1	C0	135.88	0.613	5.21
Semisplenius Capitus G	T1	C0	153.81	0.613	5.90
Semisplenius Capitus H	T1	C0	188.81	0.613	7.24
Semisplenius Capitus I	T1	C0	207.97	0.613	7.98
Total Semisplenius Capitus				5.520	44.67
Semisplenius Cervicis A	T1	C2	80.54	0.765	5.85
Semisplenius Cervicis B	T1	C3	79.91	0.765	5.81
Semisplenius Cervicis C	T1	C4	83.75	0.765	6.09
Semisplenius Cervicis D	T1	C5	88.65	0.765	6.44
Total Semisplenius Cervicis				3.060	24.19
Splenius Capitis A	C7	C0	119.27	0.773	6.25
Splenius Capitis B	T1	C0	139.86	0.773	7.33
Splenius Capitis C	T1	C0	156.12	0.773	8.19
Splenius Capitis D	T1	C0	169.64	0.773	8.90
Total Splenius Capitis				3.090	30.67
Splenius Cervicis A	T1	C1	169.98	0.477	4.67
Splenius Cervicis B	T1	C2	169.47	0.477	4.65
Splenius Cervicis C	T1	C3	184.30	0.477	5.06
Total Splenius Cervicis				1.430	14.38
Levator Scapula A	C1	T1	135.66	0.780	10.88
Levator Scapula B	C2	T1	120.24	0.780	9.64
Levator Scapula C	C3	T1	116.24	0.780	9.32
Levator Scapula D	C4	T1	99.60	0.780	7.99
Total Levator Scapula				3.120	37.83
Minor Rhomboid A	C7	T1	59.07	0.510	4.18
Minor Rhomboid B	T1	T1	46.44	0.510	3.29
Total Minor Rhomboid				1.020	7.47
Trapezius A	C0	T1	176.06	1.526	17.19
Trapezius B	C1	T1	168.37	1.526	16.44
Trapezius C	C2	T1	156.79	1.526	15.31
Trapezius D	C3	T1	148.04	1.526	14.46
Trapezius E	C4	T1	147.82	1.526	14.44
Trapezius F	C5	T1	151.46	1.526	14.79
Trapezius G	C6	T1	144.85	1.526	14.15
Trapezius H	C7	T1	140.50	1.526	13.72
Trapezius I	T1	T1	118.62	1.526	11.58
Total Trapezius				13.730	132.09
Omohyoid	T1	C0	124.07	1.175	6.35
Sternohyoid	T1	C0	141.17	1.175	5.81

6.3 Material Properties

To incorporate the mechanical properties of the various tissues of the human body into the numerical model, experimental data derived from *in vitro* tissue studies are required. Unfortunately, the experimental data for many of the tissues in the cervical spine are sometimes in a format unsuitable for numerical modelling, limited in application, or are just not available in the current literature (Panjabi, 1998). Considering what types of material data to use is a very important step, since the numerical model is only as good as its constituents.

A strong consideration regarding material constitutive models was based on the availability in LS-DYNA. Despite having nearly 200 fully functional models in its material catalog, LS-DYNA currently lacks in material models that are particularly suited for biological tissues under impact loading. A few bio-related material models, such as the fibre-reinforced hyperelastic model MAT_SOFT_TISSUE, have been implemented for tissue modelling purposes, but experience has shown these models to be unstable for certain types of impact simulation, especially using shell elements. LS-DYNA does have the capabilities for the user to create an original material model, which would be ideal for developing a material model for tissue. However, this process is very time demanding because of the extensive implementation, verification, and validation process required with a user-material. Nonetheless, due to time constraints, all tissues in the cervical spine were modeled from built-in LS-DYNA materials, with a penchant for numerical stability and ease of implementation.

6.3.1 Bone Material Model

Under physiologic loading, the mechanical properties of bone are linear and anisotropic (refer to Section 3.2). Traumatic loading beyond a certain yield strain (the onset of damage) causes the bone stiffness to soften, and permanent deformation. Unloading of the yielded bone is then along a reduced elastic modulus (refer to Figure 3-8). This type of material behaviour is best represented by a brittle damage material model. Unfortunately, anisotropic brittle damage models are complex and require material data that is currently unavailable for bone. However, the use of an elastic-plastic material model for bone in this model is an adequate choice for identifying the onset of bone damage from a single loading.

A simple isotropic power-law plasticity material model was employed to represent the bone mechanical behavior for both physiological and traumatic loading. An isotropic material law was

chosen because anisotropy in elastic-plastic models typically deals with the direction-dependency of yield stress rather than stiffness. The elastic behaviour of the power-law plasticity model is based on a simple linear stress-strain relation (Equation 6-1). Plastic behaviour is based on a non-linear function that describes the yield stress (Equation 6-2). The intersection of these two relationships, known as the yield point, is the boundary between elastic and plastic deformation. The stress-strain relationship for this model can be seen in Figure 6-15.

$$\sigma = E \cdot \varepsilon \qquad \qquad \text{Equation 6-1}$$

$$\sigma = k \cdot \varepsilon^n = k \cdot \left(\varepsilon_{yp} + \varepsilon_p \right)^n \qquad \qquad \text{Equation 6-2}$$

where E is the elastic Young's modulus, ε_{yp} is the elastic strain to yield, ε_p is the effective plastic strain, and k and n are parameters of the yield function. The three parameters for creating the power-law model (E, k, and n), can be determined from experimental data.
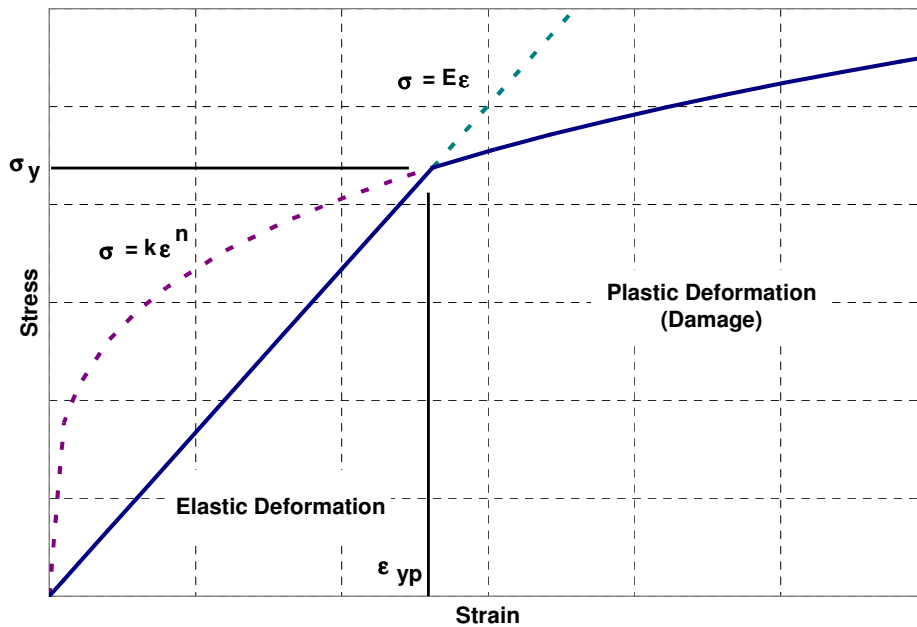
Figure 6-15: Power-Law Plasticity Model for Bone Damage Modelling

Fitting the power-law model to experimental bone data required the elastic modulus (E), the yield point (ε_{yp} and σ_y), and one other post-yield stress-strain point. The experimental data selected to generate the power-law parameters for cortical and cancellous bone were from Currey (2004), and Kopperdahl and Keaveny (1998) respectively. The mechanical properties of cortical bone reported by Currey were consistent with previous cortical bone studies (refer to Table 3-1), while Kopperdahl and Keaveny reported stiffer values for vertebral cancellous bone than previous studies. Their reasoning

for this discrepancy was that previous cancellous bone studies had certain sample end-artifacts that over predicted tissue strain. These end-artifacts were successfully removed in their study, and accurate mechanical properties were obtained.

There are no existing studies that look at the mechanical properties of the bony endplates in uniaxial tension or compression, so the material properties were assumed to be $1/3^{rd}$ the stiffness of cortical bone with the same yield and ultimate strain. The mechanical properties for the bony endplates are similar to those used by Denoziere and Ku (2006).

Table 6-9: Material Property Summary for Bone

Part	Material Model	Material Parameters	References
Cancellous Bone	Elastic-Plastic (Power-Law)	$E = 291$ MPa, $v = 0.3$ $k = 7.118$ MPa, $n = 0.2741$	Kopperdahl and Keaveny, 1998
Cortical Bone	Elastic-Plastic (Power-Law)	$E = 16700$ MPa, $v = 0.3$ $k = 440.8$ MPa, $n = 0.2772$	Currey, 2004
Bony Endplate	Elastic-Plastic (Power-Law)	$E = 5567$ MPa, $v = 0.3$ $k = 146.9$ MPa, $n = 0.2772$	Denoziere and Ku, 2006

For the complete cervical spine model, the vertebrae were modeled as rigid bodies, which is a technique used in previous full spine models. This concession was made based on reducing the required computation time for an impact simulation. The primary limitation of using rigid body vertebrae is the inability to predict failure of the bone. By reducing the vertebrae to rigid bodies, approximately 56,000 elements are removed from processing, which is almost half of the total number of deformable elements. This simplification may be justified since the validation case for the full cervical spine was based on human volunteer experiments, where significant deformation of the vertebrae would not likely occur. The deformable vertebrae can still be implemented into the full cervical spine model, with very little effort.

6.3.2 Cartilage Material Model

As described in Section 3.3, cartilage is a poroelastic material that has nonlinear mechanical properties with a strong dependency on internal fluid-flow at low strain-rates. For this reason, previous numerical models of articular cartilage have utilized a linear biphasic poroelastic model (BPE) to describe the response of cartilage during long-duration events. This model is described in detail by Mow et al (1980). In brief, the biphasic model accounts for the viscoelastic response of cartilage caused by the viscous dissipation of fluid through an incompressible and permeable solid-phase. This model has been successfully applied to many studies on the viscoelastic response of cartilage (Mow et al., 1980; Ateshian et al., 1997; DiSilvestro and Suh, 2001). However, this model is typically limited to creep or relaxation type loading behaviours.

Despite the wide use of biphasic models in biomechanics, this type of material model is not available in LS-DYNA, and is not considered necessary for the strain-rates encountered during impact loading. An alternative to the biphasic model for articular cartilage is the quasi-linear viscoelastic model (QLV). This type of model is described in detail by Fung (1993). Unlike the fluid-dissipating BPE model, this particular material model is incompressible, meaning that fluid loss does not occur. The QLV model utilizes an arbitrary strain-energy function for the quasi-static response of the material, but accounts for strain rate effects (including relaxation and creep) using a convolution integral (Equation 6-3) with a relaxation function (Equation 6-4). This is appropriate for impact conditions where the amount of fluid flow is expected to be small.

$$\sigma = \int_{0}^{t} g(t - \tau) \cdot \frac{d}{d\tau}\varepsilon \; d\tau \qquad\qquad \textbf{Equation 6-3}$$

$$g(t) = \sum_{m=1}^{N} G_m \cdot e^{-\beta_m \cdot t} \qquad\qquad \textbf{Equation 6-4}$$

where g(t) is the relaxation function characterized by G_m and β_m, which are the constants from the Prony series of N terms. This type of linear viscoelastic model is readily available in most finite element codes.

A general linear viscoelastic Maxwell model was used for articular cartilage in the cervical spine model. This model is a simple isotropic linear-elastic material with viscoelasticity being accounted for by the convolution integral seen in Equation 6-3. The assumption of incompressibility for the cartilage material is valid for the short-duration, impact modelling of the cervical spine, since *in vivo* interstitial fluid flow is expected to be negligible during this event.

The material properties used to develop the linear viscoelastic model for articular cartilage were based on DiSilvestro and Suh (2001). This study reported the relaxation testing of bovine articular cartilage in unconfined compression. To be able to fit the results of DiSilvestro and Suh (2001), the linear viscoelastic model was derived to fit the relaxation test conditions. During a relaxation test, an unloaded sample is loaded to a strain ε_1 from t = 0 to t = t_1 at a constant strain rate. The convolution integral (Equation 6-5) for this process then simplifies to:

$$\sigma_1(t) = \frac{\varepsilon_1}{t_1} \cdot \int_0^t \sum_{m=1}^{N} G_m \cdot e^{-\beta_m \cdot (t-\tau)} \, d\tau$$

Equation 6-5

$$\sigma_1(t) = \frac{\varepsilon_1}{t_1} \cdot \sum_{m=1}^{N} G_m \cdot \left(1 - e^{-\beta_m \cdot t}\right) \quad \text{for } 0 \leq t < t_1$$

Equation 6-6

where ε_1 is the relaxation strain, and t_1 is the ramp time to get to the relaxation strain. The integration of this equation results in Equation 6-6, the time-based stress of the sample during the initial ramp of a relaxation test. When the relaxation strain is held constant (from t_1 onwards), the effective strain-rate for this timespan is zero, thus the convolution integral becomes:

$$\sigma_2(t) = \frac{\varepsilon_1}{t_1} \cdot \int_0^{t_1} \sum_{m=1}^{N} G_m \cdot e^{-\beta_m \cdot (t-\tau)} \, d\tau + 0 \cdot \int_{t_1}^t \sum_{m=1}^{N} G_m \cdot e^{-\beta_m \cdot (t-\tau)} \, d\tau$$

Equation 6-7

$$\sigma_2(t) = \frac{\varepsilon_1}{t_1} \cdot \sum_{m=1}^{N} G_m \cdot \left[e^{-\beta_m \cdot (t-t_1)} - e^{-\beta_m \cdot t} \right] \quad \text{for } t_1 \leq t < \infty$$

Equation 6-8

Therefore Equation 6-8 describes the time-based stress of the sample during the holding period of a relaxation test. From the stress-time equations derived in Equation 6-6 and Equation 6-8, the Prony series constants G_m and β_m were found using the least squares method for non-linear curve fitting (R^2 = 0.991). This result can be found in Figure 6-16, where the material was ramped to a strain of 5% over 50 s. The quasi-static elastic modulus was reported to be 0.63 MPa.
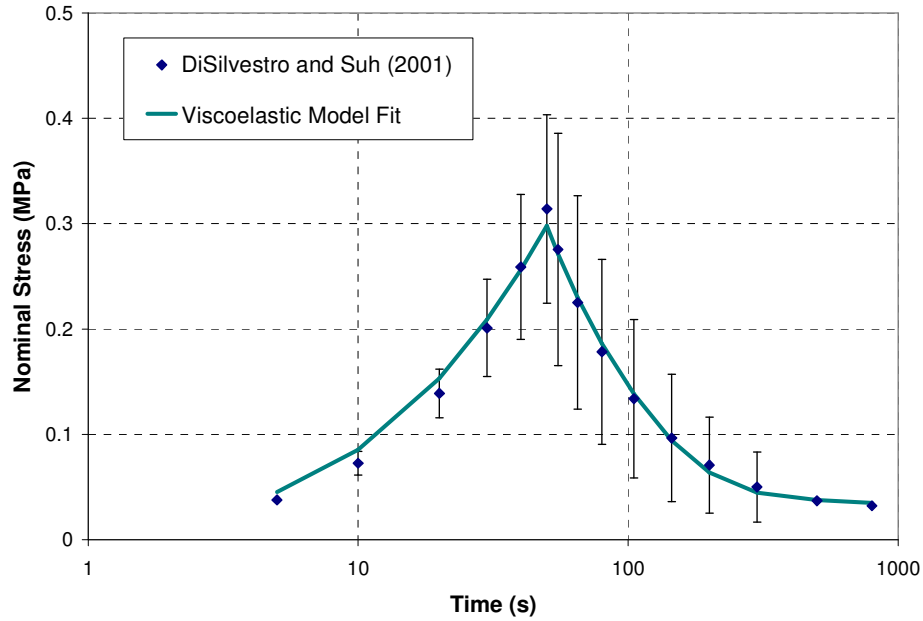
Figure 6-16: Articular Cartilage Response and Model Fit

It should be noted that the strain-rate used to load the cartilage sample was 0.001 1/s, which is considered very slow compared to possible strain-rates one would expect to see during an automotive impact (approximately 10 to 100 1/s). The result of using viscoelastic material data obtained from relaxation testing at low ramp rates can be seen in Figure 6-17, where it is shown that the current model predicts only minute differences in the stiffness for strain-rates higher than 0.1 1/s. This may be a limitation to the model and high rate testing of cartilage is required.
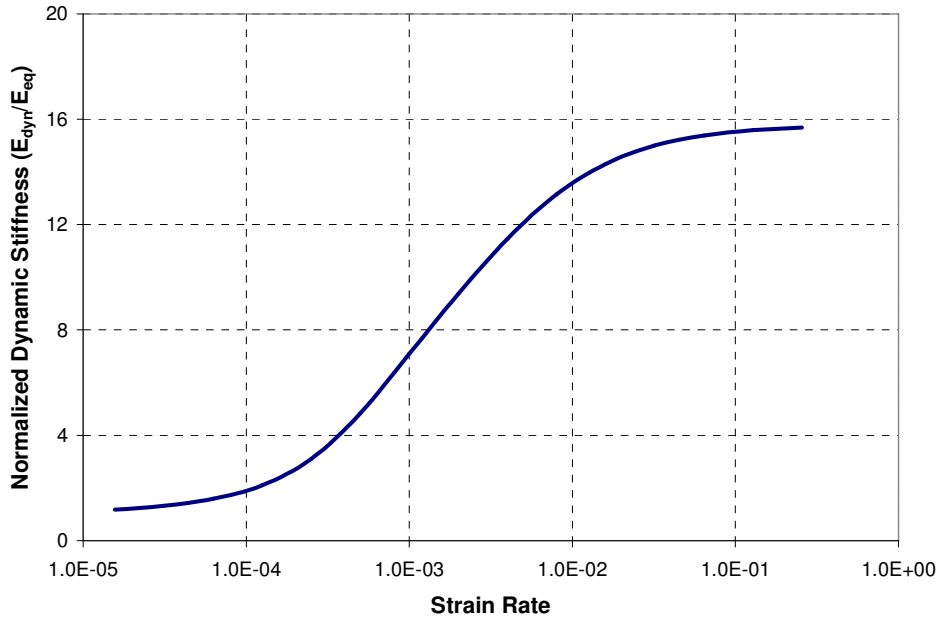
Figure 6-17: Effect of Strain-Rate on Current Cartilage Model

The constants used in the linear viscoelastic model for articular cartilage can be found in Table 6-10. For the quasi-static simulations involving the segment models, the equivalent linear elastic material model was used. This material model is also used to model the cartilagous endplates due to a lack of available material data on that specific tissue.

Table 6-10: Material Property Summary for Articular Cartilage

Part	Material Model	Material Parameters	References
Articular Cartilage and Cartilagous Endplates	Linear Viscoelastic	$N = 4$, $K = 2.0$ GPa $G_1 = 0.2100$ MPa, $\beta_1 = 0$ 1/s $G_2 = 0.0243$ MPa, $\beta_2 = 0.000303$ 1/s $G_3 = 1.0824$ MPa, $\beta_3 = 0.080807$ 1/s $G_4 = 1.9984$ MPa, $\beta_4 = 0.012927$ 1/s	DiSilvestro and Suh, 2001
	Linear Elastic	$E = 0.630$ MPa, $\nu = 0.10$	

6.3.3 Synovial Fluid Model

As mentioned in Section 6.1.2, the construction of the facet joints required a simple squeeze-film bearing model to represent the synovial fluid. In order to determine the squeeze-film relationship for each facet joint in the cervical spine model, a simplified facet joint model was developed and tested in compression. The results of the simplified compression tests were then used to define the squeeze-film relationship for the model, using the relative pressure-volume result.

A simplified model of the facet joint was developed that was similar to the fluid-based facet joint model by Kumaresan et al (1998). A quarter-model of two identical elliptical plates (rigid) were

modeled 1 mm apart. The dimensions of the plates were taken to be the average width and height of a pair of corresponding facets (see Table 6-4) associated with each level. Between the plates were fluid elements (synovial fluid) with a bulk modulus of 2.2 GPa (equivalent to water). Enclosing the outer surface of the fluid elements were shell membrane elements (synovial membrane) with a Young's modulus of 10 MPa and a Poisson's ratio of 0.4 (Kumaresan et al, 1998). The simplified facet joint model can be seen in Figure 6-18.
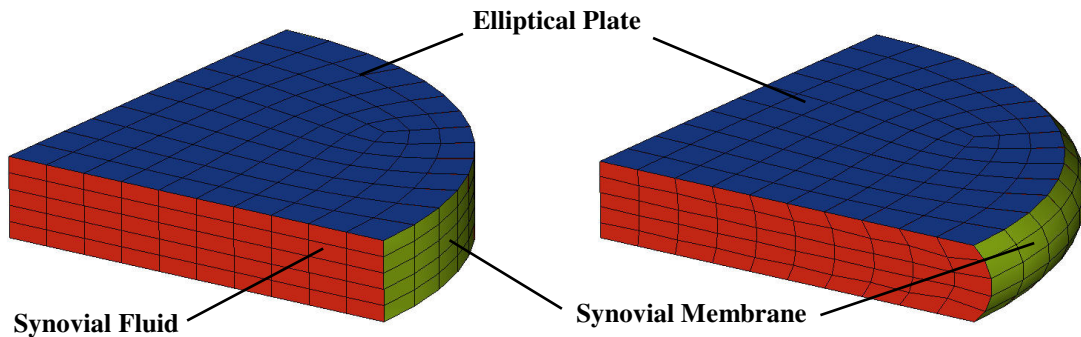
Figure 6-18: Simplified Facet Joint in Compression with Synovial Fluid

The bottom plate was fixed, while the top plate was displaced towards the bottom plate. A build-up of pressure occurred as the synovial fluid was forced out from between the elliptical plates, but contained by the synovial membrane. The corresponding volume of the facet joint was taken to be the product of the area of the elliptical plates, and their distance apart. The squeeze-film bearing model of the facet joints did not consider the additional volume of the fluid created by the bulge of the synovial fluid.

The results of this simplified model can be seen in Figure 6-19. The squeeze-film response showed that small changes to the initial volume resulted in a very little increase in pressure. The pressure-volume relationship becomes nearly linear for volume between 85% and 95% the initial volume size. These squeeze-film bearing results were applied to the models used to represent the synovial fluid in the cervical spine model. It should be noted that for relative volumes greater than 1, pressure was set at 0 MPa, since negative 'suction' pressure was not desired and tensile strength of the facet joint was provided by the capsular ligaments.
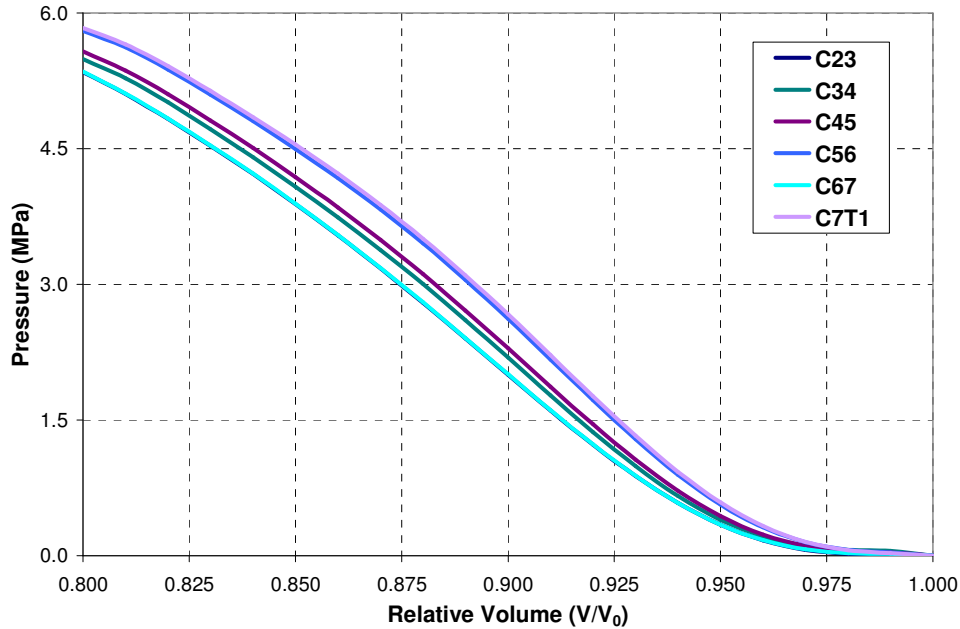
Figure 6-19: Pressure-Volume Relationship for Synovial Fluid in Cervical Spine Model

It is unknown whether this response for the synovial joint is representative of the actual synovial facet joints; however, it is expected to be significantly more biofidelic than leaving a large gap between adjacent facet joint surfaces. Incorporating the synovial fluid model allowed for the smooth transtition of forces through the facet joint.

The stiffness of this joint is directly related to the compliance of the membrane material, since the fluid is essentially incompressible at these pressures. The membrane material was selected based on the previously developed facet joint model by Kumaresan et al (1998).

6.3.4 Annulus Fibrosus Model

As discussed in Section 3.4, the mechanical properties for the annulus fibrosus are non-linear and anisotropic in nature. A structural-type AF model was developed for the cervical spine model that focused on tissue properties from the AF laminae and the AF ground substance separately. Both materials are represented using nonlinear models in accordance with the experimental data. The annular fibres were represented using orthotropic shell membrane elements.

Five annulus layers were modeled in each disc, where each layer contained a pair of lamina with alternating fibre angles. The fibre angles in the annulus of the cervical spine vary with its radial position, from +/- 25° in the outer layers, to +/- 45° in the inner layers (Cassidy et al,. 1989;

145

Marchand and Ahmed, 1990; White and Panjabi, 1990; Wagner and Lotz, 2004). Fibre angles for the intermediate layers varied between the outer and inner layer, and can be seen in Table 6-11.

Table 6-11: Model Properties of each Layer of Annulus Fibrosus Fibre Detail

Layer	Fibre Angle	C_3 (MPa)	C_4	C_5 (MPa)	C_6 (MPa)	λ^*
1 (Outer)	+/- 25°	0.0362	94.55	108.04	-110.86	1.0365
2	+/- 30°	0.0472	69.49	96.29	-99.63	1.0486
3	+/- 35°	0.0556	54.79	84.99	-88.66	1.0608
4	+/- 40°	0.0622	45.16	75.42	-79.31	1.0729
5 (Inner)	+/- 45°	0.0674	38.38	67.51	-71.56	1.0850

Because of the similarities in mechanical response between ligaments and AF laminae, the mathematical model presented by Quapp and Weiss (1998) for the fibre portion of a ligament was used to model the nonlinear behavior of the AF lamina (Quapp and Weiss, 1998). This model assumes that the lamina do not support compressive load, and that the 'toe' region is represented as an exponential function that switches to a linear function at an uncrimped stretch ratio λ^*. The nominal stress of the lamina is written as:

$$S = \begin{cases} 0 & \text{if } \lambda < 1 \\ C_3 \cdot \left[e^{C_4 \cdot (\lambda-1)} - 1 \right] & \text{if } 1 < \lambda < \lambda^x \\ C_5 \cdot \lambda + C_6 & \text{if } \lambda > \lambda^x \end{cases}$$

Equation 6-9

where C_3, C_4, C_5 and C_6 are the material parameters for the model. C_6 is determined from the condition that the nonlinear and linear regions are continuous at λ^*. For continuity in stiffness, the elastic modulus of the linear region (C_5) was set to the slope of the nonlinear region at λ^*. The nonlinear 'toe' region ($1 < \lambda < \lambda^*$) was fit, using the method of least squares, to the experimental results reported by Holzapfel et al. (2005) for both the outer and inner laminae ($R^2 > 0.999$ for both layers). The corresponding linear moduli (C_5) were found to be in excellent agreement with the experimental results reported by Skaggs et al. (1994). The gradual change in mechanical properties between the outer lamina and the inner lamina can be seen in Figure 6-20. Table 6-11 details the material parameters for the model of the AF laminae in the fibre direction.

In the full spine model, viscoelastic effect was not included in the annulus fibrosus laminae model as it was reported by Holzapfel et al (2005) that the stiffening effect from increased strain-rate was not significant.
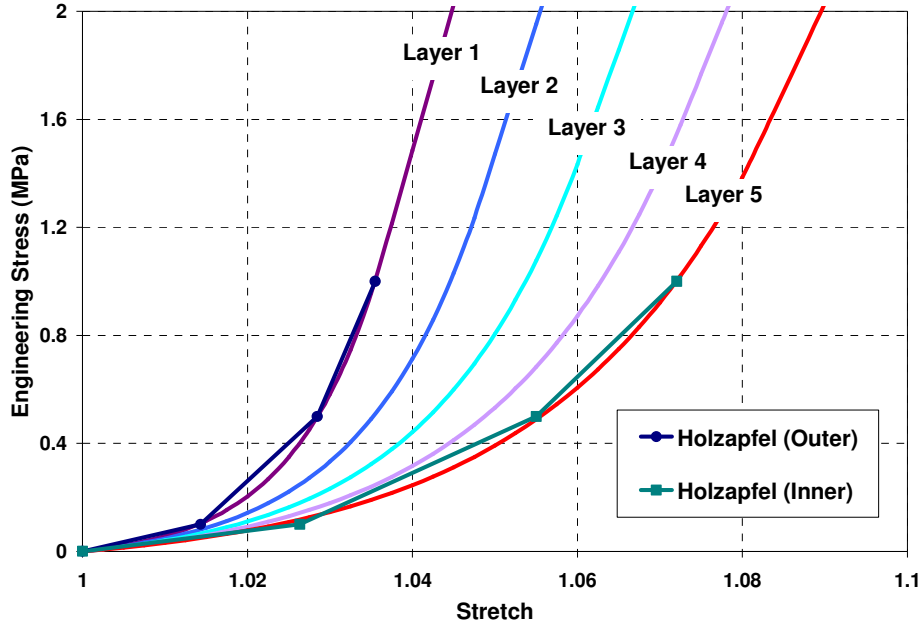
Figure 6-20: Stress-Strain Curves for Annulus Fibrosus Fibres

The AF ground substance material was modeled using the isotropic strain-energy function proposed by Hill (1978). This strain-energy function is often used to model porous rubbers of different degrees of compressibility (Storakers, 1986). The advantage of using this type of material model for the ground substance is that it can represent the nonlinearity of the tissue, while also maintaining a degree of compressibility for quasi-static simulation (unlike hyperelastic models). Details of the model can be found in Storakers (1986), and Feng and Hallquist (2003). Based on the principal stretches, the strain-energy function can be written as:

$$ W = \sum_{j=1}^{m} \frac{C_j}{b_j} \cdot \left[\lambda_1^{b_j} + \lambda_2^{b_j} + \lambda_3^{b_j} - 3 + \frac{1}{n} \cdot \left(J^{-n \cdot b_j} - 1 \right) \right] \qquad \textbf{Equation 6-10} $$

where m is the number of terms in the function, C_j and b_j are a set of material constants, n is a compressibility constant, and $J = \lambda_1 \lambda_2 \lambda_3$ denotes the relative volume. The principal nominal stresses can be written as

$$ S_i = \frac{1}{\lambda_i} \left[\sum_{j=1}^{m} C_j \cdot \left(\lambda_i^{b_j} - J^{-n \cdot b_j} \right) \right], i = 1, 2, 3 \qquad \textbf{Equation 6-11} $$

147

Equation 6-11 can be used to fit the Hill foam model to existing experimental datasets using nonlinear regression techniques such as the method of least squares. From the above equations, the shear modulus, bulk modulus, and Poisson's ratio for infinitesimal strain can be derived:

$$\mu = \frac{1}{2} \cdot \sum_{j=1}^{m} C_j \cdot b_j \qquad \textbf{Equation 6-12}$$

$$K = 2 \cdot \mu \cdot \left(n + \frac{1}{3} \right) \qquad \textbf{Equation 6-13}$$

$$\nu = \frac{n}{2 \cdot n + 1} \qquad \textbf{Equation 6-14}$$

It can be shown from Equation 6-14 when n is a very small number, the material becomes highly compressible like foam ($\nu \sim 0$), whereas a very large value of n results in the material being incompressible ($\nu \sim 0.5$). As n approaches infinity, the last term in the Hill model shrinks to zero, and the strain-energy function reduces to the Ogden hyperelastic formulation for incompressible materials (Ogden, 1984):

$$W = \sum_{j=1}^{m} \frac{C_j}{b_j} \cdot \left(\lambda_1^{b_j} + \lambda_2^{b_j} + \lambda_3^{b_j} - 3 \right) \qquad \textbf{Equation 6-15}$$

Experimental data from mechanical testing done in the radial direction (the direction perpendicular to the fibre layers) is considered as the best representative of the properties of the AF ground substance because of the minimal influence of the fibres in this direction (Fujita et al., 1997; Elliott and Setton, 2001). The experimental data used to determine the material constants of the Hill foam model were based on uniaxial tension (Fujita et al., 1997), unconfined compression (Wagner and Lotz, 2004), and confined compression (Iatridis et al., 1998). Furthermore, the material constants were constrained such that the infinitesimal shear modulus (Equation 6-12) would be within one standard deviation of the experimentally measured shear modulus (Iatridis et al., 1999).

It has been estimated that the Poisson's ratio for the annulus fibrous ground substance be between 0.3 and 0.5 (Yin and Elliot, 2005; Fujita et al., 2000). A Poisson's ratio of 0.40 was initially selected for the single segment models, considering the available experimental data (Wagner and Lotz, 2004) and past AF models (Rao and Dumas, 1991; Yoganandan et al., 1996a; Teo and Ng, 2001; Pitzen et al., 2002; Ng et al., 2004). Since the Hill foam model does not account for the fluid loss effects seen in the confined compression case, a reduced Poisson's ratio of 0.35 (n = 1.167) was used in the material model for fitting this type of data. Furthermore, for impact modelling using the full cervical spine

148

model, it is assumed that fluid loss in the AF ground substance is negligible and the material will be incompressible (Fujita et al., 2000). For this simulation case, the Ogden strain-energy formulation was used, utilizing the same material parameters as in the Hill strain-energy formulation.

Based on the experimental data, a set of material constants were found by the method of least squares. To simplify the nonlinear regression, the nonlinear material parameter b was constrained to only integer values between -4 and 4. It was found that three sets of terms were required for a good fit. It should be noted that due to the mathematical nature of the Hill foam constitutive equation, the C and b terms found using the method of least squares are not unique. Table 6-12 details the fitted model parameters, while Figure 6-21 details the quality of fit to the experimental data.

Table 6-12: Material Property Summary for Annulus Fibrosus Ground Substance

Part	Material Model	Material Parameters	References
AF Ground Substance	Non-Linear Elastic (Hill-Foam)	$m = 3$, $n = 2$ $C_1 = 0.665$, $b_1 = 2$ $C_2 = 2.730$, $b_2 = -1$ $C_3 = -0.517$, $b_3 = -3$	Fujita et al, 1997 Wagner and Lotz, 2004 Iatridis et al, 1998 Iatridis et al, 1999
	Non-Linear Elastic (Ogden-Rubber)	$C_1 = 0.665$, $b_1 = 2$ $C_2 = 2.730$, $b_2 = -1$ $C_3 = -0.517$, $b_3 = -3$	
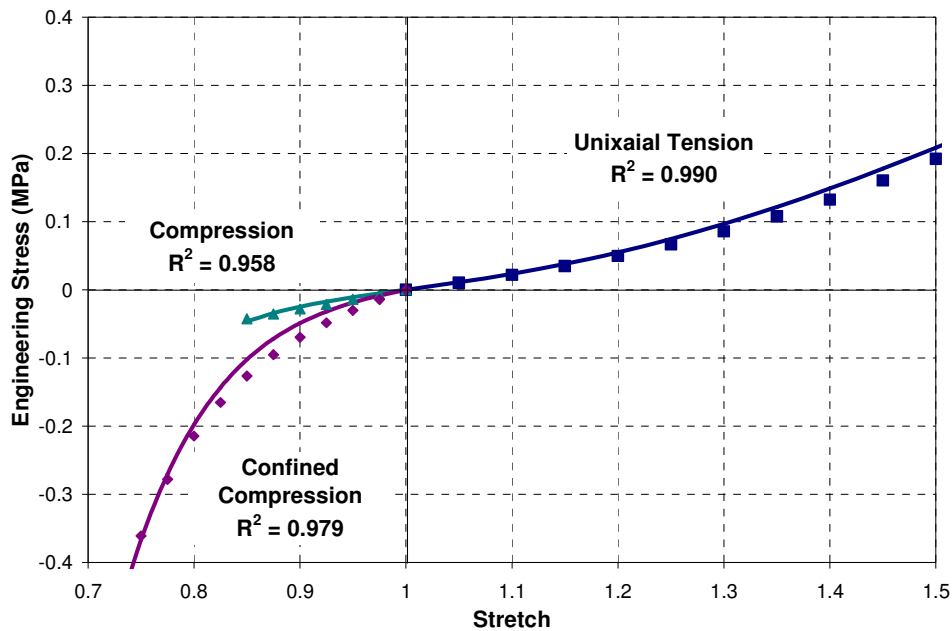
Figure 6-21: Annulus Fibrosus Ground Substance Response and Model Fit

It was reported that the annular fibres exhibited only slight viscoelastic effect for strain-rates between 0.1 to 10 mm/min (Holzapfel et al., 2005). While there was moderate stiffening and hystereses

present at 10 mm/min (compared to 0.1 mm/min), this response was deemed insignificant, and no further investigation into rate-sensitivity was made. Furthermore, there are no previous studies investigating the viscoelasticity of a single lamina of annulus fibrosus. Therefore, the viscoelastic effects were not incorporated into the annulus fibre model based on the lack of the relevant material properties.

6.3.5   Nucleus Pulposus Model

As described in Section 3.5, the nucleus pulposus is a viscoelastic material that behaves like a solid in dynamic conditions, but like a fluid in quasi-static conditions. Thus, for the quasi-static single segment simulations, the nucleus pulposus was modelled using a fluid material model with a bulk modulus of 1.720 GPa (Yang and Kish, 1988).However, for the full cervical spine model, the nucleus pulposus was modeled using the same general linear viscoelastic model described for cartilage (see Section 6.3.2), but with different constants.

The study by Iatridis et al (1997), which looked at nucleus pulposus in relaxation, is the basis for the viscoelastic model. The viscoelastic model was fit to the 0.10 strain data using the same techniques and equations described in Section 6.3.2 (R^2 = 0.999). The result of this model fit can be seen in Figure 6-22. Also in Figure 6-22 is the result of the model compared to the material data at different strains, showing good agreement and indicating the material is relatively linear in this region.
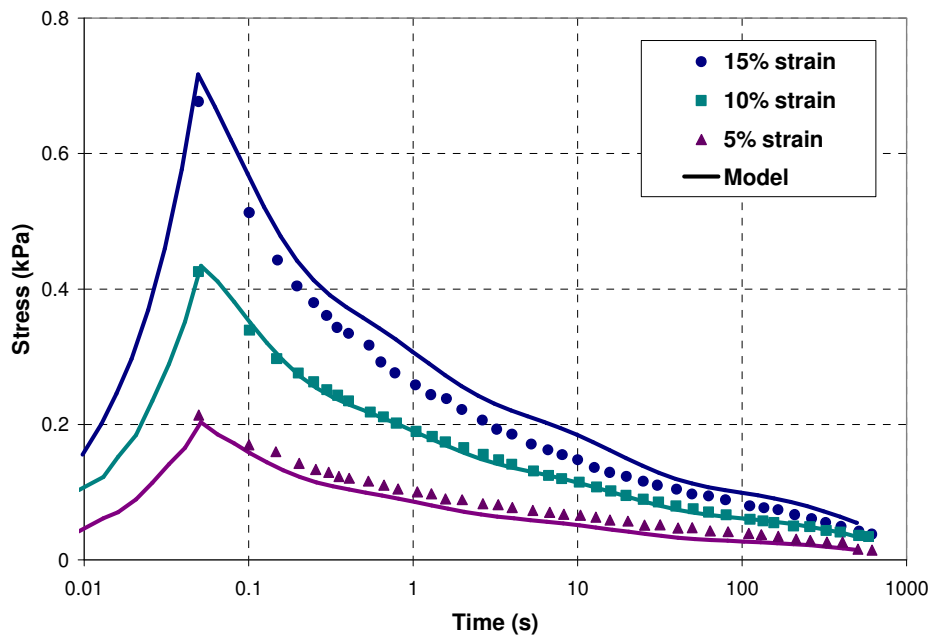
Figure 6-22: Nucleus Pulposus Response and Model Fit in Cervical Spine Model

150

The viscoelastic model fits the shear experimental data reasonably well. The parameters for the nucleus pulposus material model can be seen in Table 6-13.

Table 6-13: Material Property Summary for Nucleus Pulposus

Part	Material Model	Material Parameters	References
Nucleus Pulposus	Linear Viscoelastic	$N = 4$, $K = 1.720$ GPa $G_1 = 0.5930$ kPa, $\beta_1 = 0.001477$ 1/s $G_2 = 0.6763$ kPa, $\beta_2 = 0.061524$ 1/s $G_3 = 0.9516$ kPa, $\beta_3 = 1.017893$ 1/s $G_4 = 2.0384$ kPa, $\beta_4 = 13.20041$ 1/s	Yang and Kish, 1988 Iatridis et al, 1997
	Fluid	$K = 1.720$ GPa	

6.3.6 Ligament Material Model

A discrete nonlinear elastic spring model was used to represent each strand of a ligament in the cervical spine. Force is generated in the discrete element based on the following equation:

$$F = f(\Delta L) + g(\Delta L) \cdot h\left(\frac{d}{dt}L\right)$$

Equation 6-16

where $f(\Delta L)$ is the rate-independent force-deflection curve (nonlinear), $h(dL/dt)$ is the rate-dependent force-velocity curve, and $g(\Delta L)$ is the deflection based curve that scales $h(dL/dt)$. For modelling simplicity, $g(\Delta L)$ was equated to $f(\Delta L)$, and the model reduced to two components: the quasi-static force-deflection curve $f(\Delta L)$ and the dynamic scaling factor $h(dL/dt)$.

$$F = f(\Delta L) \cdot \left(1 + h\left(\frac{d}{dt}L\right)\right)$$

Equation 6-17

To define the quasi-static force-deflection curves, a number of different studies were used. Chazal et al (1985) identified and quantified the three distinct regions of the force-deflection response of a ligament as ratios of failure force and failure deflection (see Table 3-4). This information was used to generate the normalized force-deflection curve for the lower and middle cervical spine ligaments. The normalized force-deflection curves for the upper cervical spine were based on the average values from Chazal et al (1985).

The failure force and failure deflection data for the cervical spine ligaments was taken from Yoganandan et al (2001) (refer to Table 3-5 and Table 3-6). These values were then used to scale the normalized force-deflection curves to obtain the force-deflection curves of the ligaments. The force and deflection values for the points (A, B, and C) shown in Figure 3-17 can be found in Table 6-14 for each ligament. The three points were fit to a logist function to generate a smooth curve, and the resulting force-deflection curves for the lower and middle cervical spines can be seen in Figure 6-23 and Figure 6-24.
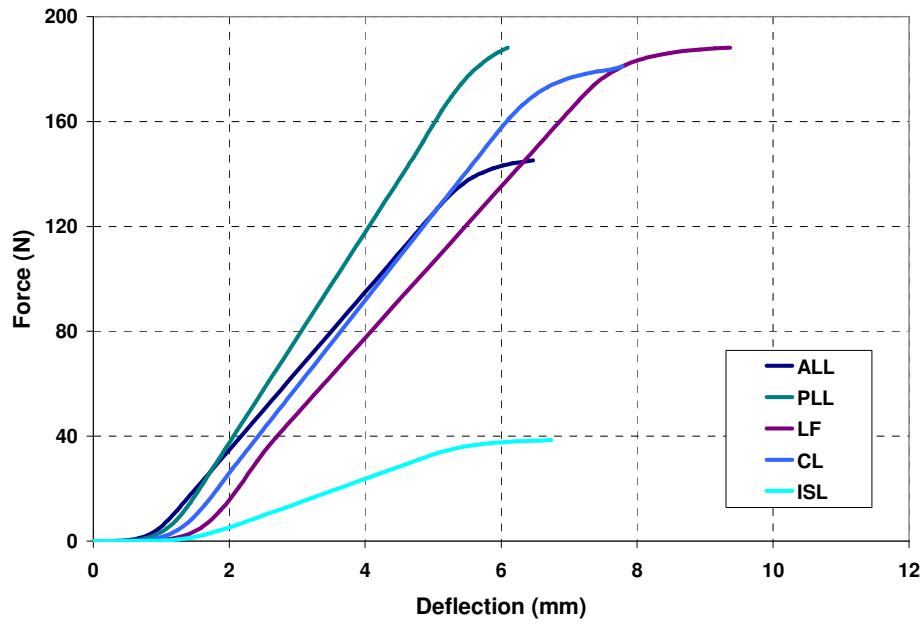
Figure 6-23: Force-Deflection Curves for the Lower (C5-T1) Cervical Spine Ligaments
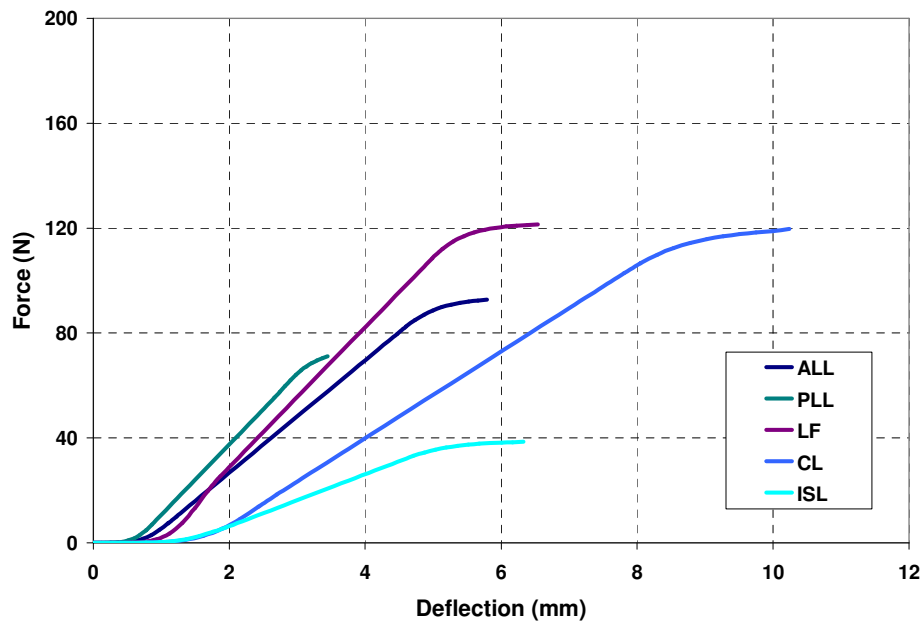
Figure 6-24: Force-Deflection Curves for the Middle (C2-C4) Cervical Spine Ligaments

Table 6-14: Force-Deflection Points for the Ligaments in the Cervical Spine Model

Ligament	Level	Point A		Point B		Point C	
		d (mm)	F (N)	d (mm)	F (N)	d (mm)	F (N)
Anterior Longitudinal	C2-C5	1.22	10.04	4.48	79.89	5.8	93
	C5-T1	1.37	15.66	5.02	124.56	6.5	145
Posterior Longitudinal	C2-C5	0.88	6.96	2.71	55.31	3.5	71
	C5-T1	1.53	18.42	4.72	146.45	6.1	188
Ligamentum Flavum	C2-C5	1.86	25.29	4.95	108.05	6.5	121
	C5-T1	2.69	26.96	7.16	115.20	9.4	129
Capsular Ligament	C0-C1	1.50	49.28	4.35	275.20	5.7	320
	C1-C2	3.06	48.36	8.85	270.04	11.6	314
	C2-C5	2.69	18.48	7.78	103.20	10.2	120
	C5-T1	2.06	27.87	5.95	155.66	7.8	181
Interspinous Ligament	C1-C5	1.94	7.84	4.69	35.45	6.3	39
	C5-T1	2.06	7.84	4.98	35.45	6.7	39
Tectorial Membrane	C0-C2	3.14	11.70	9.08	65.36	11.9	76
A. Altanto-Occipital	C0-C1	4.99	35.73	14.42	199.52	18.9	232
A. Altanto-Axial	C1-C2	2.19	40.50	6.33	226.18	8.3	263
P. Altanto-Occipital	C0-C1	4.78	12.78	13.81	71.38	18.1	83
P. Altanto-Axial	C1-C2	2.53	17.09	7.32	95.46	9.6	111
Apical	C0-C2	2.11	32.96	6.10	184.04	8.0	214
Alars (Occipital)	C0-C2	3.72	54.98	10.76	307.02	14.1	357
Alars (Atlantal)	C1-C2	3.72	54.98	10.76	307.02	14.1	357
Transverse	C1-C2	1.32	54.52	3.82	304.44	5.0	354
Vertical Crus	C0-C2	3.30	67.14	9.54	374.96	12.5	436

Since ligaments are highly sensitive to deformation rate, the full spine model required a dynamic scaling factor to account for the viscoelastic effects. To define the dynamic scaling factor, the high deformation-rate ligament study by Yoganandan et al (1989a) was used. The stiffness values of the ligaments at 25, 250, and 2500 mm/s were normalized to the stiffness of the 9 mm/s dataset for both ALL and LF to determine the dynamic stiffness. A logarithmic curve was fit to the dynamic stiffness values for deflection rate greater than 9 mm/s (see Figure 6-25), while deflection rates less than 9 mm/s did not have any increased stiffness. This logarithmic curve defined the dynamic scaling factor used in the nonlinear beam model. Note that this method scales the ligament force (and thus the stiffness) based on the instantaneous deflection rate.

An example of how this method applies to the ligaments can be seen in Figure 6-26, where the force-deflection curve is scaled depending on the deflection rate.
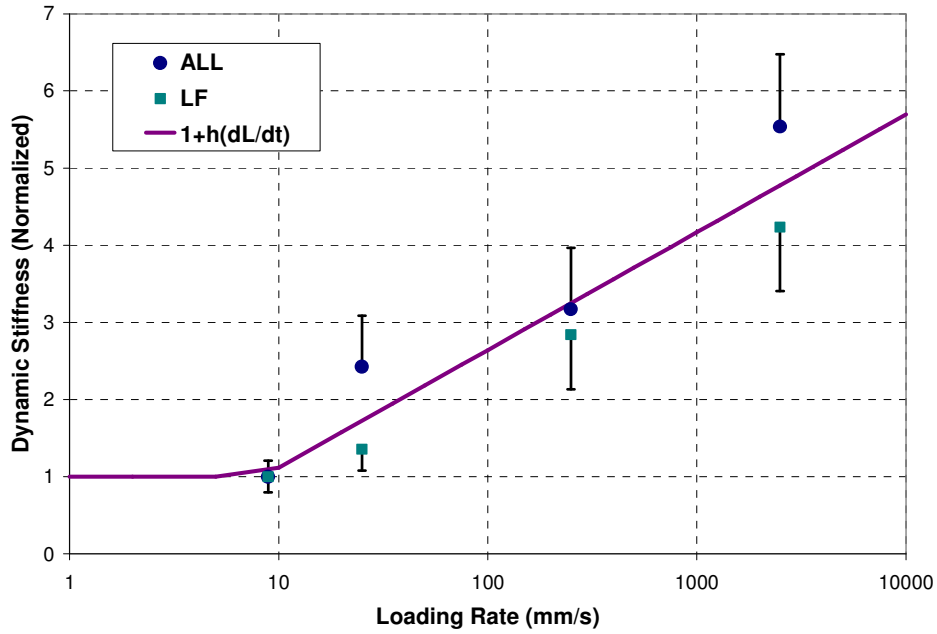
Figure 6-25: Dynamic Scaling Factor for the Ligaments in the Full Spine Model
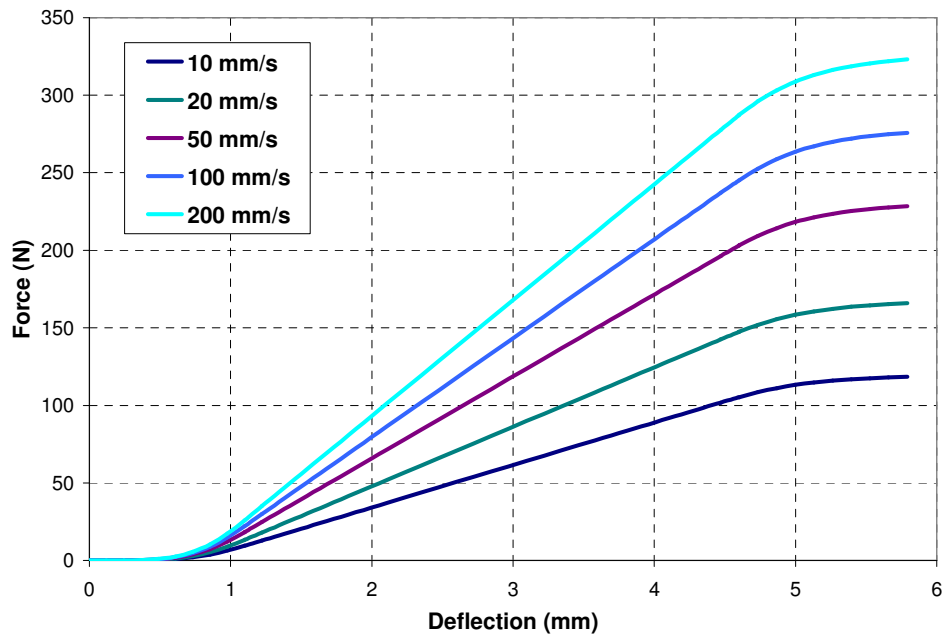
Figure 6-26: Force-Deflection Response of ALL at Increasing Deflection Rates

6.3.7 Muscle Material Model

The cervical spine muscles in the model are represented by 1D discrete elements, using the classic Hill-type muscle model. The Hill-type muscle model is a commonly used phenomenological model to explain active-passive muscle behaviour. This model is an exceptional match for cervical spine muscles since many neck impact scenarios involve active muscle behaviour, and modelling of bulk muscle is not required since the neck does not often experience direct impact. The development of the muscles in the full spine model stem from research reported by Jack Winters (Winters and Stark, 1985; Winters and Stark, 1988; Winters and Woo, 1990; Winter, 1995), since there is a lack of muscle property data in the literature that can be related to the Hill-type muscle model.

The basic Hill muscle model consists of a contractile element (CE) and a parallel elastic element (PE), with a series elastic element (SEE) for tendon-compliance often, but not always included (Figure 6-27). The parallel element is based on passive muscle properties and is dependent only on the current muscle length, while the contractile element generates the active force in the muscle, and is dependent on muscle length, velocity, and activation state.
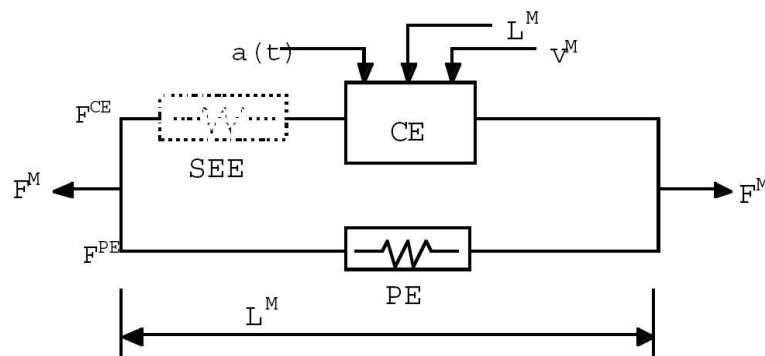
(Adapted from Hallquist, 2003)

Figure 6-27: The Hill Muscle Model Schematic Describing Active-Passive Muscle Behaviour

Active muscle force is a function of muscle length, velocity, and active state dynamics (Equation 6-18). Force-length (f_{FL}) and force-velocity (f_{FV}) relationships are nonlinear phenomena based on the current state (length and velocity) of the muscle, while active state dynamics (A) is a time-dependent function based on neural input. The product these functions determine the scale-factor that is applied to the maximum isometric force (F_{max}) produced in the muscle. F_{max} is a product of the muscle physiological cross-sectional area (PCSA, refer to Table 6-8), and the maximum muscle stress. The maximum muscle stress varies between 0.20 and 1.00 MPa (Winters and Stark, 1988), so a value of 0.5 MPa was used to determine F_{max} of each muscle.

155

$$F_{CE} = F_{max} \cdot f_{FL}(L) \cdot f_{FV}(v) \cdot A(t)$$

<div align="right">**Equation 6-18**</div>

The force-length relationship describes the isometric (no velocity) muscle force development as a function of muscle length. Isometric force is at a maximum when the muscle is at its optimum length and decreases as the muscles shortens or lengthens, approaching zero around stretches of 0.4 and 1.5 (Winters and Woo, 1990). This relationship can be described as Gaussian-shaped, and expressed in Equation 6-19:

$$f_{FL} = e^{-S_k \cdot \left(|L| - L_{opt} \right)^2}$$

<div align="right">**Equation 6-19**</div>

where L_{opt} is the optimum stretch and S_k is a model parameter. Winters (1995) suggests an L_{opt} value of 1.05 (normalized) and a S_k value of 6.25 for the force-length relationship. The shape of this curve can be seen in Figure 6-28.
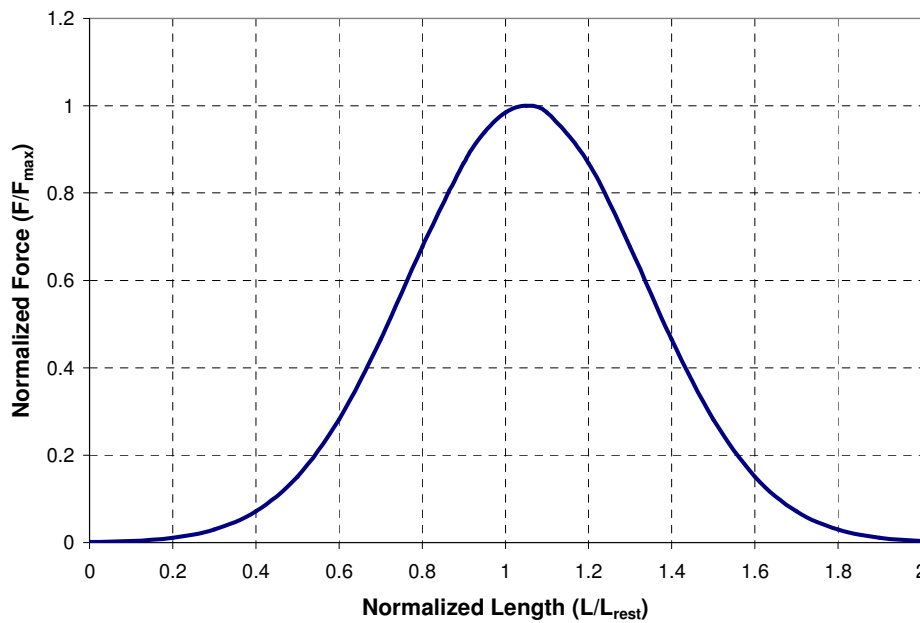
Figure 6-28: Force-Length Relationship for Hill Muscle Model

The force-velocity relationship describes the muscle force development as a function of muscle shortening or lengthening. In the isometric condition ($v = 0$), the function does not enhance nor diminish the possible amount of force generated in the muscle. When the muscle is shortening due to contaction ($v < 0$), the relationship between force-velocity is hyperbolic, with the amount of available force decreasing drastically with increasing shortening velocity (Winters and Woo, 1990). A number

of equations have been proposed to describe the shortening effect of muscle force, such as the one presented by Fung (1993) (Equation 6-20):

$$f_{FV} = \frac{1 + \dfrac{v}{v_{max}}}{1 - \dfrac{v}{v_{max} \cdot CE_{sh}}} \quad \text{for} \quad v < 0 \qquad \textbf{Equation 6-20}$$

where v is the muscle velocity ($v < 0$ for shortening), v_{max} and CE_{sh} are model parameters. The v_{max} is described as the maximum shortening velocity since f_{FV} will reach 0 when $v = v_{max}$. Winters and Woo (1990) proposed the range of v_{max} to be 2/s to 8/s times the muscle rest length, for slow and fast muscle fibres respectively, and a range of CE_{sh} to be 0.1 to 1 for slow and fast muscles. Since the ratio of fast to slow muscle fibres in the cervical spine is unknown, average values for v_{max} and CE_{sh} were used. A v_{max} of 5/s times the muscle rest length, and a CE_{sh} of 0.55 was chosen for the cervical spine model.

When the active muscle is lengthening (eccentric contraction), the amount of force available for generation is actually higher than the maximum isometric force (Winters and Woo, 1990). The maximum force increases sharply at low lengthening velocities, however this reaches an asymptotic force with increasing muscle lengthen velocity. This relationship is described in Equation 6-21:

$$f_{FV} = \frac{1 + \dfrac{v}{v_{max}} \cdot \dfrac{CE_{ml}}{CE_{shl}}}{1 + \dfrac{v}{v_{max} \cdot CE_{shl}}} \quad \text{for} \quad v > 0 \qquad \textbf{Equation 6-21}$$

where v is the muscle velocity ($v > 0$ for lengthening), v_{max}, CE_{shl}, CE_{ml} are model parameters. The v_{max} is same parameter described in Equation 6-20, while CE_{ml} is the maximum relative force from muscle lengthening. Despite limited data on eccentric contraction, Winters and Woo (1990) assumes the peak muscle force is 30% higher than peak isometric forces. Thus, the model parameter CE_{ml} was chosen to be 1.3, and CE_{shl} was calculated based on maintaining the slope continuity between the lengthening and shortening functions (0.1065). Combining both Equation 6-20 and Equation 6-21, the force-velocity relationship of muscle can be seen in Figure 6-29.
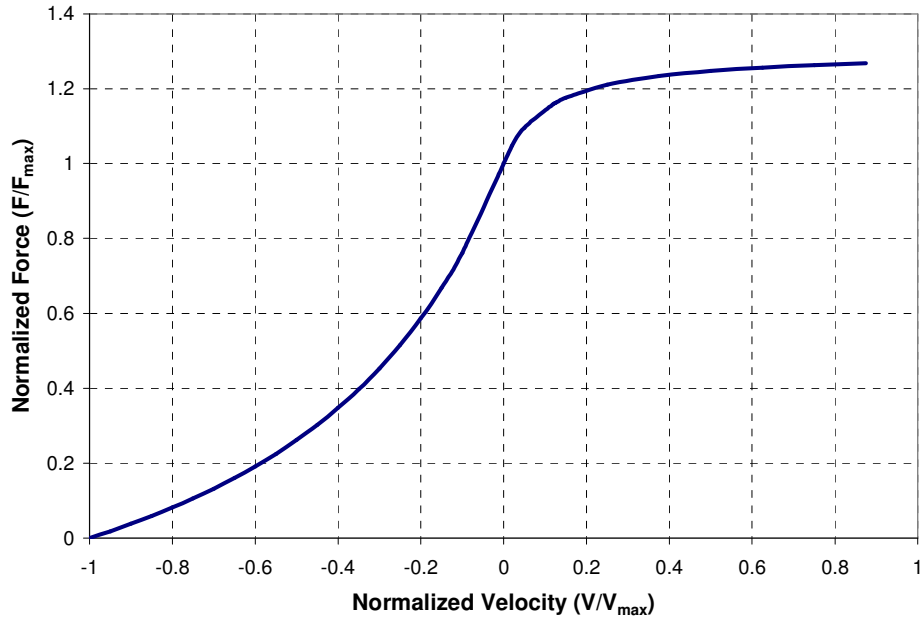
Figure 6-29: Force-Velocity Relationship for Hill Muscle Model

Muscle activation for the Hill muscle model is described by neural excitation and active state dynamics as described by Winters and Stark (1985). Neural excitation (and de-excitation) represents the process of converting an idealized neural input into an output signal resembling an EMG output. Active (and de-active) state dynamics represents the transient dynamics between the neural excitation and muscle contraction. Both neural excitation (Equation 6-22) and active state dynamics (Equation 6-23) are described using 1st order systems.

$$\frac{d}{dt}E(t) = \frac{u(t) - E(t)}{\tau_{ne}} \qquad \qquad \textbf{Equation 6-22}$$

$$\frac{d}{dt}A(t) = \frac{E(t) - A(t)}{\tau_a} \qquad \qquad \textbf{Equation 6-23}$$

where u(t) is the idealized neural input ($0 < u(t) < 1$), τ_{ne} is the neural excitation time constant, and τa is the active state time constant. When $E > A$, the muscle is in a state of activation, and $\tau_a = \tau_{ac}$; when $E < A$, the muscle is in a state of de-activation, and $\tau_a = \tau_{dc}$. The activation time constant (τ_{ac}) is smaller than the deactivation time constant (τ_{dc}), which results in muscle activation responding faster than muscle de-activation. Winters (1995) suggests a neural excitation time constant of 20 to 50 ms, an activation time constant of 5 ms to 20 ms, and a deactivation time constant of 30 ms to 50 ms. The lower time constants are for muscle composed of mainly fast muscle fibres, while the higher time constants for slow muscle fibres. Average values for τ_{ne}, τ_{ac} and τ_{dc} are used in the model (35, 15 and

158

40 ms respectively). An example of the resulting activation process for a step neural input can be seen in Figure 6-30.
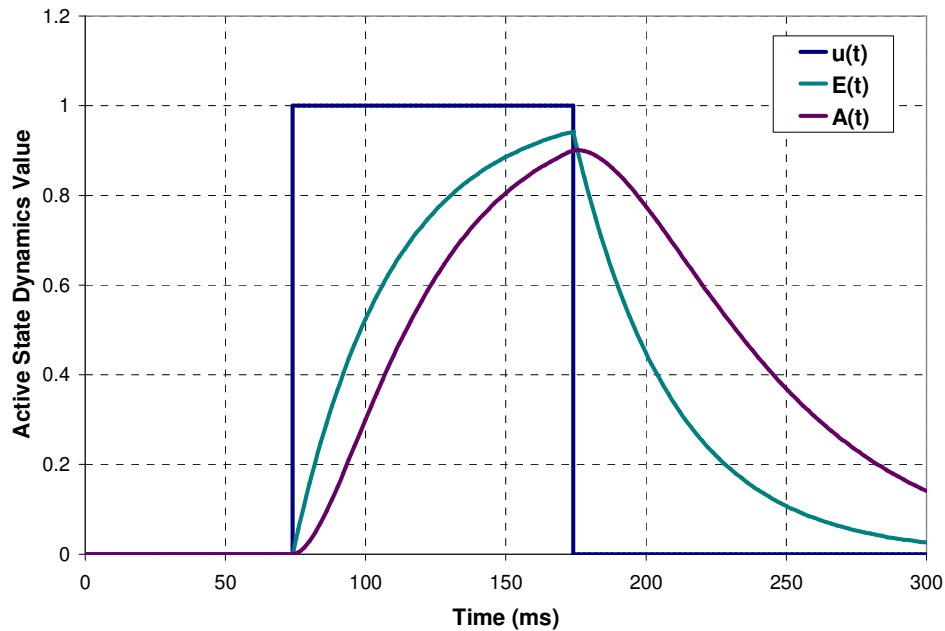
Figure 6-30: Example of Muscle Activation for Neural Input between 74 and 174 ms

The parallel (passive) element of the Hill muscle model represents the tensile behaviour of relaxed muscle and surrounding tissue. This portion the muscle behaviour typically does not generate significant force in tension until the muscle is stretched to the limits of physiological loading (Winters and Woo, 1990). There is also an assumption that the passive muscle does not carry compressive load.

While many different mathematical models can be used to represent PE of the Hill model, an exponential function is often used since muscle tissue response is nonlinear in tension (Fung, 1993). Winters and Stark (1985) proposed the following function (Equation 6-24) to represent the passive properties of the muscle in tension:

$$F_{PE} = \frac{F_{max}}{e^{K_{sh}} - 1} \cdot \left[e^{\frac{K_{sh}}{L_{max}} \cdot \left(\frac{L}{L_{rest}} - 1 \right)} - 1 \right] \quad \text{for} \quad L > L_{rest} \qquad \textbf{Equation 6-24}$$

where F_{max} and L_{rest} is the maximum force and rest length of the muscle respectively, and K_{sh} and L_{max} are model parameters. Physically, L_{max} is the strain at which the passive muscle will generate a force equal to the maximum isometric force F_{max}, while K_{sh} is the nonlinear shape parameter. Winters

(1995) suggests a K_{sh} value of 3 for parallel element in lengthening, with a L_{max} of 0.6. For lengths that are less than the rest length, the passive force is zero. The passive response of the muscle in the model can be seen in Figure 6-31.
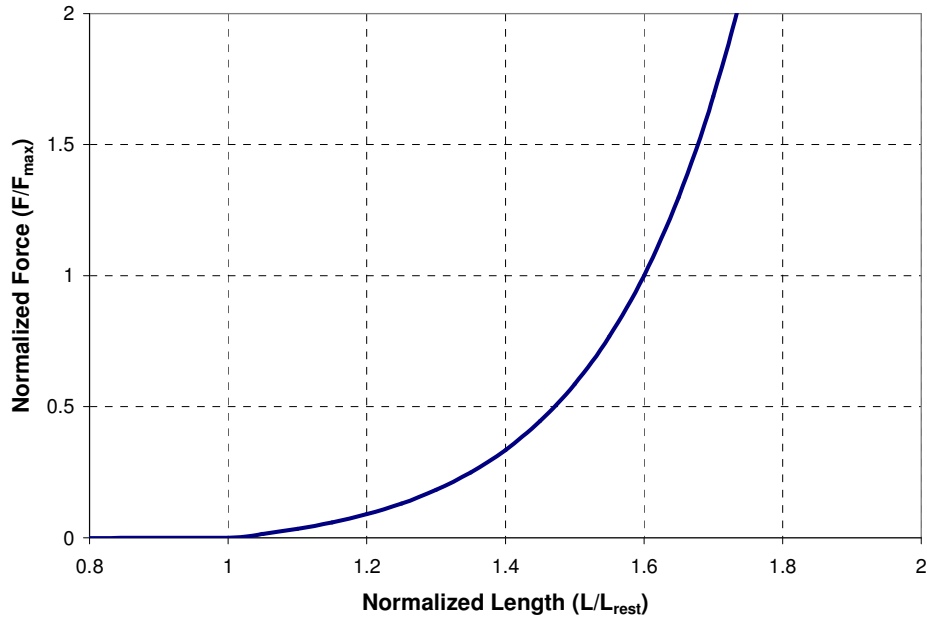
Figure 6-31: Parallel (Passive) Element Response for Hill Muscle Model

A summary of the Hill-type Muscle Model parameters used in the model can be seen in Table 6-15. Included in this table are reported the range of these values in the literature.

Table 6-15: Hill-type Muscle Model Parameter Summary for Muscles

Parameter	Range in Literature	Value in Model	Reference
σ_{max}	0.20 – 1.00 MPa	0.5 MPa	Winters and Stark, 1988; Winters, 1995
PCSA		Table 6-8	
Sk		6.25	Winters, 1995
L_{opt}		1.05	Winters, 1995
v_{max}	2 (L_{rest}) – 8 (L_{rest}) /s	5 (L_{rest}) /s	Winters and Woo, 1990
CE_{sh}	0.1 – 1	0.55	Winters and Woo, 1990
CE_{shl}		0.1065	
CE_{ml}	1.1 – 2.0	1.3	Winters and Woo, 1990
τ_{ne}	20 – 50 ms	35 ms	Winters and Stark, 1988
τ_{ac}	5 – 20 ms	15 ms	Winters and Stark, 1988; Winters, 1995
τ_{dc}	20 – 60 ms	40 ms	Winters and Stark, 1988; Winters, 1995
L_{max}	0.6 – 0.7	0.6	Winters, 1995
K_{sh}	3 – 6	3	Winters, 1995

Chapter 7

Cervical Spine Segment Model Validation

7.1   Experimental Background

The single segment models were evaluated against a number of different *in vitro* studies of the human cervical spine. Each study was selected for validation of the model based on a number of criteria. These criteria included the type of experiment and the protocols used, the usefulness of the experimental data for validation of the numerical model, the historical use of the experimental data in the cervical spine modelling community, and general agreement of the experimental data with other experimental studies. It was also important for validation purposes to examine the response of the models under both small and large loading.

For small rotational loading, the experimental results reported by Goel et al (1988a) for the upper cervical spine, and Goel et al (1988b) for the lower and middle cervical spine were used. Eight upper cervical spines segments (average age 80 years) were used in Goel et al (1988a), while nine C2-T2 cervical spines (average age 70) were used in Goel et al (1988b). Both studies reported the relative motion of each segment of the cervical spine under 0.3 Nm load in flexion, extension, axial rotation, and lateral bending. Loads were applied in four incremental steps to the superior-most vertebrae (C0 and C2 respectively), and vertebral motion was recorded at each increment. The results of each study were presented as the rotation at the 0.3 Nm load.

For evaulation of the segment models under moderate flexion or extension moments, the results from Camacho et al (1997), Nightingale et al (2002, 2006), and Wheeldon et al (2006) were used. The studies examined the flexibility of the cervical spine over a range of flexion and extension moments using either the entire cervical spine or individual motion segments. Results of each of these studies were reported results using a logarithmic function relating applied moment to rotation.

Camacho et al (1997) used 10 male heads and cervical spines (average age 66 years) in an apparatus that rigidly fixed the head to a six-axis load cell and the T2 vertebra a device that was capable of applying pure bending moments. Flexion/extension moments of 1.5 Nm were applied in 0.1 Nm increments, and allowed to creep for 50 seconds at each increment to record the resulting vertebral rotation. In a similar study, Wheeldon et al (2006) used 13 cervical spines (C2 to T1) from 'young'

161

donors (average age 33 years). Pure bending moments from 2 Nm extension to 2 Nm flexion were applied to the spines.

Nightingale et al (2002) used 52 female spinal segments (average age 51 years) from the C0-C2, C3-C4, C5-C6, and C7-T1 levels with a small preload of 0.5 N. Loads of +/- 3.5 Nm were applied at 0.5 Nm increments and held for 30 seconds to reach an equilibrium position. In a follow-up study, Nightingale et al (2006) used 41 male spinal segments (average age 66 years) from the C0-C2, C4-C5, and C6-C7 levels.

To evaluate the model in translation, the experimental results from Panjabi et al (1986) and Shea et al (1991) were used. Panjabi et al (1986) used 18 single segment units (C2-C3 to C7-T1) from four cervical spines (average age 55 years). Maximum loads of 50 N were applied in four increments and each step held for 30 seconds before displacements were recorded. Motion segment stiffness for compression, tension, and shear (anterior, posterior, and lateral) was reported as the slope of the load-displacement curve at 25 N.

Shea et al (1991) used 35 two-disc motion segments (grouped into C2-C5 and C5-T1) from 18 cervical spines (average age 74 years). Displacements were applied to the motion segments at rates of 5 mm/s, which they reported had no significant difference in results obtained at rates of 0.5 mm/s (Shea et al., 1991). Motion segment stiffness for tension, and shear (anterior and posterior) was reported as the slope of the load-displacement curve at 100 N, while stiffness in compression was reported at 500 N. These values were doubled to represent the stiffness of only one segment, based on the assumption that each segment was of equal stiffness.

7.2   Simulation Methods

All single segment models were simulated in quasi-static conditions in all modes of loading (three translational and three rotational directions). For each segment, the inferior endplate of the inferior vertebra was fully constrained, and a prescribed motion was applied in the direction of primary loading to the centre of the superior vertebral body. The superior vertebra was unconstrained in the five other degrees of freedom. The reaction load generated by the prescribed motion was recorded. No preload was applied to the superior vertebra to simulate *in vivo* loading conditions.
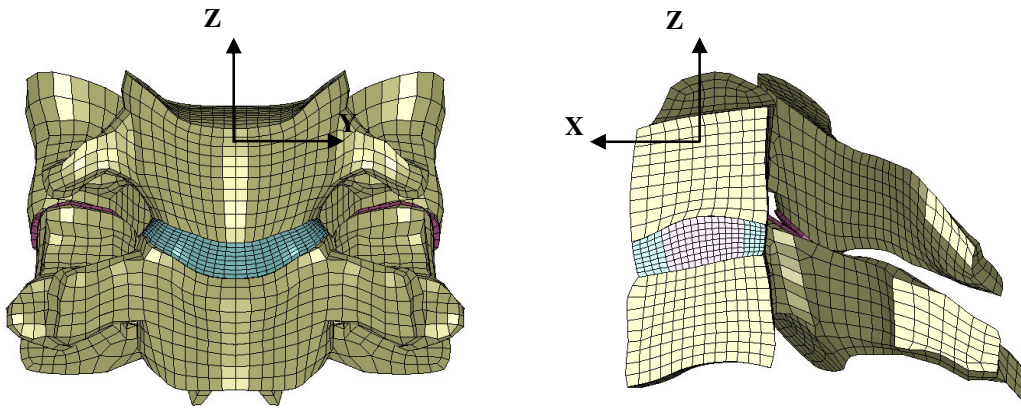
Figure 7-1: Coordinate System for Single Segment Models (C45 Model Shown)

All six degrees of freedom (three translational, three rotational) were investigated in both positive and negative directions. Due to symmetry, only the positive motion in translational Y direction, and rotational X and Z direction were simulated. Nine separate simulations were conducted for each segment model from C23 to C7T1. A summary of the direction of motion for the single segment simulations can be seen in Table 7-1. Only the rotational simulations were conducted for the upper cervical spine segment model. The maximum applied displacements and rotations are indicated in Table 7-1.

Table 7-1: Description of Single Segment Model Simulations and their Maximum Displacements

Direction of Motion	X	Y	Z
Translation			
Positive (+)	Anterior Shear (3 mm)	Lateral Shear (3 mm)	Tension (1.5 mm)
Negative (–)	Posterior Shear (3 mm)		Compression (1.5 mm)
Rotation			
Positive (+)	Lateral Bending (20°)	Flexion (25°)	Axial Rotation (20°)
Negative (–)		Extension (25°)	

All simulations were run using LS-DYNA version 970 revision 6763.086 using single precision calculations on a single Linux workstation. The models took between 1½ and 5 hours to run each simulation, depending on the load case and model, on a single 2.4 GHz machine. Mass-scaling or other methods of reducing run-times were not enabled for the single segment models.

7.3 Simulation Results

The following section presents the results of the single segment model simulations in all directions of loading. Despite the simulation methods of applying a quasi-static displacement to the model and recording the resistant load, the results in this section are presented as displacement versus load in accordance with the published experimental results.

To decrease the size and complexity of this section, the results of the simulations are presented in the Appendices. Appendix A presents the complete results of the single segment models, including the coupled displacements of the superior vertebra in each mode of loading. Appendix B presents the complete flexion-extension results of each segment model as compared to the experimental data.

Many of the experimental studies examined the response of the cervical spine segment at small loads (0.3 Nm or 25 N). This level of load primarily involved the response of the intervertebral disc since deformations were not large enough for the ligaments to contribute to the response significantly. In the case of the upper cervical spine however, small loads that generate large displacements involve the ligaments. The results from Goel et al (1988) provided the basis for validating the disc model in flexion, extension, axial rotation, and lateral bending. The results from Panjabi et al (1986b) provided the basis for validating the disc in tension, compression, and shear.

7.3.1   Flexion and Extension Results

Validation of the model in flexion and extension is particularly important if the eventual application of the full cervical spine model is to simulate frontal or rearward impacts, since this is the primary mode of spine loading. Consequently, it is also the motion that is most often studied for the cervical spine, and has the most available experimental data to validate the model.

An example of the motion of the segment model in flexion and extension can be seen in Figure 7-2. The deformation of the intervertebral disc agrees with qualitative observation that the nucleus pulposus tended to shift posterior in flexion while the disc bulged in the anterior and was concave in the posterior, and vice versa for the extension case (White and Panjabi, 1990). The stiffness of the spinal segment at small rotations was provided primarily by the annulus fibrosus fibres. At larger rotations, the ligaments begin to dominate the flexion response, while compression of the facet joints increased the stiffness of the motion segment in extension.

164

| Flexion | Initial Position | Extension |
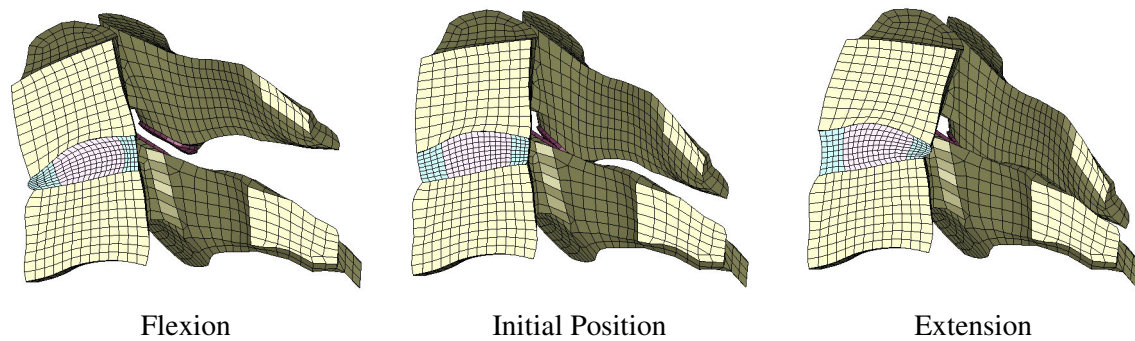
Figure 7-2: Segment Deformation during Flexion and Extension

Examining the results in Appendix A, it was observed that rotation in the sagittal plane was not coupled to any other motion except for anterior-posterior translation, where displacement was quite significant. In flexion, the superior vertebra was inclined to move in the anterior direction, while in extension the trend was to move in the posterior direction. These results are similar to the coupled motions reported by Moroney et al., (1988) and Panjabi et al (2001b).

The model was initially compared to the experimental results reported by Goel et al (1988a, 1988b) for motion segment response at small moments (0.3 Nm). The model response in flexion was very good (Figure 7-3), with all motion segments being within one standard deviation of the experimental average, except for the C7-T1 motion segment, which was more compliant than the experimental data. On the extension side (Figure 7-4), the lower cervical spine motion segments were slightly more compliant than the experimental response, while the motion between the occipital bone (C0) and the atlas (C1) was much stiffer.
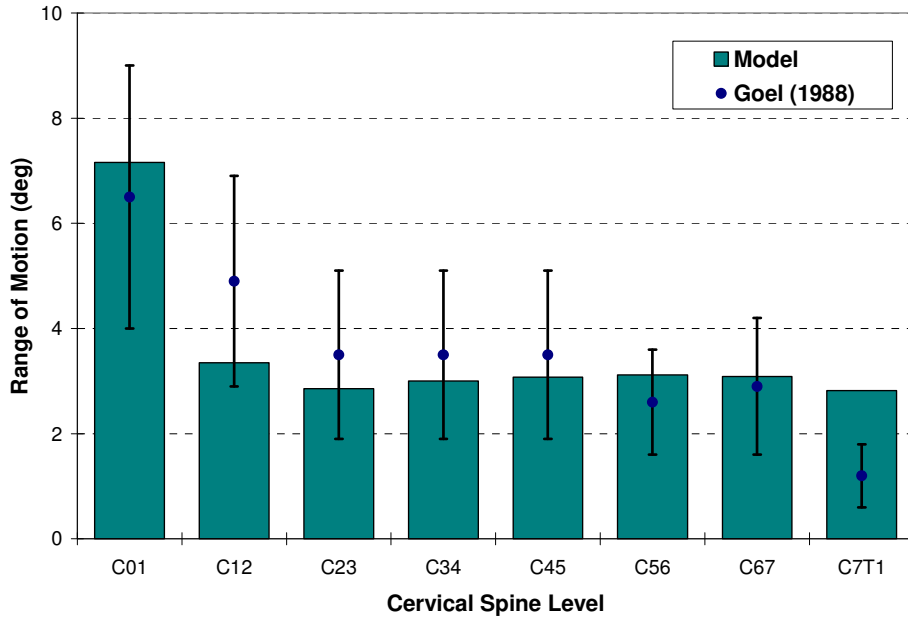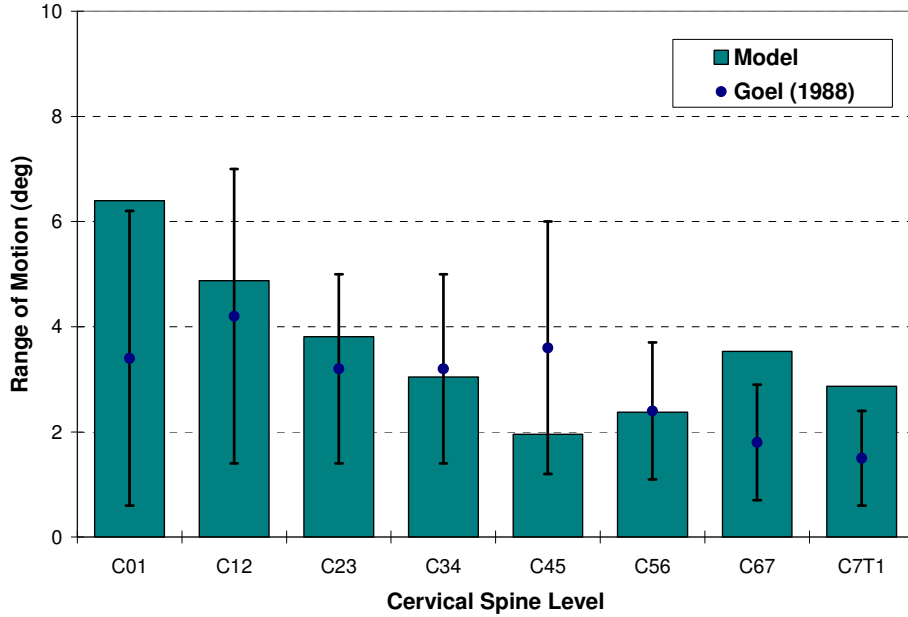
Figure 7-3: Flexion Angle of Each Segment under a Small Moment (0.3 Nm)
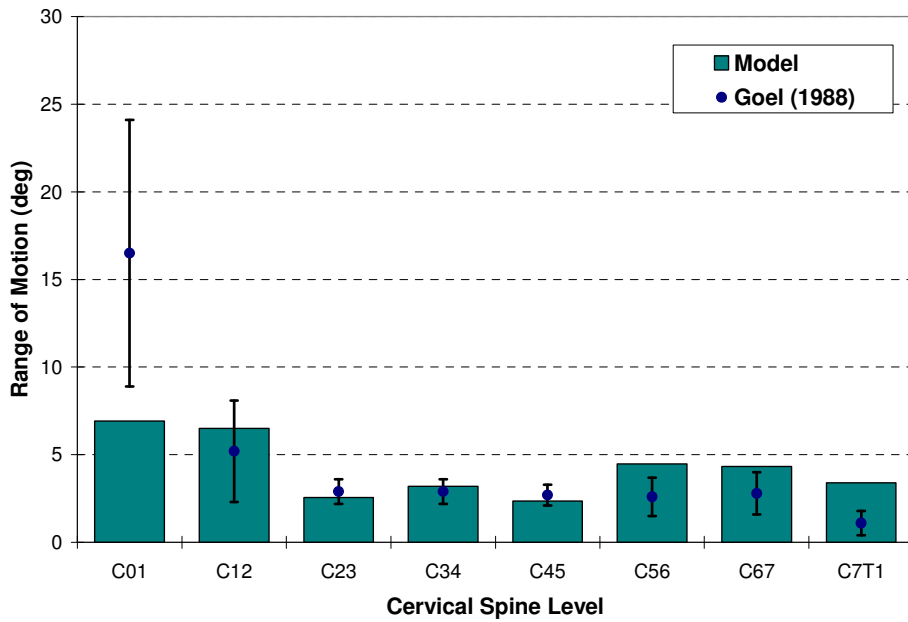
Figure 7-4: Extension Angle of Each Segment under a Small Moment (0.3 Nm)

Comparing the flexion and extension response of the single segment models to the larger deformation studies by Camacho et al (1997), Nightingale et al (2002, 2006) and Wheeldon et al (2006), the model also performed very well. The response of the C4-C5 motion segment can be seen in Figure 7-5 and Figure 7-6, while the entire set of motion segment results for large flexion and extension moments

can be seen in Appendix B. The general results show that the model is in good agreement with experimental data for the range considered between moderate flexion and extension loads for nearly all motion segments. The segment that does not fully agree with the experimental data is again the C7-T1 model, which is more compliant in extension than the experimental data.
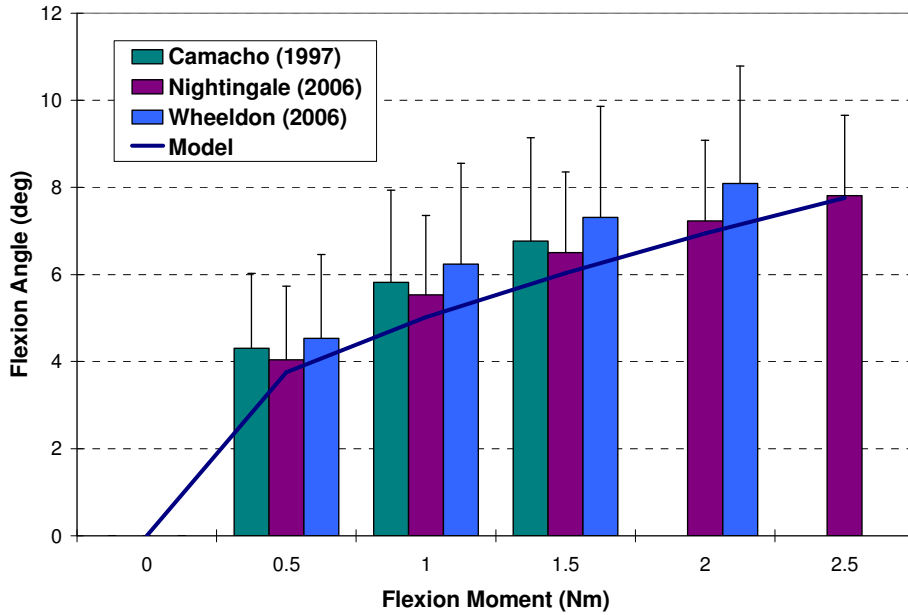
Figure 7-5: Response for C45 Segment under a Range of Quasi-Static Flexion Moments
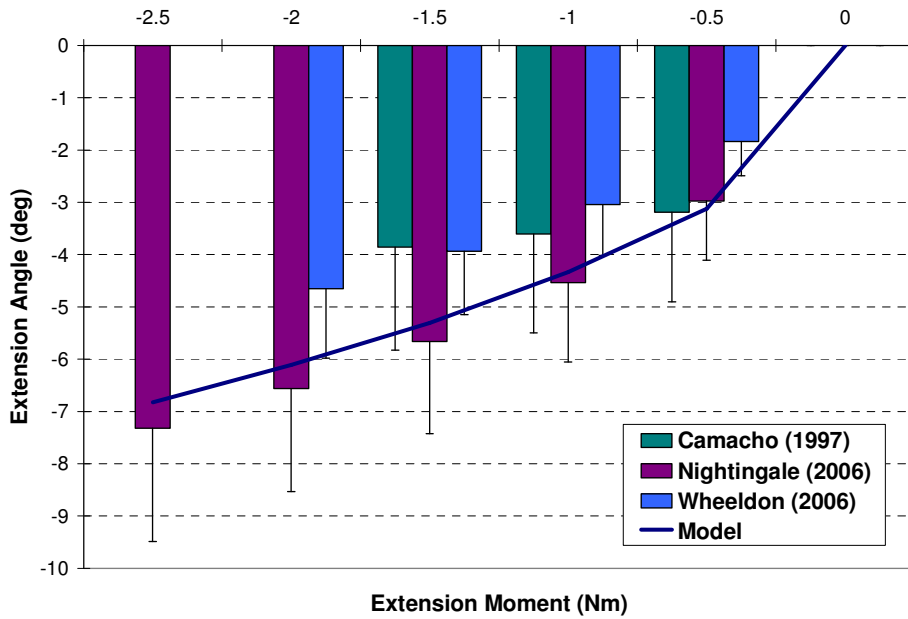
Figure 7-6: Response for C45 Segment under a Range of Quasi-Static Extension Moments

7.3.2 Lateral Bending and Axial Rotation Results

Lateral bending and axial rotation are motions that have a significant coupled relationship in the cervical spine because of the facet joint geometry (see Section 2.2.2). This is also the dominant motion of the cervical spine in lateral impact, and should be thoroughly examined if using the cervical spine model for lateral impact simulation.

An example of the motion of the segment model in lateral bending can be seen in Figure 7-7. It can be seen in this figure that the pronounced motion was a lateral bend, but a noticeable rotational motion can also be seen. This coupled motion is much easier seen in Figure 7-9, where the applied lateral bending moment produced a complementary axial rotation. This motion agrees well with results reported by Moroney et al., (1988).

Initial Position   Lateral Bending
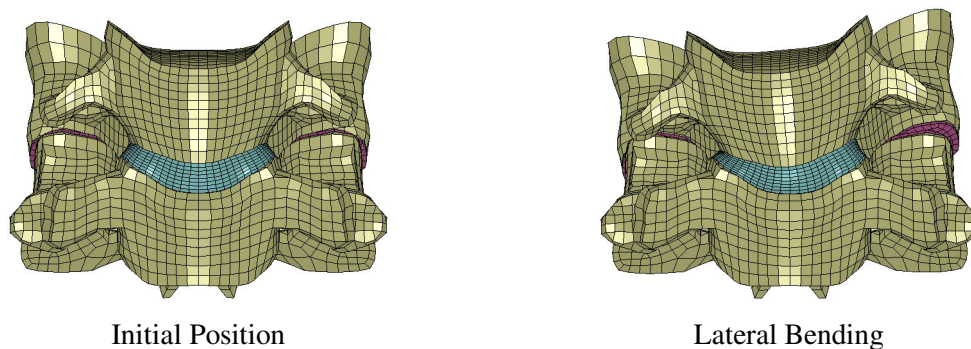
Figure 7-7: Segment Deformation during Lateral Bending

This coupling effect was also noticeable when applying an axial rotation to the motion segment. While this is not as apparent in Figure 7-8, the coupled motion is easily seen in Figure 7-10 where the applied rotational moment produces a complementary lateral bend.

Initial Position   Axial Rotation
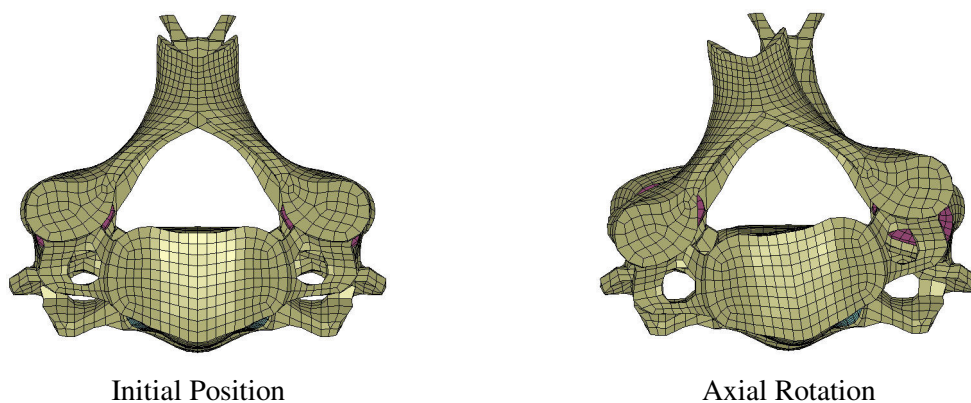
Figure 7-8: Segment Deformation during Axial Rotation
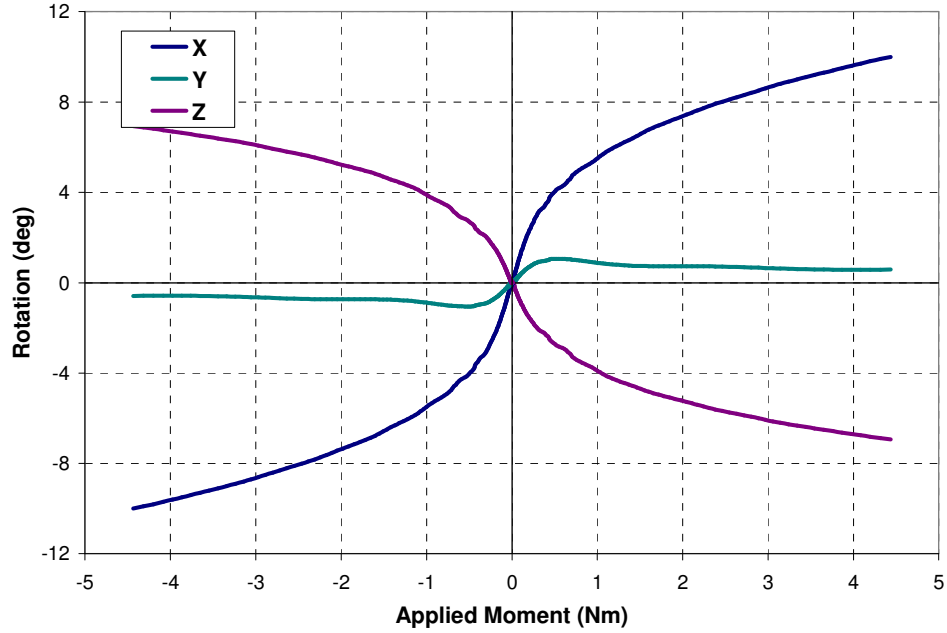
Figure 7-9: Coupled Motion of the C3-C4 Motion Segment in Applied Lateral Bending
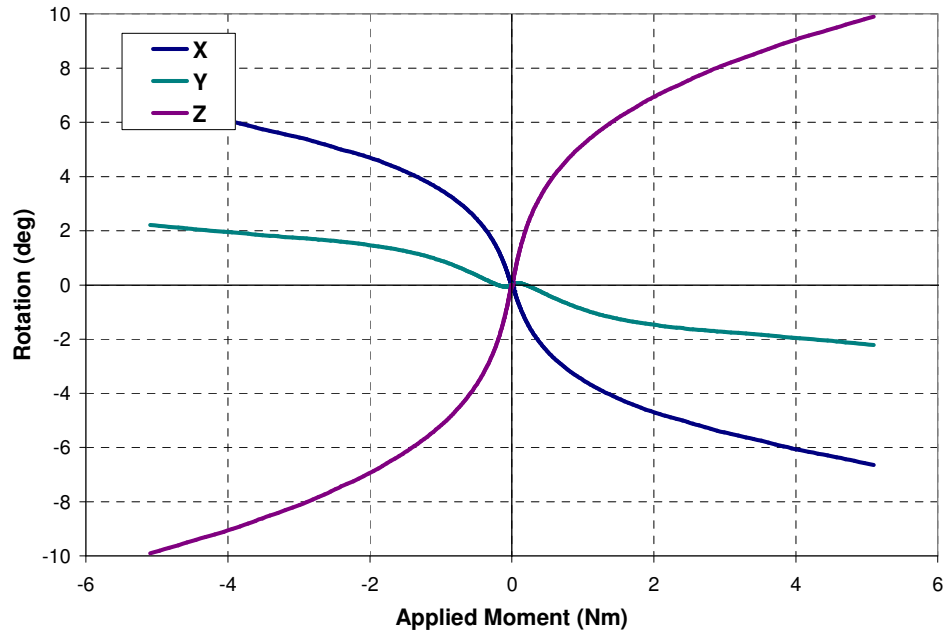
Figure 7-10: Coupled Motion of the C3-C4 Motion Segment in Applied Axial Rotation

The response of the models to small lateral moments (0.3 Nm) reported by Goel et al (1988a, 1988b) is very good (Figure 7-11), with most of the motion segments being within one standard deviation of the experimental average. Exceptions include the C0-C1, C6-C7, and C7-T1 motion segments, which

are just slightly more flexible than the experimental data. In axial rotation (Figure 7-12), the middle and lower cervical spine motion segments agree very well with the experimental response, while the relative axial motion of the upper cervical spine differs slightly. The results indicate that the C0-C1 joint is lax in axial rotation, while the C1-C2 is slightly stiff.

Figure 7-11: Lateral Angle of Each Segment under a Small Moment (0.3 Nm)
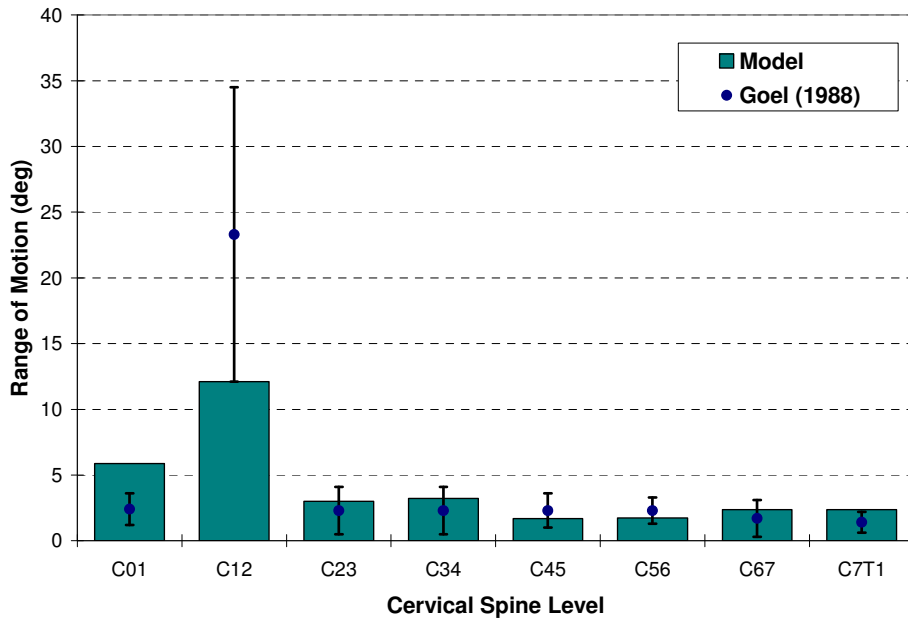
Figure 7-12: Rotation Angle of Each Segment under a Small Moment (0.3 Nm)

For larger axial rotations, only experimental data for the upper cervical spine joint is readily available. Comparing the axial rotational response of the C012 spine segment to the response reported in Chang et al (1992) revealed that the model was in good agreement with the experimental results. As the axial rotation increases, it is apparent that model response is more compliant than the post-mortem human subject for very large rotations. Nevertheless, the upper cervical spine model is representative in low to moderate axial rotation, and sufficient for frontal and rear impact response.
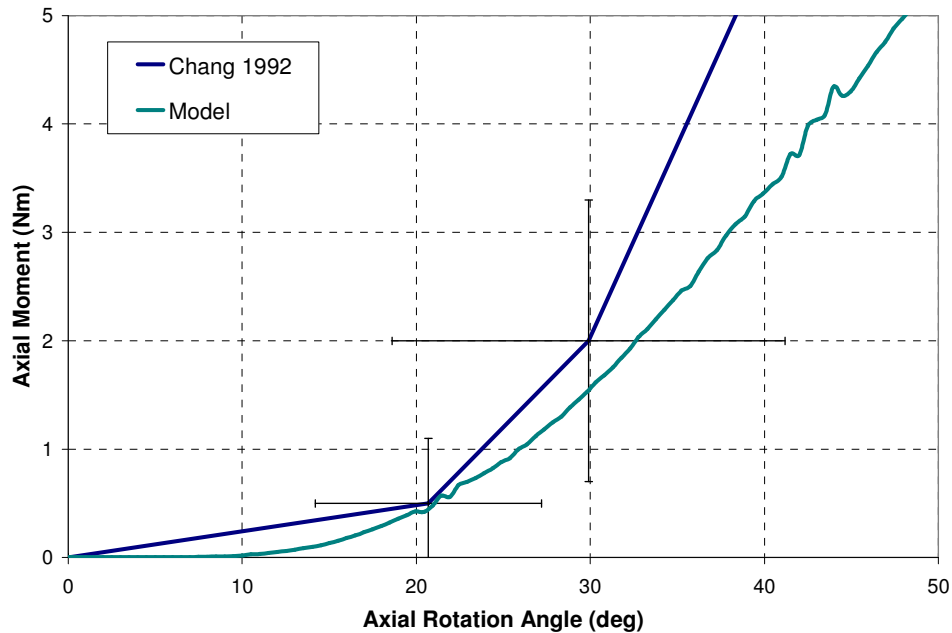
Figure 7-13: Rotation Response for C012 Segment under Large Rotational Moment

7.3.3   Tension and Compression

Tensile and compressive loading is present in the cervical spine during a frontal impact due to the inertial loading of the head. Furthermore, the tension or compression coupled with large flexion or extension moments are often the cause of serious cervical spine injury (Yoganandan et al., 1989c).

An example of the motion of a segment model in tension and compression can be seen in Figure 7-14. The response of intervertebral disc is similar to that described by White and Panjabi (1990). Under low to moderate compressive loads, the nucleus pulposus forces the annulus fibrosus to bulge outward. This mechanism provides for nearly all the compressive strength of the spine segment. At higher compressive loads, deformation of the vertebral endplate into the vertebrae became more apparent. Tensile loading resulted in a slight concavity of the annulus fibrosus. At low displacements,

the annulus fibrosus fibre provided most of the tensile resistance, since many of the ligaments were still lax.

| Tension | Initial Position | Compression |
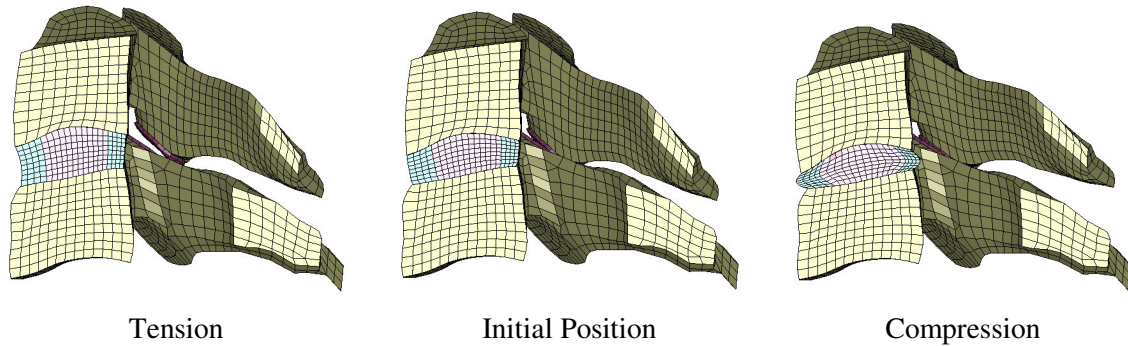
Figure 7-14: Segment Deformation during Tension and Compression

Compressive loading was coupled with either a significant flexion or extension motion, as the incompressible nucleus pulposus acted as a pivot for the superior vertebra (refer to Appendix A). In four of the six motion segments, a significant flexion motion was produced. This does not agree with Panjabi et al (1986) who reported that all compression loads were coupled with an extension motion. A small extension motion was coupled with the model in tensile loading, although this motion was rather insignificant. The type of coupled motion is dependant on the location of the applied tension and compression load. This aspect is discussed in Section 7.4.

A typical response of a cervical spine segment model in tension and compression can be found in Figure 7-15. In compression, there is generally a small 'toe' region of relatively low, but increasing, compression stiffness. This is followed by a period of linear response, until the stiffness of the segment in compression begins to decrease when plastic deformation takes place in the vertebrae (typically around 1000 N). The stiffness of the segment is much less in tension than it is in compression, with a relatively large 'toe' region. Tensile loading was not simulated to a point where plastic deformation began to occur in the vertebrae.
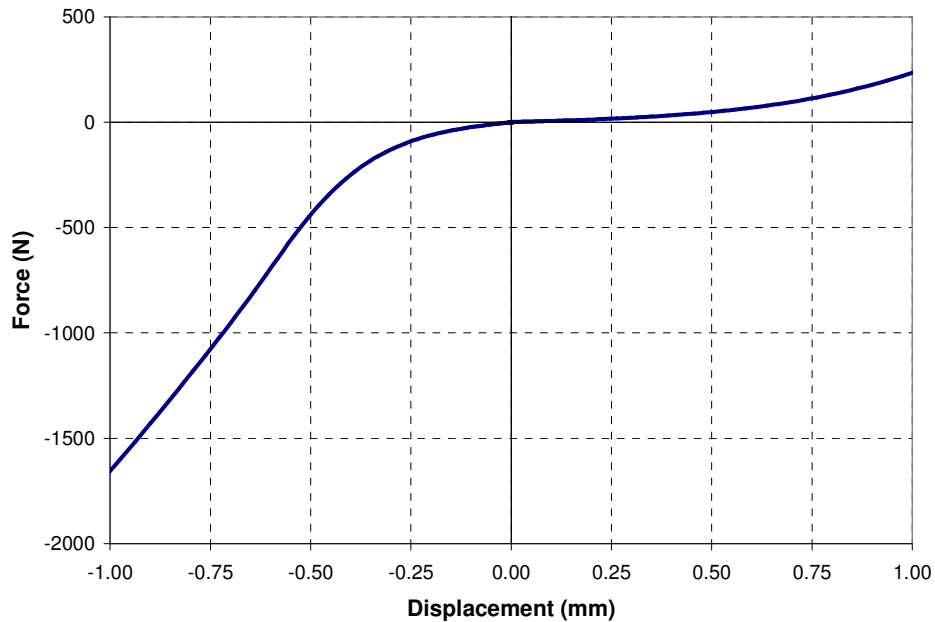
Figure 7-15: Tension/Compression Response for C45 Segment

The response of the segment models were compared to the segment stiffness reported by Panjabi et al (1986) and Shea et al (1991). The stiffness for each motion segment in tension and compression can be seen in Figure 7-16 and Figure 7-17. For simplicity, the average model response is compared to the experimental results, which can be seen Table 7-2. The model response agrees with the experimental results, being within one standard deviation from the experimental average. However, it should be noted that the reported results from both studies have large statistical spreads.

Table 7-2: Segment Model Response in Tension and Compression

	Tension		Compression	
	25 N	100 N	25 N	500 N
Model Average	88.8 N/mm	288.7 N/mm	275.4 N/mm	2181.7 N/mm
Panjabi et al (1986)	75.0 (+/- 49.0) N/mm		338.0 (+/- 399.9) N/mm	
Shea et al (1991)		386 (+/- 248) N/mm		1914 (+/- 488) N/mm
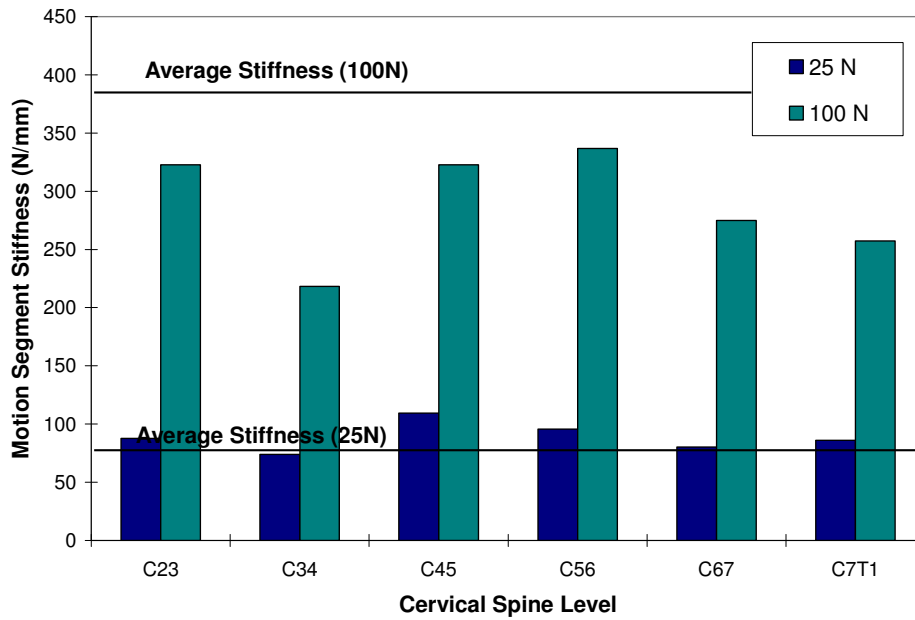
Figure 7-16: Stiffness of Each Segment at 25 N and 100 N Tension
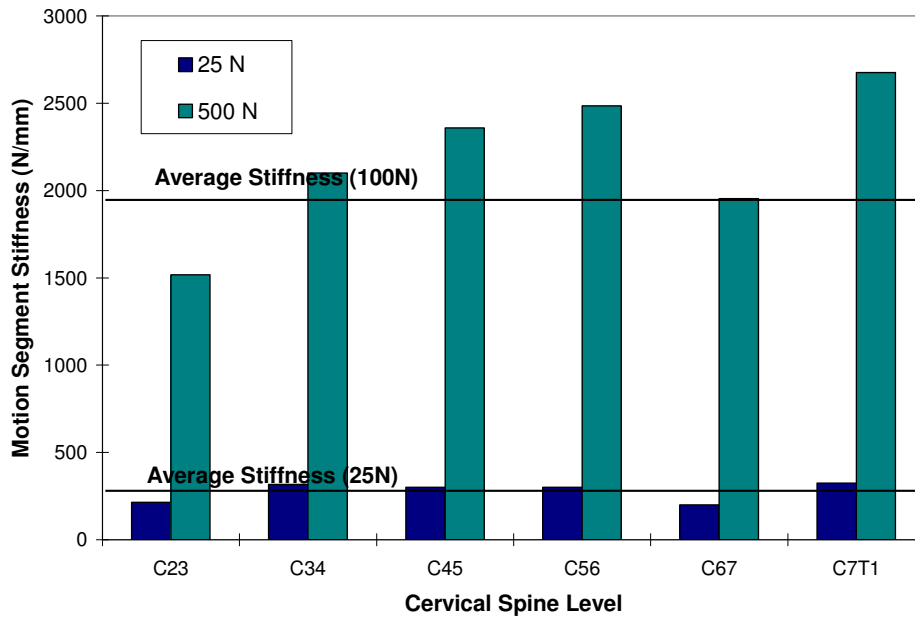
Figure 7-17: Stiffness of Each Segment at 25 N and 500 N Compression

174

7.3.4   Anterior, Posterior, and Lateral Shear

Only a few studies have looked at the load-displacement results of the cervical spine segment in shear, since these motions are often considered a by-product of more dominate modes of loading such as flexion or extension. Many cervical spine models over-look shear loading as a validation case, despite the fact that anterior shear can occur in the cervical spine in frontal impact cases, posterior shear in rear impact cases, and lateral shear in lateral impact cases.

An example of the motion of a segment model in anterior and posterior shear can be seen in Figure 7-18. These results are similar to those seen in Figure 7-2, since anterior and posterior shear were strongly coupled to flexion and extension respectively. Motion in anterior and posterior shear was restricted by the posterolateral annulus fibres, although only half of these fibres provided resistance.

Anterior Shear   Initial Position   Posterior Shear
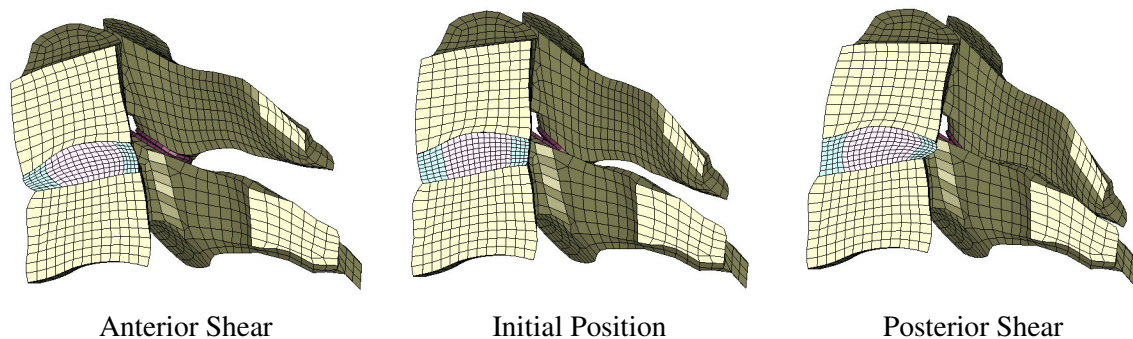
Figure 7-18: Segment Deformation during Anterior and Posterior Shear

The motion of a segment in lateral shear was similar to that of lateral bending. This can be seen when comparing Figure 7-19 with Figure 7-7. Furthermore, lateral shear was coupled with lateral bending and axial rotation, which is seen in Appendix A. This type of coupled motion was also reported by Panjabi et al (1986). Resistance to lateral shear was provided by the stretched fibres on the 'far' side of the disc (opposite the direction of motion), and the compressed annulus fibrosus on the 'near' side.

Initial Position   Lateral Shear
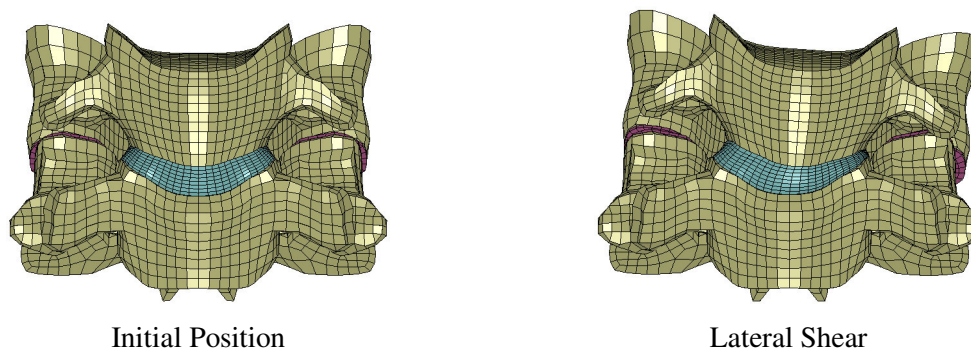
Figure 7-19: Segment Deformation during Lateral Shear

A typical response of a cervical spine segment model in shear can be found in Figure 7-20. Each direction exhibits the classic 'toe' region of low stiffness at small displacements, increasing in stiffness until the load-displacement response is linear. The general trend for the segment models was anterior and posterior shear were nearly equivalent in load-displacement response, while response in lateral shear was significantly stiffer. This partially agrees with Panjabi et al (1986) who reported that the range of motion of the cervical spine segment in the transverse plane was nearly equal.
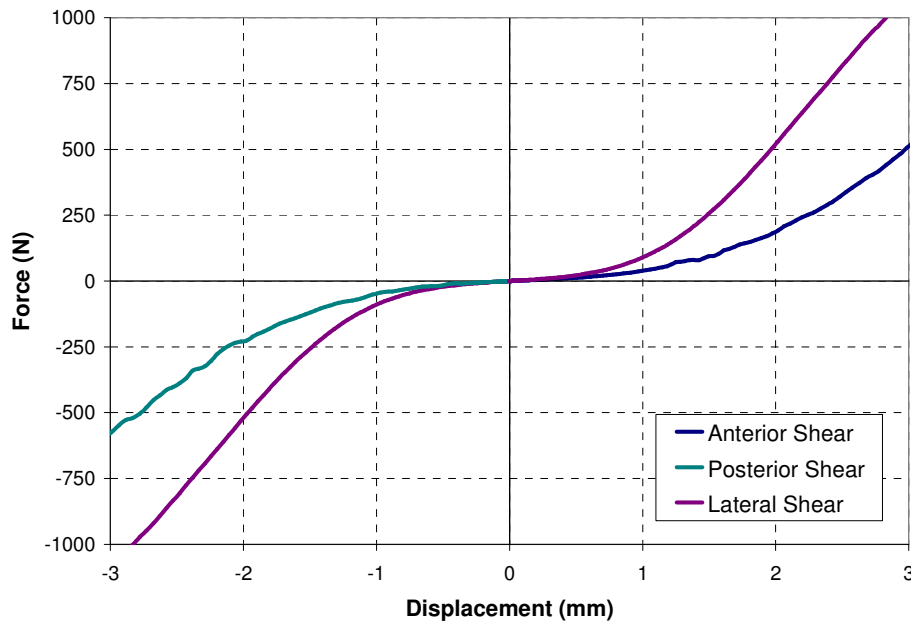
Figure 7-20: Anterior, Posterior, and Lateral Shear Response for C45 Segment

The response of the segment models were again compared to the segment stiffness reported by Panjabi et al (1986) and Shea et al (1991). The stiffness for each motion segment in anterior, posterior, and lateral shear can be seen in Figure 7-21, Figure 7-22, and Figure 7-23 respectively. For simplicity, the average model response is compared to the experimental results, which can be seen Table 7-3. Lateral shear was not tested in Shea et al (1991), but the model stiffness at 100 N was determined and reported in the table. The model response in anterior shear tends to be too stiff compared to Panjabi et al (1986), but too flexible compared to Shea et al (1991). In posterior shear, the model average is within one standard deviation of both Panjabi et al (1986) and Shea et al (1991), but are considerably more flexible than the experimental averages. Finally, the model response in lateral shear agrees well with Panjabi et al (1986). Again, it should be noted that the reported results from both studies have large statistical spreads.

Table 7-3: Segment Model Response in Anterior, Posterior, and Lateral Shear

	Anterior Shear		Posterior Shear		Lateral Shear	
	25 N	100 N	25 N	100 N	25 N	100 N
Model Average	54.4 N/mm	134.4 N/mm	39.4 N/mm	109.8 N/mm	61.1 N/mm	193.7 N/mm
Panjabi et al (1986)	38.4 (+/- 14.1) N/mm		70.6 (+/- 41.2) N/mm		71.4 (+/- 42.7) N/mm	
Shea et al (1991)	246 (+/- 70) N/mm		228 (+/- 138) N/mm			
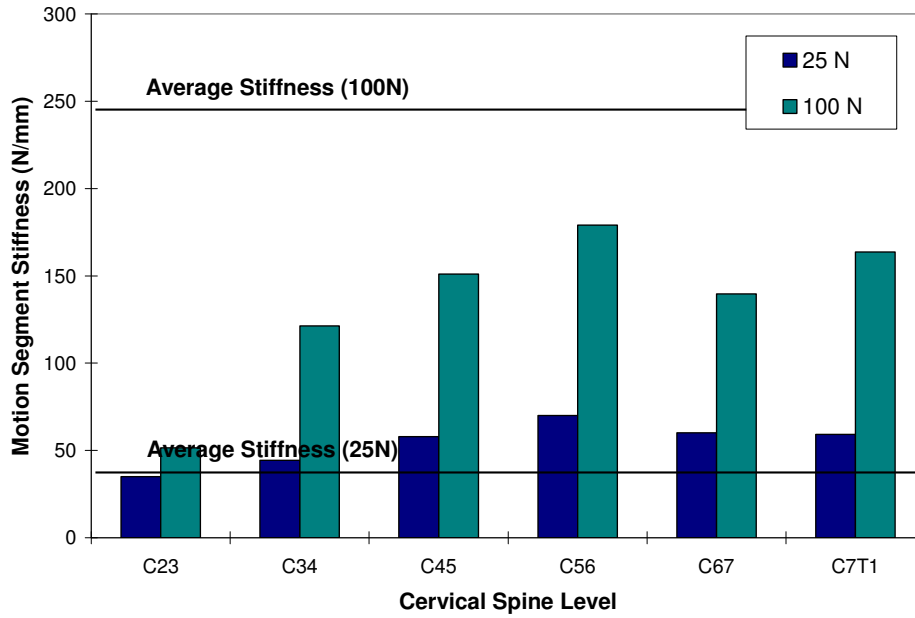
Figure 7-21: Stiffness of Each Segment at 25 N and 100 N in Anterior Shear
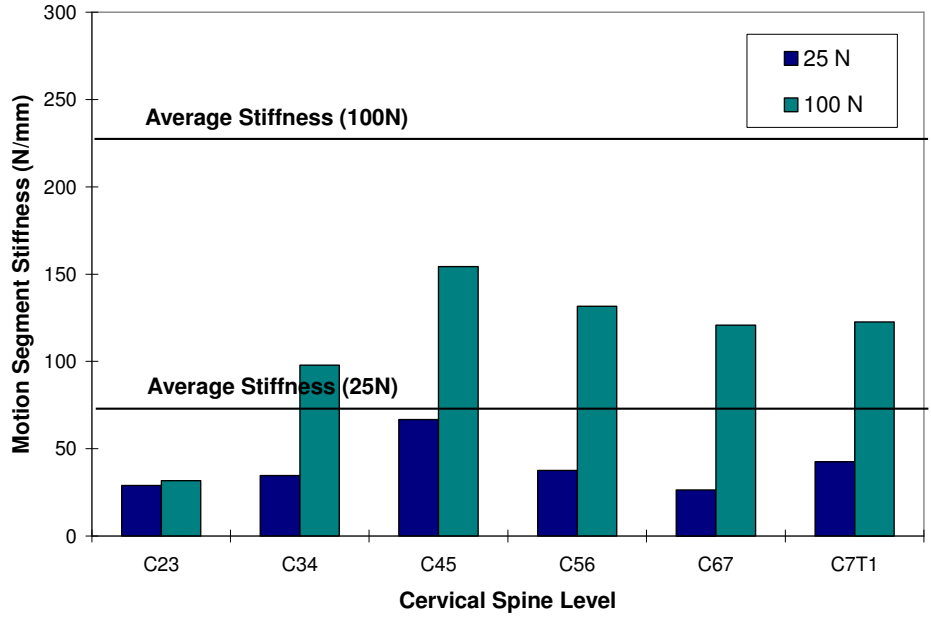
Figure 7-22: Stiffness of Each Segment at 25 N and 100 N in Posterior Shear
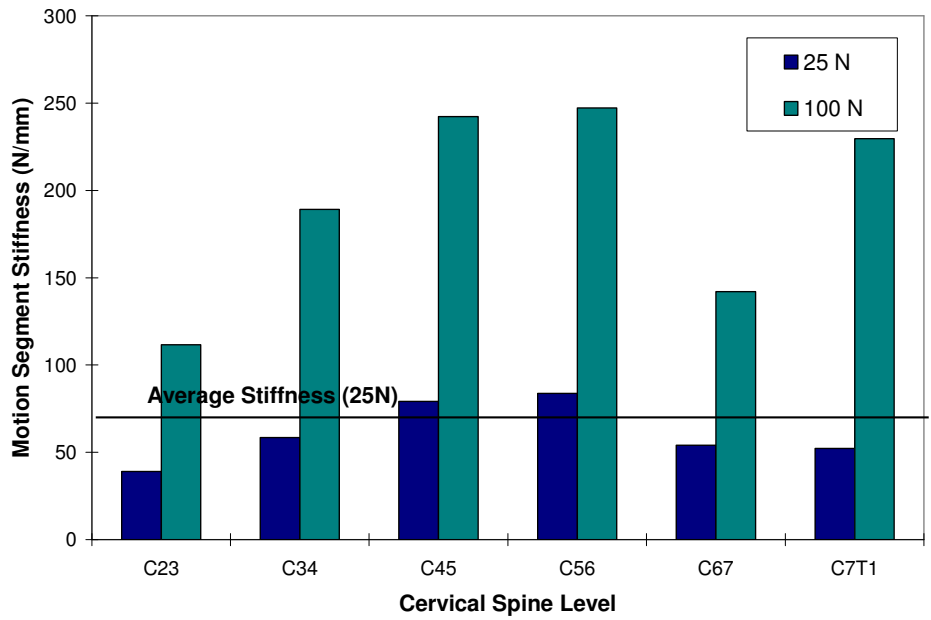
Figure 7-23: Stiffness of Each Segment at 25 N and 100 N in Lateral Shear

7.4 Discussion

The intent of the single segment simulations was to identify the quasi-static response of the cervical spine to evaluate the model against available experimental data. A number of different experimental studies were chosen to address all modes of loading to gauge the accuracy of model as thoroughly as possible. Previous cervical spine segment models have never been simulated in shear loading or tension (Yoganandan et al., 1996b; Clausen et al., 1997; Natarajan et al., 2000; Ng and Teo, 2001). Incorporating shear and tension loading in the model assessment is important for cervical spine models since these motions are coupled with dominate motions such as flexion and extension. Furthermore, in the case of frontal impact, anterior shear and tension loading have a large influence on the response of the cervical spine (see Section 8.4).

The results of the simulations reported in Section 7.3 show that the single segment models were generally representative of *in vitro* cervical spine segments based on various experimental studies and observations. The single segment models showed mostly excellent agreement with the experimental data. Nevertheless, some disparities between the segment model response and the experimental data were found. Many of differences between the single segment models and the experimental data may be partially attributed to the variation in experimental sample age, disc degeneration, specimen sex, specimen geometry, and fixation techniques. These are all typical sources of experimental variation found in biological material testing, and are reflected in the large standard deviations seen in almost all of the experimental data presented in this chapter.

The cause for many of the differences between the segment models and the experimental data was likely due to the initial positioning of the two adjacent vertebrae. It is speculated that gap between the articular surfaces in the facet joint was larger than tested experimentally. This would explain why most segments were too flexible in extension, since contact between the articular surfaces will provide structural support in extension. In many cases in the numerical simulations, contact between articular surfaces would occur only after a significant amount of extension rotation. However, segments C45 and C67 had small facet gaps, and their extension response compared well with the experimental data.

An overly large facet gap would also have a significant impact on the segment response in lateral bending, axial rotation, anterior shear, and compression. This may be the reason why the stiffness in anterior shear is much lower than the experimental results. Unfortunately, no measure of the facet

joint gaps in the cervical spine have been published, nor were actual CT scans of a human cervical spine made available.

Another difference between the segment models and the experiment are the difference in preconditioning of the segments prior to testing and the definition of the 'zero position'. While the 'zero position' in the numerical models was the initial model position, the 'zero position' using experimental methods is much more difficult to define. It was reported by Panjabi et al (1986) that because small loads would easily cause the spine segments to displace, they 'arbitrarily chosen the origin' on which they measured the spine displacements. This ramification may be significant since results of physiological loading are often dealing with displacements in fractions of a millimeter, and rotations in fraction of a degree.

Finally, when dealing with translational loading, the point where the load was applied and the displacement was measured had a significant effect on the results. In most experiments, the upper vertebra was cast in a resin or cement, and a device applied load to the entire vertebra. However, in the numerical model, all loads were applied to a point located in the exact centre of the superior vertebral body. Kumaresan et al (1999b) showed in their numerical model that by moving this point load a few millimeters either posterior or anterior, the response of the disc in compression changed significantly.

This sensitivity was seen in the current single segment models for compression, as well as in tension and shear. Because four of six segment models produced coupled flexion motion during compression, while the experimental results produced only coupled extension motion (Panjabi et al., 1986), it would appear that the compressive load should have been applied posterior to the vertebral centre in accordance to the experimental study. This effect was not present for rotational-based modes of loading.

7.5   Vertebra Trauma in Compression

As an initial investigation into simulating trauma in the cervical spine, the material model for bone included a damage-like response in the form of plastic deformation (see Section 6.3.1). Based on strain criteria, this type of trauma modelling can provide insight into the load-threshold for the vertebrae as well as the mechanism of injury.

Each compression simulation was designed such that the compressive load would exceed a normal physiologic level in order to achieve damage (plastic deformation) within the vertebrae. The load

corresponding to the onset of damage in each type of bone (cancellous, cortical, and endplate) was recorded to identify when sub-traumatic loading may occur. The compressive force causing the onset of bone damage is not necessarily the failure force of the bone, since bone damage can occur prior to any complete rupture or fracture mechanism (Kopperdahl and Keaveny, 1998). The compressive load in each segment at the onset of bone damage can be seen in Figure 7-24.
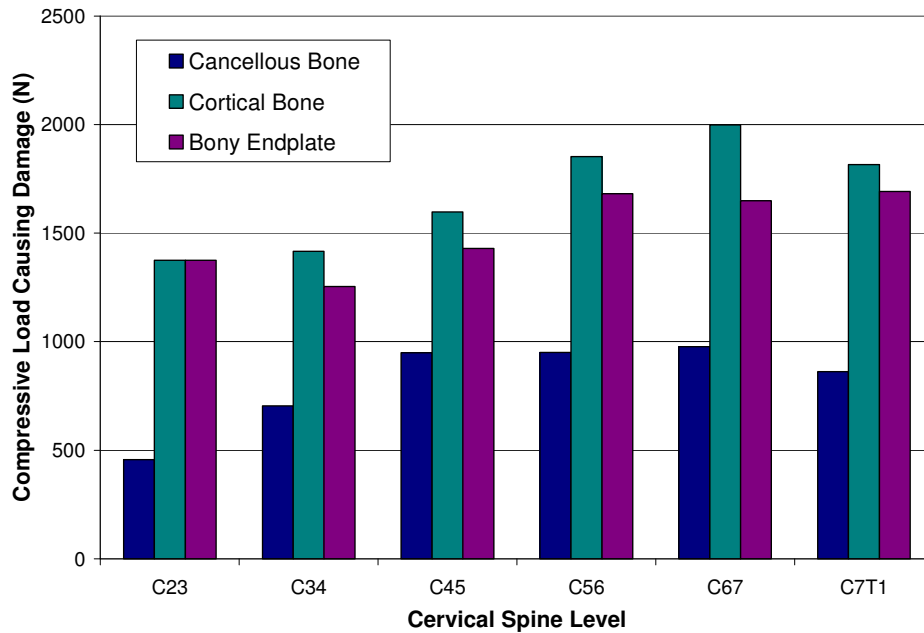
Figure 7-24: Compressive Load at the Onset of Bone Damage for Each Cervical Spine Level

Damage to the cancellous bone always occurred much sooner than cortical bone or the bony endplates. Cancellous bone damage was typically concentrated in the centre of each vertebral body, which can be seen in Figure 7-25. Bony endplate damage typically began in the centre of the endplate in the area adjacent to the nucleus pulposus. Endplate damage also occurred along the rim where the endplate met the cortical bone. Cortical bone was often present on the anterior wall of the vertebral body. This type of bone damage pattern is consistent with wedge or comminuted type fractures (refer to Figure 4-7). It should be noted that using shell elements for the cortical bone and bony endplates may not have properly captured the damage phenomenon since through-thickness response was neglected.

As mentioned earlier, the results shown in Figure 7-24 indicate a load at which bone damage will begin to occur. It is expected that damaged bone will continue to provide structural strength to the vertebra until an ultimate strength is reached, wherein the bone will fracture and fail (refer to Section

3.2). Therefore, it is likely that the ultimate compressive load of the vertebral segment be larger than the loads shown in Figure 7-24.
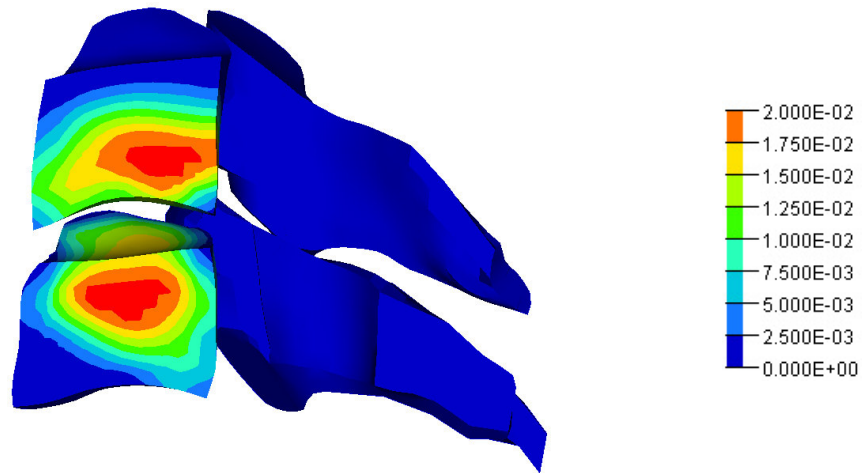
Figure 7-25: Plastic Strain in C4 and C5 Cancellous Bone under 1770 N Compression

Thus, while the results of bone damage in the vertebrae cannot be validated against a specific experimental study, the results appear to be realistic for the cervical spine. Yamada (1970) reported the compressive breaking load of cervical vertebra to decrease from 4100 N in young adults to 1850 N for old adults. White and Panjabi (1990) reported that the compressive strength of the cervical vertebrae (C3 to C7) to be between 1500 N and 1750 N. Studies on the compressive strength of ligamentous cervical spines have produced failure forces between 960 N and 6840 N in various impact cases (McElhaney et al., 1983; Pintar et al., 1989; Yoganandan et al., 1991; Pintar et al., 1995; Nightingale et al., 1996).

Chapter 8

Frontal Impact of the Complete Spine Model

8.1 Experimental Background

The full cervical spine model was evaluated against the human volunteer tests done by the Naval Biodynamics Laboratory (NBDL) to simulate frontal impact. This extensive program studied the head and neck response of seated volunteers under frontal, lateral, and oblique impact conditions. In total, more than 300 tests on 16 instrumented human subjects were done by the NBDL, with most of the test data available to the public from the National Highway and Traffic Safety Administration (NHTSA).

The series of sled tests used to validate the full cervical spine model were conducted in the early 1980's on a 12-inch HYGE Accelerator sled. The sleds were initially at rest before being rapidly accelerated down the sled track using a specific acceleration profile (see Figure 8-1). Included in these tests were a series of 39 frontal impact tests grouped by peak sled acceleration (8, 10, 12, or 15 G) (Wismans et al., 1986). These tests are the basis for the evaluating the full cervical spine model in frontal impact. The average sled acceleration time histories for each case can be found in Figure 8-1.
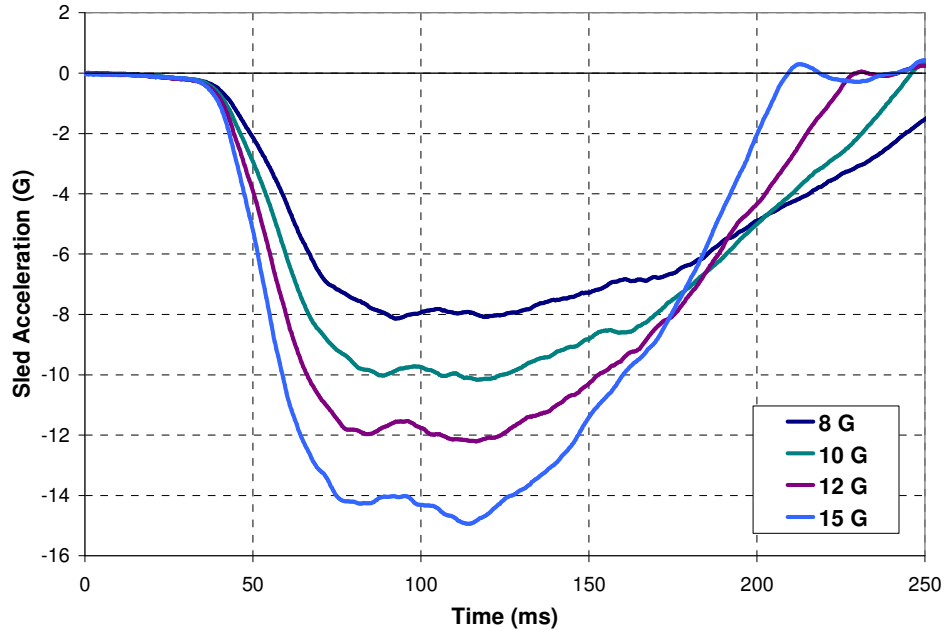
Figure 8-1: Average Sled Acceleration Time Histories from the NBDL Study

For each test, a human volunteer sat upright in a rigid seat fixed to the sled, and constrained by shoulder straps, a lap belt, and an inverted V-pelvic strap fixed to the lap belt. This type of occupant restraint sufficiently constrained the subject to limit the amount of vertical or lateral displacement of the T1 vertebra (Wismans et al., 1986; Thunnissen et al., 1995). The three-dimensional motions of the head and T1 vertebra were monitored using a cluster of accelerometers mounted to each subject. The typical instrumentation setup of each human volunteer can be seen in Figure 8-2.

(Adapted from van der Horst, 2002)

Figure 8-2: Instrumented Human Volunteer for the NBDL Sled Test Experiments

184

All 39 frontal impact tests were conducted using eight human volunteers, whose anthropometric measurements can be found in Table 8-1. Despite the wide range in body size, the sled test results between different subjects were consistent. It should be noted that the volunteers were taken from a pool of young and physically fit marines.

Table 8-1: Summary of the Anthropometric Details of Each Volunteer

Subject	Weight	Standing Height	Sitting Height	Neck Length	Estimate Head Mass	
					Mass	Inertia (Iyy)
H00118	73.8 kg	185.5 cm	97.9 cm	17.2 cm	4.79 kg	0.0303 kgm^2
H00120	83.0 kg	172.6 cm	91.1 cm	17.2 cm	5.14 kg	0.0331 kgm^2
H00127	62.1 kg	172.3 cm	89.8 cm	16.2 cm	4.40 kg	0.0252 kgm^2
H00131	67.6 kg	167.0 cm	90.0 cm	15.6 cm	4.98 kg	0.0311 kgm^2
H00132	79.8 kg	172.9 cm	89.6 cm	14.1 cm	5.05 kg	0.0319 kgm^2
H00133	61.2 kg	161.7 cm	86.8 cm	16.5 cm	4.70 kg	0.0286 kgm^2
H00135	68.9 kg	171.6 cm	90.7 cm	15.0 cm	4.23 kg	0.0240 kgm^2
H00136	88.9 kg	185.4 cm	92.3 cm	17.3 cm	4.77 kg	0.0292 kgm^2
Average	73.2 kg	173.6 cm	91.0 cm	16.1 cm	4.76 kg	0.0292 kgm^2

As mentioned above, the T1 vertebra of each subject was adequately constrained to limit movement in the vertical (Z) or lateral (Y) directions (Wismans et al., 1986). Initially, it was believed that the acceleration of the T1 vertebra in the frontal (X) direction was the sole input for transferring acceleration from the sled to the head during each test (Ewing et al., 1968). A re-analysis of the study by Wismans et al (1986) revealed that there is also a significant amount of T1 rotation during the frontal impact that was not present in the experimental dataset due to T1 accelerometer slippage (Thunnissen et al., 1995).

8.2 Simulation Methods

The full cervical spine model consisted of the head, all eight vertebra, intervertebral discs, ligaments, and neck musculature as described in Chapter 6. Each vertebra was modeled as a rigid body, with the same mass and inertia properties as found in the deformable vertebra, since the additional mass from the musculature was added via point masses rather than lumping the mass in with the vertebra. The viscoelastic component of each material model, including any incompressibility assumption, was enabled as described in Section 6.3. The coordinate system for the model can be seen in Figure 8-3.
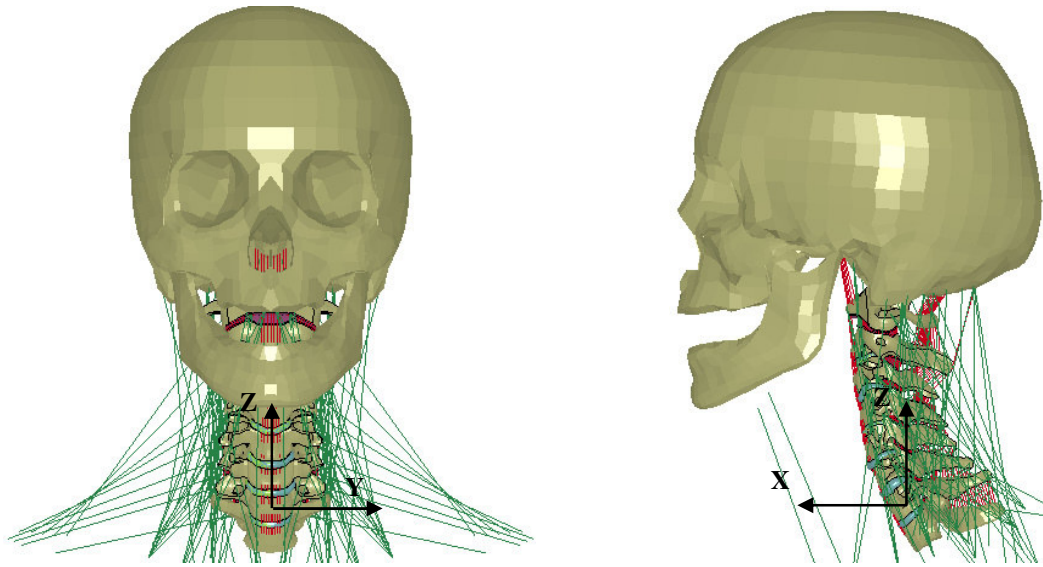
Figure 8-3: Coordinate System for Full Cervical Spine Model

The full cervical spine model was used to investigate the 15 G frontal impact condition, since this was the most severe case. This was accomplished by prescribing a motion to the T1 vertebra based on the acceleration and rotation response recorded in the experimental data. The average experimental T1 acceleration for the 15 G case can be seen in Figure 8-4, while the average T1 rotation (as reported by Thunnissen et al., 1995) can be seen in Figure 8-5. All other motion for the T1 was constrained.

Each simulation was run to 250 ms, despite the fact that the experimental data was available to 300 ms. Most of the inertial loading on the head was already reduced to near zero by 250 ms, so simulating to 300 ms was considered unnecessary.
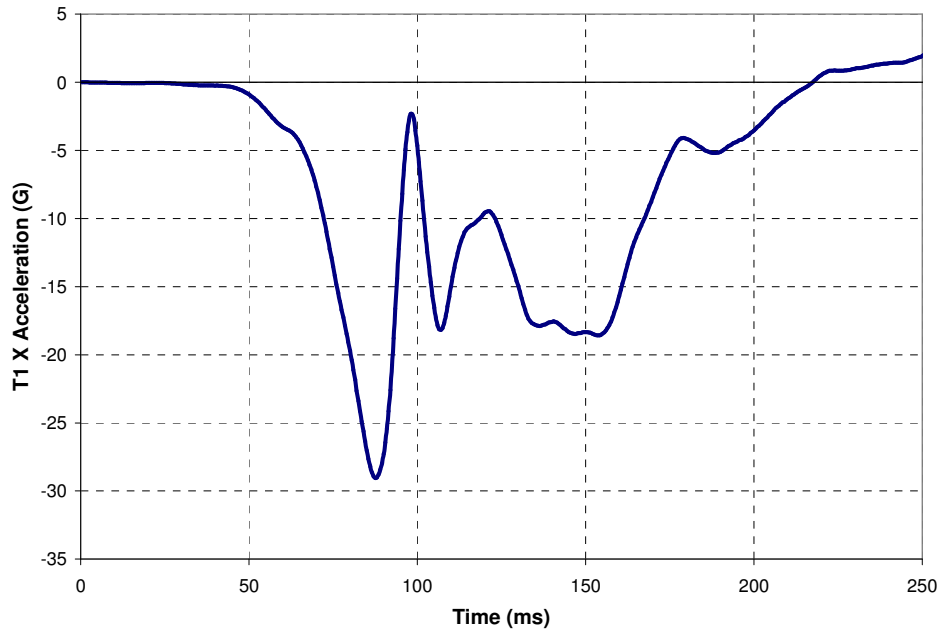
Figure 8-4: Prescribed T1 Acceleration Time History (X Direction) for 15 G Impact Case
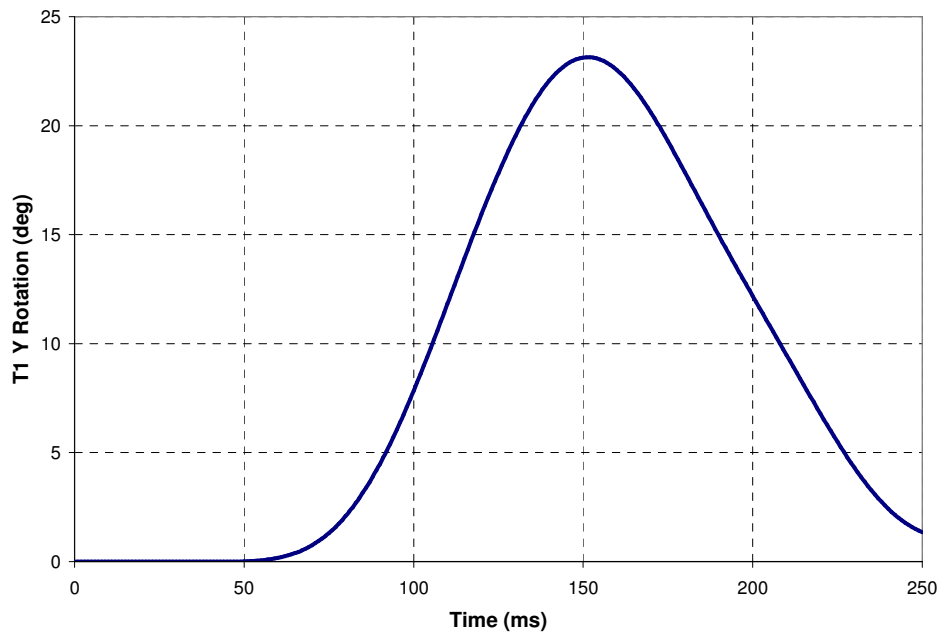
Figure 8-5: Prescribed T1 Rotation Time History (Y Direction) for 15 G Impact Case

Activation of the muscles via the idealized neural input u(t) was implemented in the full cervical spine model based on the estimated reaction of the human volunteer to the sled acceleration. Siegmund et al (2003) determined from rear impact tests, that the muscles in the cervical spine activate around 74 ms after the onset of sled acceleration. Therefore, full neural excitation began at t

= 74 ms and held for 100 ms, where it returned to zero neural excitation. The resulting muscle activation scheme for the 15 G impact case can be seen in Figure 8-6. It should be noted that for simplicity, activation for both flexors and extensors were modeled using the same scheme.

Gravity was not accounted for in the simulation, since this would require a muscle activation scheme to stabilize the head prior to the applied impact. The lack of a realistic initial loading condition on the cervical spine is not considered a significant shortcoming, since accelerations seen on the head are magnitudes greater than the constant 1 G gravity load. It was reported that the addition of gravity in the 15 G frontal impact case resulted in a 5% increase in head rotation, and even smaller difference in model acceleration for a multi-body model (van der Horst, 2002).
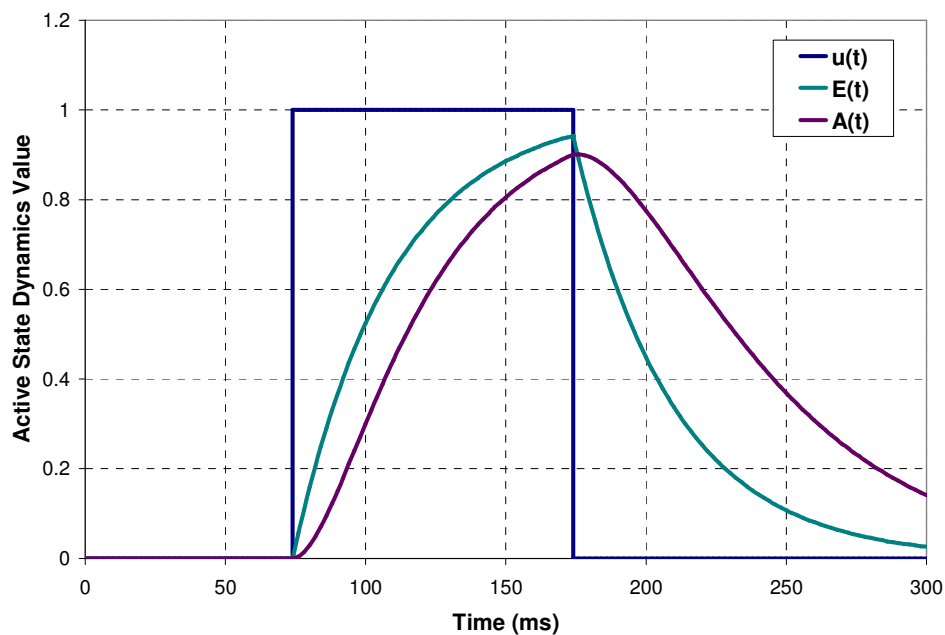
Figure 8-6: Muscle Activation for 15 G Frontal Impact Case

All simulations were run using LS-DYNA version 970 revision 6763.086 using single precision calculations on a single Linux workstation. The model took over 124 hours to run on a single 2.4 GHz machine. To reduce this simulation time, mass scaling was invoked to increase the minimum timestep to 0.45 µs from 0.17 µs, which reduced processing time by approximately 76 hours. The only 7.22 gm of mass was added to the model (mainly to the nucleus pulposus elements) for an increase of 0.15%. There was no difference in simulation results, therefore the mass-scaling method was used throughout the simulations.

8.3 Simulation Results

The results of the simulation of the 15 G frontal impact cases can be seen in the following section. The accelerations of the centre of gravity (C.G.) of the head in the model were compared to the experimental results using the acceleration of the three motions in the sagittal plane (horizontal 'X' and vertical 'Z' linear acceleration, and rotational 'Y' acceleration). The model head trajectory was also compared to the experimental corridors (average response +/- one standard deviation). These results can be seen in Figure 8-8 to Figure 8-11.

The graphical response of the model can be seen in Figure 8-7. For all cases, there was very little motion occurring from 0 ms to 75 ms of the simulation. From 75 ms, the T1 vertebra moves away from the head, since the head remains relatively stationary because of its inertia. This resulted in the cervical spine being stretched in tension. Also around this time, the head began to move and rotate towards the chest. Muscle activation began at 74 ms, which reduced the tensile forces in the cervical spine to near zero by 100 ms.

From 100 ms, the head continued to move downward and rotate, as the cervical spine began to bend in flexion. The head reached its lowest point and greatest rotation at 160 ms. At this point, the cervical spine was loaded in a combined flexion-compression mode, with some anterior shear. This was also the point of maximum tissue stress, and the most likely time for injury to occur.

After reaching the maximum displacement point, the head and cervical spine began to rebound back to a neutral position. The rebound phase produced less severe loads on the cervical spine and head. By the end of the simulation (250 ms), the head and cervical spine returned to a position similar to the initial position.

**Model
Response**
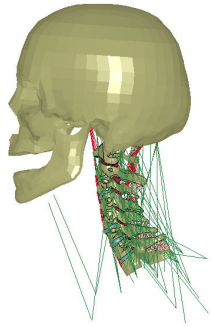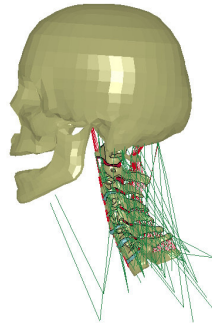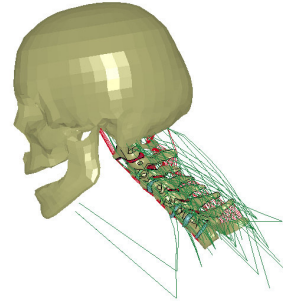
Time **40 ms** **70 ms** **100 ms** **130 ms**
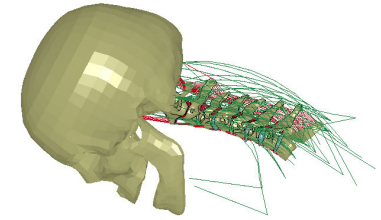
**Model
Response**
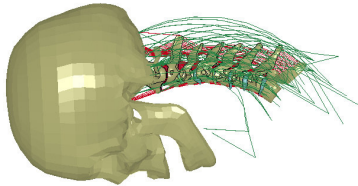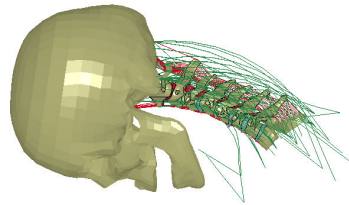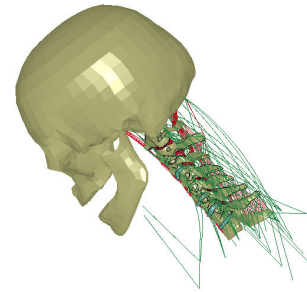
Time **160 ms** **190 ms** **220 ms** **250 ms**
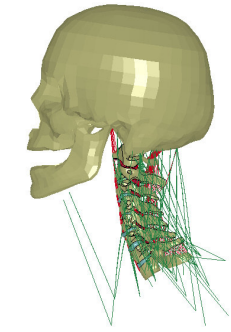
Figure 8-7: Time-Lapsed Head and Neck Displacement during Frontal Impact Simulation

The response of the head and cervical spine in the model simulation was considered realistic when compared to the experimental results from the NBDL tests (Figure 8-8 to Figure 8-10). In general, the trends in acceleration time-history predicted by the model agreed with the experimental response. Furthermore, the magnitudes of the head accelerations predicted by the model were similar to those from the experimental study. However, there were a few areas in the simulation where the model did not accurately reproduce the response of the human volunteers.

The most noticeable difference between the full cervical spine model and the experimental response was that the model did not accurately predict the first horizontal (X) acceleration peak at 98 ms, as seen in Figure 8-8. Instead, the model predicted two smaller acceleration peaks (one at 92 ms and other at 112 ms). The double-peak effect did not appear in either the vertical or the rotational acceleration responses of the model. After the two smaller accelerations peaks, the response of the model in horizontal acceleration agreed well with the experimental response.
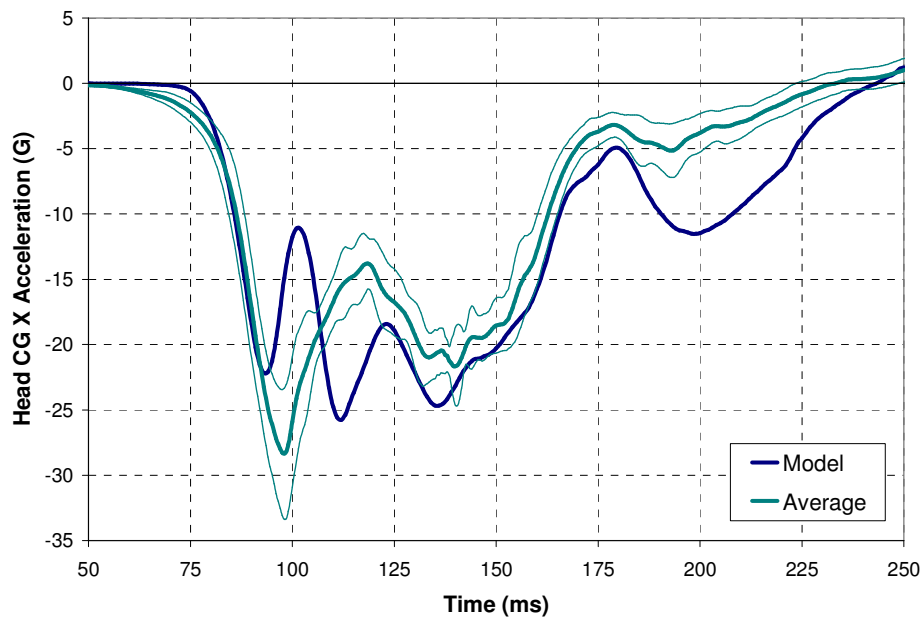
Figure 8-8: Head C.G. Horizontal Acceleration (X Direction) in 15 G Frontal Impact

There was also a noticeable lag between the model and the experiment in the vertical (Z) acceleration direction at the beginning of the response (Figure 8-9). This is likely causing the over-prediction of the first acceleration peak at 90 ms. At this peak, the model over predicts the experimental average by

roughly 60% (8 Gs). There was also a slight lag between the model and the experiment in the horizontal direction (Figure 8-8). Oddly enough, the response of the model leads the experimental response when considering the rotational acceleration of the head (see Figure 8-10).
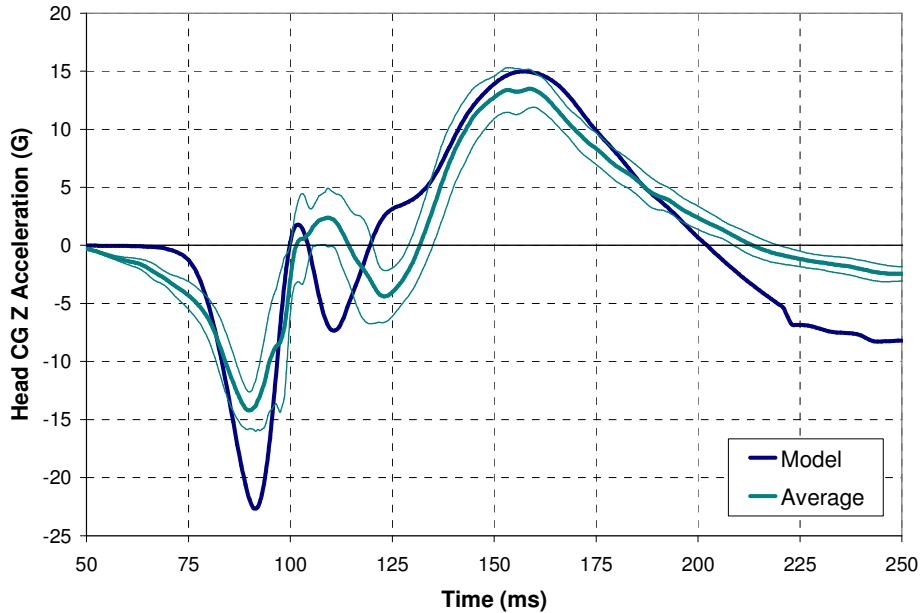
Figure 8-9: Head C.G. Vertical Acceleration (Z Direction) in 15 G Frontal Impact

The model response in rotational acceleration agreed well with the experimental response, predicting an accurate peak rotational acceleration (although a few milliseconds earlier than the experimental average). However, the model does not accurately predict the minor acceleration peak occurring at 125 ms.
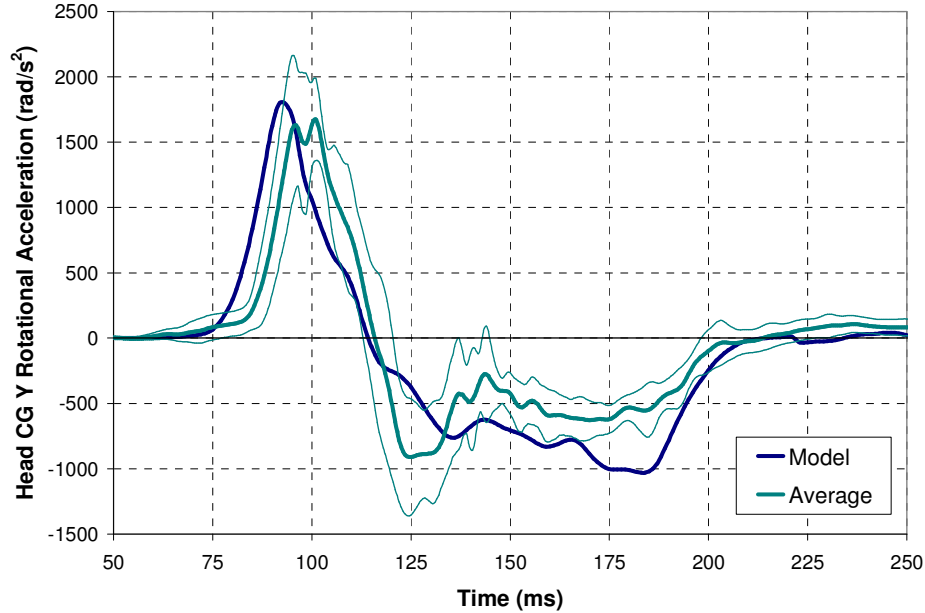
Figure 8-10: Head C.G. Rotational Acceleration (Y Direction) in 15 G Frontal Impact

The trajectory of the model head during the 15 G frontal impact, which can be seen in Figure 8-11, fell within the experimental corridor. Despite some disparity between the experimental acceleration and the model acceleration, no major differences were seen comparing the position of the head to the experimental corridors. This highlights the fact that it is not appropriate to validate a cervical spine model using only head trajectory as a measure since this can hide any errors present in the acceleration histories.
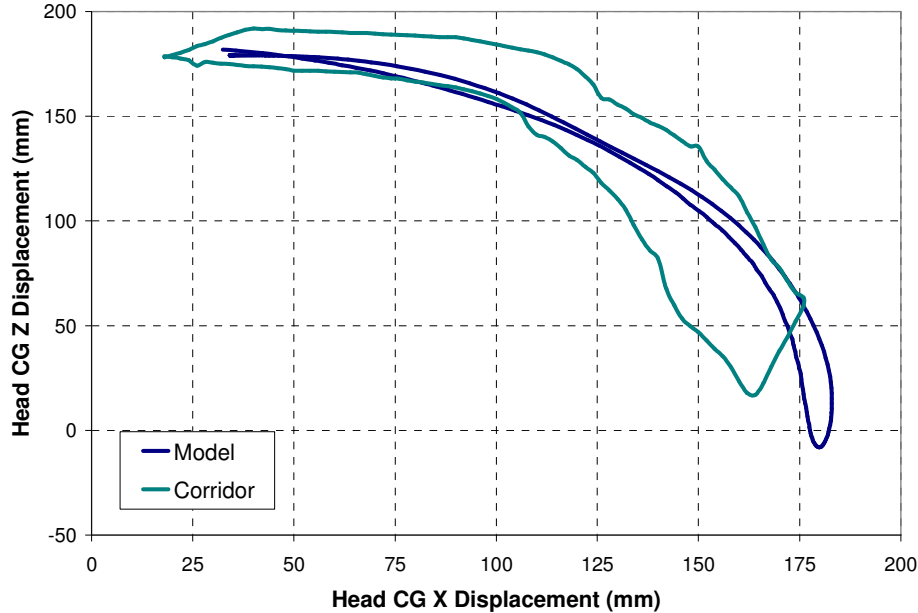
Figure 8-11: Head C.G. Trajectory in 15 G Frontal Impact

Since flexion is the predominant mode of cervical spine loading in frontal impact, the relative flexion angle between each spine segment was measured during the simulation (Figure 8-12). The maximum flexion angle was reached between 150 ms and 175 ms for all cervical spine levels. The lowest two cervical levels (C7T1 and C67) reached a maximum flexion between 14 deg and 15 deg, while the rest of the cervical spine had a maximum flexion level between 11 deg and 12 deg. These flexion angles were beyond the angles used to validate each single segment model (Appendix B). Also noticeable in Figure 8-12 is a significant delay in the response between the C23, C34, and C45 segments. This may be one of the localized sources of the delay seen at the head in Figure 8-8 and Figure 8-9.

At maximum flexion angle, the posterior portions of the interspinous ligament of all levels reached stretches near the experimental failure deformation. In the case of the lowest two cervical levels, the interspinous ligament exceeded the experimental failure deformation, which indicatied that localized ligament injury should have occurred. All remaining ligaments were not exposed to high levels of stretch, and were not at risk of injury. No pain was reported by any of the volunteers after each sled test, indicating that no severe injury had occurred during the impact.
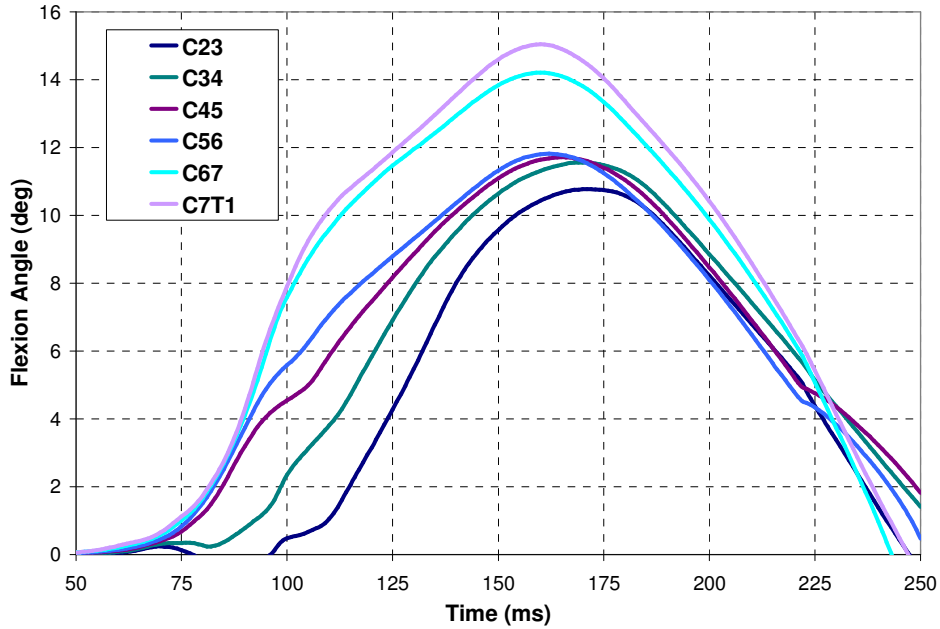
Figure 8-12: Flexion Angle for Each Level of the Cervical Spine in 15 G Frontal Impact

Using the current FMVSS208 standard for measuring neck injury (N_{IJ}), the response of the model in the 15 G frontal impact was assessed for injury. The moments and forces were calculated at the occipital condyles in a manner similar to Mertz and Patrick (1967), who used the rigid body motion of the head to determine neck loading. Axial force was calculated as the product of the head mass (4.376 kg) and the relative acceleration between the head and T1, in the line defined by the occipital condyles and T1. The bending moment was calculated as the product of the head inertia in the sagittal plane (23300 kg mm^2) and the rotational acceleration of the head. These values were calculated concurrently, and plotted on the N_{IJ} chart seen in Figure 8-13.

As expected, the model results indicated that the occupant was not experiencing an injurious neck load, having a maximum N_{IJ} value of 0.21 that occurred at 100 ms. At this instance, the maximum occipital bending moment and axial force were reached, calculated to be 38 Nm in flexion and 708 N in tension respectively. Consequently, a flexion moment of 38 Nm is below the flexion tolerance of 60 Nm proposed by Mertz and Patrick (1971) as the threshold of pain.
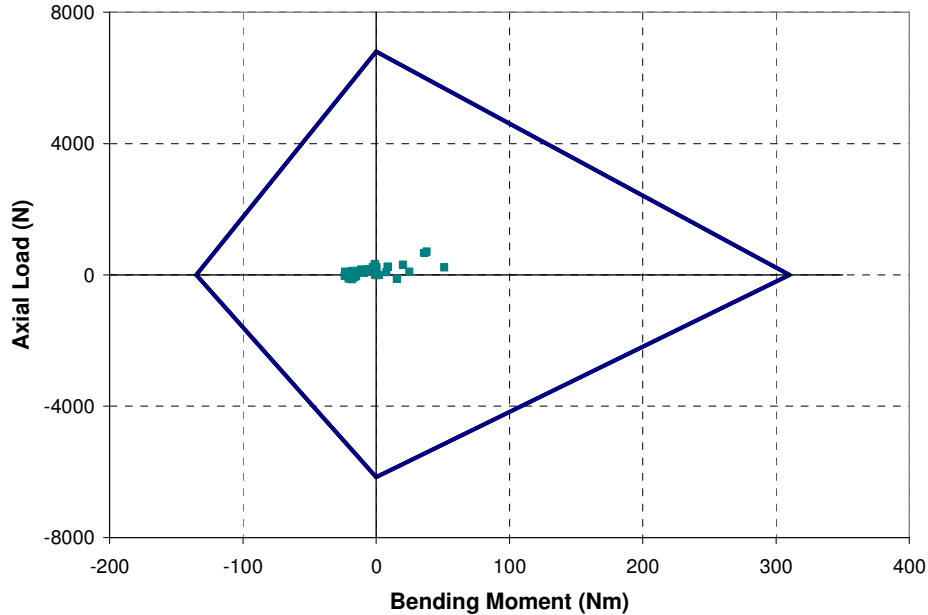
Figure 8-13: NIJ Assessment for Simulated 15 G Frontal Impact

8.4 Discussion

The 15 G frontal impact case was fully investigated with the full cervical spine model to evaluate the biofidelity the full cervical spine model under dynamic loading conditions. The results of the full cervical spine simulation in frontal impact agree reasonably well compared to the experimental data. The response of the model seen in Figure 8-8 to Figure 8-10 tended to be more representative of the human volunteer response than other numerical models of the cervical spine validated using the same impact case (Meyers et al., 2004; Brolin et al., 2005). Furthermore, many of the previous full spine models used head trajectory rather than acceleration as the measure for model evaluation (Van der Horst, 2000). Choosing to assess the model based on head trajectory alone is inadequate, since this method can mask or dilute errors in the model response seen in the head accelerations.

The most significant differences in the model response compared to the experimental response was the double peak found in the horizontal acceleration (Figure 8-8), and the delay in vertical acceleration (Figure 8-9). The double peak response in the model fails to capture the correct loading at the most significant time in the impact, during maximum loading. During this stage of the impact, the neck is just beginning to stretch in tension as the head remains stationary by the T1 vertebra

accelerates away. The cervical spine appeared to behave like a spring that went through a few cycles of loading and unloading. This would indicate that the model has a higher natural frequency in tension than an actual human volunteer.

In a simple spring-mass-damper system, natural frequency increases with increasing stiffness, decreasing mass, and decreasing damping. Since the mass in the simplified system is essentially the head (where the simulation and experiment agreed), the most likely cause for the higher natural frequency was that the model was either too stiff, or lacked damping (viscoelastic effect). At this stage of the simulation, elongation of the cervical spine was relatively small, so the mechanical effects of the ligaments were minor. This indicated the source of high frequency was found in either the intervertebral discs or the muscles. It should be noted that response of the single segments in tension and compression agreed reasonably well with quasi-static experimental data (Section 7.3.3), suggesting the lack of viscoelastic characterization of the annulus fibrosus was a source of model error.

However, another source of model inaccuracy may be due to the lack of representation of the non-structural soft tissues of the neck. These soft tissues reside in the vascular system (carotid artery and jugular vein), the digestive system (pharynx and esophagus), the respiratory system (larynx and trachea), the nervous system (spinal cord), the integumentary system (skin), and adipose tissue (fat). Furthermore, bulk muscle tissue was not represented in the model as the mass was simplified to nodal masses (Section 6.1.5). All of these missing soft tissues may contribute to the mass and damping required to reduce the natural frequency of the model to biofidelic levels.

The other main difference between the model and the experimental response, as mentioned previously, was the delay apparent in the vertical acceleration time-history (Figure 8-9), and slightly in the horizontal acceleration time-history (Figure 8-8). Analyzing the response of each individual motion segment of the cervical spine (Figure 8-12) revealed that a delay in flexion response exists in the C23 and C34 motion segments. However, upon reviewing the quasi-static flexion response of these segments (Appendix B), it is clear that the model response agrees with the experimental data.

The most likely source of the delay in the response of the model comes from the low anterior shear stiffness that was seen in all motion segments (Figure 7-21). Anterior shear was the primary motion coupled with flexion (Appendix A), and was a significant mode of loading seen during the frontal

impact simulation. Furthermore, the anterior shear stiffness of the C23 and C34 segments at large shear loads were the most flexible in the entire cervical spine (Figure 7-21).

Another aspect to consider in future studies for better representing the initial conditions of the cervical spine model. The initial state of the head and neck model was such that no tissue preload was present at the beginning of the simulation. This was done to maintain a neutral position of the cervical spine prior to the impact simulation. This, of course, is not the case in a living person. It is estimated that compressive forces of approximately 100 N to 300 N can exist on the cervical spine during physiological movement (Bernhardt et al., 1999; Ito et al., 2005). Moreover, the response of the cervical spine has been shown to increase in stiffness under the influence of preload (Shea et al., 1991). A preload would likely decrease the amount of delay seen in the model head and neck response.

To achieve physiological preloading, the cervical spine model must reach an equilibrium state under gravitational load, which would require an initial muscle activation scheme to keep the head in a neutral position. Because the cervical spine, with all its musculature, is such a complex structure, achieving this goal would be very difficult and require an in-depth study and analysis. Furthermore, it is realistic to assume that cervical spine muscles are not at their rest length in the neutral head position, and that some initial muscle stretch and passive load is present. This further complicates the process of achieving an initial equilibrium position for the cervical spine to use prior to the frontal impact simulation. The effect of gravity was shown be negligible on a multi-body model response (Van der Horst, 2002), but the initial stretch and activation of the muscles is expected to have a significant influence on the head and neck response.

Finally, active muscle properties have been shown to have a significant influence on the response of the cervical spine in frontal impact (Van der Horst, 2000; Deng and Fu, 2002; Brolin et al., 2005). The activation scheme and Hill-type muscle model parameters chosen for the cervical spine model were based on average values for generalized muscle listed in the literature (refer to Table 6-15), since these specific cervical spine muscle properties have yet to be identified. Thus, current choice of muscle model parameters may not accurately reflect those of cervical spine muscles. Additionally, the muscle activation response of the human volunteers during the 15 G frontal impact experiment was never recorded, so the current muscle activation scheme may not reflect the actual subject response.

8.5 Active Muscle Study

As mentioned in the previous section, active muscles have a strong effect on the response of the cervical spine during frontal impact (Deng and Fu, 2002; Van der Horst, 2002; Brolin et al., 2005). The current muscle implementation for the cervical spine model is based on average Hill-type model parameter values determined from ranges proposed by Winters (Winters and Stark, 1988; Winters and Woo, 1990; Winters, 1995). However, due to lack of complete material data, the accuracy of these Hill-type muscle model parameters as it pertains to cervical spine muscles is unknown.

A preliminary study was conducted on the influence of the active muscle properties on the response of the cervical spine during 15 G frontal impact. The study focused on identifying the significant changes to the response of the model based on changes to the muscle parameters proposed by Winters to determine if legitimate changes to the muscle model can result in improved biofidelity of the full cervical spine model.

Four different studies were undertaken looking at various properties of muscle, and compared to the baseline model that was simulated and discussed in Section 8.3. The first muscle study looked at the difference in response between active and purely passive muscles. The active (baseline) model used the activation scheme shown in Figure 8-6, whereas the passive model set $A(t) = 0$ to mimic the response of a post-mortem human subject.

The second study looked at varying the maximum muscle stress that was used to calculate the maximum muscle force. Winters and Stark (1988) reported a maximum muscle stress range between 0.20 MPa and 1.00 MPa, and a value of 0.50 MPa was chosen for the baseline model. The baseline model was compared to a low-end model using 0.20 MPa and a high-end model using 1.00 MPa to calculate the muscle force.

The third study looked at the change in cervical spine response depending on the initial activation time of the muscles. In the baseline model, the muscles were activated at $t = 74$ ms, which was determined by Siegmund et al (2003). The low-end model muscles were activated 10 ms earlier than the baseline model (at $t = 64$ ms), and the high-end model muscles were activated 10 ms later (at $t = 84$ ms). This range is typical for occupants in impact, and signifies the variability of the occupant's awareness to the oncoming impact (Siegmund et al., 2003). Activation was held for 100 ms from the initial activation time for all cases.

Finally, the last study looked at the composition of the cervical spine muscles in terms of slow and fast muscle fibres. Slow-twitch muscle fibres are predominately used for endurance-related activities, while fast-twitch muscle fibres are for proving short bursts of strength. A few studies into the fibre composition of the major cervical spine muscles indicate that large muscles such as the longus colli, sternocleidomastoid, and trapezius, contain an even number of slow and fast-twitch muscle fibres (Uhlig et al., 1995). Muscles that are predominately used for stability, such as the multifidius, contain mainly slow-twitch muscle fibres (Boyd-Clark et al., 2001). The muscle type study will look at the effect of varying the composition of the muscles between all slow-twitch fibres, to all fast-twitch fibres.

The low-end model represented muscles comprised solely of slow muscle fibre, and the high-end model represented muscles of fast muscle fibres. The type of muscle fibre had an effect on the force-velocity relationship on the muscle, as well as an effect on the muscle activation scheme due to the variation in activation time-constants. The effected model parameters included v_{max}, CE_{sh}, τ_{ne}, τ_{ac}, and τ_{dc}, which are all described in Section 6.3.7.

The muscle model properties for each test case can be seen in **Error! Reference source not found.**. The results of each test case are presented in the following sections.

Table 8-2: Active Muscle Study Test Setup

Study Type	Active vs. Passive	Maximum Muscle Force	Activation Time	Muscle Type (Slow vs Fast)
Low-End	A(t) = 0	σ_{max} = 0.20 MPa	64 ms	v_{max} = 2/s, CE_{sh} = 0.1, τ_{ne} = 50 ms, τ_{ac} = 20 ms, τ_{dc} = 50 ms
Baseline	A(t) = *function*	σ_{max} = 0.50 MPa	74 ms	v_{max} = 5/s, CE_{sh} = 0.55, τ_{ne} = 35 ms, τ_{ac} = 15 ms, τ_{dc} = 40 ms
High-End	-	σ_{max} = 1.00 MPa	84 ms	v_{max} = 8/s, CE_{sh} = 1.0, τ_{ne} = 20 ms, τ_{ac} = 5 ms, τ_{dc} = 30 ms

8.5.1 Active vs. Passive Muscle Response

The results of the active vs. passive muscle study can be seen in Figure 8-14 and Figure 8-15. It was clear that the response of the full cervical spine model without activated musculature deviated significantly from the experimental response. The response of the passive model was also more violent compared to the response of the active model. This result reinforces the notion that active musculature plays a considerable role in the motion of the head during frontal impact, as well as reducing the risk of head or neck injury to the occupant.
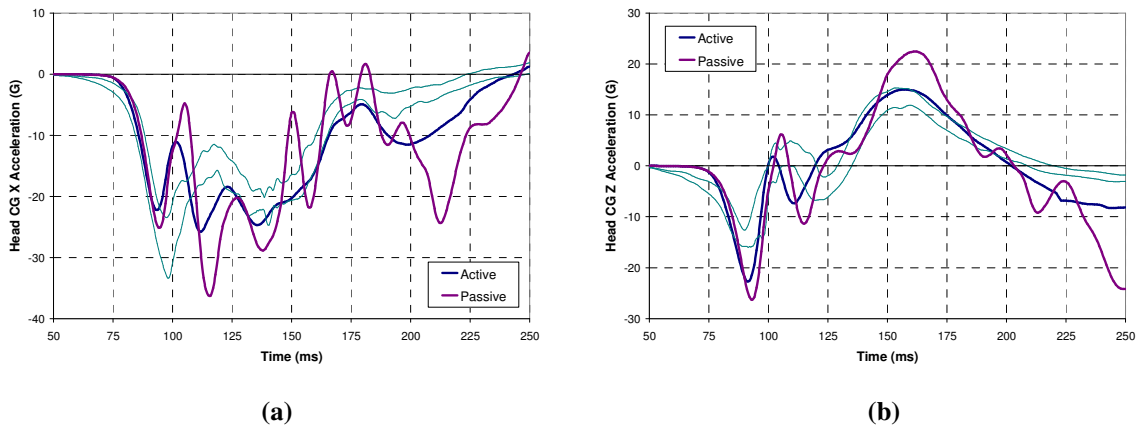
(a)   **(b)**

Figure 8-14: Active vs. Passive Muscle Study in (a) Horizontal and (b) Vertical Acceleration
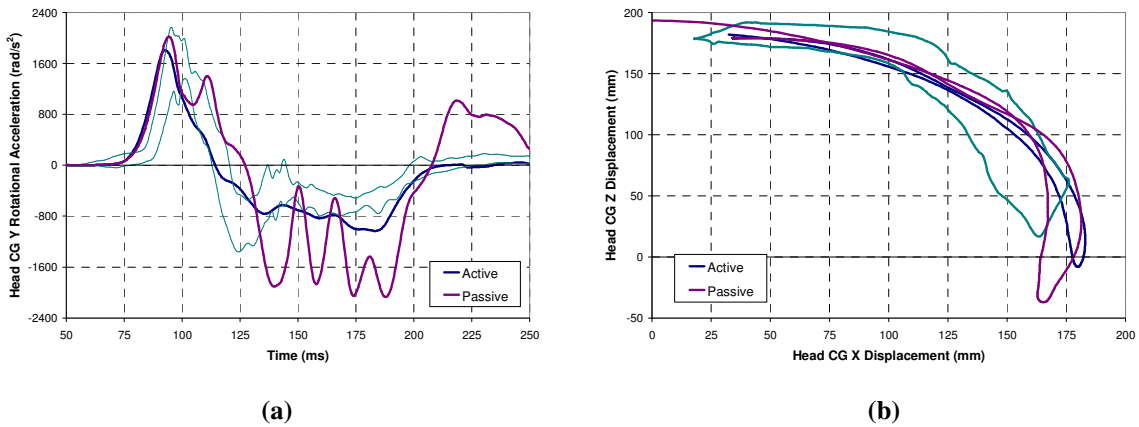

(a)   **(b)**

Figure 8-15: Active vs. Passive Muscle Study in (a) Rotational Acceleration and (b) Trajectory

The results of this study indicate that activate muscle properties must be included if simulating human volunteer in frontal impact for the 15 G impact case. It should also be noted that the response of the passive model displays a significant amount of oscillation that has been discussed in Section 8.4. This suggests that the active muscles in the cervical spine model dampen out the natural frequency of the spine, and implies that much of the unwanted model oscillation stems from the intervertebral discs.

8.5.2 Maximum Muscle Force Study

The results of the maximum muscle force study can be seen in Figure 8-16 and Figure 8-17. For the most part, the change in maximum muscle force did not drastically affect the response of the head and neck during the impact. However, there were noticeable reductions in peak acceleration with

increasing maximum muscle force. This would indicate that stronger neck muscles would result in less head or neck acceleration during impact, suggesting lower probability of injury.

Nevertheless, the most biofidelic response of all three test cases appeared to be the baseline case with a σ_{max} of 0.50 MPa. However, based on the experimental results, it is likely that an optimal σ_{max} would exist somewhere between 0.50 MPa and 1.00 MPa. Modifying the maximum muscle stress to values below 0.5 MPa would result in a response that was far too lax, as seen in Figure 8-17b.

(a)   (b)
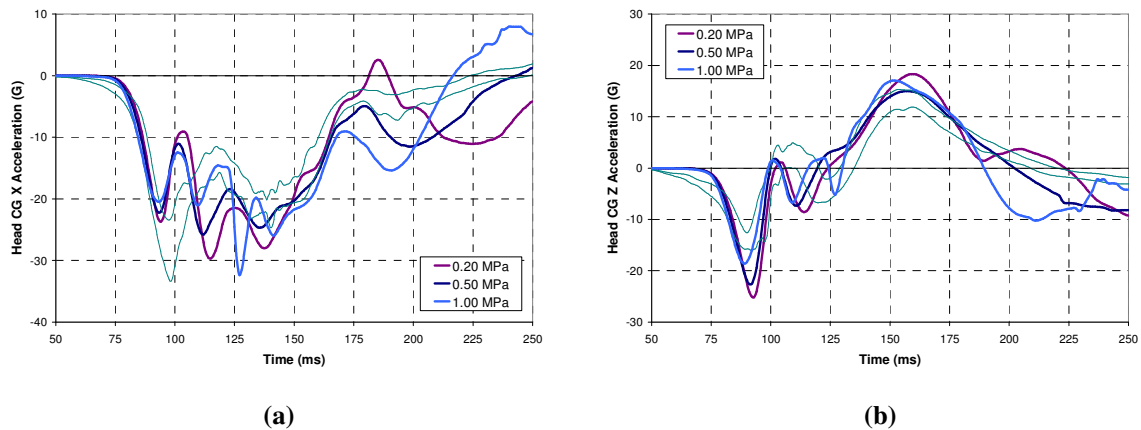
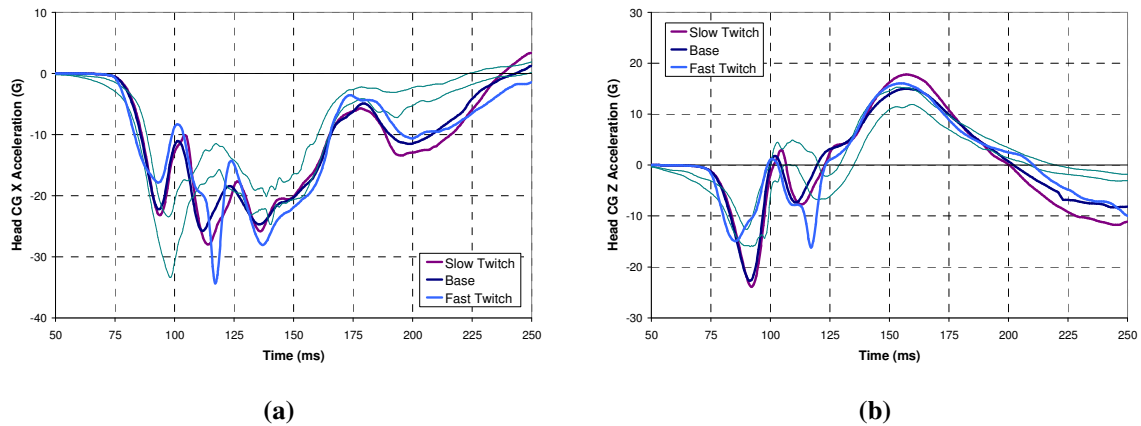**Figure 8-16: Maximum Muscle Force Study in (a) Horizontal and (b) Vertical Acceleration**

(a)   (b)
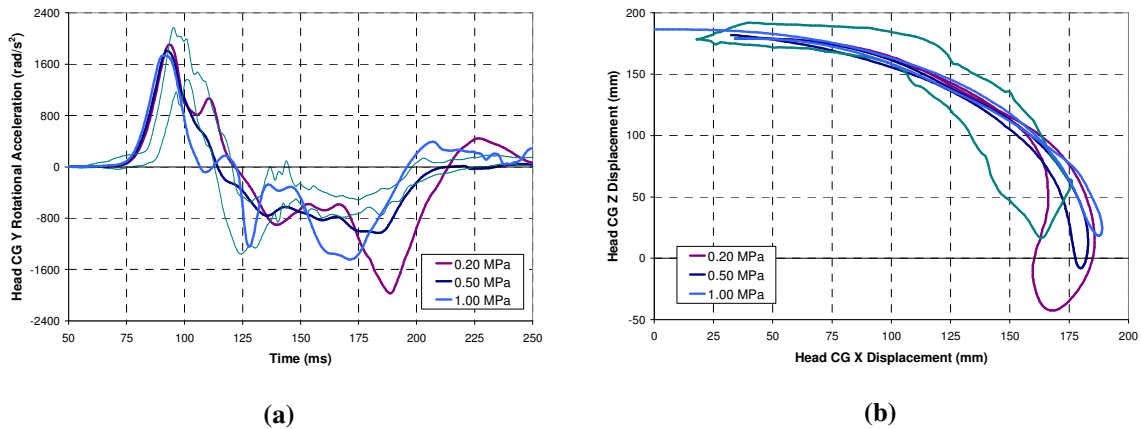
Figure 8-17: Maximum Muscle Force Study in (a) Rotational Acceleration and (b) Trajectory

8.5.3 Activation Time Study

The results of the activation time study can be seen in Figure 8-18 and Figure 8-19. There was very little difference between the responses of all three tests cases, particularly in head trajectory. For the 10 ms early response case, the erroneous time delay between the experimental data and the simulation

was reduced, which caused the peak vertical head acceleration (Figure 8-18b) also reduce to experimental levels. However, the early response case in head rotational acceleration (Figure 8-19a) was worse than either the baseline case, or the delayed response case. There was little difference in acceleration delay between the baseline and the 10 ms delayed response case.

The general trend found in this study was that peak accelerations were reduced with earlier muscle response. This would indicate that a person with quicker reflexes, or who was more aware of the oncoming impact, would have a reduced chance of head or neck injury.

| (a) | (b) |
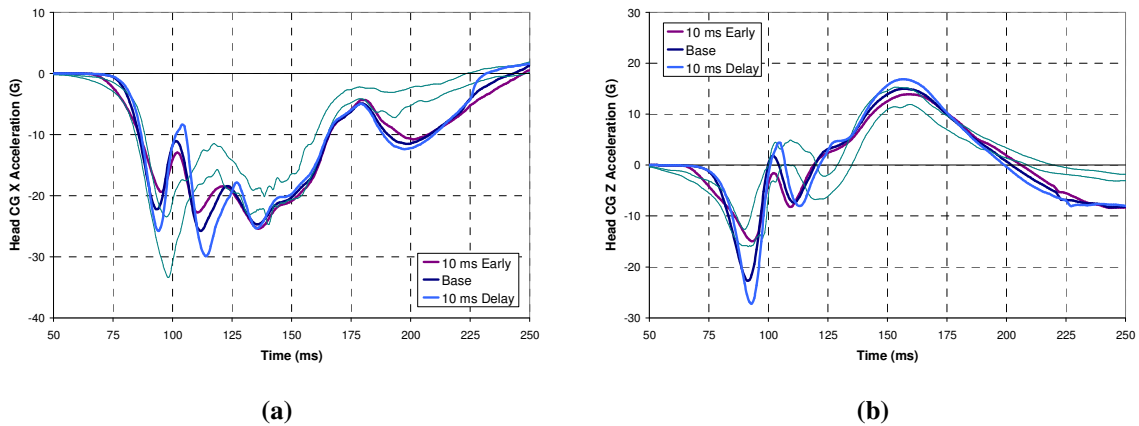
Figure 8-18: Activation Time Study in (a) Horizontal and (b) Vertical Acceleration

| (a) | (b) |
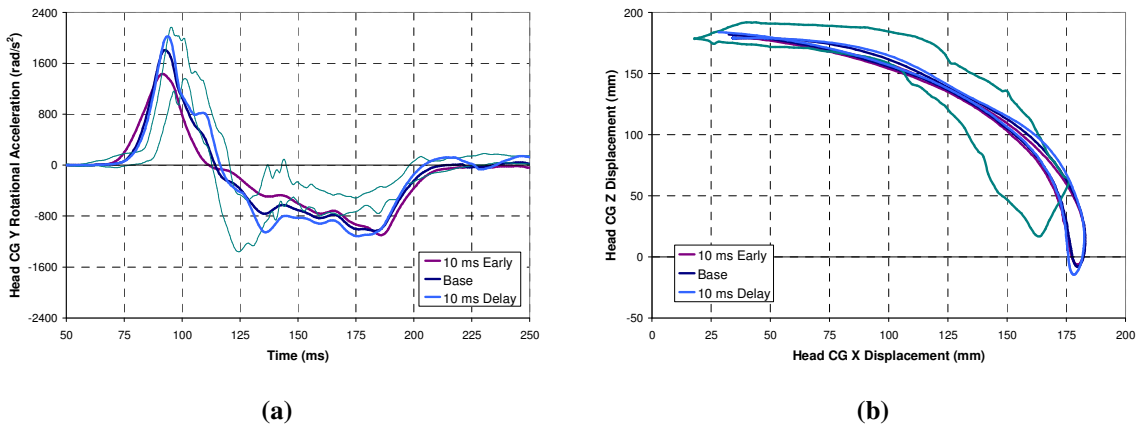
Figure 8-19: Activation Time Study in (a) Rotational Acceleration and (b) Trajectory

It was concluded, from the results of this study, that a muscle activation time of 74 ms was representative of the human volunteers, and that the delay in the head acceleration was caused by factors other than the onset of muscle activation.

8.5.4 Muscle Type Study

The results of the muscle type study can be seen in Figure 8-20 and Figure 8-21. There was not a significant difference between the responses of the baseline model and of the slow muscle fibre model. However, it was evident that the fast muscle model response differed in the initial 125 ms from the other two test cases. The primary reason for this difference was due to the change in muscle activation between the models, rather than change in force-velocity relationship. The fast muscle model was able to reach activation quicker than the other models, resulting in decreased peak loading.

(a)   (b)

Figure 8-20: Muscle Type Study in (a) Horizontal and (b) Vertical Acceleration

(a)   (b)
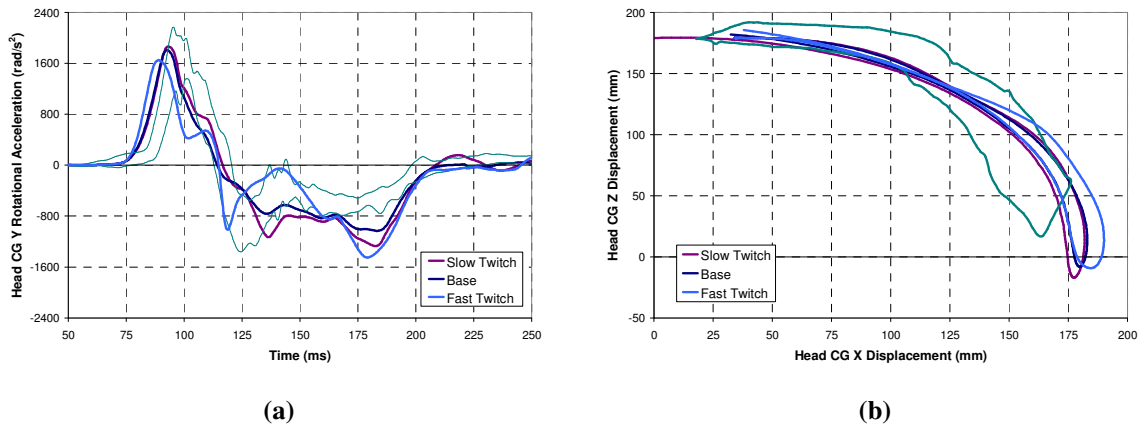
Figure 8-21: Muscle Type Study in (a) Rotational Acceleration and (b) Trajectory

Based on the results of the muscle type study, it is reasonable to assume that the baseline muscle model using model parameters for an even composition of slow and fast twitch muscle fibres is representative of cervical spine muscles.

Chapter 9

Conclusions

Cervical spine injuries caused by motor vehicle accidents continue to be a costly burden on society. Automotive manufacturers are continuously trying to reduce occupant risk of injury in crash through the innovation of novel protection techniques. To design better safety devices, a comprehensive understanding of the response of the human body from impact loading is essential. Numerical models of the human body are an emerging technology that is increasingly being employed to simulate and analyze the human body in crash. Human body simulation is a highly effective method that will be a main tool for injury and injury protection research in the many years to come.

The purpose of this research was to develop a cervical spine model that would produce realistic response in frontal impact loading. The model was developed with a focus on accurate representation of the cervical spine at the local tissue level. Material models were developed based on fundamental experimental studies. These tissues were assembled to create a single segment model that was validated using a wide variety of experimental data. Finally, the single segment models were assembled to create a full cervical spine model that was validated in frontal impact.

The single segment models were constructed from the basic building blocks of the cervical spine: the intervertebral disc (annulus fibrosus and nucleus pulposus), the vertebrae, the ligaments, and the facet joints. Each model (including the upper cervical spine model) was validated in all modes of loading, and at different levels of load when possible. This allowed for the assessment of the cervical spine model at each isolated level. The results of the validation indicate that the cervical spine segments performed very well in flexion, compression, and tension. Segment response to lateral bending and axial rotation was also good, but the validation case was limited to small loads. The models response in extension often proved too compliant compared to the experimental data. Furthermore, the single segment models did not fully agree with the experimental shear response, again being more flexible.

It was hypothesized that much of the disparity between the model response and the experimental data in extension was the result of initial positioning of the vertebrae in the segment models differing from

the experimental tests. This caused the gap between the facet joint surfaces to be too large, which reduced the effectiveness of the facet joints to provide stiffness in extension. Furthermore, the large facet gap was also assumed to have an impact on the response from lateral bending, axial rotation, and anterior shear. In the case of anterior shear, all segment models were more complaint than the average stiffness values reported in the literature.

An initial studying into vertebral body trauma prediction was done using the segment models in pure compression. The results showed that damage initiated in the cancellous bone of the vertebral body between 500 N and 1000 N. Damage continued in the cancellous bone, until the bony endplates began to accumulate damage around 1400 N and 1800 N for the middle and lower cervical spine respectively. Damage to the cortical bone occurred soon after the onset of endplate damage. The results were in reasonable agreement with published studies.

The full cervical spine model was assembled from the single segment models using rigid vertebrae rather than deformable vertebrae. The model was validated using the 15 G frontal impact sled test data from the National Biodynamics Laboratory. Active muscles were used to simulate the response of the human volunteers used in the study. The model response was in reasonable agreement with the experimental data, and compared better than previous finite element cervical spine models. However, the model did exhibit significant oscillation during the most severe loading that caused a deviation from the experimental response. The head trajectory agreed well with the experimental data, suggesting that trajectory should not be the lone measure used for model validation purposes.

A complementary study involving the active muscle properties was undertaken to identify areas were the model response could be improved. It was shown that active muscles are required for biofidelic response of the head and neck, and that minor changes to the activation scheme can change the model response during peak loading. It was also shown that the Hill-type muscle model parameters initially selected for the model provided good muscle response.

In conclusion, the developed cervical spine model is representative of the human cervical spine, for both quasi-static loading and dynamic frontal loading. This is a particularly significant achievement since the model was developed from the fundamental tissue properties, and not calibrated or modified to reach a better agreement with the experimental data. Furthermore, it appears that the model is well suited for additional enhancement in the future.

Chapter 10

Recommendations

Notwithstanding the positive results from the cervical spine simulations, there are aspects of the model that can be improved upon with further research and development. The recommendations discussed in this chapter are based on the experience of developing the numerical model for both quasi-static and dynamic loading, and the knowledge gained through rigorous study of the previous literature involving the mechanics of the cervical spine. Furthermore, a number of recommendations are made that focus on enhancing the capabilities of the model for the future goal of predicting injury to the spine at the tissue level.

10.1 Improved Material Properties

One of the most important aspects of the cervical spine model was the use of local tissue data to define the mechanical properties of most materials. Using the mechanical test data from various independent studies, the cervical spine model was able to represent the load-displacement response of the quasi-static *in vitro* model very well. However, it was recognized that some of the experimental data used to define the material properties in the model was not ideal.

A significant amount of tissue testing is done at low levels of loading deemed to be non-injurious, with the intention of analyzing the physiological response of the tissue. However, in many cases, the response of the tissue in the numerical model exceeded the level of loading at which the material model was based, and this is expected to be the case in impact scenarios. While all material models were verified that no unusual responses occurred at deformations outside of the experimental range, there was no guarantee that the response outside this range was accurate. This argument also applies to the use of viscoelastic material properties in the dull cervical spine model for dynamic loading.

For instance, most viscoelastic characterization for biological material is reported using relaxation or creep techniques. While this type test data is suitable for long duration loading, this regime of strain-rates is much lower than rates typically seen in impact events such as automotive crash. Using

relaxation test data to predict impact response is an extrapolation of sorts, and may produce erroneous results.

Utilizing the mechanical properties of tissue tested in the appropriate regimes of loading and environments would certainly improve the accuracy of the model. It is recommended that future cervical tissue research be reviewed on a periodic basis for studies that involve the types of loading suitable for numerical modelling. It is also recommended, if feasible, that in-house testing of cervical spine tissues be studied. This would allow for first-hand insight into the mechanics of the tissue (for the purposes of developing better tissue models) and allow for the control of test procedures and analysis of specific mechanical properties important for numerical analysis.

10.2 Appropriate Material Constitutive Models

The mechanics of biological tissue are often complicated, since most tissue is heterogeneous, nonlinear, orthogonal, viscoelastic, and susceptible to damage. This type of behaviour is not accurately represented by the classical theories of continuum mechanics. Furthermore, these material responses are generally under-represented in finite element codes such as LS-DYNA, which tend to focus on material models for metals, foams, composites, and concretes. In order to advance the accuracy and capabilities of the cervical spine model, numerical representation of the complex responses of the local tissue is essential.

For instance, the current bone material model utilizes a simple isotropic power-law material model commonly used for modelling plastic deformation in metals. In real life, vertebral cancellous bone is moderately orthotropic, and behaves similar to a ceramic when overloaded and damaged. There are also viscoelastic effects associated with bone stemming from the presence of marrow in cancellous bone, and the presence of a collagen matrix in cortical bone. Since most of the traumatic injuries associated with the cervical spine involve fracture to the vertebra, accurate modelling the bone material is desired for realistic injury response.

It is recommended for the future enhancement of the cervical spine model, that better representative material models be developed in LS-DYNA that incorporate the appropriate material characteristics of each particular tissue. Investigation into alternative material models already incorporated into LS-DYNA is also recommended. In particular, models should include nonlinearity, viscoelasticity (based on relaxation functions and/or strain-rate data), and damage (as a representation of injury).

10.3 Model Detail and Construction

The use of nonlinear discrete elements to characterize the ligaments was a practical and robust choice of material and element type, given the type of mechanical data available. However, shell elements were the initial formulation choice for the ligaments in the cervical spine model. It was assumed that shell elements would provide more realistic representation of ligament under general loading than discrete elements would. However, it was found that the shell elements were numerical unstable for large tensile deformations. This was most apparent for the capsular ligaments, which often loaded in biaxial tension due to their cylinder-like geometry. This instability was neither mesh nor material model-dependant, and was likely caused by the low shear strength of the ligament material since increasing this value improved the model stability. Nonetheless, it is believed that a functional shell-based ligament model is the best representation for the future of cervical spine model, and it is recommended that efforts be made to rectify this problem.

The lack of the original cervical spine geometry (from CT scans or other imaging techniques) was a significant disadvantage for developing the model. The initial intention of the cervical spine project was to develop and enhance a model that was representative of a 50th percentile male. However, it was later revealed that the original model (Deng et al., 1999) was smaller than the desired size. Efforts were made to scale the original model to the correct size, and reposition the vertebrae such that the most significant components of the spine (primarily the intervertebral discs) would have dimensions similar to those reported for the 50th percentile male. By adjusting the vertebrae to get proper disc dimensioning, it is likely that the facet gaps were enlarged to a point that was not typical of a spine in a neutral position. It would have been more appropriate to build the model around the geometry of a cervical spine scanned from a person representative of a 50th percentile male rather than adjust the geometry of a spine that was not to size.

Finally, it was thought that omitting the non-structural soft tissues of the neck would not affect the response of the cervical spine in dynamic loading. However, after running the frontal impact simulations, it was found that the cervical spine oscillated at a higher frequency than did the human volunteers. The high frequency in the model of the model response may have been caused by a lack of structural damping due to the current characterization of soft tissue viscoelasticity, but it was hypothesized that a source of neck damping would be found in the viscoelastic effects of the non-structural soft tissues. It is recommended that a preliminary study into effects on the dynamic

response of the cervical spine due to the presence of these soft tissues be done prior to any major modelling. The addition of these tissues to the current model would be a significant undertaking, since proper interaction between all of these tissues with the cervical spine would be required.

10.4 Physiological Response of Muscles

The study involving the active muscle properties indicated the response of the cervical spine in dynamic loading was largely influenced by the activation of the musculature. It is evident from the results that the response of the model can be greatly improved through the optimization of the activation muscle behaviour. While 'optimization' is a term often used interchangeably with 'calibration', finding a realistic solution to the muscle activation would be valid process since it would generate the correct loading seen in the local cervical spine tissues due to the frontal impact.

A number of aspects should be considered when improving the physiological response of the muscles. Currently the muscle activates at 100% neural excitation at 74 ms, and deactivates to 0% neural excitation at 174 ms. Furthermore, both the flexors and the extensors are activated together. A reasonable approach to identify the optimal muscle activation scheme would be to vary the activation and deactivation times, activate the flexors and extensors separately, and vary the level of neural excitation.

It is also recommended that an initial muscle activation scheme be developed such that the position of the head and neck is maintained under gravitational loading. This would provide the proper initial loading on the soft tissues prior to the impact simulation.

Due to the length of time required to run the full cervical spine model, it is suggested that a multi-body model calibrated to the full cervical spine model be used to develop an optimal muscle activation scheme. This would significantly reduce the amount of time required to run the study.

10.5 Future Direction of the Cervical Spine Model

In the immediate future, the cervical spine model should be used to evaluate the response in loading conditions other than frontal impact. Human volunteer data exists for lateral, rear, and oblique impact loading, which can be simulated using the cervical spine model by applying the accelerations to the T1 vertebra in the corresponding direction of motion. Muscle activation schemes would have to be

changed to correspond with human response in a different direction. This may be particularly difficult for lateral and oblique loading, since the combination of muscles used to react to the applied motion is not as clearly defined. Nevertheless, this is an important step in the progress of the cervical spine model, as it has the potential to validate the model in nearly all forms of loading seen in automotive crash.

A long-term goal of the cervical spine model would be the development of a injury predicting model for both quasi-static and dynamic loading conditions. This would have major application in such fields as automobile safety, personal protective equipment, and sports injury.

To reach this goal, a serious push in the research of the injury mechanisms of local spine tissues is required. The development of advanced numerical material models would also be required to effectively simulate injury of a tissue (see Section 10.2). It should be the effort of future work on the model to progress towards this end goal.

References

Acaroglu, E.R., Iatridis, J.C., Setton, L.A., Foster, R.J., Mow, V.C., and Weidenbaum, M., 1995. Degeneration and Aging Affect the Tensile Behavior of Human Lumbar Anulus Fibrosus. *Spine* 20(24), 2690 – 2701.

Adams, M.A., and Green, T.P., 1993. Tensile Properties of the Annulus Fibrosus: I. The Contribution of Fibre-Matrix Interactions to Tensile Stiffness and Strength. *European Spine Journal* 2, 203 - 208.

Agur, A.M.R., and Dalley, A.F., 2005. *Grant's Atlas of Anatomy* 11th Ed. Lippincott Williams and Wilkins, Philadelphia.

Alem, N.M., Nusholtz, G.S., and Melvin, J.W., 1984. Head and Neck Response to Axial Impacts. *Proceedings from the 28th Stapp Car Crash Conference*, 275 – 288. SAE 8416675.

Ateshian, G.A., Warden, W.H., Kim, J.J., Grelsamer, R.P., and Mow, V.C., 1997. Finite Deformation Biphasic Material Properties of Bovine Articular Cartilage from Confined Compression Experiments. *Journal of Biomechanics* 30(11), 1157 – 1164.

Argenson, C., de Peretti, F., Ghabris, A., Eude, P., Lovet, J., and Hovorka, I., 2002. Classification of Lower Cervical Spine Injuries. *European Journal of Orthopaedic Surgery and Traumatology* 7(4), 215 – 229.

Bass, E.C., Ashford, F.A., Segal, M.R., and Lotz, J.C., 2004. Biaxial Testing of Human Annulus Fibrosus and its Implications for a constitutive Formulation. *Annals of Biomedical Engineering* 32(9), 1231 – 1242.

Belytschko, T., Kulak, R.F., and Schutlz, A.B., 1974. Finite Element Stress Analysis of an Intervertebral Disc. *Journal of Biomechanics* 7, 277 – 285.

Bernhardt, P., Wilke, H.J., Wenger, K.H., Jungkunz, B., Bohm, A., and Claes, L.E., 1999. Multiple Muscle Force Simulation in Axial Rotation of the Cervical Spine. *Clinical Biomechanics* 14(1), 32 – 40.

Best, B.A., Guilak, F., Setton, L.A., Zhu, W., Saed-Nejad, F., Ratcliffe, A., Weidenbaum, M., and Mow, V.C., 1994. Compressive Mechanical Properties of the Human Annulus Fibrosus and Their Relationship to Biochemical Composition. *Spine* 19(2), 212 – 221.

Bogduk, N., and Mercer, S., 2000. Biomechanics of the Cervical Spine I: Normal Kinematics. *Clinical Biomechanics* 15, 633 – 648.

Bostrom, O., Svensson, M.Y., and Aldman, B., 1996. A New Neck Injury Criterion Candidate – Based on Injury Findings in the Cervical Spine Ganglia After Experimental Neck Extension Trauma. *Proceedings of the International IRCOBI Conference on the Biomechanics of Injury*, 123 – 136.

Bowman, S.M., Keaveny, T.M., Gibson, L.J., Hayes, W.C., and McMahon, T.A., 1994. Compressive Creep Behavior of Bovine Trabecular Bone. *Journal of Biomechanics* 27(3), 301 – 310.

Boyd-Clark, L.C., Briggs, C.A., and Galea, M.P., 2001. Comparative Histochemical Composition of Muscle Fibres in a Pre- and a Postvertebral Muscle of the Cervical Spine. *Journal of Anatomy* 199, 709 – 716.

Bozic, K.J., Keyak, J.H., Skinner, H.B., Bueff, H.U., and Bradford, D.S., 1994. Three-Dimensional Finite Element Modeling of a Cervical Vertebra: An Investigation of Burst Fracture Mechanism. *Journal of Spinal Disorders* 7(2), 102 – 110.

Brinkmann, P., and Horst, M., 1985. The Influence of Vertebral Body Fracture, Intradiscal Injection, and Partial Discectomy on the Radial Bulge and Height of Human Lumbar Discs. *Spine* 10(2), 138.

Brolin, K., and Halldin, P., 2004. Development of a Finite Element Model of the Upper Cervical Spine and a Parameter Study of Ligament Characteristics. *Spine* 29(4), 376 – 385.

Brolin, K., Halldin, P., and Leijonhufvud, I., 2005. The Effect of Muscle Activation on Neck Response. *Traffic Injury Prevention* 6, 67 – 76.

Bursac, P.M., Obitz, T.W., Eisenberg, S.R., and Stamenovic, D., 1999. Confined and Unconfined Stress Relaxation of Cartilage: Appropriateness of a Transversely Isotropic Analysis. *Journal of Biomechanics* 32, 1125 – 1130.

Caler, W.E., and Carter, D.R., 1989. Bone Creep-Fatigue Damage Accumulation. *Journal of Biomechanics* 22, 625 – 635.

Camacho, D.L.A., Nightingale, R.W., Robinette, J.J., Vanguri, S.K., Coates, D.J., and Myers, B.S., 1997. Experimental Flexibility Measurements for the Development of a Computational Head-Neck Model Validated for Near-Vertex Head Impact. *Proceedings from the 41st Stapp Car Crash Conference*, 473 – 486. SAE 973345.

Camacho, D.L.A., Nightingale, R.W., and Myers, B.S., 1999. Surface Friction in Near-Vertex Head and Neck Impact Increases Risk of Injury. *Journal of Biomechanics* 32, 293 – 301.

Carter, D.R., and Hayes, W.C., 1977. The Compressive Behavior of Bone as a Two-Phase Porous Structure. *Journal of Bone and Joint Surgery* 59A, 954 – 962.

Carter, J.W., 2002. *Compressive Cervical Spine Injury: The Effect of Injury Mechanisms on Structural Injury Pattern and Neurologic Injury Potential*. PhD Thesis. University of Washington.

Cassidy, J.J., Hiltner, A., and Baer, E., 1989. Hierarchical Structure of the Intervertebral Disc. *Connective Tissue Research* 23(1), 75 – 88.

Chancey, V.C., Nightingale, R.W., Van Ee, C.A., Knaub, K.E., and Myers, B.S., 2003. Improved Estimation of Human Neck Tensile Tolerance: Reducing the Range of Reported Tolerance Using Anthropometrically Correct Muscles and Optimized Physiologic Initial Conditions. *Proceedings from the 47th Stapp Car Crash Conference*, 135 – 153. SAE 2003-22-0008.

Chang, H., Gilbertson, L.G., Goel, V.K., Winterbottom, J.M., Clark, C.R., and Patwardhan, A., 1992. Dynamic Response of the Occipito-Atlanto-Axial (C0-C1-C2) Complex in Right Axial Rotation. *Journal of Orthopaedic Research* 10(3), 446 – 453.

Chazel, J., Tanguy, A., Bourges, M., Gaurel, G., Escande, G., Guillot, M., and Vanneuville, G., 1985. Biomechanical Properties of Spinal Ligaments and a Histological Study of the Supraspinal Ligament in Traction. *Journal of Biomechanics* 18(3), 167 – 176.

Cheng, R., Yang, K.H., Levine, R.S., King, A.I., and Morgan, R., 1982. Injuries to the Cervical Spine Caused by a Distributed Frontal Load to the Chest. *Proceedings from the 36th Stapp Car Crash Conference*, 1 – 39. SAE 821155.

Clausen, J.D., Goel, V.K., Traynelis, V.C., and Scifert, J., 1997. Unicinate Process and Luschka Joints Influence the Biomechanics of the Cervical Spine: Quantification Using a Finite Element Model of the C5-C6 Segment. *Journal of Orthopaedic Research* 15, 342 – 347.

Clemens, H.J., and Burow, K., 1972. Experimental Investigation on Injury Mechanisms of Cervical Spine at Frontal and Rear-Front Vehicle Impacts. *Proceedings from the 26th Stapp Car Crash Conference*, 76 – 104. SAE 720960.

Cody, D.D., Goldstein, S.A., Flynn, M.J., and Brown, E.B., 1991. Correlations Between Vertebral Regional Bone Mineral Density and Whole Bone Fracture Load. *Spine* 16(2), 146 – 154.

Cowin, S.C., 2001. *Bone Mechanics Handbook* 2nd Ed. CRC Press LLC., Boca Raton, Florida.

Cripton, P.A., Dumas, G.A., and Nolte, L.P., 2001. A Minimally Invasive Technique for Measuring Intervertebral Disc Pressure In Vitro: Application to the Cervical Spine. *Journal of Biomechanics* 34, 545 – 549.

Cross, N., 2003. The Ligamentum Nuchae. *Massage Today* 3.

Currey, J.D., 2004. Tensile Yield in Compact Bone is Determined by Strain, Post-Yield Behaviour by Mineral Content. *Journal of Biomechanics* 37, 549 – 556.

Daffner, R.H., Sciulli, R.L., Rodriguez, A., and Protech, J., 2006. Imaging for Evaluation of Suspected Cervical Spine Trauma: A 2-Year Analysis. *Injury, International Journal of the Care of the Injured*, In Press.

Davis, J., Kaufman, K.R., and Lieber, R.L., 2003. Correlation between Active and Passive Isometric Force and Intramuscular Pressure in the Isolated Rabbit Tibialis Anterior Muscle. *Journal of Biomechanics* 36, 505 – 512.

Dauvilliers, F., Bendjellal, F., Weiss, M., Lavaste, F., and Tarriere, C., 1994. Development of a Finite Element Model of the Neck. *Proceedings from the 38th Stapp Car Crash Conference*, 77 – 91. SAE 942210.

De Jager, M., Suren, A., Thunnissen, J., and Wismans, J., 1994. A Three-Dimensional Head-Neck Model: Validation for Frontal and Lateral Impacts. *Proceedings from the 38th Stapp Car Crash Conference*, 93 – 109. SAE 942211.

De Jager, M., Suren, A., Thunnissen, J., and Wismans, J., 1996. A Global and a Detailed Mathematical Model for Head-Neck Dynamics. *Proceedings from the 40th Stapp Car Crash Conference*, 93 – 109. SAE 962430.

Denoziere, G., and Ku, D.N., 2006. Biomechanical Comparison Between Fusion of Two Vertebrae and Implantation of an Artificial Intervertebral Disc. *Journal of Biomechanics* 39(4), 766 – 775.

Deng, B., Begeman, P.C., Yang, K.H., Tashman, S., and King, A.I., 2000. Kinematics of Human Cadaver Cervical Spine during Low Speed Rear-End Impacts. *Proceedings from the 44th Stapp Car Crash Conference*. SAE 2000-01-SC13.

Deng, Y.C., and Goldsmith, W., 1987. Response of a Human Head/Neck/Upper-Torso Replica to Dynamic Loading-II: Analytical/Numerical Model. *Journal of*

Deng, Y.C., Li, X., and Liu, Y., 1999. Modeling of the Human Cervical Spine Using Finite Element Techniques. *Proceedings from the 43rd Stapp Car Crash Conference*. SAE 1999-01-1310.

Deng, Y.C., and Fu, J., 2002. Simulation and Identification of the Neck Muscle Activities During Head and Neck Flexion Whiplash. *Proceedings from the 46th Stapp Car Crash Conference*. SAE 2002-01-0017.

DiSilvestro, M.R., and Suh, J.K.F., 2001. A Cross-Validation of the Biphasic Poroviscoelastic Model of Articular Cartilage in Unconfined Compression, Indentation, and Confined Compression. *Journal of Biomechanics* 34, 519 – 525.

Duncan, N.A., Bass, E.C., and Lotz, J.C., 1995a. A Fiber-Reinforced Multi-Shell Composite Finite Element Model of the Human Annulus Fibrosus. *Advances in Bioengineering* 31, 15 – 16.

Duncan, N.A., Bass, E.C., and Lotz, J.C., 1995b. The Nonlinear Load-Displacement Response of the Human Annulus Fibrosus in Axial Tension and Compression: Finite Element Predictions. *Advances in Bioengineering* 31, 17 – 18.

Duncan, N.A., Ashford, F.A., and Lotz, J.C., 1996. The Effect of Strain Rate on the Axial Stress-Strain Response of the Human Annulus Fibrosus in Tension and Compression: Experiment and Poroelastic Finite Element Predictions. *Advances in Bioengineering* 33, 402 – 402.

Dvorak, J., and Panjabi, M.M., 1987. Functional Anatomy of the Alar Ligaments. *Spine* 12, 183 – 189.

Dvorak, J., Hayek, J., and Zehnder, R., 1987. CT-Functional Diagnostics of the Rotatory Instability of the Upper Cervical Spine. *Spine* 12(8), 726 – 731.

Dvorak, J., Schneider, E., Saldinger, P., and Rahn, B., 1988. Biomechanics of the Craniocervical Region: The Alar and Transverse Ligaments. *Journal of Orthopaedic Research* 6, 452 – 461.

Ebara, S., Iatridis, J.C., Setton, L.A., Foster, R.J. Mow, V.C., and Weidenbaum, M., 1996. Tensile Properties of Nondegenerate Lumbar Annulus Fibrosus. *Spine* 21(4), 452 – 461.

Eberlein, R., Holzapfel, G.A., and Schulze-Bauer, C.A.J., 2001. An Anisotropic Model for Annulus Tissue and Enhanced Finite Element Analyses of Intact Lumbar Disc Bodies. *Computer Methods in Biomechanics and Biomedical Engineering* 4, 209 – 229.

Eberlein, R., Holzapfel, G.A., and Frohlich, M., 2004. Multi-Segment FEA of the Human Lumbar Spine Including the Heterogeneity of the Annulus Fibrosus. *Computational Mechanics* 34, 147 – 163.

Elliot, D.M., and Setton, L.A., 2000. A Linear Material Model for Fiber-Induced Anisotropy of the Anulus Fibrosus. *Journal of Biomechanical Engineering* 122, 173 – 179.

Elliot, D.M., and Setton, L.A., 2001. Anisotropic and Inhomogeneous Tensile Behavior of the Human Annulus Fibrosus: Experimental Measurement and Material Model Predictions. *Journal of Biomechanical Engineering* 123, 256 – 263.

Eppinger, R., Sun, E., Bandak, F., Haffner, M., Khaewpong, N., Maltese, M., Kuppa, S., Nguyen, T., Takhounts, E., Tannous, R., Zhang, A., and Saul, R., 1999. *Development of Improved Injury Criteria for the Assessment of Advanced Automotive Restraint Systems II*. National Highway Traffic Safety Administration, Docket No. 1999-6407-5.

Ewing, C.L., Thomas, D.J., Beeler, G.W., Patrick, L.M., and Gillis, D.B., 1968. Dynamic Response of the Head and Neck of the Living Human to –Gx Impact Acceleration. *Proceedings from the 12th Stapp Car Crash Conference* 424 – 439. SAE 680792.

Ewing, C.L., Thomas, D.J., Patrick, L.M., Beeler, G.W., and Smith, M.J., 1969. Living Human Dynamic Response to –Gx Impact Acceleration III – Accelerations Measured on the Head and Neck. *Proceedings from the 13th Stapp Car Crash Conference* 400 – 415. SAE 690817.

Ewing, C.L., and Thomas, D.J., 1973. Torque versus Angular Displacement Response fo Human Head to –Gx Impact Acceleration. *Proceedings from the 17th Stapp Car Crash Conference* 309 – 342. SAE 730976.

Ewing, C.L., Thomas, D.J., Lustick, L., Becker, E., Willems, G., and Muzzy, W.H., 1975. The Effect of the Initial Position of the Head and Neck on the Dynamic Response of the Human and Neck to –Gx Impact Acceleration. *Proceedings from the 19th Stapp Car Crash Conference* 487 – 512. SAE 751157.

Ewing, C.L., Thomas, D.J., Lustick, L., Muzzy, W.H., Willems, G., and Majewski, P.L., 1976. The Effect of Duration, Rate of Onset, and Peak Sled Acceleration on the Dynamic Response of the Human Head and Neck. *Proceedings from the 20th Stapp Car Crash Conference* 3 – 41. SAE 760800.

Ewing, C.L., Thomas, D.J., Lustick, L., Muzzy, W.H., Willems, G.C., and Majewski, P., 1977a. Dynamic Response of the Human Head and Neck to +Gy Impact Acceleration. *Proceedings from the 21st Stapp Car Crash Conference* 549 – 586. SAE 770928.

Ewing, C.L., Thomas, D.J., Majewski, P.L., Black, R., and Lustick, L., 1977b. Measurement of Head, T1, and Pelvic Response to –Gx Impact Acceleration. *Proceedings from the 21st Stapp Car Crash Conference* 509 – 545. SAE 770927.

Evans, F.G., and Lebow, M., 1957. Strength of Human Compact Bone Under Repetitive Loading. *Journal of Applied Physiology* 10, 127 – 130.

Feng, W.W., and Hallquist, J.O., 2003. On Constitutive Equations for Elastomers and Elastomeric Foams. *Proceedings from the 4th European LS-DYNA Users Conference* D-11, 15 – 28.

Fondrk, M., Bahniuk, E., Davy, D.T., and Michaels, C., 1988. Some Viscoplastic Characteristics of Bovine and Human Cortical Bone. *Journal of Biomechanics* 21(8), 623 – 630.

Francis, C.C., 1955. Variations in the Articular Facets of the Cervical Vertebrae. *Anatomical Record* 122, 589 – 602.

Fujita, Y., Duncan, N.A., and Lotz, J.C., 1997. Radial Tensile Properties of the Lumbar Annulus Fibrosus are Site and Degeneration Dependent. *Journal of Orthopaedic Research* 15, 814 – 819.

Fujita, Y., Wagner, D.R., Biviji, A.A., Duncan, N.A., and Lotz, J.C., 2000. Anisotropic Shear Behavior of the Annulus Fibrosus: Effect of Harvest Site and Tissue Prestrain. *Medical Engineering and Physics* 22, 349 – 357.

Fung, Y.C., 1993. *Biomechanics: Mechanical Properties of Living Tissue* 2nd Ed. Springer, New York, NY.

Galante, J.O., 1967. Tensile Properties of the Human Lumbar Annulus Fibrosus. *Acta Orthopaedica Scandinavica Supplement* 100, 1 – 89.

Gilad, I., and Nissan, M., 1986. A Study of Vertebra and Disc Geometric Relations of the Human Cervical and Lumbar Spine. *Spine* 11(2), 154 – 157.

Goel, V.K., Clark, C.R., McGowan, D., and Goyal, S., 1984. An In-Vitro Study of the Kinematics of the Normal, Injured and Stabilized Cervical Spine. *Journal of Biomechanics* 17(5), 363 – 376.

Goel, V.K., Clark, C.R., Gallaes, K., and Liu, Y.K., 1988a. Moment-Rotation Relationships of the Ligamentous Occipito-Atlanto-Axial Complex. *Journal of Biomechanics* 21, 673 – 680.

Goel, V.K., Clark, C.R., Harris, K.G., and Schulte, K.R., 1988b. Kinematics of the Cervical Spine: Effects of Multiple Total Laminectomy and Facet Wiring. *Journal of Orthopaedic Research* 6, 611 – 619.

Goel, V.K., and Kim, Y.E., 1989. Effects of Injury on the Spinal Motion Segment Mechanics in the Axial Compression Mode. *Clinical Biomechanics* 4, 161 – 167.

Goel, V.K., Monroe, B.T., Gilbertson, L.G., and Brinkmann, P., 1995. Interlaminar Shear Stresses and Laminae Separation in a Disc. *Spine* 20(6), 689 – 698.

Goel, V.K., and Clausen, J.D., 1998. Prediction of Load Sharing Among Spinal Components of a C5-C6 Motion Segment Using the Finite Element Approach. *Spine* 23(6), 684 – 691.

Gray, H., 1918. *Anatomy of the Human Body*. Lea & Febiger, Philadelphia; Bartleby.com, 2000.

Green, T.P., Adams, M.A., and Dolan, P. 1993. Tensile Properties of the Annulus Fibrosus: I. Ultimate Tensile Strength and Fatigue Life. *European Spine Journal* 2, 209 - 214.

Hakim, N.S., and King, A.I., 1979. A Three Dimensional Finite Element Dynamic Response Analysis of a Vertebra with Experimental Verification. *Journal of Biomechanics* 12, 277 – 292.

Halldin, P.H., Brolin, K., Kleiven, S., von Holst, H., Jakobsson, L., and Palmertz, C., 2000. Investigation of Conditions that Affect Neck Compression-Flexion Injuries Using Numerical Techniques. *Proceedings from the 44th Stapp Car Crash Conference*. SAE 2000-01-SC10.

Hallquist, J.O., 2003. *LS-DYNA Keyword Users Manual Version 970*. Livermore Software Technology Co., Livermore, CA.

Hansson, T.H., Keller, T.S., and Panjabi, M.M., 1987. A Study of the Compressive Properties of Lumbar Vertebral Trabeculae: Effects of Tissue Characteristics. *Spine* 12(1), 56 – 62.

Hawkins, D., and Bey, M., 1997. Muscle and Tendon Force-Length Properties and Their Interactions In Vivo. *Journal of Biomechanics* 30, 63 – 70.

Hayes, W.C., and Mockros, L.F., 1971. Viscoelastic Properties of Human Articular Cartilage. *Journal of Applied Physiology* 31, 562 – 568.

Hayes, W.C., and Bodine, A.J., 1978. Flow-Independent Viscoelastic Properties of Articular Cartilage Matrix. *Journal of Biomechanics* 11, 407 – 419.

Hill, R., 1978. Aspects of Invariance in Solid Mechanics. *Advances in Applied Mechanics* 18, 1 – 75.

Hochman, M., and Tuli, S., 2005. Cervical Spondylotic Myelopathy: A Review. *The Internet Journal of Neurology* 4(1).

Hodgson, V.R., and Thomas, L.M., 1980. Mechanisms of Cervical Spine Injury During Impact to the Protected Head. *Proceedings from the 24th Stapp Car Crash Conference*, 17 – 42. SAE 801300.

Holzapfel, G.A., Schulze-Bauer, C.A.J., Feigl, G., and Regitnig, P., 2005. Single Lamellar Mechanics of the Human Lumbar Annulus Fibrosus. *Biomechanics and Modeling in Mechanobiology* 3, 125 – 140.

Hori, R.Y., and Mockros, L.F., 1976. Indentation Tests of Human Articular Cartilage. *Journal of Biomechanics* 9, 259 – 268.

Hu, A.S., Bean, S.P., and Zimmerman, R.M., 1977. Response of Belted Dummy and Cadaver to Rear Impact. *Proceedings from the 21st Stapp Car Crash Conference*, 589 – 625. SAE 770929.

Huang, C.Y., Stankiewicz, A., Ateshian, G.A., and Mow, V.C., 2005. Anisotropy, Inhomogeneity, and Tension-Compression Nonlinearity of Human Glenohumeral Cartilage in Finite Deformation. *Journal of Biomechanics* 38, 799 – 809.

Iatridis, J.C., Weidenbaum, M., Setton, L.A., and Mow, V.C., 1996. Is the Nucleus Pulposus a Solid or a Fluid? Mechanical Behaviors of the Nucleus Pulposus of the Human Intervertebral Disc. *Spine* 21, 1174 – 1184.

Iatridis, J.C., Setton, L.A., Foster, R.J., Rawlins, B.A., Weidenbaum, M., and Mow, V.C., 1998. Degeneration Affects the Anisotropic and Nonlinear Behaviors of Human Anulus Fibrosus in Compression. *Journal of Biomechanics* 31, 535 – 544.

Iatridis, J.C., Kumar, S., Foster, R.J., Weidenbaum, M., and Mow, V.C., 1999. Shear Mechanical Properties of Human Lumbar Annulus Fibrosus. *Journal of Orthopaedic Research* 17, 732 – 737.

Iatridis, J.C., and ap Gwynn, I., 2004. Mechanisms for Mechanical Damage in the Intervertebral Disc Annulus Fibrosus. *Journal of Biomechanics* 31, 535 – 544.

Iatridis, J.C., MacLean, J.J., and Ryan, D.A., 2005. Mechanical Damage to the Intervertebral Disc Annulus Fibrosus Subjected to Tensile Loading. *Journal of Biomechanics* 38, 557 – 565.

Ito, S., Ivancic, P.C., Panjabi, M.M., and Cunningham, B.W., 2004. Soft Tissue Injury Threshold during Simulated Whiplash. *Spine* 29(9), 979 – 987.

Ito, S., Ivancic, P.C., Pearson, A.M., Tominga, Y., Gimenez, S.E., Rubin, W., and Panjabi, M.M., 2005. Cervical Intervertebral Disc Injury During Simulated Frontal Impact. *European Spine Journal* 14, 356 – 365.

Kallieris, D., Mattern, R., Miltner, E., Schmidt, G., and Stein, K., 1991. Considerations for a Neck Injury Criterion. *Proceedings from the 35th Stapp Car Crash Conference*, 401 – 417. SAE 912916.

Kasra, M., and Grynpas, M.D., 1998. Static and Dynamic Finite Element Analyses of an Idealized Structural Model of Vertebral Trabecular Bone. *Journal of Biomechanical Engineering* 120, 267 – 272.

Kasra, M., Parnianpour, M., Shirazi-Adl, A., Wang, J.L., and Grynpas, M.D., 2004. Effect of Strain Rate on Tensile Properties of Sheep Disc Annulus Fibrosus. *Technology and Health Care* 12, 333 – 342.

Kazarian, L.E., 1975. Creep Characteristics of the Human Spinal Column. *Orthopedic Clinics of North America* 6, 3.

Keaveny, T.M., Morgan, E.F., Niebur, G.L., and Yeh, O.C., 2001. Biomechanics of Trabecular Bone. *Annual Review of Biomedical Engineering* 3, 307 – 333.

Kempson, G.E., Freeman, M.A.R., and Swanson, S.A.V., 1971. The Determination of a Creep Modulus for Articular Cartilage from Indentation Tests on the Human Femoral Head. *Journal of Biomechanics* 4, 239 – 250.

King, A.I., 2000. Fundamentals of Impact Biomechanics: Part I – Biomechanics of the Head, Neck, and Thorax. *Annual Reviews in Biomedical Engineering* 2, 55 – 81.

Kleinberger, M., 1993. Application of Finite Element Techniques to the Study of Cervical Spine Mechanics. *Proceedings from the 37th Stapp Car Crash Conference*, 261 – 272. SAE 933131.

Klinich, K.D., Ebert, S.M., Van Ee, C.A., Flannagan, C.A.C., Prasad, M., Reed, M.P., and Schneider, L.W., 2004. Cervical Spine Geometry in the Automotive Seated Posture: Variations with Age, Stature, and Gender. *Proceedings from the 48th Stapp Car Crash Conference*, 301 – 330. SAE 2004-22-014.

Klisch, S.M. and Lotz, J.C., 1999. Application of a Fiber-Reinforced Continuum Theory to Multiple Deformations of the Annulus Fibrosus. *Journal of Biomechanics* 32, 1027 – 1036.

Klisch, S.M., and Lotz, J.C., 2000. A Special Theory of Biphasic Mixtures and Experimental Results for Human Annulus Fibrosus Tested in Confined Compression. *Journal of Biomechanical Engineering* 122, 180 – 188.

Knaub, K., and Myers, B.S., 1998. Project F.2(c) Cervical Spine Muscle. *National Highway Traffic Safety Administration*, NHTSA-98-3588-133.

Knaub, K., Van Ee, C., Cheng, C., Poon, B., Spritzer, C., and Myers, B.S., 1999. Measurement of Human Neck Muscle Volume Geometry and Physiologic Cross-Sectional Area in 5th, 50th, and 95th Percentile Subjects Using Cadaveric Dissection and MRI. *National Highway Traffic Safety Administration*, NHTSA-98-3588-34.

Kopperdahl, D.L., and Keaveny, T.M., 1998. Yield Strain Behavior of Trabecular Bone. *Journal of Biomechanics* 31, 601 – 608.

Kopperdhal, D.L., Pearlman, J.L., and Keaveny, T.M., 2000. Biolmechanical Consequences of an Isolated Overload on the Human Vertebral Body. *Journal of Orthopaedic Research* 18, 685 – 690.

Kosmopoulos, V., and Keller, T.S., 2003. Finite Element Modeling of Trabecular Bone Damage. *Computer Methods in Biomechanics and Biomedical Engineering* 6(3), 209 – 216.

Kotha, S.P., and Guzelsu, N., 2003. Effect of Bone Mineral Content on the Tensile Properties of Cortical Bone: Experiments and Theory. *Journal of Biomechanical Engineering* 125, 785 – 793.

Kraemer, J.D., Kolditz, M., and Gowin, R., 1985. Water and Electrolyte Content of the Human Intervertebral Discs under Variable Load., *Spine* 10, 69 – 71.

Kulak, R.F., Belytschko, T.B., Schultz, A.B., and Galante, J.O., 1976. Nonlinear Behavir of the Human Intervertebral Disc Under Axial Load. *Journal of Biomechanics* 9, 377 – 386.

Kumaresan, S., Yoganandan, N., Pintar, F.A., Voo, L.M., Cusick, J.F., and Larson, S.J., 1997. Finite Element Modeling of Cervical Laminectomy with Graded Facetectomy. *Journal of Spinal Disorders* 10(1), 40 – 46.

Kumaresan S., Yoganandan, N., and Pintar, F.A., 1998. Finite Element Modeling Approaches of Human Cervical Spine Facet Joint Capsule. *Journal of Biomechanics* 31, 371 – 376.

Kumaresan S., Yoganandan, N., and Pintar, F.A., 1999a. Finite Element Analysis of the Cervical Spine: A Material Property Sensitivity Study. *Clinical Biomechanics* 14, 41 – 53.

Kumaresan, S., Yoganandan, N., Pintar, F.A., and Maiman, D.J., 1999b. Finite Element Modeling of the Cervical Spine: Role of Intervertebral Disc Under Axial and Eccentric Loads. *Medical Engineering and Physics* 21, 689 – 700.

Lee, I.H., Choi, H.Y., Lee, J.H., and Han, D.C., 2004. Development of Finite Element Human Neck Model for Vehicle Safety Simulation. *International Journal of Automotive Technology*, 5(1), 33 – 46.

Lee, K.E., Franklin, A.N., Davis, M.B., and Winkelstein, B.A., 2006. Tensile Cervical Facet Capsule Ligament Mechanics: Failure and Subfailure Responses in the Rat. *Journal of Biomechanics* 39, 1256 – 1264.

Li, L.P., Buschmann, M.D., and Shirazi-Adl, A., 2003. Strain-Rate Dependent Stiffness of Articular Cartilage in Unconfined Compression. *Journal of Biomechanical Engineering* 125, 161 – 168.

Lin, H.S., Liu, Y.K., Ray, G., and Nikravesh, P., 1978. Systems Identification for Material Properties of the Intervertebral Joint. *Journal of Biomechanics* 11, 1 – 14.

Lindahl, O., 1976. Mechanical Properties of Dried Defatted Spongy Bone. *Acta Orthopaedica Scandinavica* 47, 11 – 19.

Linde, F., Norgaard, P., Hvid, I., Oggaard, A., and Soballe, K., 1991. Mechanical Properties of Trabecular Bone Dependency on Strain Rate. *Journal of Biomechanics* 24, 803 – 809.

Lotz, J.C., Biviji, A.A., Fujita, Y., and Duncan, N.A., 1995. Time-Independent Shear Moduli of the Human Annulus Fibrosus. *Proceedings from the ASME Bioengineering Conference* 29, 253 – 254.

Lu, Y.M., Hutton, W.C., and Gharpuray, V.M., 1996. Do Bending, Twisting, and Diurnal Fluid Changes in the Disc Affect the Propensity to Prolapse? A Viscoelastic Finite Element Model. *Spine* 21(22), 2570 – 2579.

Maak, T.G., Tominaga, Y., Panjabi, M.M., and Ivancic, P.C., 2006. Alar, Transervse, and Apical Ligament Strain due to Head-Turned Rear Impact. *Spine* 31(6), 632 – 638.

Maat, G.J.R., and Mastwijk, R.W., 2000. Avulsion Injuries of Vertebral Endplates. *International Journal of Osteoarchaeology* 10, 142 – 152.

Marchand, F., and Ahmed, A.M., 1990. Investigation of the Laminate Structure of the Lumbar Disc Anulus Fibrosus. *Spine* 15(5), 402 – 410.

Markolf, K.L., and Morris, J.M., 1974. The Structural Components of the Intervertebral Disc. *Journal of Bone and Joint Surgery* 56, 675.

Martinez, J.B., Oloyede, V.O.A., and Broom, N.D., 1997. Biomechanics of Load-Bearing of the Intervertebral Disc: An Experiment and Finite Element Model. *Medical Engineering and Physics* 19(2), 145 – 156.

McElhaney, J.H., 1966. Dynamic Response of Bone and Muscle Tissue. *Journal of Applied Physiology* 21, 1231 – 1236.

McElhaney, J.H., Paver, J.G., McCrackin, H.J., and Maxwell, G.M., 1983. Cervical Spine Compression Responses. *Proceedings from the 27th Stapp Car Crash Conference*, 163 – 177. SAE 831615.

McElhaney, J.H., Doherty, B.J., Paver, J.G., Myers, B.S., and Gray, L., 1988. Combined Bending and Axial Loading Responses of the Human Cervical Spine. *Proceedings from the 32nd Stapp Car Crash Conference*, 21 – 28. SAE 881709.

Meakin, J.R., Reid, J.E., and Hukins, D.W.L., 2001. Replacing the Nucleus Pulposus of the Intervertebral Disc. *Clinical Biomechanics* 16, 560 – 565.

Mercer, S.B., and Bogduk, N., 1999. The Ligaments and Anulus Fibrosus of Human Adult Cervical Intervertebral Discs. *Spine* 24(7), 619 – 628.

Mercer, S.B., and Bogduk, N., 2003. Clinical Anatomy of Ligamentum Nuchae. *Clinical Anatomy* 16(6), 484 – 493.

Merrill, T., Goldsmith, W., and Deng, Y.C., 1984. Three-Dimensional Response of a Lumped Parameter Head-Neck Model Due to Impact and Impulsive Loading. *Journal of Biomechanics* 17(2), 81 – 95.

Mertz, H.J., and Patrick, L.M., 1967. Investigation of the Kinematics and Kinetics of Whiplash. *Proceedings from the 11th Stapp Car Crash Conference* 267 – 317. SAE 670919.

Mertz, H.J., and Patrick, L.M., 1971. Strength and Response of the Human Neck. *Proceedings from the 15th Stapp Car Crash Conference* 2903 – 2928. SAE 710855.

Meyer, F., Bourdet, N., Deck, C., Willinger, R., and Raul, J.S., 2004. Human Neck Finite Element Model Development and Validation Against Original Experimental Data. *Proceedings from the 48th Stapp Car Crash Conference*, 177 – 206. SAE 2004-22-0008.

Moore, K.L., and Dalley, A.F., 2006. *Clinically Oriented Anatomy* 5th Ed. Lippincott Williams and Wilkins, Philadelphia.

Morgan, E.F., and Keaveny, T.M., 2001. Dependence of Yield Strain of Human Trabecular Bone on Anatomic Site. *Journal of Biomechanics* 34, 569 – 577.

Moroney, S.P., Schultz, A.B., Miller, J.A.A., and Andersson, G.B.J., 1988. Load-Displacement Properties of Lower Cervical Spine Motion Segments. *Journal of Biomechanics* 21(9), 769 – 779.

Morris, A.P., and Thomas, P., 1996. Neck Injuries in the UK Co-operative Crash Injury Study. *Proceedings from the 40th Stapp Car Crash Conference*, 317 – 329. SAE 962433.

Mosekilde, Li., and Mosekilde, Le., 1986. Normal Vertebral Body Size and Compressive Strength: Relations to Age and to Vertebral and Iliac Trabecular Bone Compressive Strength. *Bone* 7, 207 – 212.

Mosekilde, Li., Mosekilde, Le., and Danielsen, C.C., 1987. Biomechanical Competence of Vertebral Trabecular Bone in Relation to Ash Density and Age in Normal Individuals. *Bone* 8, 79 – 85.

Mow, V.C., Kuei, S.C., Lai, W.M., and Armstrong, C.G., 1980. Biphasic Creep and Stress Relaxation of Articular Cartilage in Compression: Theory and Experiments. *Journal of Biomechanical Engineering* 102, 73 – 84.

Mow, V.C., and Guo, X.E., 2002. Mechano-Electrochemical Properties of Articular Cartilage: Their Inhomogeneities and Anisotropies. *Annual Reviews in Biomedical Engingeering* 4, 175 – 209.

Myers, B.S., McElhaney, J.H., Richardson, W.J., Nightingale. R.W., and Doherty, B.J., 1991. The Influence of End Condition on Human Cervical Spine Injury. *Proceedings from the 35th Stapp Car Crash Conference*, 391 – 399. SAE 912915.

Myers, B.S., Van Ee, C.A., Camacho, D.L.A., Woolley, C.T., and Best, T.M., 1995. On the Structural and Material Properties of Mammalian Skeletal Muscle and its Relevance to Human Cervical Impact Dynamics. *Proceedings from the 39th Stapp Car Crash Conference*, 203 – 214. SAE 952723.

Myklebust, J.B., Pintar, F.A., Yoganandan, N., Cusick, J.F., Maiman, D., Myers, T.J., and Sances, A., 1988. Tensile Strength of Spinal Ligaments, *Spine* 13, 526 – 531.

Nalla, R.K., Stolken, J.S., Kinney, J.H., and Ritchie, R.O., 2005. Fracture in Human Cortical Bone: Local Fracture Criteria and Toughening Mechanisms. *Journal of Biomechanics* 38, 1517 – 1525.

Natarajan, R.N., Ke, J.H., and Andersson, G.B.J., 1994. A Model to Study the Disc Degeneration Process. *Spine* 19(3), 259 – 265.

Natarajan, R.N., and Andersson, G.B.J., 1999. The Influence of Lumbar Disc Height and Cross-Sectional Area on the Mechanical Response of the Disc to Physiologic Loading. *Spine* 24(18), 1873 – 1881.

Natarajan, R.N., Chen, B.H., An, H.S., and Andersson, G.B.J., 2000. Anterior Cervical Fusion: A Finite Element Model Study on Motion Segment Stability Including the Effect of Osteoporosis. *Spine* 25(8), 955 – 961.

National Highway Traffic Safety Administration, 2002. *Federal Motor Vehicle Safety Standards and Regulations No. 208 "Occupant Crash Protection"*. United States Department of Transportation.

Ng, H.W., and Teo, E.C., 2001. Nonlinear Finite-Element Analysis of the Lower Cervical Spine (C4-C6) Under Axial Loading. *Journal of Spinal Disorders* 14(3), 201 – 210.

Ng, H.W., and Teo, E.C., 2003. Finite Element Analysis of Cervical Spinal Instability Under Physiologic Loading. *Journal of Spinal Disorders* 16(1), 55 – 65.

Ng, H.W., Teo, E.C., and Lee, V.S., 2004. Statistical Factorial Analysis on the Material Property Sensitivity of the Mechanical Response of the C4-C6 Under Compression, Anterior and Posterior Shear. *Journal of Biomechanics* 37, 771 – 777.

Nightingale, R.W., McElhaney, J.H., Richardson, W.J., and Myers, B.S., 1996. Dynamic Responses of the Head and Cervical Spine to Axial Impact Loading. *Journal of Biomechanics* 29(3), 307 – 318.

Nightingale, R.W., McElhaney, J.H., Camacho, D.L., Kleinberger, M., Winkelstein, B.A., and Myers, B.S., 1997. The Dynamic Responses of the Cervical Spine: Buckling, End Conditions, and Tolerance in Compressive Impacts. *Proceedings from the 41st Stapp Car Crash Conference*, 451 – 471. SAE 973344.

Nightingale, R.W., Winkelstein, B.A., Knaub, K.E., Richardson, W.J., Luck, J.F., and Myers, B.S., 2002. Comparative Strengths and Structural Properties of the Upper and Lower Cervical Spine in Flexion and Extension. *Journal of Biomechanics* 35, 725 – 732.

Nightingale, R.W., Chancey, V.C., Luck, J.F., Tran, L., Ottaviano, D., and Myers, B.S., 2004. The Human Cervical Spine in Tension: Effects of Frame and Fixation Compliance on Structural Responses. *Traffic Injury Prevention* 5, 151 – 155.

Nightingale, R.W., Chancey, V.C., Ottaviano, D., Luck, J.F., Tran, L., Prange, M., and Myers, B.S., *In Press*. Flexion and Extension Structural Properties and Strengths for Male Cervical Spine Segments. *Journal of Biomechanics*.

Noailly, J., Lacroix, D., and Planell, J.A., 2005. Finite Element Study of a Novel Intervertebral Disc Substitute. *Spine* 30(20), 2257 – 2264.

Nusholtz, G.S., Melvin, J.W., Huelke, D.F., Alem, N.M., and Blank, J.G., 1981. Response of the Cervical Spine to Superior-Inferior Head Impact. *Proceedings from the 25th Stapp Car Crash Conference*, 197 – 237. SAE 811005.

Nusholtz, G.S., Huelke, D.F., Lux, P., Alem, N.M., and Montavlo, F., 1983. Cervical Spine Injury Mechanisms. *Proceedings from the 27th Stapp Car Crash Conference*, 179 – 197. SAE 831616.

Ogden, R.W., 1984. *Non-Linear Elastic Deformations.* Ellis Horwood Ltd., Chichester, Great Britain.

Pal, G.P., Routal, R.V., and Saggu, S.K., 2001. The Orientation of the Articular Facets of the Zygapophyseal Joints at the Cervical and Thoracic Region. *Journal of Anatomy* 198, 431 – 441.

Panjabi, M.M., Jorneus, L., and Greenstein, G., 1984. Physical Properties of Lumbar Spine Ligaments. *Orthopaedic Research Society Conference* 30, 112.

Panjabi, M.M., Summers, D.J., Pelker, R.R., Videman, T., Friedlaender, G.E., and Southwick, W.O., 1986. Three-Dimensional Load-Displacement Curves Due to Forces on the Cervical Spine. *Journal of Orthopaedic Research* 4, 152 – 161.

Panjabi, M.M., Dvorak, J., Duranceau, J., Yamamoto, I., Gerber, M., Rauschining, W., and Bueff, H.U., 1988. Three-Dimensional Movements of the Upper Cervical Spine. *Spine* 13(7), 726 – 730.

Panjabi, M.M., Oxland, T.R., and Parks, E.H., 1991a. Quantitative Anatomy of Cervical Spine Ligaments Part 1: Upper Cervical Spine. *Journal of Spinal Disorders* 4, 270 – 276.

Panjabi, M.M., Oxland, T.R., and Parks, E.H., 1991b. Quantitative Anatomy of Cervical Spine Ligaments Part 2: Middle and Lower Cervical Spine. *Journal of Spinal Disorders* 4, 277 – 285.

Panjabi, M.M., Dvorak, J., Crisco, J.J., Oda, T., Hilibrand, A., and Grob, D., 1991c. Flexion, Extension, and Lateral Bending of the Upper Cervical Spine in Response to Alara Ligament Transections. *Journal of Spinal Disorders* 4(2), 157 – 167.

Panjabi, M.M., Dvorak, J., Crisco, J.J., Oda, T., Wang, P., and Grob, D., 1991d. Effects of Alar Ligament Transection on Upper Cervical Spine Rotation. *Journal of Orthopaedic Research* 9, 584 – 593.

Panjabi, M.M., Duranceau, J., Goel, V., Oxland, T., and Takata, K., 1991e. Cervical Human Vertebrae: Quantitative Three-Dimensional Anatomy of the Middle and Lower Regions. *Spine* 16(8), 7 – 12.

Panjabi, M.M., Oxland, T., Takata, K., Goel, V., Duranceau, J., and Krag, M., 1993. Articular Facets of the Human Spine: Quantitative Three-Dimensional Anatomy. *Spine* 18(10), 1298 – 1310.

Panjabi, M.M., and Myers, B.S., 1995. Cervical Spine Protection Report. *National Organizing Committee for Standards in Athletic Equipment*.

Panjabi, M.M., Yoldas, E., Oxland, T.R., and Crisco, J.J., 1996. Subfailure Injury of the Rabbit Anterior Cruciate Ligament. *Journal of Orthopaedic Research* 14, 216 – 222.

Panjabi, M.M., 1998. Cervical Spine Models for Biomechanical Research. *Spine* 23(24), 2684 – 2699.

Panjabi, M.M., Crisco, J.J., Lydon, C., and Dvorak, J., 1998. The Mechanical Properties of Human Alar and Transverse Ligaments at Slow and Fast Extension Rates. *Clinical Biomechanics* 13(2), 112 – 120.

Panjabi, M.M., Chen, N.C., Shin, E.K., and Wang, J-L., 2001a. The Cortical Shell Architecture of Human Cervical Vertebral Bodies. *Spine* 26(22), 2478 – 2484.

Panjabi, M.M., Crisco, J.J., Vasavada, A., Oda, T., Cholewicki, J., Nibu, K., and Shin, E., 2001b. Mechnical Properties of the Human Cervical Spine as Shown by Three-Dimensional Load-Displacement Curves. *Spine* 26(24), 2692 – 2700.

Panjabi, M.M., Ito, S., Pearson, A.M., and Ivancic, P.C., 2004a. Injury Mechanisms of the Cervical Intervertebral Disc during Simulated Whiplash. *Spine* 29(11), 1217 – 1225.

Panjabi, M.M., Pearson, A.M., Ito, S., Ivancic, P.C., Gimenez, S.E., and Tominga, Y., 2004b. Cervical Spine Ligament Injury during Simulated Frontal Impact. *Spine* 29(21), 2395 – 2403.

Panjabi, M.M., Ito, S., Ivancic, P.C., and Rubin, W., 2005. Evaluation of the Intervertebral Neck Injury Criterion Using Simulated Rear Impacts. *Journal of Biomechanics* 38, 1694 – 1701.

Penning, L., and Wilmink, J.T., 1986. Rotation of the Cervical Spine. *Spine* 12(8), 732 – 738.

Pezowicz, C.A., Roberston, P.A., and Broom, N.D., 2005. Intralamellar Relationships within the Collagenous Architecture of the Annulus Fibrosus Imaged in its Fully Hydrated State. *Journal of Anatomy* 207, 299 – 312.

Pintar, F.A., 1986. *The Biomechanics of Spinal Elements*. PhD Thesis, Marquette University.

Pintar, F.A., Yoganandan, N., Sances, A., Reinartz, J., Harris, G., and Larson, S.J., 1989. Kinematic and Anatomical Analysis of the Human Cervical Spine Column Under Axial Loading. *Proceedings from the 33rd Stapp Car Crash Conference*, 191 – 214. SAE 892436.

Pintar, F.A., Sances, A., Yoganandan, N., Reinartz, J., Maiman, D.J., Suh, J.K., Unger, G., Cusisck, J.F., and Larson, S.J., 1990. Biodynamics of the Total Human Cadaveric Cervical Spine. *Proceedings from the 34th Stapp Car Crash Conference*, 55 – 72. SAE 902309.

Pintar, F.A., Yoganandan, N., Voo, L., Cusick, J.F., Mainman, D.J., and Sances, A., 1995. Dynamic Characteristics of the Human Cervical Spine. *Proceedings from the 41st Stapp Car Crash Conference*, 195 – 202. SAE 952722.

Pitzen, T., Matthis, D., and Steudel, W.I., 2002. Posterior Element Injury and Cervical Spine Flexibility Following Anterior Cervical Fusion and Plating. *European Journal of Trauma* 1, 24 – 30.

Pitzen, T., Schmitz, B., Georg, T., Barbier, D., Beuter, T., Steudel, W.I., and Reith, W., 2004. Variation of Endplate Thickness in the Cervical Spine. *European Spine Journal* 13, 235 – 240.

Pooni, J.S., Hukins, D.W.L., Harris, P.F., Hilton, R.C., and Davies, K.E., 1986. Comparison of the Structure of Human Intervertebral Discs in the Cervical, Thoracic and Lumbar Regions of the Spine. *Surgical and Radiologic Anatomy* 8, 175 – 182.

Provenzano, P.P., Heisey, D., Hayasho, K., Lakes, R.S., and Vanderby, R., 2001. Sub-Failure Damage in Ligament. *Proceedings of the 2001 Bioengineering Conference (ASME)* 50, 49 – 50.

Przybylski, G.J., Patel, P.R., Carlin, G.J., and Woo, S.L-Y., 1998. Quantitative Anthropometry of the Subatlantal Cervical Longitudinal Ligaments. *Spine* 23(8), 893 – 898.

Pugh, J.W., Rose, R.M., and Radin, E.L., 1973. Elastic and Viscoelastic Properties of Trabecular Bone: Dependence on Structure. *Journal of Biomechanics* 6, 475 – 485.

Puttlitz, C.M., Rousseau, M.A., Xu, Z., Hu, S., Tay, B.K.B., and Lotz, J.C., 2004. Intervertebral Disc Replacement Maintains Cervical Spine Kinetics. *Spine* 29(24), 2809 – 2814.

Quapp, K.M., and Weiss, J.A., 1998. Material Characterization of Human Medial Collateral Ligament. *Journal of Biomechanical Engineering* 120, 757 – 763.

Race, A., Broom, N.D., and Roberstson, P., 2000. Effect of Loading Rate and Hydration on the Mechanical Properties of the Disc. *Spine* 25(6), 662 – 669.

Rao, A.A., and Dumas, G.A., 1991. Influence of Material Properties on the Mechanical Behaviour of the L5-S1 Intervertebral Disc in Compression: A Nonlinear Finite Element Study. *Journal of Biomedical Engineering* 13, 139 – 151.

Reilly, D.T., Burstein, A.H., and Frankel, V.H., 1974. The Elastic Modulus for Bone. *Journal of Biomechanics* 7, 271 – 275.

Reilly, D.T., and Burstein, A.H., 1975. The Elastic and Ultimate Properties of Compact Bone Tissue. *Journal of Biomechanics* 8, 393 – 405.

Richter, M., Wilke, H.J., Kluger, P., Claes, L., and Puhl, W., 2000. Load-Displacement Properties of the Normal and Injured Lower Cervical Spine in vitro. *European Spine Journal* 9, 104 – 108.

Robertson, A., Branfoot, T., Barlow, I.F., and Giannoudies, P.V., 2002. Spinal Injury Patterns Resulting From Car and Motorcycle Accidents. *Spine* 27(24), 2825 – 2830.

Robbins, D.H., 1983. *Anthropometric Specifications for Mid-Sized Male Dummy, Volume 2*. University of Michigan Transportation Research Institute, UMTRI-83-53-2.

Rockoff, S.D., Sweet, E., and Bleustein, J., 1969. The Relative Contribution of Trabecular and Cortical Bone to the Strength of Human Lumbar Vertebrae. *Calcified Tissue Research* 3, 163.

Rohlmann, A., Zilch, H., Bergmann, G., and Kolbel, R., 1980. Material Properties of Femoral Cancellous Bone in Axial Loading. Part I: Time Independent Properties. *Acta Orthopaedia Trauma Surgery* 97, 95 – 102.

Saha, S., and Hayes, W.C., 1976. Tensile Impact Properties of Human Compact Bone. *Journal of Biomechanics* 9, 243 – 251.

Schmidt, G., Kallieris, D., Barz, J., and Mattern, R., 1974. Results of 49 Cadaver Tests Simulating Frontal Collision of Front Seat Passengers. *Proceedings from the 18th Stapp Car Crash Conference*, 283 – 291. SAE 741182.

Schulte, K., Clark, C.R., and Goel, V.K., 1989. Kinematics of the Cervical Spine Following Discectomy and Stabilization. *Spine* 14(10), 1116 – 1121.

Selard, E., Shirazi-Adl, A., and Urban, J.P., 2003. Finite Element Study of Nutrient Diffusion in the Human Intervertebral Disc. *Spine* 28(17), 1945 – 1953.

Setton, L.A., Zhu, W., and Mow, V.C., 1993a. The Biphasic Poroviscoelastic Behavior of Articular Cartilage: Role of the Surface Zone in Governing the Compressive Behavior. *Journal of Biomechanics* 26, 581 – 592.

Setton, L.A., Zhu, W., Weidenbaum, M., Ratcliffe, A., and Mow, V.C., 1993b. Compressive Properties of the Cartilaginous End-Plate of the Baboon Lumbar Spine. *Journal of Orthopaedic Research* 11, 228 – 239.

Skaggs, D.L., Weidenbaum, M., Iatridis, J.C., Ratcliffe, A., and Mow, V.C., 1994. Regional Variation in Tensile Properties and Biochemical Composition of the Human Lumbar Annulus Fibrosus. *Spine* 19(12), 1310 – 1319.

Shea, M., Edwards, W.T., White, A.A., and Hayes, W.C., 1991. Variations of Stiffness and Strength along the Human Cervical Spine. *Journal of Biomechanics* 24(2), 95 – 107.

Shim, V.P.W., Liu, J.F., and Lee, V.S., 2006. A Technique for Dynaimic Tensile Testing of Human Cervical Spine Ligaments. *Experimental Mechanics* 46, 77 – 89.

Shirazi-Adl, A., Shrivastava, S.C., and Ahmed, A.M., 1984. Stress Analysis of a Lumbar Disc-Body Unit in Compression: A Three Dimensional Nonlinear Finite Element Study. *Spine* 9, 120 – 134.

Shirazi-Adl, A., Ahmed, A.M., and Shrivastava, S.C., 1986. A Finite Element Study of a Lumbar Motion Segment Subjected to Pure Sagittal Plane Moments. *Journal of Biomechanics* 19(4), 331 – 350.

Shiradi-Adl, A., 1989. On the Fibre Composite Material Models of Disc Annulus – Comparison of Predicted Stresses. *Journal of Biomechanics* 22(4), 357 – 365.

Siegmund, G.P., Myers, B.S., Davis, M.B., Bohnet, H.F., and Winkelstein, B.A., 2001. Mechanical Evidence of Cervical Facet Joint Capsule Injury during Whiplash. *Spine* 26, 2095 – 2101.

Silver, F.H., Ebrahimi, A., and Snowhill, P.B., 2002. Viscoelastic Properties of Self-Assembled Type I Collagen Fibers: Molecular Basis of Elastic and Viscous Behaviors. *Connective Tissue Research* 43, 569 – 580.

Simon, B.R., Coats, R.S., and Woo, S.L.Y., 1984. Relaxation and Creep Quasilinear Viscoelastic Models for Normal Articular Cartilage. *Journal of Biomechanical Engineering* 106, 159 – 164.

Spilker, R.L., 1980. Mechanical Behavior of a Simple Model of an Intervertebral Disk Under Compressive Loading. *Journal of Biomechanics* 13, 895 – 901.

Spilker, R.L., Daugirda, D.M., and Schultz, A.B., 1984. Mechanical Response of a Simple Finite Element Model of the Intervertebral Disc under Complex Loading. *Journal of Biomechanics* 17, 103 – 112.

Spilker, R.L., Jakobs, D.M., and Schultz, A.B., 1986. Material Constants for a Finite Element Model of the Intervertebral Disk with a Fiber Composite Annulus. *Journal of Biomechanical Engineering* 108, 1 – 11.

Storakers, B., 1986. On Material Representation and Constitutive Branching in Finite Compressible Elasticity. *Journal of the Mechanics and Physics of Solids* 34, 125 – 145.

Teo, E.C., and Ng, H.W., 2001. Evaluation of the Role of Ligaments, Facets and Disc Nucleus in Lower Cervical Spine Under Compression and Sagittal Moments Using Finite Element Method. *Medical Engineering and Physics* 23, 155 – 164.

Thunnissen, J., Wismans, J., Ewing, C.L., and Thomas, D.J., 1995. Human Volunteer Head-Neck Response in Frontal Flexion: A New Analysis. *Proceedings from the 39th Stapp Car Crash Conference* 439 – 460. SAE 952721.

Ueno, K., and Liu, Y.K., 1987. A Three-Dimensional Nonlinear Finite Element Model of Lumbar Intervertebral Joint in Torsion. *Journal of Biomechanical Engineering* 109, 200 – 209.

Uhlig, Y., Weber, B.R., Grob, D., and Muntener, M., 1995. Fiber Composition and Fiber Transformations in Neck Muscles of Patients with Dysfunction of the Cervical Spine. *Journal of Orthopaedic Research* 13, 240 – 249.

Van der Horst, M.J., 2002. *Human Head Neck Response in Frontal, Lateral and Rear End Impact*. PhD Thesis, Eindhoven University of Technology.

Van Ee, C.A., Chasse, A.L., and Myers, B.S., 2000a. Quantifying Skeletal Muscle Properties in Cadaveric Test Specimens: Effects of Mechanical Loading, Postmortem Time, and Freezer Storage. *Journal of Biomechanical Engineering* 122, 9 – 14.

Van Ee, C.A., Nightingale, R.W., Camacho, D.L.A., Chancey, V.C., Knaub, K.E., Sun, E.A., and Myers, B.S., 2000b. Tensile Properties of the Human Muscular and Ligamentous Cervical Spine. *Proceedings from the 44th Stapp Car Crash Conference*. SAE 2000-01-SC07.

Van Slightenhorst, C., Cronin, D.S., and Brodland, G.W., 2006. High Strain Rate Compressive Properties of Bovine Muscle Tissue Determined using a Split Hopkinson Bar Apparatus. *Journal of Biomechanics* 39, 1852 – 1858.

Viano, D.C., King, A.I., Melvin, J.W., and Weber, K., 1989. Injury Biomechanics Research: An Essential Element in the Prevention of Trauma. *Journal of Biomechanics* 22(5), 403 – 417.

Virgin, W., 1951. Experimental Investigations into Physical Properties of Intervertebral Disc. *Journal of Bone and Joint Surgery* 33, 607.

Ward, S.R., and Lieber, R.L., 2005. Density and Hydration of Fresh and Fixed Human Skeletal Muscle. *Journal of Biomechanics* 38(11), 2317 – 2320.

Wagner, D.R., and Lotz, J.C., 2004. Theoretical Model and Experimental Results for the Nonlinear Elastic Behavior of Human Annulus Fibrosus. *Journal of Orthopaedic Research* 22, 901 – 909.

Walker, L.B., Harris, E.H., and Pontius, U.R., 1973. Mass, Volume, Center of Mass, and Mass Moment of Inertia of Head and Head and Neck of Human Body. *Proceedings from the 17th Stapp Car Crash Conference*. SAE 730985.

Weiss, J.A., Bonifasi-Lista, C., and Gardiner, J.C., 2001. Determination of Ligament Shear Properties Using a Finite Element Parameter Estimation Technique. *Proceedings of the 2001 Bioengineering Conference (ASME)* 50, 43 – 44.

Wen, N., Lavaste, F., Santin, J.J., and Lassau, J.P., 1993. Three-Dimensional Biomechanical Properties of the Human Cervical Spine in vitro. *European Spine Journal* 2, 2 – 11.

Wheeldon, J.A., Pintar, F.A., Knowles, S., and Yoganandan, N., 2006. Experimental Flexion/Extension Data Corridors for Validation of Finite Element Models of the Young, Normal Cervical Spine. *Journal of Biomechanics* 39, 375 – 380.

White, A.A., and Panjabi, M.M., 1990. *Clinical Biomechanics of the Spine*. 2nd Ed. J.B. Lippincott Co., Philadelphia.

Whyne, C.M., Hu, S.S., and Lotz, J.C., 2001. Parametric Finite Element Analysis of Vertebral Bodies Affected by Tumors. *Journal of Biomechanics* 34, 1317 – 1324.

Whyne, C.M., Hu, S.S., and Lotz, J.C., 2003. Burst Fracture in the Metastatically Involved Spine. *Spine* 28(7), 652 - 660.

Wilcox, R.K., Allen, D.J., Hall, R.M., Limb, D., Barton, D.C., and Dickson, R.A., 2004. A Dynamic Investigation of the Burst Fracture Process Using a Combined Experimental and Finite Element Approach. *European Spine Journal* 13, 481 – 488.

Williams, J.L., and Belytschko, T.B., 1983. A Three-Dimensional Model of Human Cervical Spine for Impact Simulation. *Journal of Biomechanical Engineering* 105, 321 – 331.

Winkelstein, B.A., Nightingale, R.W., Richardson, W.J., and Myers, B.S., 2000a. The Cervical Facet Capsule and its Role in Whiplash Injury. *Spine* 25(10), 1238 – 1246.

Winkelstein, B.A., and Myers, B.S., 2000b. Experimental and Computational Characterization of Three-Dimensional Cervical Spine Flexibility. *Proceedings from the 44th Stapp Car Crash Conference*. SAE 2000-01-SC11.

Winkelstein, B.A., McLendon, R.F., Barbir, A., and Myers, B.S., 2001. An Anatomical Investigation of the Human Cervical Facet Capsule, Quantifying Muscle Insertion Area. *Journal of Anatomy* 198, 445 – 461.

Winters, J.M., and Stark, L., 1985. Analysis of Fundamental Human Movement Patterns Through the Use of In-Depth Antagonistics Muscle Models. *IEEE Transactions in Biomedical Engineering* 12, 826 – 839.

Winters, J.M., and Stark, L., 1988. Estimated Mechanical Properties of Synergistic Muscles Involved in Movements of a Variety of Human Joints. *Journal of Biomechanics* 21(12), 1027 – 1041.

Winters, J.M., and Woo, S.L.Y., 1990. *Multiple Muscle Systems: Biomechanics and Movement Organization*. Springer-Verlag, New York.

Winters, J.M., 1995. How Detailed Should Muscle Models be to Understand Multi-Joint Movement Coordination?. *Human Movement Science* 14, 401 – 442.

Wismans, J., and Spenny, C.H., 1983. Performance Requirements for Mechanical Neck in Lateral Flexion. *Proceedings from the 27th Stapp Car Crash Conference*, 137 – 148. SAE 831613.

Wismans, J., and Spenny, C.H., 1984. Head-Neck Response in Frontal Flexion. *Proceedings from the 28th Stapp Car Crash Conference*, 161 – 171. SAE 841666.

Wismans, J., van Oorashot, H., and Woltring, H.J., 1986. Omni-Directional Human Head-Neck Response. *Proceedings from the 30th Stapp Car Crash Conference* 313 – 331. SAE 861893.

Wismans, J., Philippens, M., van Ooraschot, E., Kallieris, D., and Mattern, R., 1987. Comparison of Human Volunteer and Cadaver Head-Neck Response in Frontal Flexion. *Proceedings from the 31st Stapp Car Crash Conference*, 1 – 13. SAE 872194.

Woo, S.L.Y., Simon, B.R., Kuei, S.C., and Akeson, W.H., 1980. Quasi-Linear Viscoelastic Properties of Normal Articular Cartilage. *Journal of Biomechanical Engineering* 102, 85 – 90.

Wu, H-C., and Yao, R-F., 1976. Mechanical Behavior of Human Annulus Fibrosus. *Journal of Biomechanics* 9, 1 – 17.

Yahia, L.H., Audet, J., and Drouin, G., 1991. Rheological Properties of the Human Lumbar Spine Ligaments. *Journal of Biomedical Engineering* 13(5), 399 – 406.

Yamada, H. 1970. *Strength of Biological Materials*. Williams and Wilkins Co., Baltimore.

Yamazaki, K., Ono, K., and Kaneoka, K., 2000. A Simulation Analysis of Human Cervical Spine Motion During Low Speed Rear-End Impacts. *Proceedings from the 44th Stapp Car Crash Conference*. SAE 2000-01-0154.

Yang, K.H., and Kish, V.L., 1988. Compressibility Measurement of Human Intervertebral Nucleus Pulposus. *Journal of Biomechanics* 21, 865.

Yao, J., Turteltaub, S.R., and Ducheyne, P., 2006. A Three-Dimensional Nonlinear Finite Element Analysis of the Mechanical Behavior of Tissue Engineered Intervertebral Discs Under Complex Loads. *Biomaterials* 27, 377 – 387.

Yeh, O.C., and Keaveny, T.M., 2001. Relative Roles of Microdamage and Microfracture in the Mechanical Behavior of Trabecular Bone. *Journal of Orthopaedic Research* 19, 1001 – 1007.

Yin, L., and Elliot, D.M., 2005. A Homogenization Model of the Annulus Fibrosus. *Journal of Biomechanics* 38, 1674 – 1684.

Yoganandan, N., Sances, A., Maiman, D.J., Myklebust, J.B., Pech, P., and Larson, S.J., 1986. Experimental Spinal Injuries with Vertical Impact. *Spine* 11(9), 855 – 860.

Yoganandan, N., Pintar, F., Butler, J., Reinartz, J., Sances, A., and Larson, S.J., 1989a. Dynamic Response of Human Cervical Spine Ligaments. *Spine* 14(10), 1102 – 1110.

Yoganandan, N., Pintar, F., Haffner, M., Jentzen, J., Mainma, D.J., Weinshel, S.S., Larson, S.J., Nichols, H., and Sances, A., 1989b. Epidemiology and Injury Biomechanics of Motor Vehicle Related Trauma to the Human Spine. *Proceedings from the 33rd Stapp Car Crash Conference*, 223 – 242. SAE 892438.

Yoganandan, N., Sances, A., and Pintar, F.A., 1989c. Biomechanical Evaluation of the Axial Compressive Responses of the Human Cadaveric and Manikin Necks. *Journal of Biomechanical Engineering* 111, 250 – 255.

Yoganandan, N., Pintar, F.A., Sances, A., Reinartz, J., and Larson, S.J., 1991. Strength and Kinematic Response of Dynamic Cervical Spine Injuries. *Spine* 16(10), S511 – S517.

Yoganandan, N., Kumaresan, S., Voo, L., and Pintar, F.A., 1996a. Finite Element Applications in Cervical Spine Modeling. *Spine* 21(15), 1824 – 1834.

Yoganandan, N., Kumaresan, S., Voo, L., Pintar, F.A., and Larson, S.J., 1996b. Finite Element Modeling of the C4-C6 Cervical Spine Unit. *Medical Engineering and Physics* 18(7), 569 – 574.

Yoganandan, N., Pintar, F.A., Mainman, D.J., Cusick, J.F., Sances, A., and Walsh, P.R., 1996c. Human Head-Neck Biomechanics Under Axial Tension. *Medical Engineering and Physics* 18(4), 289 – 294.

Yoganandan, N., Kumaresan, S., and Pintar, F.A., 2000a. Geometric and Mechanical Properties of Human Cervical Spine Ligaments. *Journal of Biomechanical Engineering* 122, 623 – 629.

Yoganandan, N., Pintar, F.A., Stemper, B.D., Schlick, M.B., Philippens, M., and Wismans, J., 2000b. Biomechanics of Human Occupants in Simulated Rear Crashes: Documentation of Neck Injuries and Comparison of Injury Criteria. *Proceedings from the 44th Stapp Car Crash Conference*. SAE 200-01-SC14.

Yoganandan, N., Kumaresan, S., and Pintar, FA., 2001. Biomechanics of the Cervical Spine Part 2: Cervical Spine Soft Tissue Responses and Biomechanical Modeling, *Clinical Biomechanics* 16, 1 – 27.

Yoganandan, N., Knowles, S.A., Maiman, D.J., and Pintar, F.A., 2003. Anatomic Study of the Morphology of Human Cervical Facet Joint. *Spine* 28(20), 2317 – 2323.

Zhang, Q.H., Teo, E.C., Ng, H.W., and Lee, V.S., 2006. Finite Element Analysis of Moment-Rotation Relationships for Human Cervical Spine. *Journal of Biomechanics* 39, 189 – 19.

Appendix A

Single Segment Model Results

The following appendix contains the results of the single segment model simulations that were analyzed and discussed in Chapter 7. Reported in this section are the motions of the superior vertebra in each segment due to the applied load. Motions in all six degrees-of-freedom are reported (translations on one graph, rotations on another) for each simulation case.

C0-C1-C2 Motion Segment Model under Applied Moment
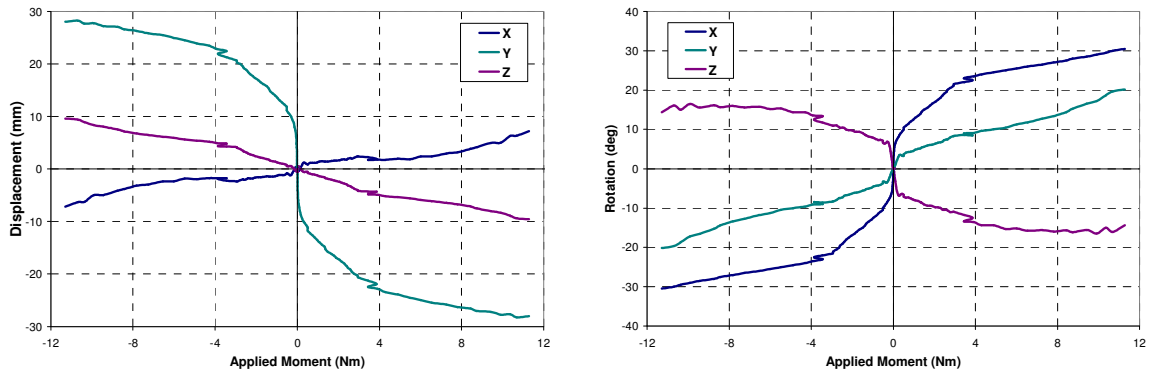
Figure A-1:   Coupled Motion in Applied Lateral Bending
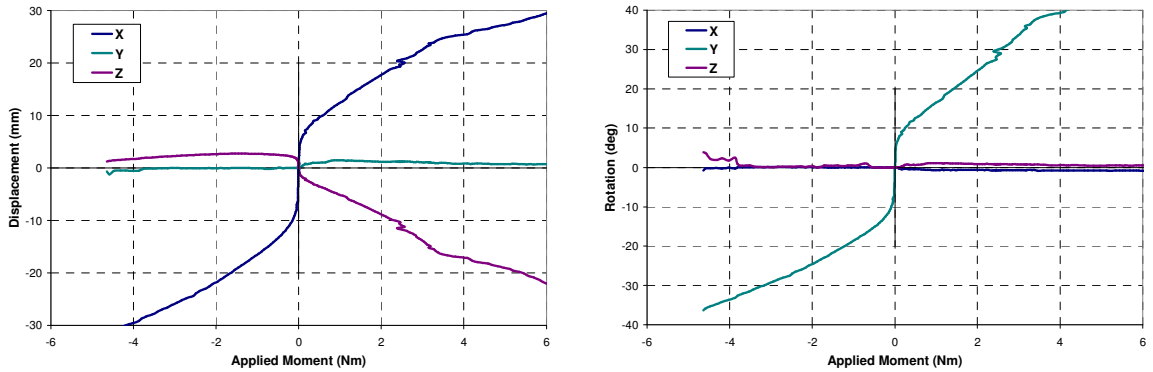
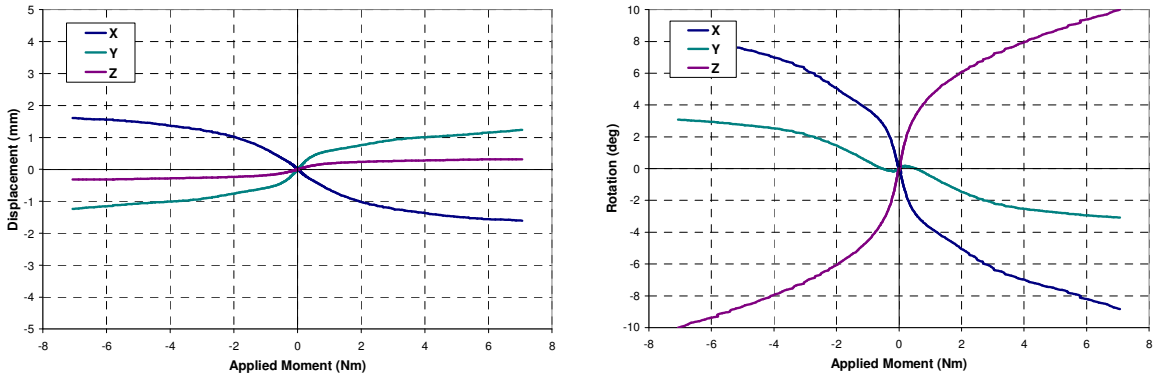**Figure A-2:   Coupled Motion in Applied Flexion and Extension**
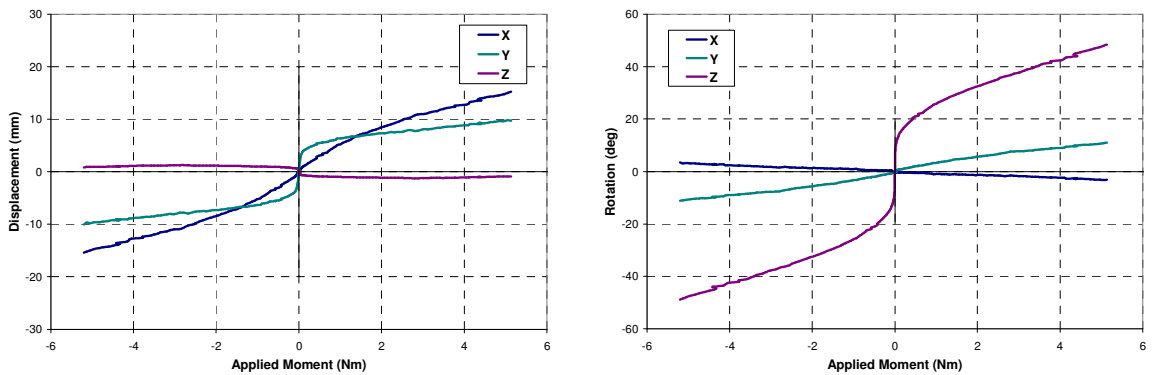
Figure A-3:   Coupled Motion in Applied Axial Rotation

228

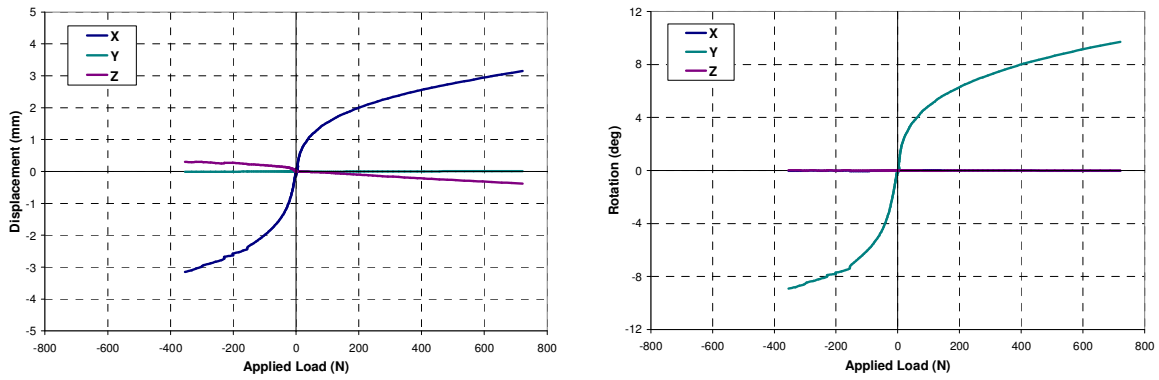## C2-C3 Motion Segment Model under Applied Force
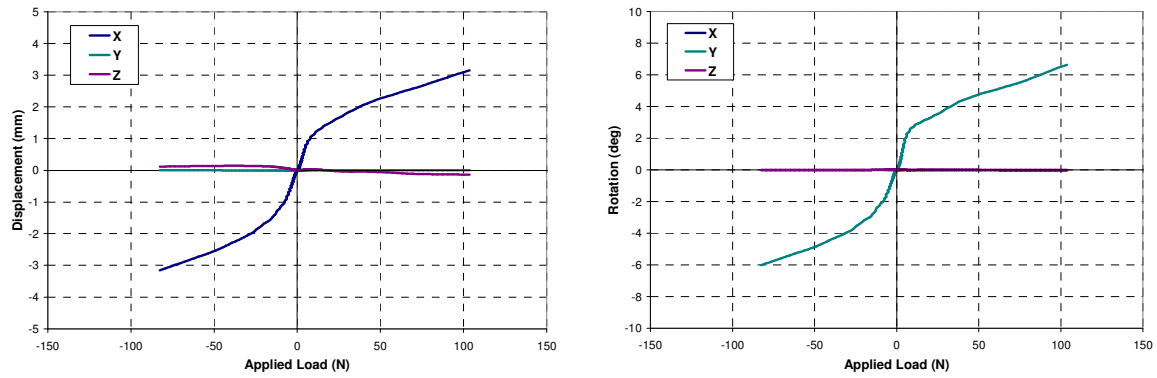
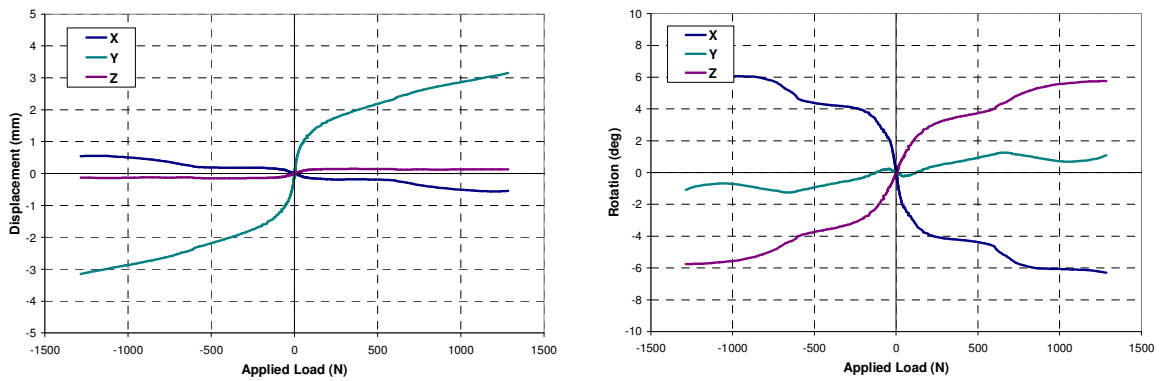**Figure A-4:   Coupled Motion in Applied Anterior and Posterior Shear**
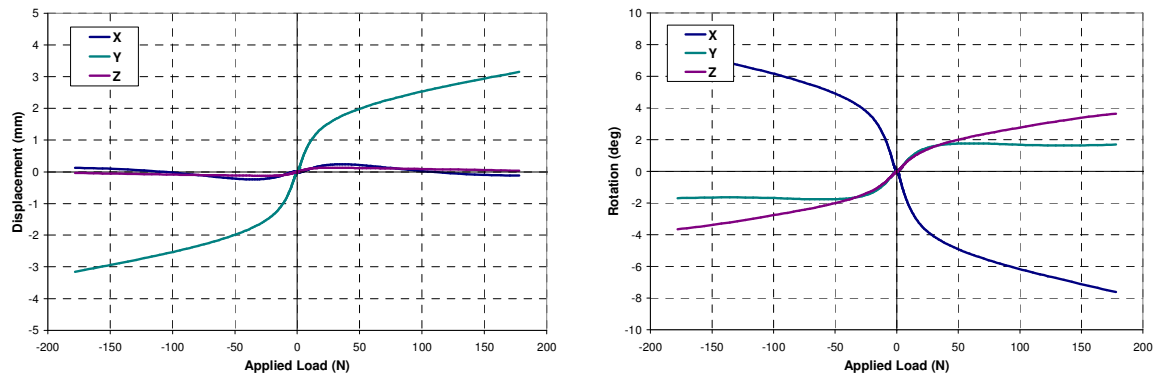
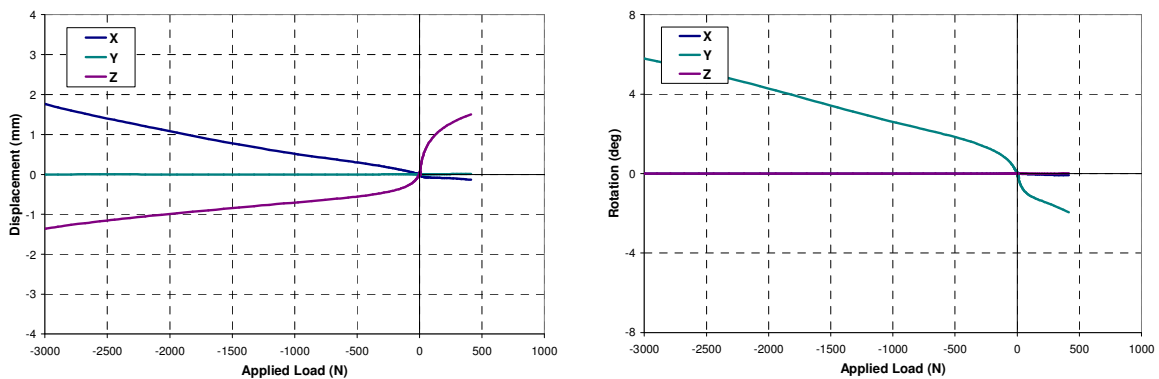**Figure A-5:   Coupled Motion in Applied Lateral Shear**
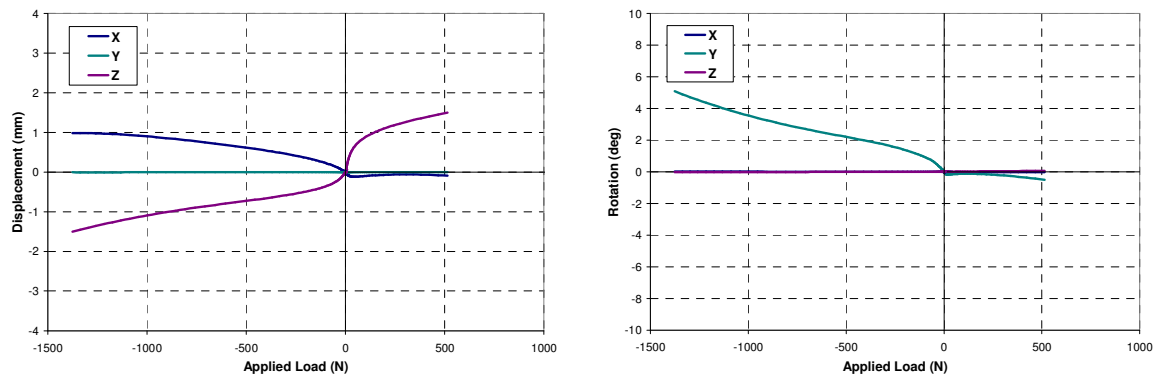
Figure A-6:   Coupled Motion in Applied Tension and Compression

229

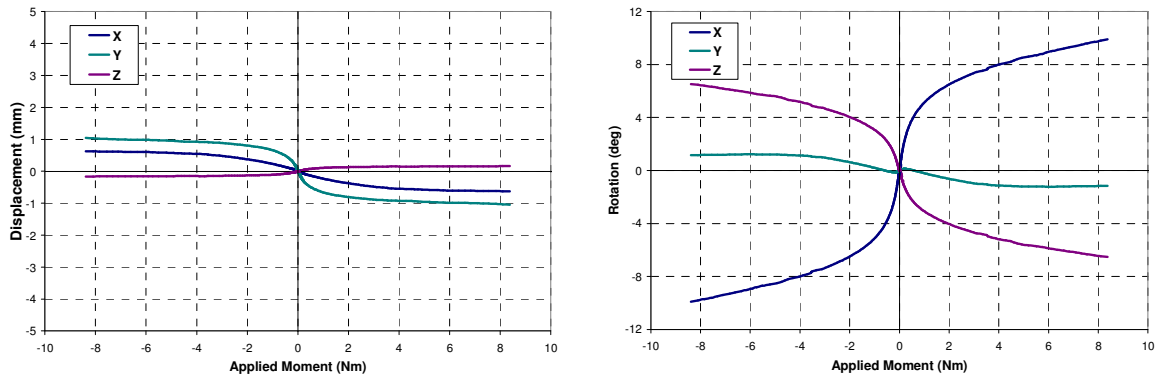## C2-C3 Motion Segment Model under Applied Moment
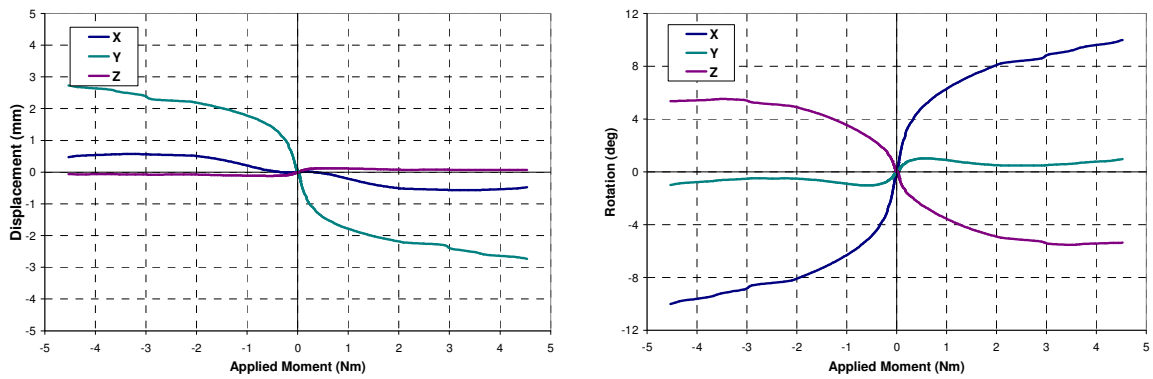
Figure A-7:   Coupled Motion in Applied Lateral Bending
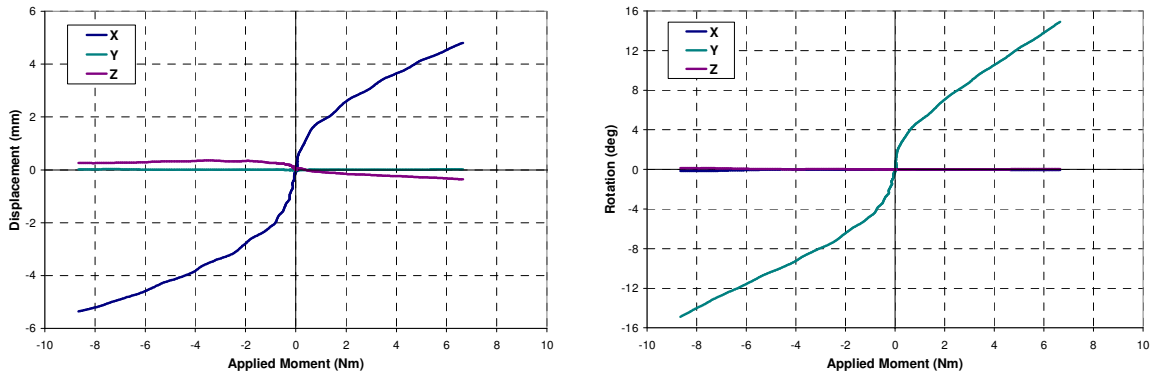
Figure A-8:   Coupled Motion in Applied Flexion and Extension
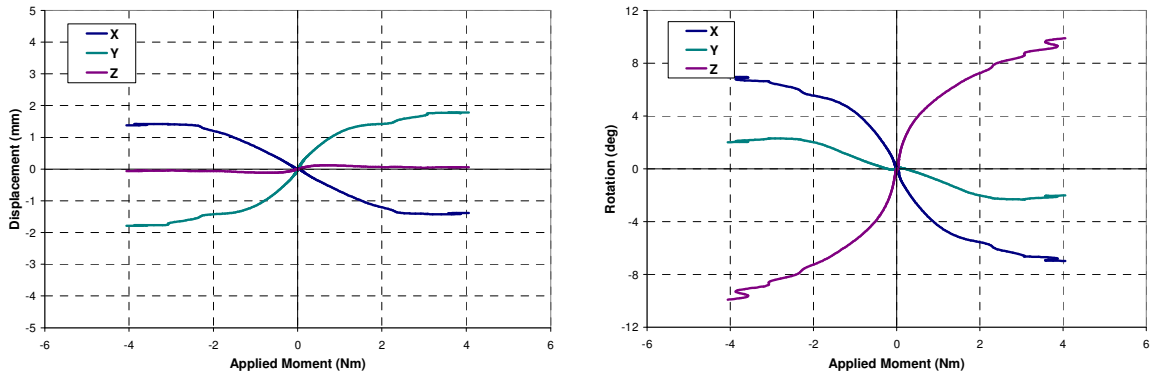
Figure A-9:   Coupled Motion in Applied Axial Rotation

C3-C4 Motion Segment Model under Applied Force
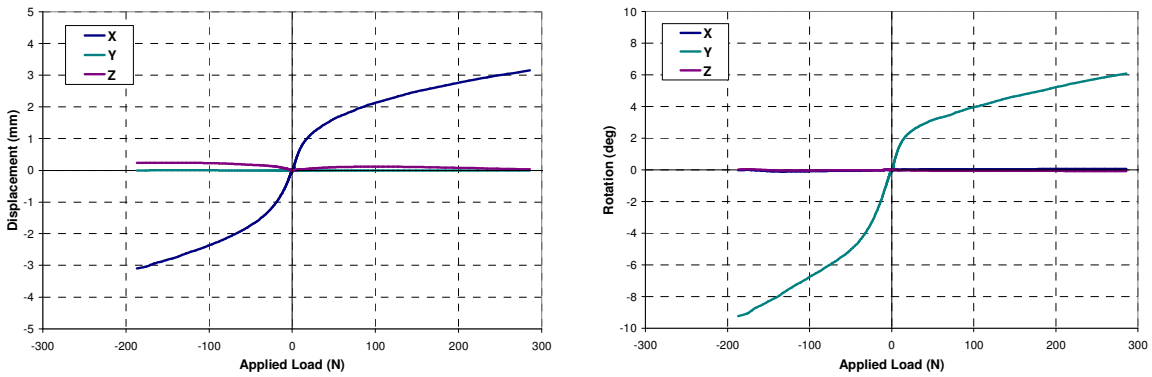
Figure A-10: Coupled Motion in Anterior and Posterior Shear
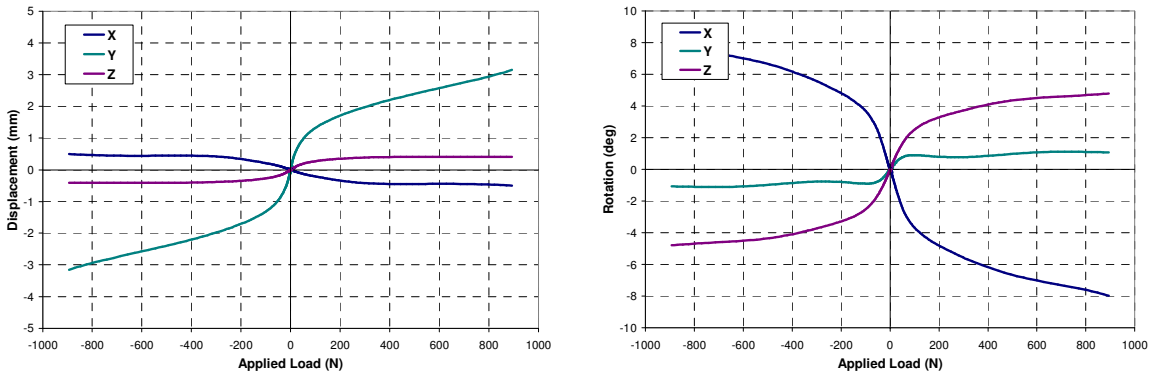
Figure A-11: Coupled Motion in Lateral Shear
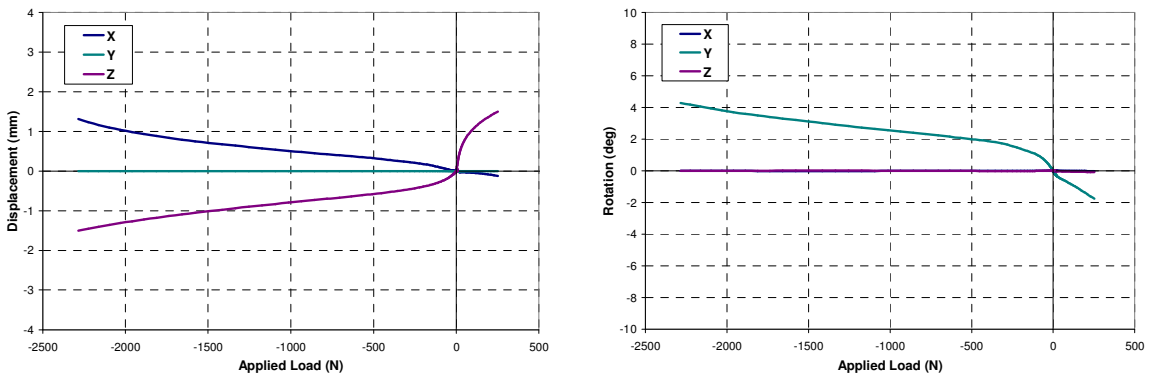
Figure A-12: Coupled Motion in Tension and Compression

231

C3-C4 Motion Segment Model under Applied Moment
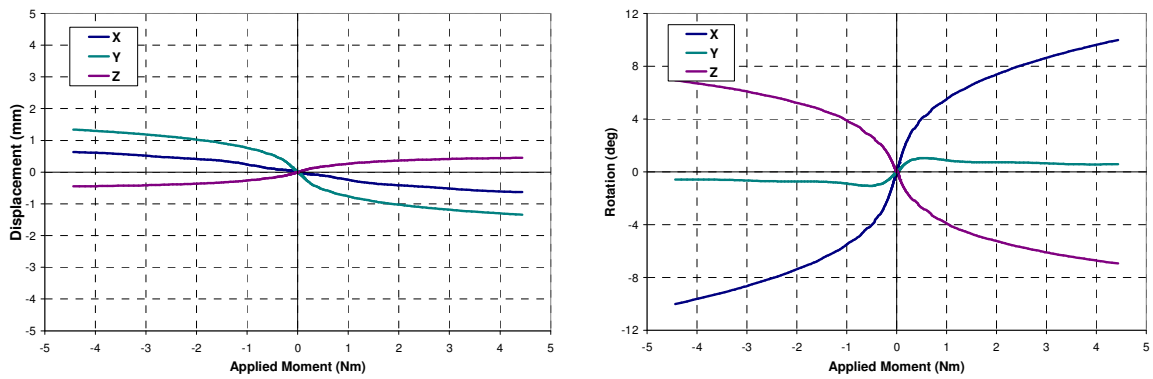
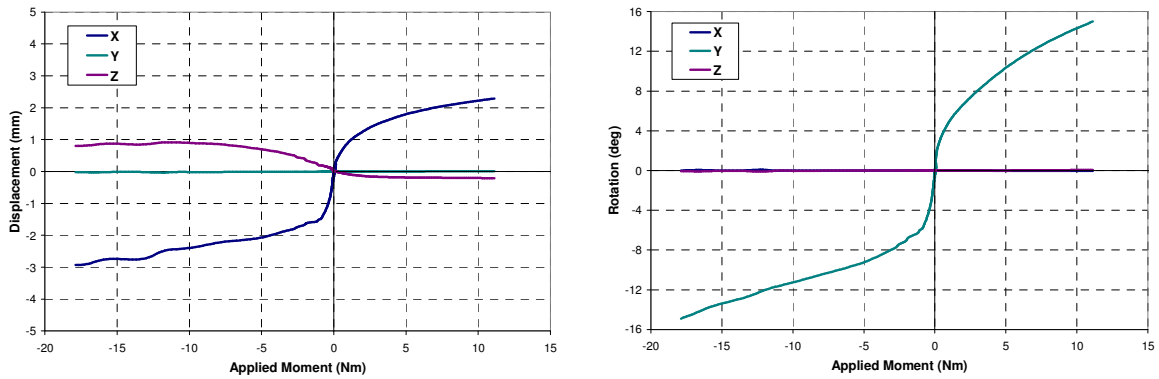**Figure A-13: Coupled Motion in Applied Lateral Bending**
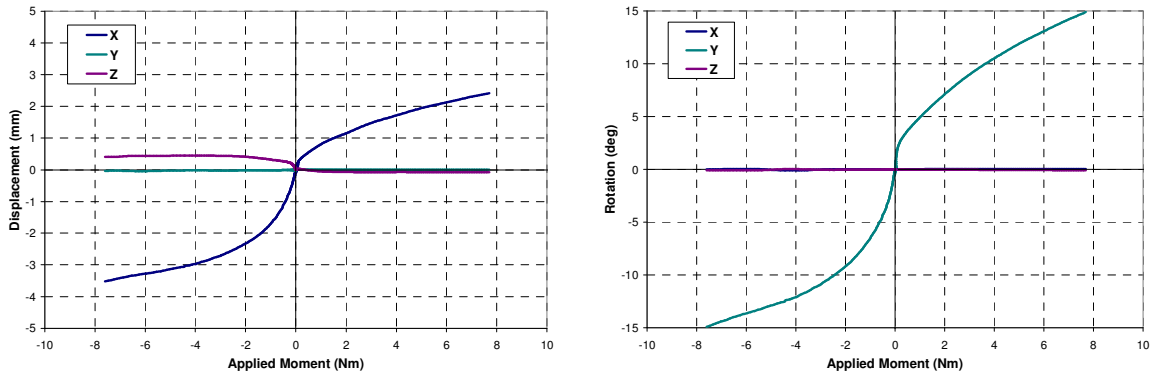
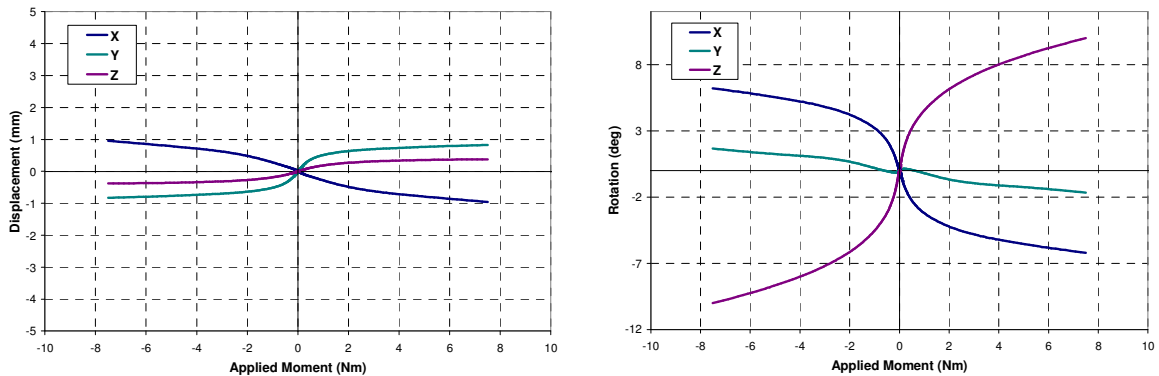**Figure A-14: Coupled Motion in Applied Flexion and Extension**
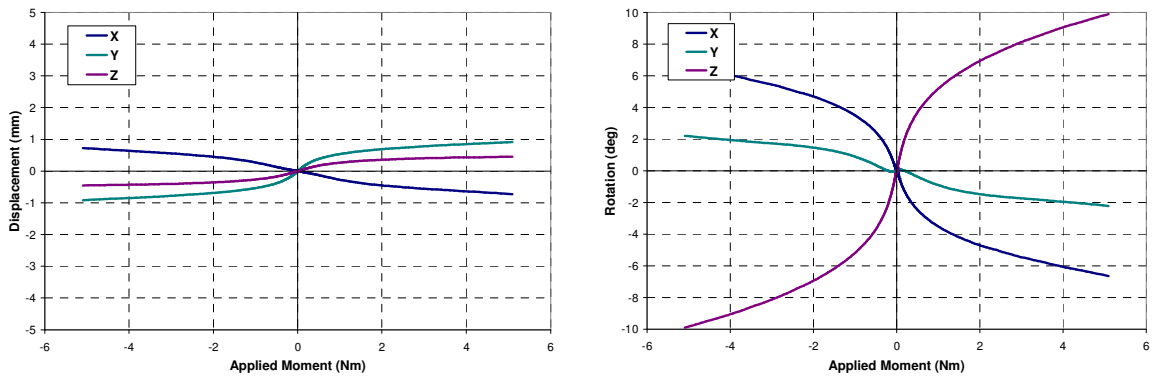
Figure A-15: Coupled Motion in Applied Axial Rotation

C4-C5 Motion Segment Model under Applied Force
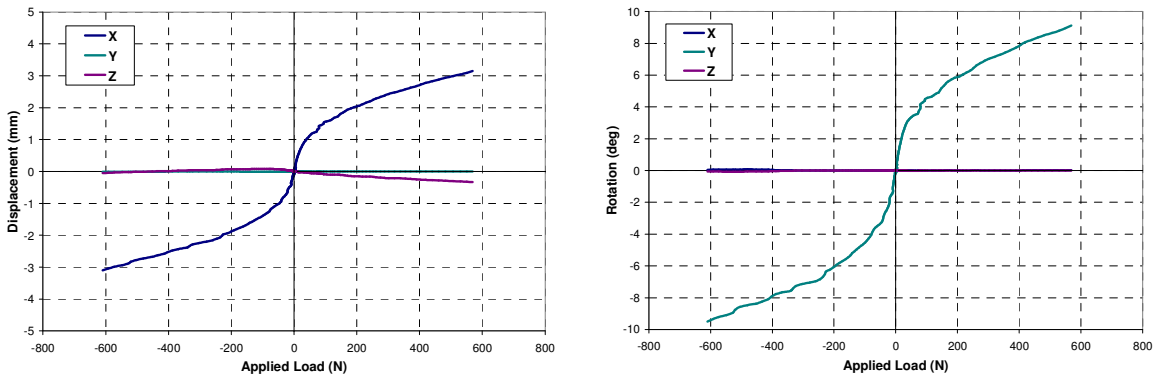
Figure A-16: Coupled Motion in Applied Anterior and Posterior Shear
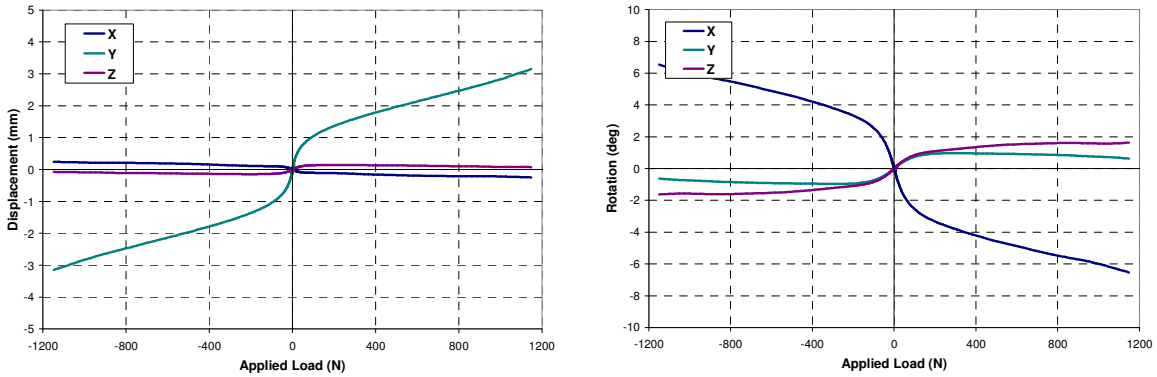
Figure A-17: Coupled Motion in Applied Lateral Shear
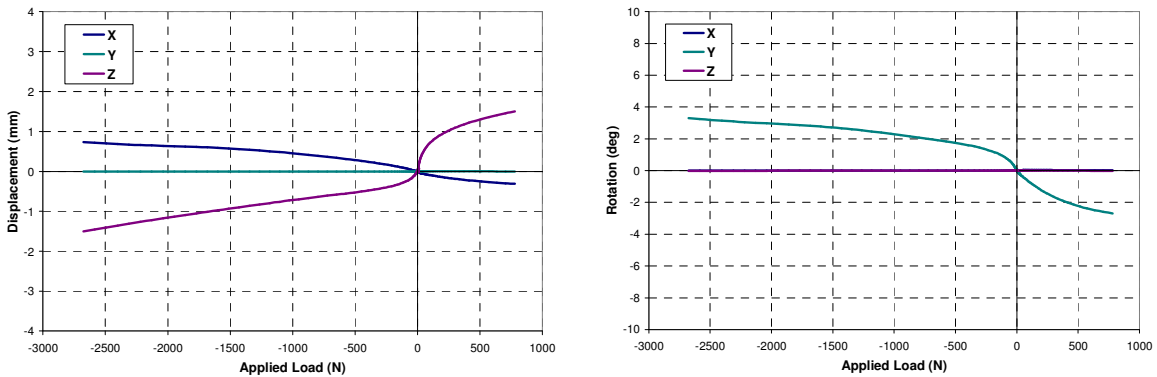
Figure A-18: Coupled Motion in Applied Tension and Compression

C4-C5 Motion Segment Model under Applied Moment
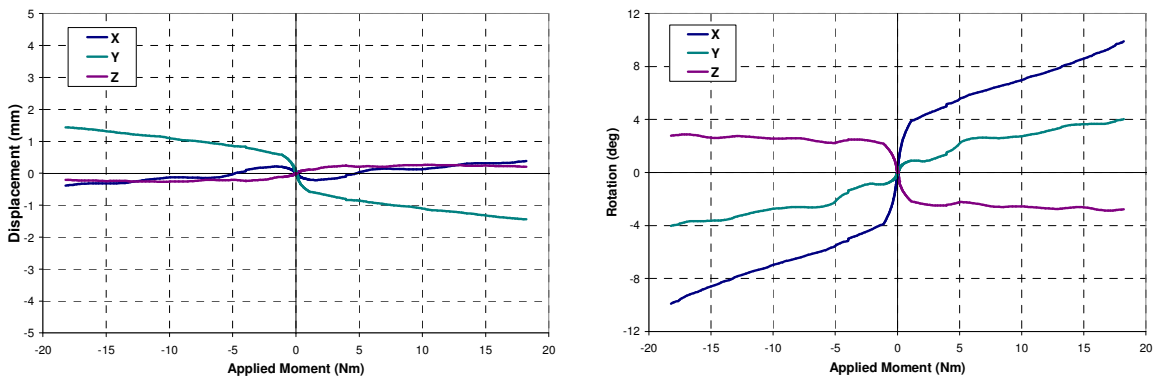
Figure A-19: Coupled Motion in Applied Lateral Bending
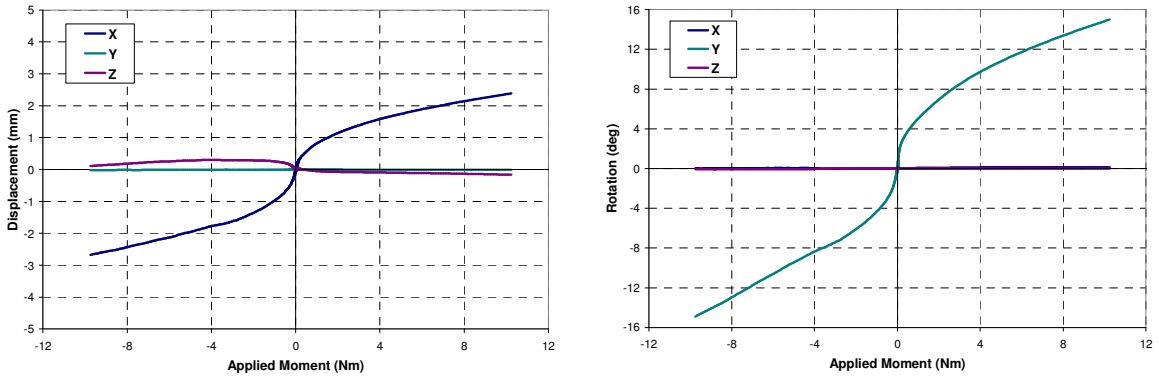
Figure A-20: Coupled Motion in Applied Flexion and Extension
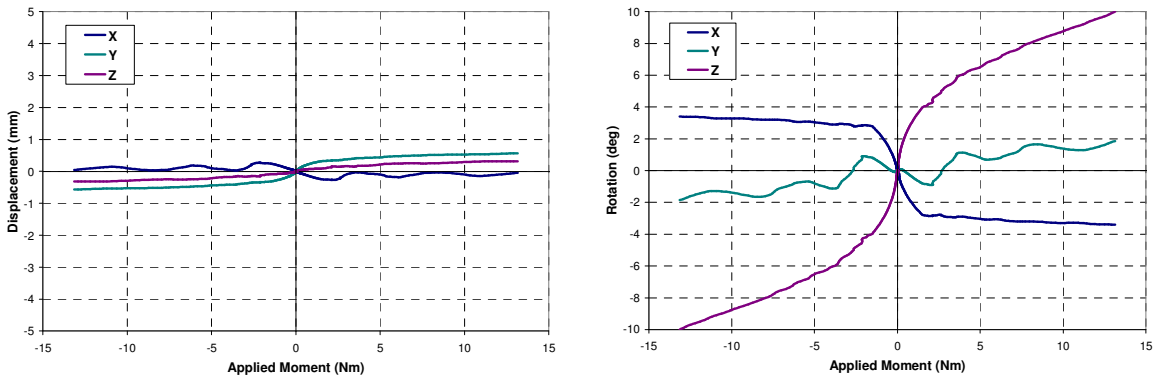
Figure A-21: Coupled Motion in Applied Axial Rotation

234

C5-C6 Motion Segment Model under Applied Force
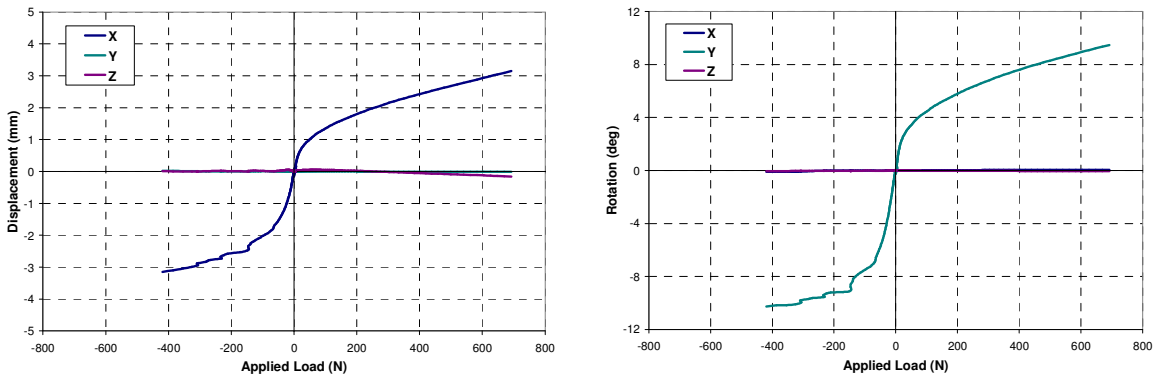
Figure A-22: Coupled Motion in Applied Anterior and Posterior Shear
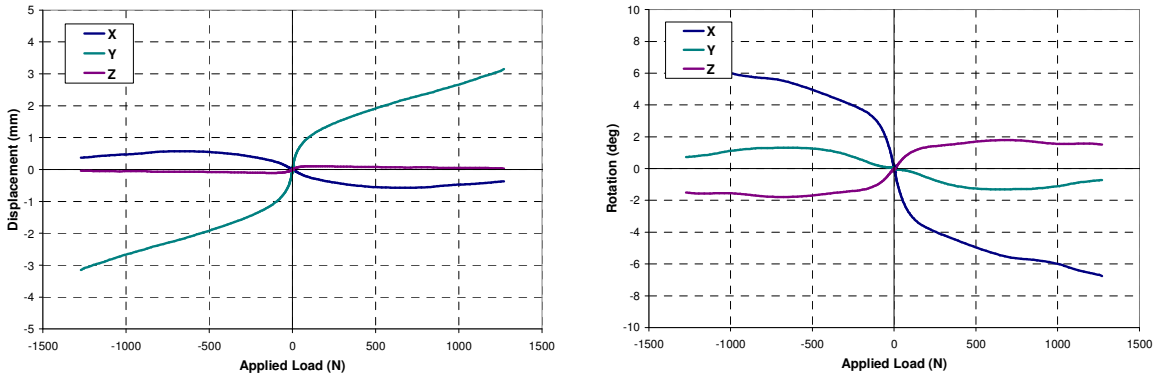
Figure A-23: Coupled Motion in Applied Lateral Shear
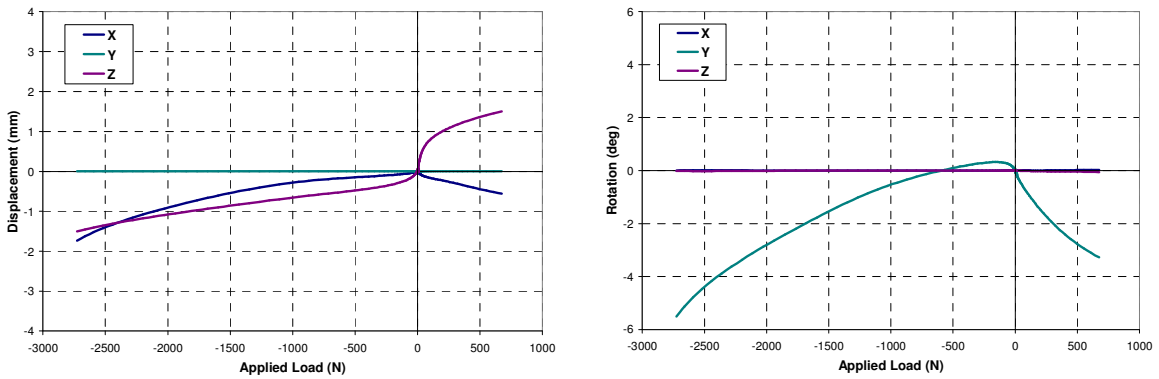
Figure A-24: Coupled Motion in Applied Tension and Compression

C5-C6 Motion Segment Model under Applied Moment
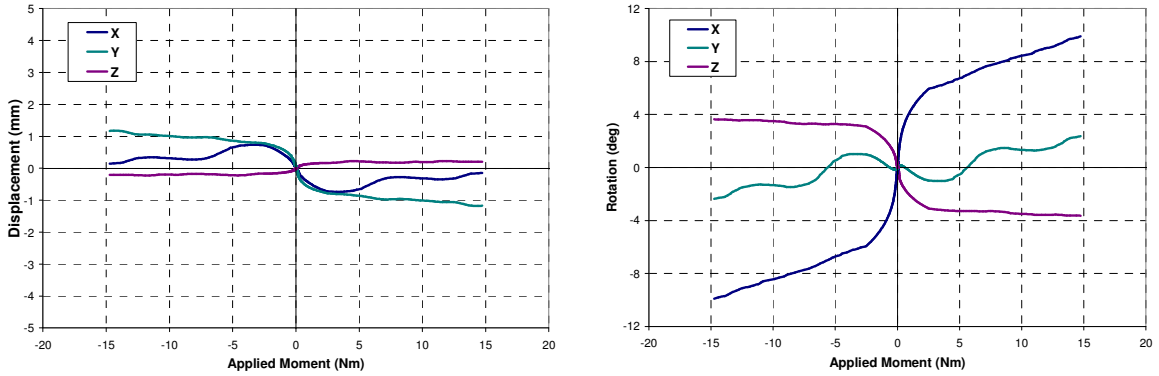
Figure A-25: Coupled Motion in Applied Lateral Bending
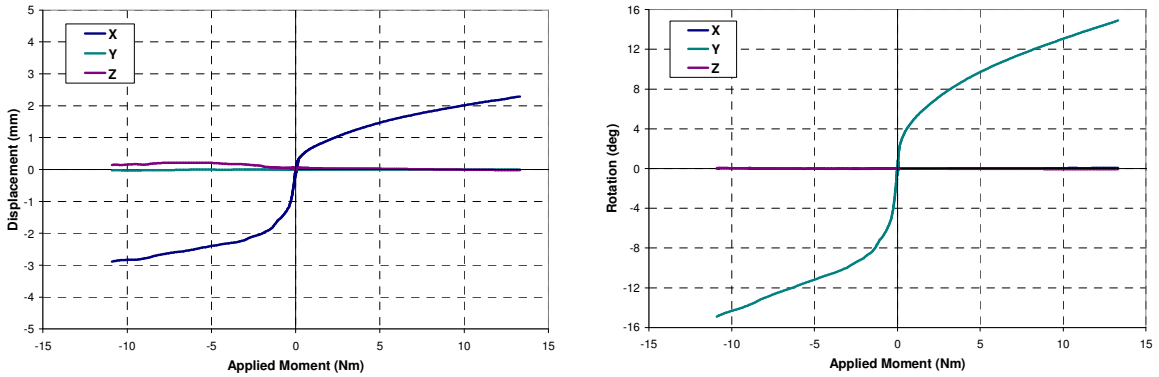
Figure A-26: Coupled Motion in Applied Flexion and Extension
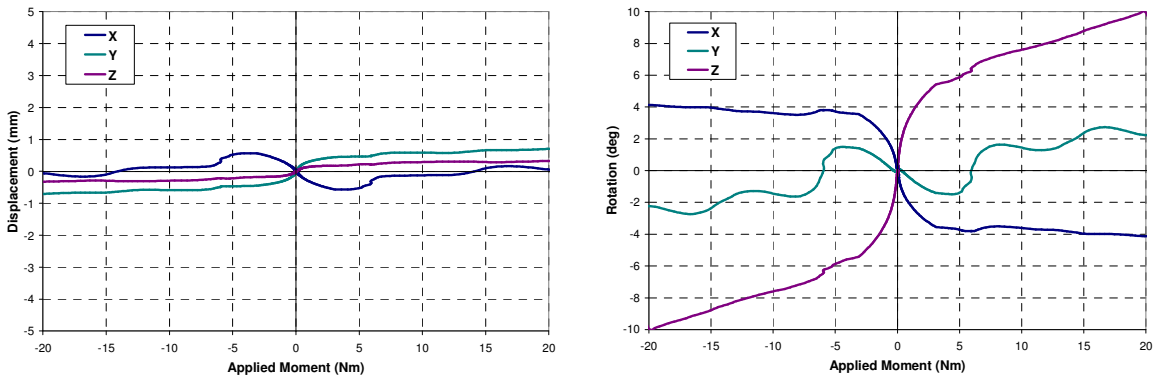
Figure A-27: Coupled Motion in Applied Axial Rotation

C6-C7 Motion Segment Model under Applied Force
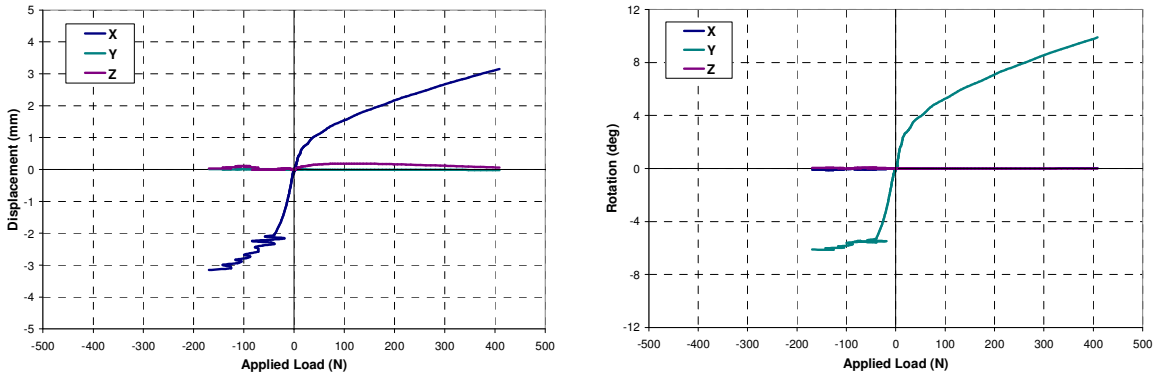
Figure A-28: Coupled Motion in Applied Anterior and Posterior Shear
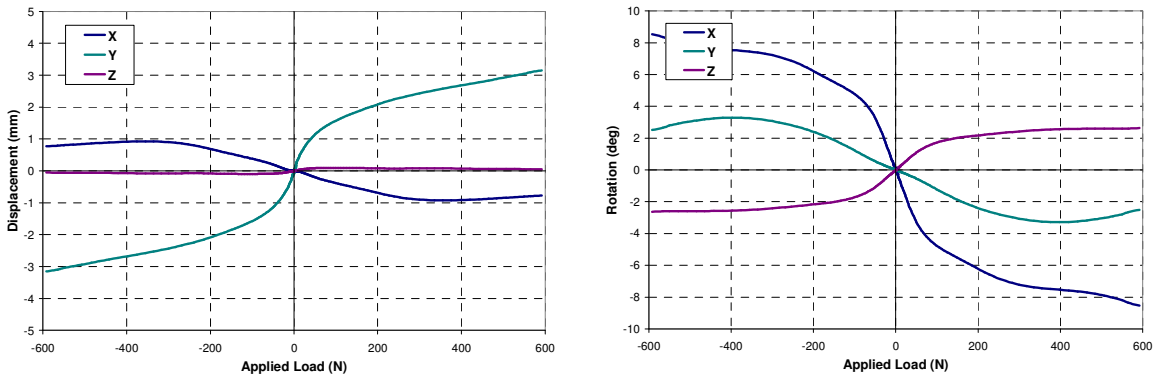
Figure A-29: Coupled Motion in Applied Lateral Shear
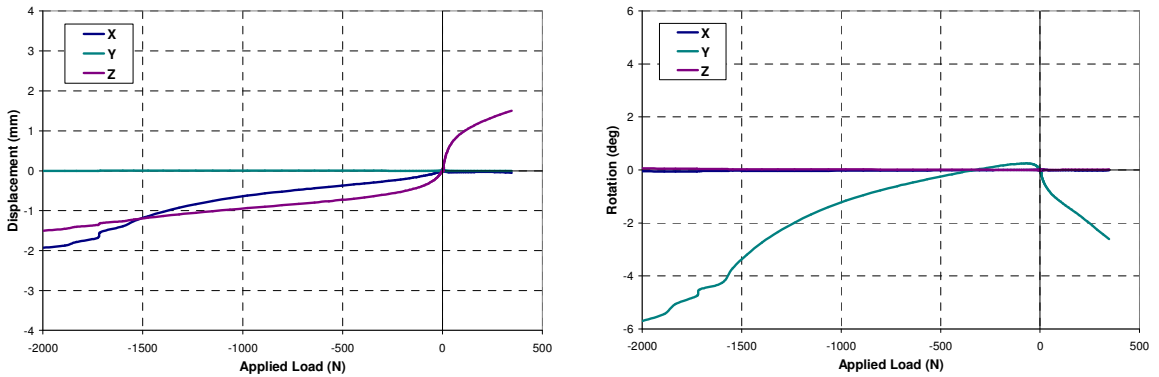
Figure A-30: Coupled Motion in Applied Tension and Compression

237

C6-C7 Motion Segment Model under Applied Moment
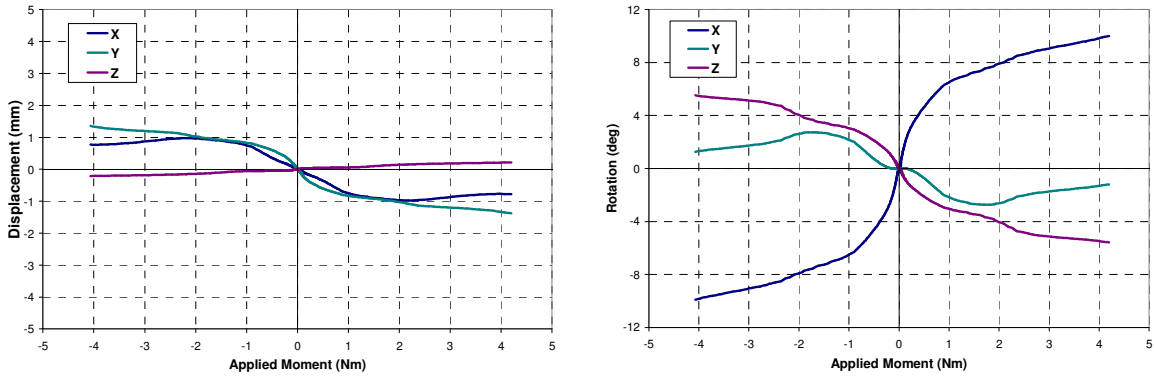
Figure A-31: Coupled Motion in Applied Lateral Bending
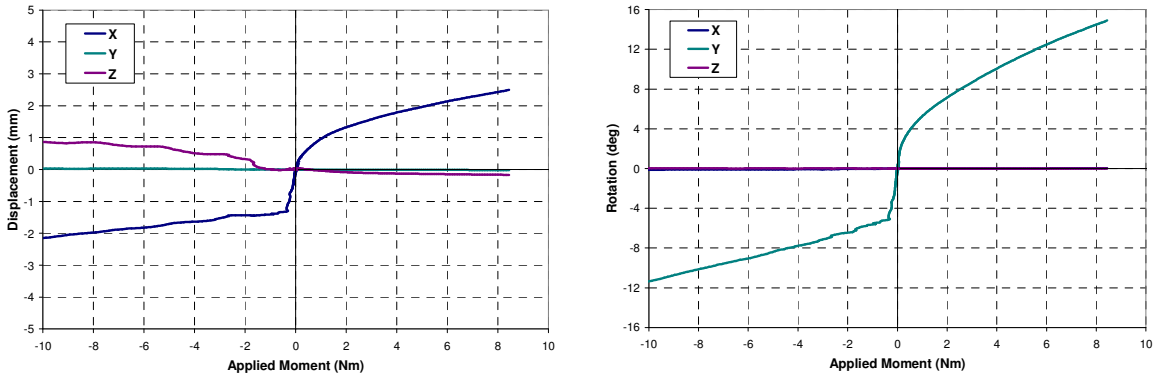
Figure A-32: Coupled Motion in Applied Flexion and Extension

Figure A-33: Coupled Motion in Applied Axial Rotation

C7-T1 Motion Segment Model under Applied Force

Figure A-34: Coupled Motion in Applied Anterior and Posterior Shear

Figure A-35: Coupled Motion in Applied Lateral Shear

Figure A-36: Coupled Motion in Applied Tension and Compression

239

C7-T1 Motion Segment Model under Applied Moment

Figure A-37: Coupled Motion in Applied Lateral Bending

Figure A-38: Coupled Motion in Applied Flexion and Extension

Figure A-39: Coupled Motion in Applied Axial Rotation

Appendix B

Single Segments in Flexion/Extension

The following appendix contains the results of the single segment model simulations that were analyzed and discussed in Chapter 7. Reported in this section are the response of the segment models in flexion and extension. The relative sagittal rotation (Y) between the superior and inferior vertebra is reported for bending moments ranging from 2.5 Nm flexion to 2.5 Nm extension. These results are compared to the results of the experimental studies by Camacho et al (1997), Nightingale et al (2002, 2006), and Wheeldon et al (2006).

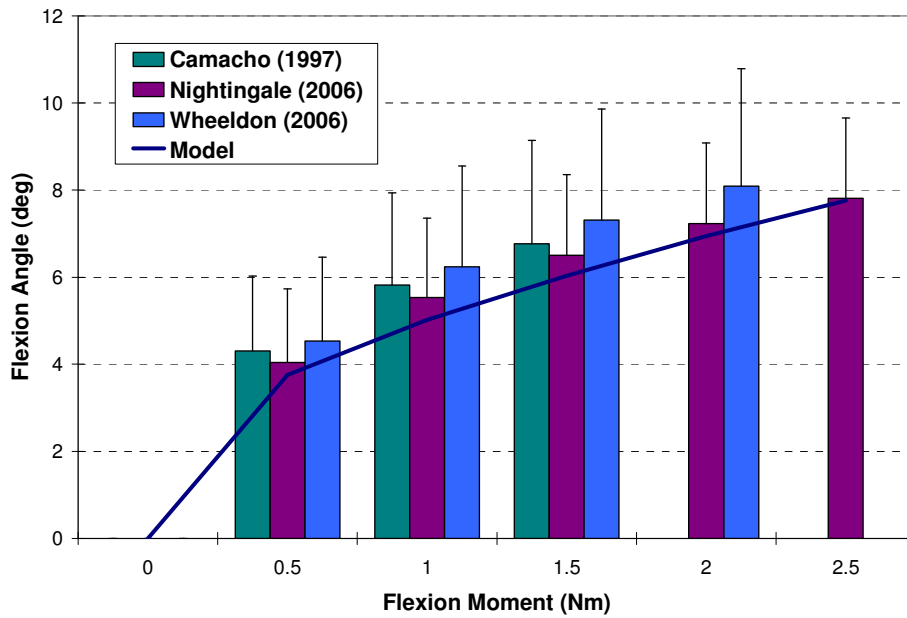## B.1 C0-C1-C2 Motion Segment Model under Flexion/Extension Moment
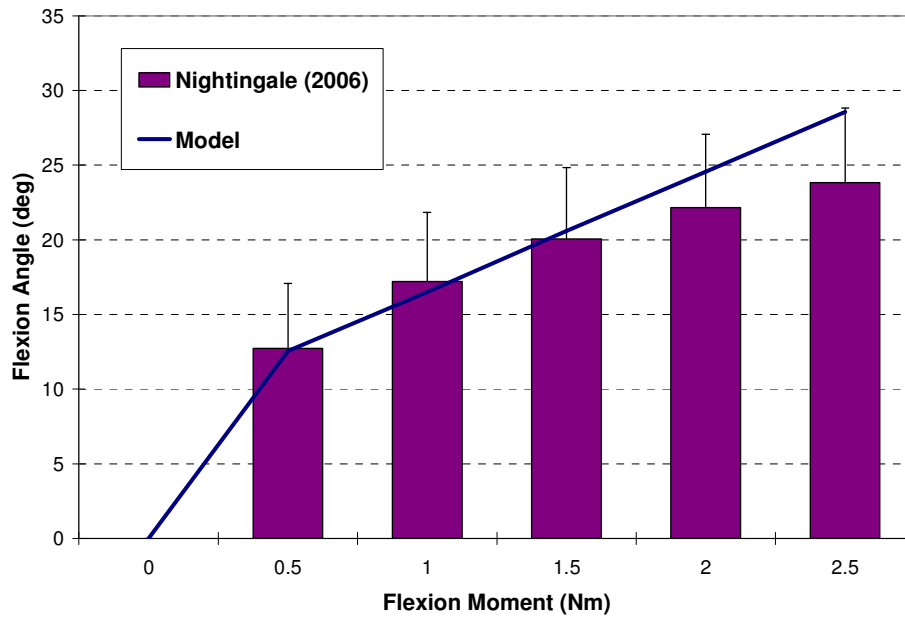
Figure B-1: Response under a Range of Quasi-Static Flexion Moments
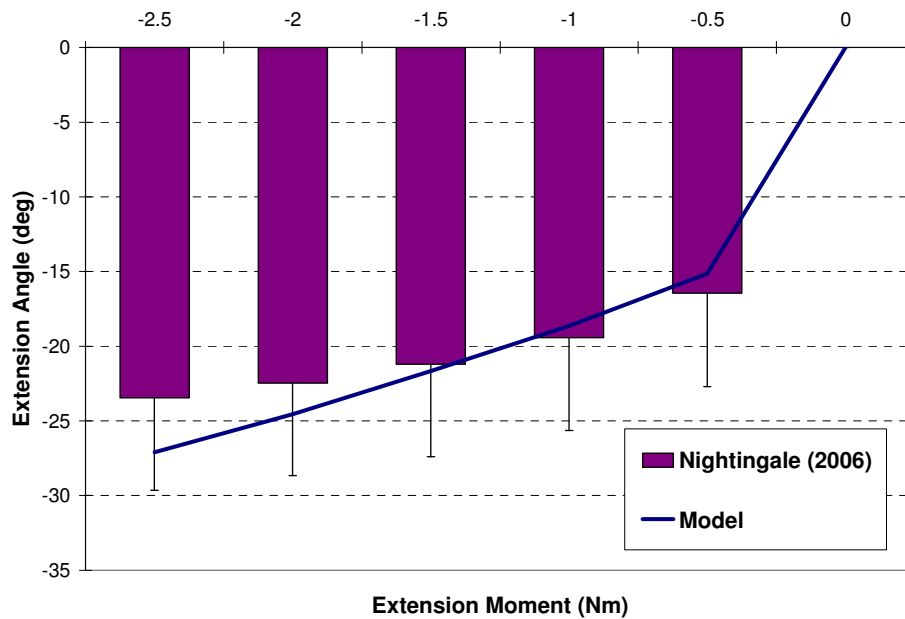
Figure B-2: Response under a Range of Quasi-Static Extension Moments

242

B.2 C2-C3 Motion Segment Model under Flexion/Extension Moment
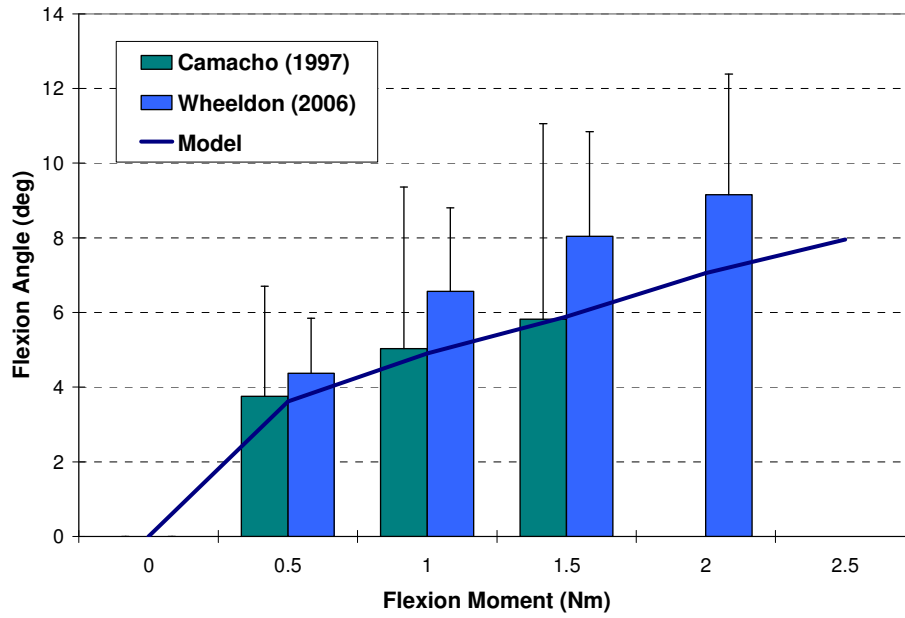
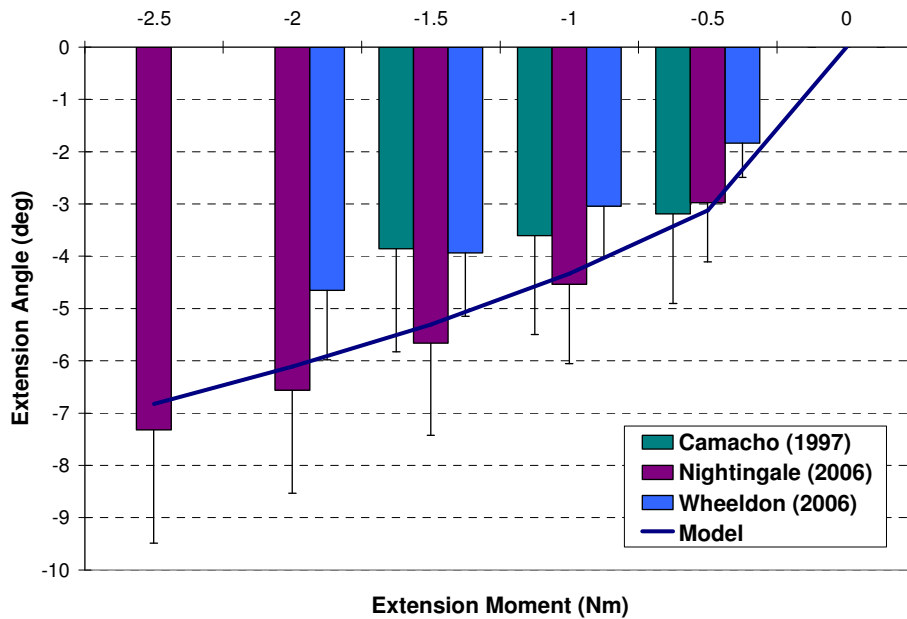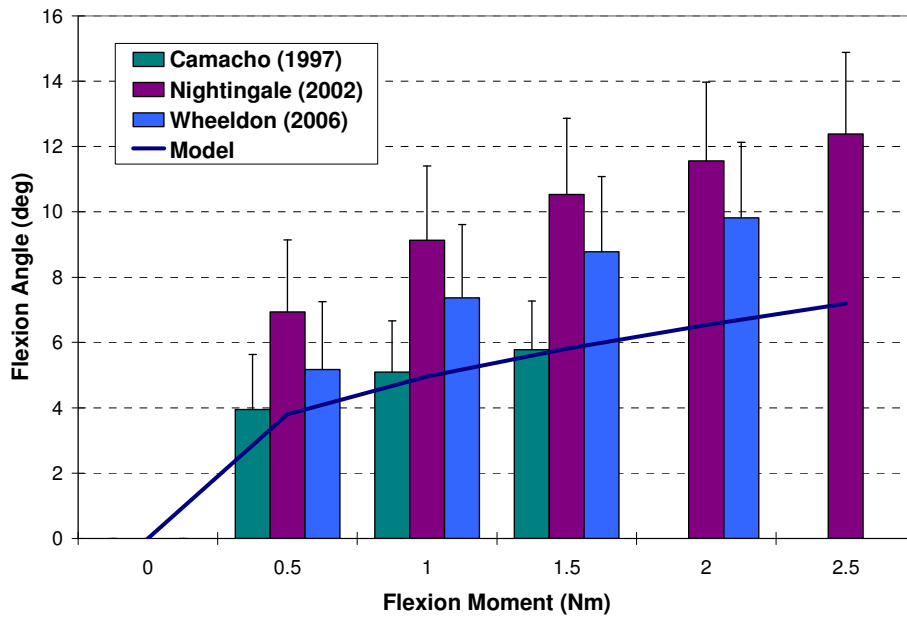**Figure B-3:   Response under a Range of Quasi-Static Flexion Moments**
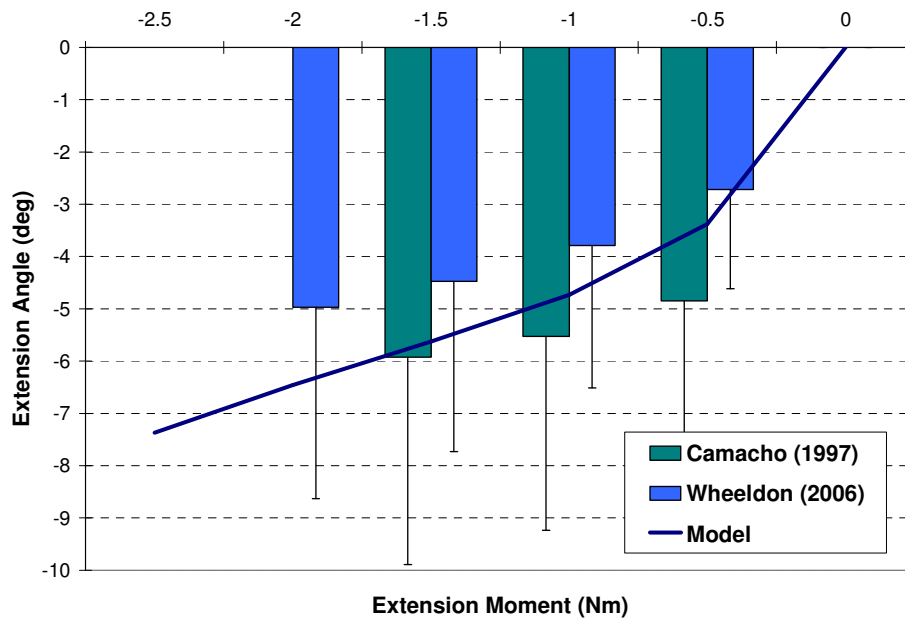
Figure B-4:   Response under a Range of Quasi-Static Extension Moments

B.3 C3-C4 Motion Segment Model under Flexion/Extension Moment
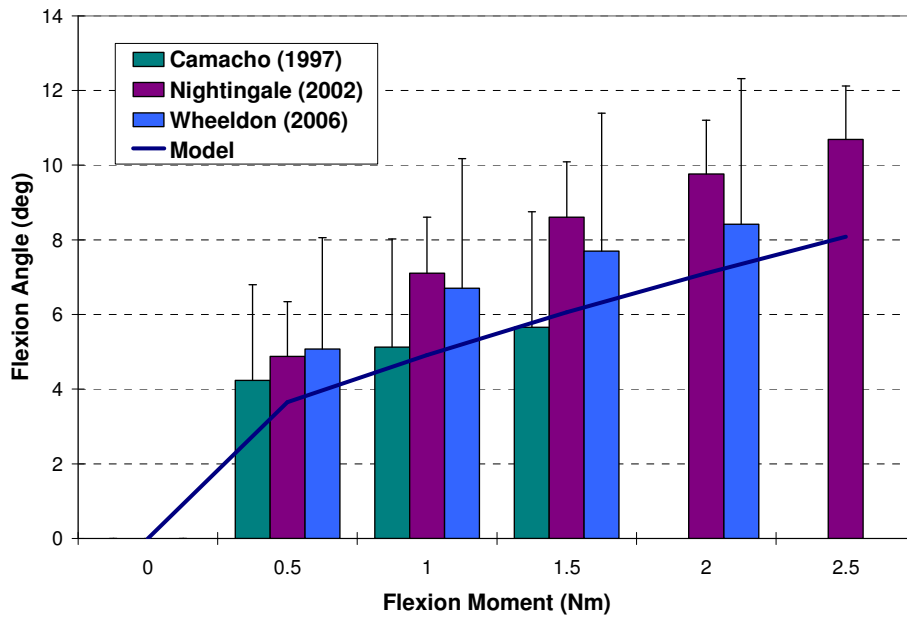
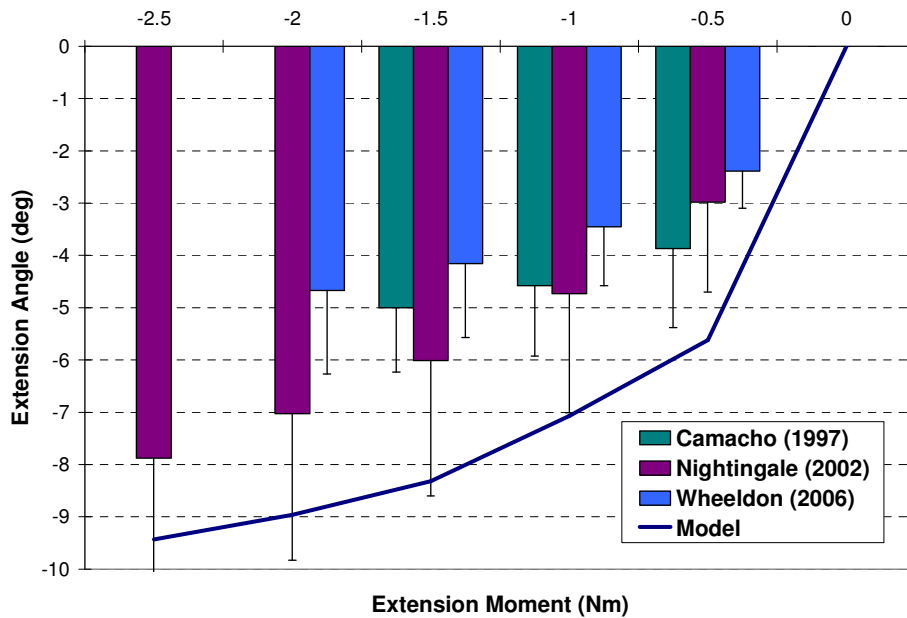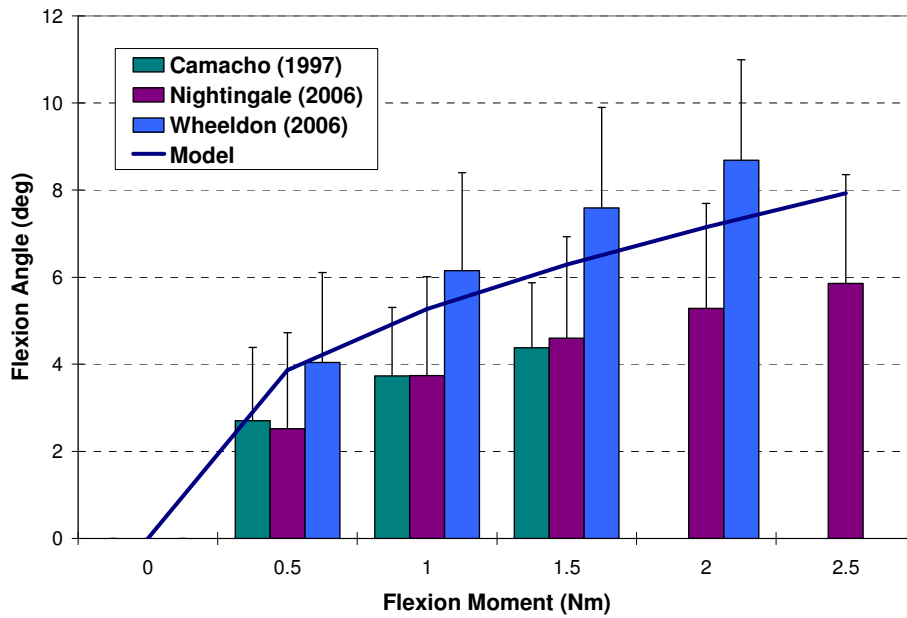**Figure B-5:   Response under a Range of Quasi-Static Flexion Moments**
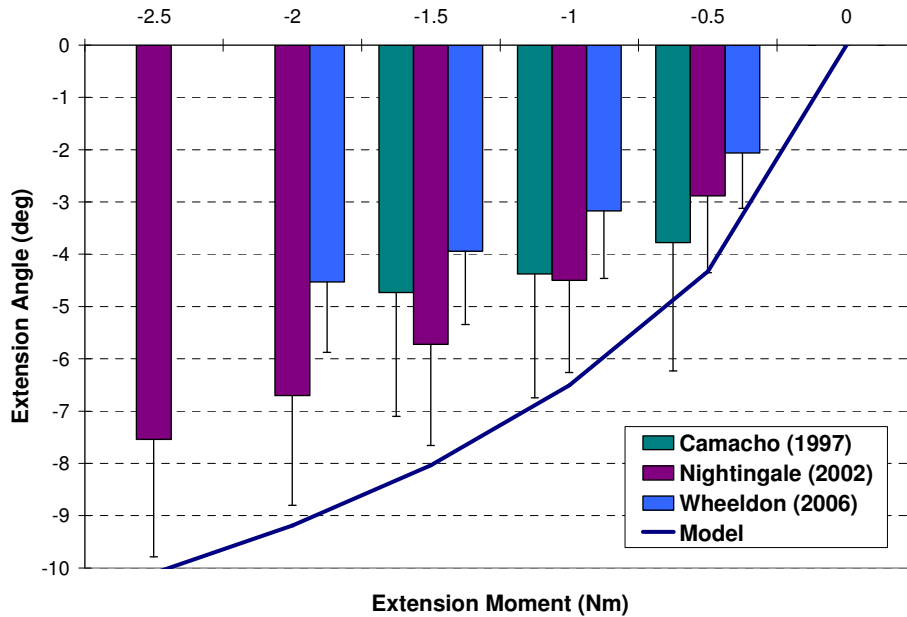
Figure B-6:   Response under a Range of Quasi-Static Extension Moments

B.4 C4-C5 Motion Segment Model under Flexion/Extension Moment

Figure B-7: Response under a Range of Quasi-Static Flexion Moments

Figure B-8: Response under a Range of Quasi-Static Extension Moments

B.5 C5-C6 Motion Segment Model under Flexion/Extension Moment

Figure B-9: Response under a Range of Quasi-Static Flexion Moments

Figure B-10: Response under a Range of Quasi-Static Extension Moments

B.6 C6-C7 Motion Segment Model under Flexion/Extension Moment

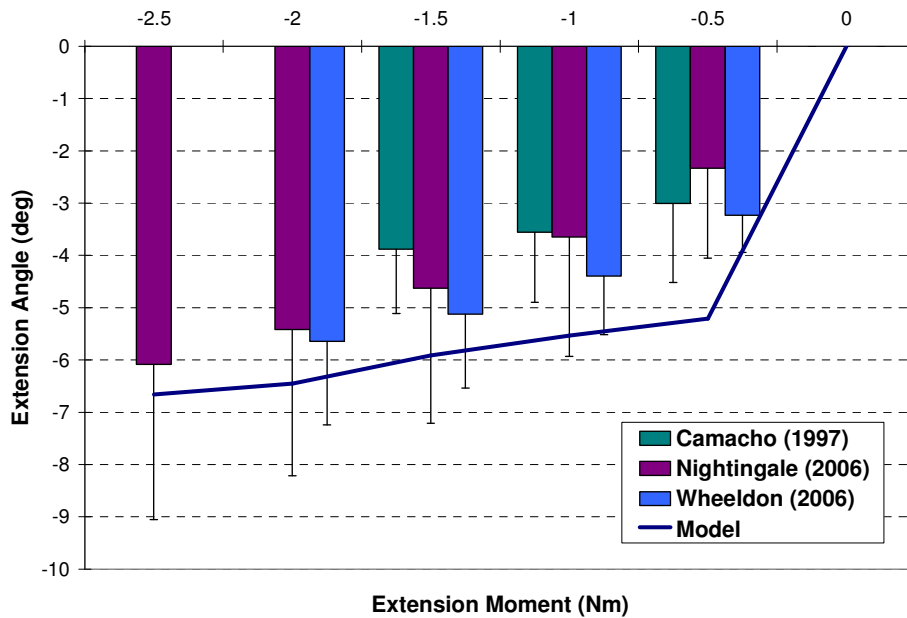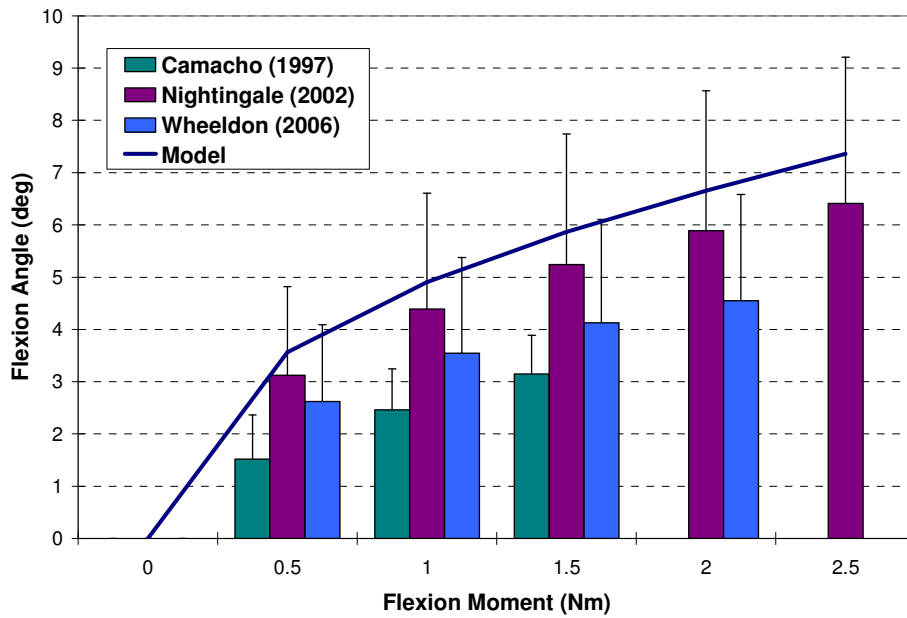**Figure B-11: Response under a Range of Quasi-Static Flexion Moments**

Figure B-12: Response under a Range of Quasi-Static Extension Moments

B.7 C7-T1 Motion Segment Model under Flexion/Extension Moment

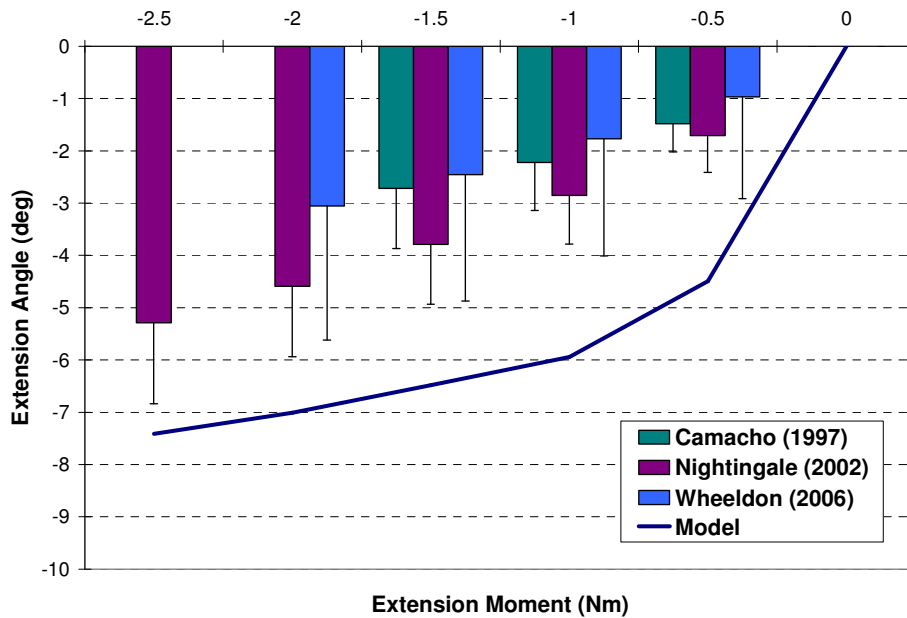**Figure B-13: Response under a Range of Quasi-Static Flexion Moments**

Figure B-14: Response under a Range of Quasi-Static Extension Moments